DESIGN OF BIODEGRADABLE ALIPHATIC AROMATIC POLYESTER FILMS FOR AGRICULTURAL APPLICATIONS USING RESPONSE SURFACE METHODOLOGY

By

Thitisilp Kijchavengkul

A DISSERTATION

Submitted to
Michigan State University
in partial fulfillment of the requirements
for the degree of

DOCTOR OF PHILOSOPHY

Packaging

2010

ABSTRACT

DESIGN OF BIODEGRADABLE ALIPHATIC AROMATIC POLYESTER FILMS FOR AGRICULTURAL APPLICATIONS USING RESPONSE SURFACE METHODOLOGY

By

Thitisilp Kijchavengkul

Degradation of an aliphatic aromatic copolyester film, poly(butylene adipate-*co*-terephthalate) or PBAT, under atmospheric, laboratory simulated solar radiation, phosphate buffer solution, manure, food and yard compost environments was investigated. Methodologies and equipment were developed to measure biodegradation of PBAT films in compost environments using a direct measurement respirometric system (DMR), and to determine the gel content in PBAT films due to crosslinking by differential scanning calorimetry and Fourier transform infrared spectroscopy. A response surface methodology (RMS) was used to design films for agriculture applications with the required optical, physical, mechanical, and biodegradable properties for exposure to different amount of solar radiation. Field and laboratory experiments were carried out to verify and corroborate the performance of the designed films.

The performance of PBAT films in tomato production for two consecutive seasons was compared to commercial low density polyethylene mulch film. Changes in light transmission, mechanical properties, molecular weight, thermal behavior and functional groups of the films were used to investigate the effects of solar radiation on PBAT. Exposure of PBAT films to solar radiation produced crosslinked structures of combined phenyl radicals within the film structure. The behavior was replicated when the films were exposed to simulated laboratory UV radiation. The presence of crosslinked

structures not only decreased the mechanical properties of the film due to embrittlement, but also hindered the biodegradation process by limiting the access of water and microorganisms to the polymer chains as confirmed by scanning electron microscope and the DMR system.

To prevent the formation of the PBAT crosslinked structures from recombination of free radicals, a chain breaking antioxidant, butylated hydroxytoluene (BHT), was incorporated in the formulation. RSM was used to determine the optimal concentrations of carbon black (CB) and BHT for the design of mulch film. Light transmission, final tensile strength, final gel content, and the pattern of reduction of number average molecular weight (M_n) were selected as the response surfaces for determination of the film formulation. Twenty percent light transmission or less, a final tensile strength of at least 6.35 MPa, a maximum gel content of 0.30 g gel/g polymer, and a specific reduction pattern of M_n were established as the mulch films design criteria. A contour plot of suitable concentrations of CB and BHT for the formulation of mulch film for crop production in Michigan or regions with similar solar radiation was established. Furthermore, a model including CB and an antioxidant concentration with the four design criteria was developed for the formulation of mulch films for general exposure radiation. Therefore, the proposed model is not restricted by different crops or geographical regions.

To my parents, Suchitra and Thavorn Kijchavengkul, brother and sister,

Vorasilp and Vorakul,

and in memory of my grandmother, Penkhae Osothsilp

ACKNOWLEDGMENTS

Although only my name is on the front cover, this dissertation would not have been possible without contribution from many people throughout my Ph.D. study at Michigan State University. I owe my gratitude to all these wonderful people.

My deepest gratitude is to my major advisor, Dr. Rafael Auras. I have been fortunate to have him as an advisor who gave me freedom to conduct research and guidance when I was struggle, as a mentor who taught me how to excel in research, teaching, and community outreach, and as a friend whom I could talk to, especially during the time of my mother's illness. He has always encouraged me to try harder and think differently in order to solve a problem. His patience and advice helped me overcome many situations and finish this dissertation.

Dr. Maria Rubino's insightful comments and criticisms helped me crystallize research ideas and become a better researcher. She introduced me to Instrumental analysis in PKG 817 and her teaching of instrumental analysis has inspired a major part in this dissertation.

I am grateful to Dr. Susan Selke who has taught me so much about critical thinking and reasoning to substantiate my thoughts through her class assignments and her comments on article manuscripts. I am thankful for countless manuscript revisions and grammar corrections.

Dr. Mathieu Ngouajio always gave me advices throughout the two-year field experiment of tomato production. He also helped me understand the needs of vegetable growers regarding mulch films.

I am thankful to Dr. Rodney Thomas Fernandez for his advice about agriculture industry point of view and countless revisions of manuscripts and writing. His comments from different views helped me understand and improve my research.

I would like to thank Dr. Robert Tempelman for his statistics teaching that inspired the use of response surface methodology in this dissertation. I would like to thank Dr. Ramani Narayan for his guidance and advice on biodegradation of polymer. I am grateful to Dr. Stanley and Carol Flegler for their teaching and advices on scanning electron microscope, as well as, for inviting me to a wonderful thanksgiving dinner. I am indebted to many staff members at chemistry department, Dr. Kathryn Severin, Dr. Daniel Holmes, and Dr. Rui Huang, for their guidance on various advanced instruments.

I would like to express my gratitude to faculty from school of packaging. I am thankful to Dr. Bruce Harte for his advice as a packaging graduate association advisor and making my study at school of packaging a wonderful experience. I am grateful to Dr. Diana Twede for her teaching and training on accelerated UV chamber. I would like to thank current and former school of packaging staffs, Robert Bob Hurwitz, Linda Estill, April Meersdom, Colleen Wager, and Kelby Thayer, for their various forms of support during my M.S. and Ph.D. studies.

I would like to thank my friends in former and current RAA research group for their supports and intellectual inputs. I am indebted to Dr. Ngouajio's students and staffs

for their helps in the tomato farm. I am grateful to all of my friends in school of packaging, Ploy, Little Tom, Sukeewan, Waree, Oh, Hall, Chaiyatas, Kate, Hayati etc. Their support and care helped keep me sane and focus throughout the whole difficult years. I greatly appreciate their friendship.

None of this would have been possible without continuous love, support, and patience from my family. I would like to express my heart-felt gratitude to my parents. Mom and dad, they have believed in me, never had any doubt in me, and given me strength for all these years. For my brother, Vip, I am thankful for introducing me to MSU and helping me adjust to this new environment. For my sister, Vav, I am grateful for everything you have done for me. She took care of family business, so I could come to MSU and pursued my dream.

I would like to acknowledge the Northern Technologies International, Inc. for providing the PBAT films used in the tomato production trials. Finally, I would like to express my gratitude to Michigan State University Project GREEEN for the financial support that funded parts of the research in this dissertation, and the Graduate School Dissertation Completion Fellowships (DCF) program for financial stipend during the spring 2010 semester.

TABLE OF CONTENTS

LIST OF TABLES

LIST OF FIGURES

LIST OF SCHEMES

LIST OF SYMBOLS AND ABBREVIATIONS

•	=	Free radical
+	=	Coded level of +1 in RSM CCD
-	=	Coded level of -1 in RSM CCD
0	=	Coded level of 0 in RSM CCD
^{1}H-NMR	=	Proton nuclear magnetic resonance
$^{1}O_2$	=	Singlet oxygen
25w	=	25 micron thick white PBAT film in experimental plot design
$^{3}O_2$	=	Triplet oxygen
35w	=	35 micron thick white PBAT film in experimental plot design
α	=	(1) Distance from the center point to the star point in CCD (2) Type I error
β_o	=	Intercept in the second-order RSM model
β_1	=	Linear main effect of carbon black in the second-order RSM model
β_2	=	Linear main effect of antioxidant in the second-order RSM model
β_3	=	Linear main effect of total radiation in the second-order RSM model
β_{11}	=	Quadratic main effect of carbon black in the second-order RSM model
β_{22}	=	Quadratic main effect of antioxidant in the second-order RSM model
β_{33}	=	Quadratic main effect of total radiation in the second-order RSM model

β_{12}	=	Interaction effect of carbon black and antioxidant in the second-order RSM model
β_{13}	=	Interaction effect of carbon black and total radiation in the second-order RSM model
β_{23}	=	Interaction effect of antioxidant and total radiation in the second-order RSM model
τ	=	Blocking effect in the second-order RSM model
Δt	=	Difference of the onset time of the melting peak between the unexposed and the exposed samples
A	=	(1) Adipic acid monomer (2) Absorbance of the test sample at 796 cm^{-1} (3) Coded level of $+\alpha$ in RSM CCD
a	=	Coded level of $-\alpha$ in RSM CCD
a	=	Adjusted parameter in the equation $M_n = y_O + ae^{bx}$
AnOx	=	Antioxidant
$AnOx_C$	=	Coded level of antioxidant
A_o	=	Absorbance of the sample with 0% gel content at 796 cm^{-1}
ATR	=	Attenuated total reflectance
B	=	(1) 1,4 butanediol monomer (2) Black PBAT film in experimental plot design
b	=	Reduction rate in the equation $M_n = y_O + ae^{bx}$
BA	=	Ester repeat unit consisting of 1,4 butanediol and adipic acid
BHT	=	Butylated hydroxytoluene
BI	=	Biofilms found in SEM micrographs
BT	=	Ester repeat unit consisting of 1,4 butanediol and terephthalic acid

C	=	CO_2 concentration determined and corrected by the calibration curve (ppm) used in equation 3-2
$\%C_{mat}$	=	% carbon content of test material in equation 3-3
C/N	=	Carbon to nitrogen ratio
CB	=	(1) Carbon black (2) Chain breaking antioxidant
CB_C	=	Coded level of carbon black
CB-A	=	Chain breaking acceptor
CB-D	=	Chain breaking donor
CCD	=	Central composite design
$CDCl_3$	=	Deuterated chloroform
CHN	=	Carbon hydrogen nitrogen
CMR	=	Cumulative measurement respirometric
CT	=	Crystalline regions found in SEM micrographs
CV	=	Cavities found in SEM micrographs
d	=	Days
Da	=	Dalton (unit of molecular weight)
DAQ	=	Data acquisition
DF	=	Degree of freedom
DSC	=	Differential scanning calorimetry
DMR	=	Direct measurement respirometric
E	=	Cohesive energy
$E\{Y\}$	=	Estimate of interested parameter in the second-order RSM model
EBA	=	Ethylene butyl acrylate

ESR	=	Electron spin resonance
EVA	=	Ethylene vinyl acetate
F	=	(1) Flow rate (scc/min) in equation 3-2 (2) Fraction of filler
f	=	Polymer fraction
FTIR	=	Fourier transform infrared
GC	=	Gas chromatography
g	=	guard row in experimental plot design
gCO_2	=	Mass of evolved CO_2 used in equation 3-2
gCO_2-gCO_2b	=	Mass of total evolved CO_2 minus blank CO_2 used in equation 3-3
Gel	=	Estimated gel content of PBAT exposed to x MJ/m^2 of UV radiation in the equation $Gel = Gel_a(1 - e^{-Gel_b x})$
Gel_a	=	Estimated maximum gel content of PBAT sample in the equation $Gel = Gel_a(1 - e^{-Gel_b x})$
Gel_b	=	Gel-forming rate in the equation $Gel = Gel_a(1 - e^{-Gel_b x})$
g_{mat}	=	Mass of test material in equation 3-3
GMR	=	Gravimetric measurement respirometric
GND	=	Ground in electronic circuit
GPC	=	Gel permeation chromatography
H_f	=	Heat of fusion
hr	=	Hours
hν	=	Photon energy (h = Planck's constant, ν = electromagnetic wave frequency)
HDPE	=	High density polyethylene

IR	=	Infrared
k	=	Rate constant
L/D	=	Length to diameter ratio of the extruder screw
LDPE	=	Low density polyethylene
LLDPE	=	Linear low density polyethylene
M	=	Black LDPE film in experimental plot design
MD	=	Machine direction
MFC	=	Mass flow controller
min	=	Minutes
M_n	=	(1) Number average molecular weight (2) Number average molecular weight of PBAT film exposed to x MJ/m^2 of UV radiation in the equation $M_n = y_O + ae^{bx}$
M_w	=	Weight average molecular weight
MWD	=	Molecular weight distribution
n	=	Avrami exponent
n_1, n_2	=	Numbers of replicate for each test material and blank in equation 3-4
NDIR	=	Non-dispersive infrared
NMR	=	Nuclear magnetic resonance
NPN	=	Negative-positive-negative transistor
O.D.	=	Optical density
PAR	=	Photosysthetically active radiation
PBA	=	Poly(butylene adipate)
PBAT	=	Poly(butylene adipate-*co*-terephthalate)

PBT	=	Poly(butylene terephthalate)
PCL	=	Poly(ε-caprolactone)
PD	=	Peroxide decomposing antioxidant
PD-C	=	Catalytic peroxide decomposer
PD-S	=	Stoichiometric peroxide decomposer
PE	=	Polyethylene
PET	=	Polyethylene terephthalate
PGA	=	Poly(glycolic acid)
PHA	=	Poly(hydroxyalkanoates)
PHB	=	Poly(hydroxybutylate)
PHBV	=	Poly(hydroxybutylate-*co*-valerate)
PHV	=	Poly(hydroxyvalerate)
PLA	=	Poly(lactide) or poly(lactic acid)
PP	=	Polypropylene
ppm	=	part per million
PS	=	Polystyrene
PTFE	=	Poly(tetrafluoroethylene)
PVOH	=	Poly(vinyl alcohol)
r	=	Degree of randomness
R•	=	Free radical
R^2	=	Coefficient of determination
R_C	=	Coded level of total radiation
RH	=	(1) Relative humidity (2) Polymer in degradation scheme

ROH	=	Alcohol
ROOH	=	Hydroperoxide
RSM	=	Response surface methodology
s	=	(1) Standard deviation (2) Seconds
S*	=	Excited metal complex
scc	=	Standard cubic centimeter
S_e	=	Standard error (%)
SEM	=	Scanning electron microscopy
T	=	Terephthalic acid monomer
t	=	(1) Time between each measuring sequence (min) used in equation 3-2 (2) t-distribution value for 95% probability with n_1+n_2-2 degree of freedom
TD	=	Titianium dioxide found in SEM micrographs
T_g	=	Glass transition temperature
THF	=	Tetrahydrofuran
T_m	=	Melting temperature
TMS	=	Tetramethylsilane
TS	=	Estimated tensile strength of PBAT exposed to x MJ/m^2 of UV radiation from the equation $TS = TS_O + TS_a e^{-TS_b x}$
TS_o	=	Estimated final tensile strength from the equation $TS = TS_O + TS_a e^{-TS_b x}$
TS_a	=	Total amount of tensile strength reduction from the beginning to the end of the exposure from the equation $TS = TS_O + TS_a e^{-TS_b x}$

TS_b	=	Reduction rate from the equation $TS = TS_O + TS_a e^{-TS_b x}$
UV	=	Ultraviolet
W_d	=	Weight of dried gel in equation 4-1
wk	=	Weeks
W_s	=	Weight of the specimen tested in equation 4-1
X_g	=	Gel content
XRD	=	X-ray diffraction
y_o	=	Adjusted parameter in the equation $M_n = y_O + ae^{bx}$

Chapter 1 Introduction

1.1 Introduction and motivation

Since the early 1950s, commercial fresh vegetable production has transitioned from bare ground systems to plasticulture. Plasticulture is defined by the American Society of Plasticulture as "the use of plastics in agriculture for both plant and animal production including; plastic mulch, drip irrigation, row covers, low tunnels, high tunnels, greenhouses, silage bags, hay bales and in food packaging and nursery pots and containers for growing transplants" (Lamont and Orzolek 2004). Mulching by putting a thin plastic film directly over the soil surface with drip irrigation has become a standard technique for vegetable growers in the U.S. and around the world. In 1999, more than 185,000 acres in the U.S, were covered with plastic mulch and it was estimated that by 2006 the U.S. acreages would be 400,000 acres (Miles 2003). Hussain and Hamid (2003) reported that in 2002, global acreages were approximately 10 million acres. According to the Center for Plasticulture at Penn State University, U.S. growers use approximately 100,000 tons of plastic mulch films annually (Kaplan 2003). Espi *et al.* (2006) estimated that global volume for mulch film was 771,000 tons per year.

The advantages and purposes of using mulch films in vegetable production are to control or alter the soil temperature, maintain soil humidity, maintain raised-bed soil structure, reduce seed germination time, provide early or out of season crop production for produce with better market value, reduce weeds and plant diseases, provide efficiency in the usage of water and fertilizers, and increase yields and improve produce quality (Espi *et al.* 2006; Jensen 2004; Lamont 2004; Olson 2007).

Despite all these advantages, there are several major concerns about using mulch films including the costs of removal and disposal of the used plastics and environmental issues. Most of the used mulch films are not typically recycled, since they are often contaminated with soil, moist vegetation, and water, making them difficult to be recovered. Therefore, most used mulch films are disposed of by landfilling, open burning or on-site dumping (Garthe 2004).

The use of biodegradable mulch films seems to be a promising solution to solve these problems because the films can degrade right in the field; therefore, the growers' expenses for removal and disposal of used films should be greatly reduced, and the amount of waste accumulating in landfills or being open-burned should be reduced.

Early use of photodegradable plastic mulch during the 1970s and 1980s, wrongly named degradable mulch films, discouraged the current use and implementation of new biodegradable mulch films because they were too expensive and their breakdown was unpredictable. Moreover, their use increased the costs of weed control, and the cost of pick up and removal of mulch films that broke down prematurely in the field (Giacomell *et al.* 2000). Since new truly biodegradable materials obtained from petroleum and natural resources are commercially available, a new opportunity for using biodegradable polymers as agricultural mulch films has become more viable. Current commercial biodegradable polymers such as poly(lactic acid) (PLA), poly(butylene adipate-*co*-terephthalate) (PBAT), poly (ε-caprolactone) (PCL), and starch-based polymer blends or copolymers can degrade when exposed to bioactive environments such as soil and compost. The degradation rate of these biopolymers can be manipulated and modified by controlling the exposure conditions and the characteristics of the polymers. However, to

this date no optimal biodegradable mulch film has been developed, but aromatic-aliphatic copolyesters such as PBAT have shown the most potential due to their field performance.

Furthermore, knowledge of manipulating those factors affecting biodegradation or photodegradation opens up the opportunity to design new biodegradable mulch films with proper field performance and total biodegradation after crop harvesting.

1.2 Goal and objectives

Due to extensive outdoor use, plastic mulch film can degrade because of long-term exposure to sunlight (for at least 2-3 months) especially due to UV wavelengths (190-400 nm). Plastics tend to undergo both chain scission and crosslinking as a result of photodegradation.

Therefore, the overall goal of this research is to develop biodegradable mulch films that possess photo-stability and strength requirements for the agricultural industry, ability to provide the desired longevity, and finally total biodegradability in soil after harvesting.

To achieve the overall goal, specific objectives of this dissertation are to determine the rate of crosslinking of PBAT films due to photodegradation and to design PBAT films that do not crosslink. Therefore, regarding the performance and biodegradability of the biodegradable mulch films these two required attributes will not be compromised.

1.3 Hypotheses

In order to reach the specified goal and objectives, the following hypotheses are set as target statements to be proved or disproved

1.3.1 First hypothesis: film performance

Null hypothesis (H_o): There are no differences in performance between biodegradable film and commercial LDPE mulch film throughout the growing season under Michigan conditions.

Alternative hypothesis (H_a): There are some differences in performance between biodegradable film and commercial LDPE mulch film throughout the growing season under Michigan conditions.

Performance of mulch film is in regard to film integrity, ability to suppress weed growth, to maintain soil moisture and structure, to alter soil temperature, and marketable yield. Those performance attributes are directly related to changes of mechanical, optical, and chemical structure of the plastic film over time.

1.3.2 Second hypothesis: photodegradation

H_o*:* Exposure to UV light does not affect any property of the biodegradable film including mechanical properties, optical properties, chemical structure, or biodegradability.

H_a: Exposure to UV light affects some properties of the biodegradable film including mechanical properties, optical properties, chemical structure, and biodegradability.

1.4 Dissertation outline

This dissertation is divided into a literature review section (chapter 2), to review the state of the plasticulture industry and agricultural film waste management and to understand and acquire knowledge of the biodegradable polymers and various modes of related degradation, such as photodegradation and biodegradation, and a research plan to test the hypotheses.

The research in this dissertation is divided into 3 phases: design and creation of assessment tools, determination of the performance of the commercial and biodegradable mulch films under field and lab studies, and design of a biodegradable film formulation for mulch film (Figure 1-1).

Research work in phase I was to develop new measuring tools in order to assess performance of biodegradable mulch films, such as biodegradation of films as a function of time and degree of crosslinking or gel content in the polymer structure. As a result of phase I completion, the direct measurement respirometric (DMR) system was constructed to measure biodegradability of the polymers (chapter 3) and the techniques of differential scanning calorimetry (DSC) and Fourier transform infrared (FTIR) spectroscopy were also used to measure the degree of crosslinking or, in this case, gel content in the polymer structure (chapter 4).

In phase II (chapter 5), field experiments for two consecutive growing seasons and laboratory simulation experiments were conducted using PBAT film and commercial LDPE mulch film as a control for comparison to determine the performance of both films under field and laboratory conditions. As a result, the required design properties for biodegradable mulch film, such as mechanical and optical properties, molecular weight, gel content, and biodegradability, were obtained. In addition, the concepts of hydrolysis and biodegradation of aliphatic-aromatic copolyester in various media were further explored in chapter 6.

In Phase III (chapter 7), with information, knowledge, and findings from phases I and II, the research work in phase III was to determine the optimal formulation of PBAT, carbon black, and antioxidants for biodegradable mulch films using response surface methodology (RSM) in order to achieve the ultimate goal of biodegradable mulch films with total biodegradation without compromising required properties of the mulch film including photo-stability.

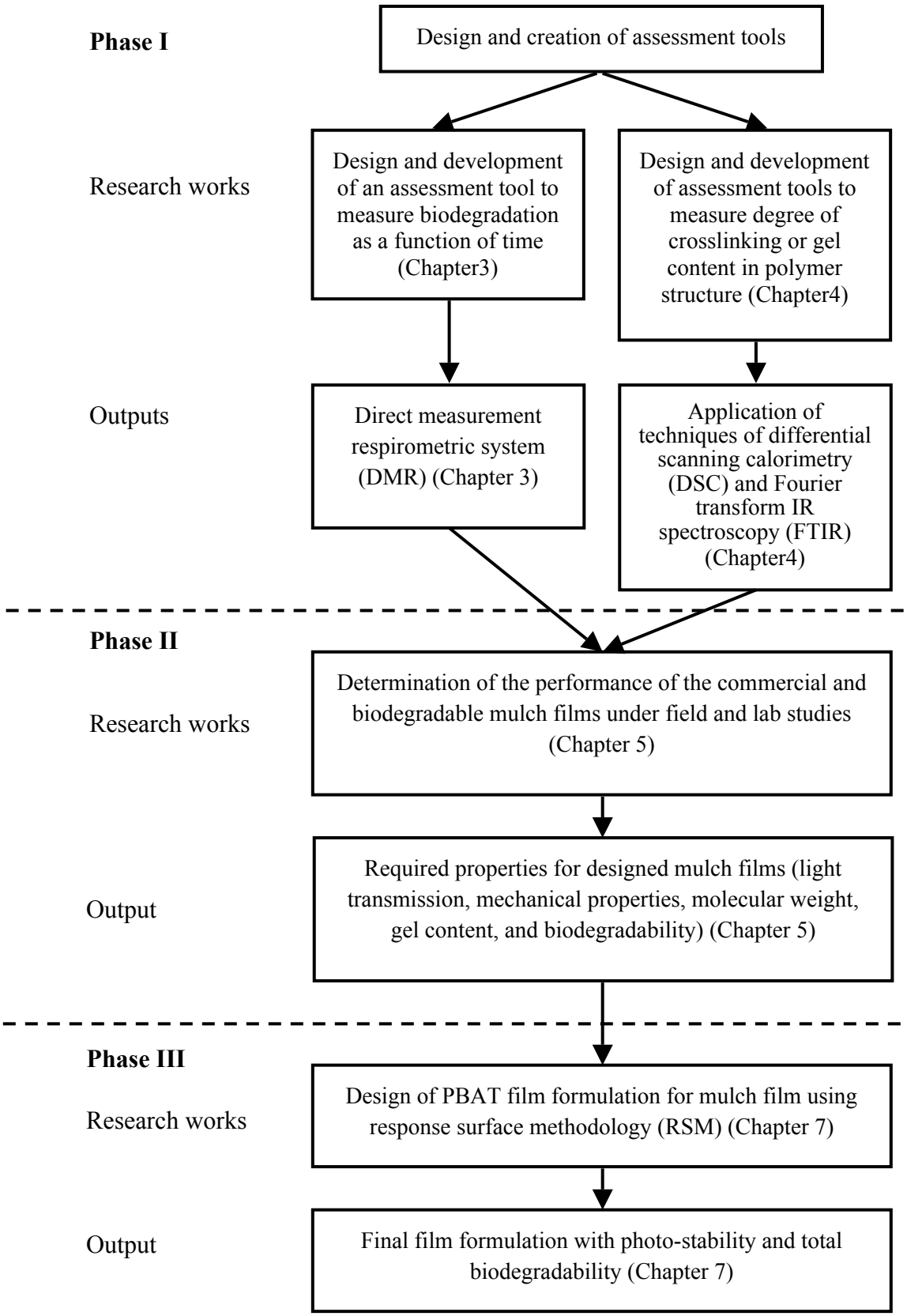

Figure 1-1. Research plan and outline of this dissertation

REFERENCES

REFERENCES

Espi, E, Salmeron, A, Fontecha, A, Garcia, Y and Real, AI (2006). "Plastic films for agricultural applications." Journal of Plastic Film and Sheeting **22**: 85-102.

Garthe, J (2004). Managing used agricultural plastics. Production of Vegetables, Strawberries, and Cut Flowers Using Plasticulture. W Lamont ed. Ithaca, NY, Natural Resource, Agriculture, and Engineering Service (NRAES).

Giacomell, GA, Garrison, SA, Jensen, M, Mears, DR, Paterson, JW, Roberts, WJ and Wells, OS (2000). Advances of plasticulture technologies 1977 – 2000. The 15th International Congress for Plastics in Agriculture, Hershey, PA.

Hussain, I and Hamid, H (2003). Plastics in agriculture. Plastics and the Environment. A L Andrady ed. Hoboken, NJ, John Wiley & Sons, Inc**:** 185-209.

Jensen, MH. (2004). "Plasticulture in the global community - view of the past and future." Retrieved Nov 20, 2006, from http://www.plasticulture.org/history_global_community.htm.

Kaplan, JK. (2003). "Dress-for-success mulch." Retrieved Aug 8, 2008, from http://plasticulture.cas.psu.edu/default.html.

Lamont, W (2004). Plastic mulches. Production of Vegetables, Strawberries, and Cut Flowers Using Plasticulture. W Lamont ed. Ithaca, NY, Natural Resource, Agriculture, and Engineering Service (NRAES).

Lamont, W and Orzolek, M. (2004). "Plasticulture glossary of terms." Retrieved Nov 25, 2006, from http://www.plasticulture.org/what_glossary.htm.

Miles, C. (2003). "Alternative to plastic mulch." Retrieved Sep 20, 2006, from http://agsyst.wsu.edu/AltMulch.htm#2003.

Olson, SM. (2007). Mulching. Vegetable Production Handbook for Florida 2007-2008. S M Olson and E Simonne ed. Gainesville, FL, The Institute of Food and Agricultural Sciences, University of Florida.

Chapter 2 Literature review

2.1 Plasticulture

According to the American Society for Plasticulture, plasticulture is "the use of plastic in agriculture", which includes but is not limited to plastic mulch films (Figure 2-1 left), drip irrigation tape, row covers, low tunnels, high tunnels (Figure 2-1 right), silage bags, hay bale wraps, and plastic trays and pots used in transplant and bedding plant production (Orzolek 2004). The history of plasticulture dates back to 1948 when polyethylene (PE) was first used as a greenhouse film by professor Emery Myers Emmert at the University of Kentucky in order to replace more expensive glass (Anderson 1994; Jensen 2004).

Figure 2-1. (left) tomato plots covered with mulch films; (right) high tunnel or overwintering house. **For interpretation of the references to color in this and all other figures, the reader is referred to the electronic version of this dissertation.**

Up to 2008, the only comprehensive published data differentiating the use of agricultural plastics in the U.S. into categories was done by Amidon Recycling for the American Plastic Council in 1994 (Amidon 1994). This study reported the most

commonly used plastics in different application as shown in Table 2-1. Approximately 66.5% of agricultural plastics are used for nursery containers, 28.8% for various types of plastic films, and 4.7% for pesticide containers. The estimated consumption of agricultural plastics in the U.S. has increased steadily from 519 million pounds in 1994 to 850 million pounds in 1998 and to 1000 million pounds in 2001 (Lawrence 2007).

Hussain and Hamid (2003) reported that global plastic consumption in agriculture and related areas accounted for 2.48 million tons (1 tons = 2,000 pounds) of plastics annually.

In Western Europe, plastic films are the major type of plastic used in plasticulture. In 1997, out of 700,000 tons of total plastics used in agriculture in Western Europe, 500,000 tons or 71% were plastic films, of which greenhouse films accounted for 50%, and mulch and silage films were approximately 25% each as shown in Figure 2-2a (Hussain and Hamid 2003). Low density polyethylene (LDPE) was the most commonly used plastic. Western Europe used 570,000 tons of LDPE per annum, of which 350,000 were used in the form of film and tubing, see Figure 2-2b (Hussain and Hamid 2003).

Table 2-1. Estimated quantities of agricultural plastics used annually in the U.S. from 1992 data. Adapted from Amidon (1994)

Applications	**Main plastic types**	**Amount in million pounds** *(percent in total)*
Film		
Greenhouse and nursery film	LDPE	25.0
Mulch film	LDPE	60.0
Fumigation film	LDPE	12.5
Photodegradable mulch film	LDPE with additives	3.0
Drip irrigation tape or tubing	LDPE	13.5
Silage bag	LDPE	8.0
Hay and silage bale stretch wrap	LDPE	25.0
Haysleeve covers	LDPE	2.5
Total amount/Total percentage		***149.5 (28.8%)***
Nursery containers		
Pots and trays	HDPE	190.0
	PP	85.0
	PS	70.0
Total amount/Total percentage		***345.0 (66.5%)***
Pesticide containers	HDPE	*24.5 (4.7%)*
Total		***519.0 (100%)***

LDPE = Low density polyethylene

HDPE = High density polyethylene

PP = Polypropylene

PS = Polystyrene

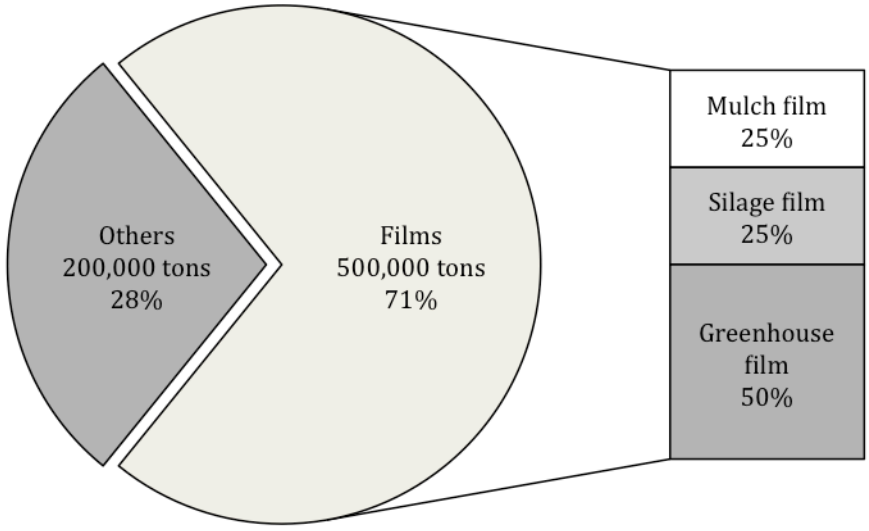

(a)

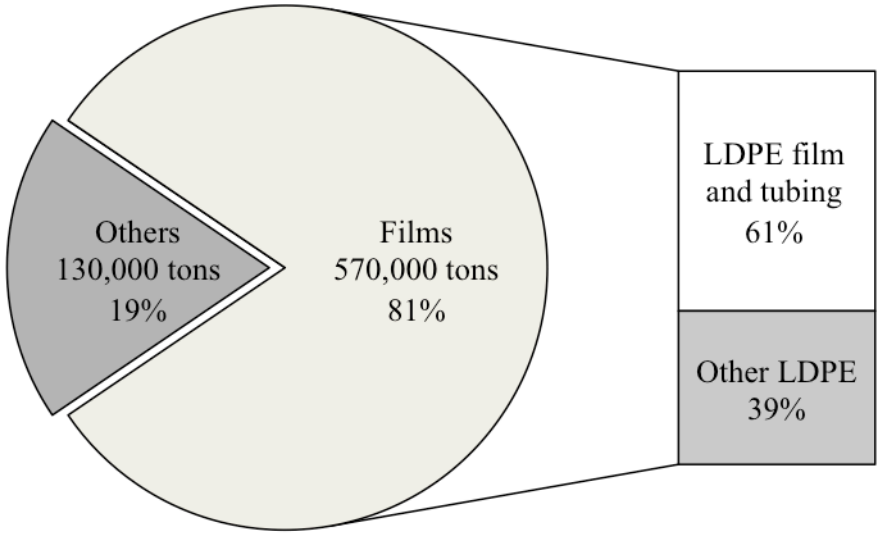

(b)

Figure 2-2. Total 700,000 tons of agricultural plastic used in Western Europe in 1997 categorized by (a) form of uses and (b) materials used

2.2 Plastic mulch films

Plastic mulch films are thin plastic films that growers use to cover raised soil beds in order to maintain soil structure, moisture, and temperature and to suppress weed growth. Plastic mulch films were first used in the late 1950s in university research and have been used commercially for vegetable production since the early 1960s (Hussain and Hamid 2003; Lamont 2004a; Lamont 2004b). Use of plastic mulch and drip irrigation, watering systems that directly deliver water to the plant root zone using flexible plastic tubing or tape (Ross 2004) has become standard for growers worldwide due to their many advantages. In 2002, approximately 10 million acres of land were covered with plastic mulch globally (Hussain and Hamid 2003). Espi *et al.* (2006) estimated that global volume use of mulch film was 771,000 tons per year. According to the Center for Plasticulture at Pennsylvania State University, American growers use approximately 100,000 tons of plastic mulch films annually (Kaplan 2003).

Kijchavengkul *et al.* (2008a) described the mulch film cycle of conventional and biodegradable films for single cropping, such as tomato in Michigan (Figure 2-3). The cycle starts when the herbicide is first applied to the field and the beds are raised in spring. Then the drip irrigating tubes are installed and mulch films are laid to cover the soil beds. A week after or so, the crops are planted onto the mulch covered beds through pre-punched holes. During the growing season of 2-6 months, fertilizer, pesticides, and stakes and twine are applied to the beds and plants.

After harvest in the fall, there are several end-of-life scenarios for conventional and biodegradable mulch films. For conventional films, they can be left in place for reuse in the next season, or they can be disposed of by energy-recovery incineration,

landfilling, open burning, or theoretically recycling. Dirtiness of the used mulch films inhibits the recycling process. However, no more than one additional season of use is attainable; then they are disposed of. For used biodegradable mulch films, there are two more disposal options: removing and composting them in a compost pile, or plowing the soil and the biodegradable mulch films together. If the latter option is used the films must be totally biodegraded.

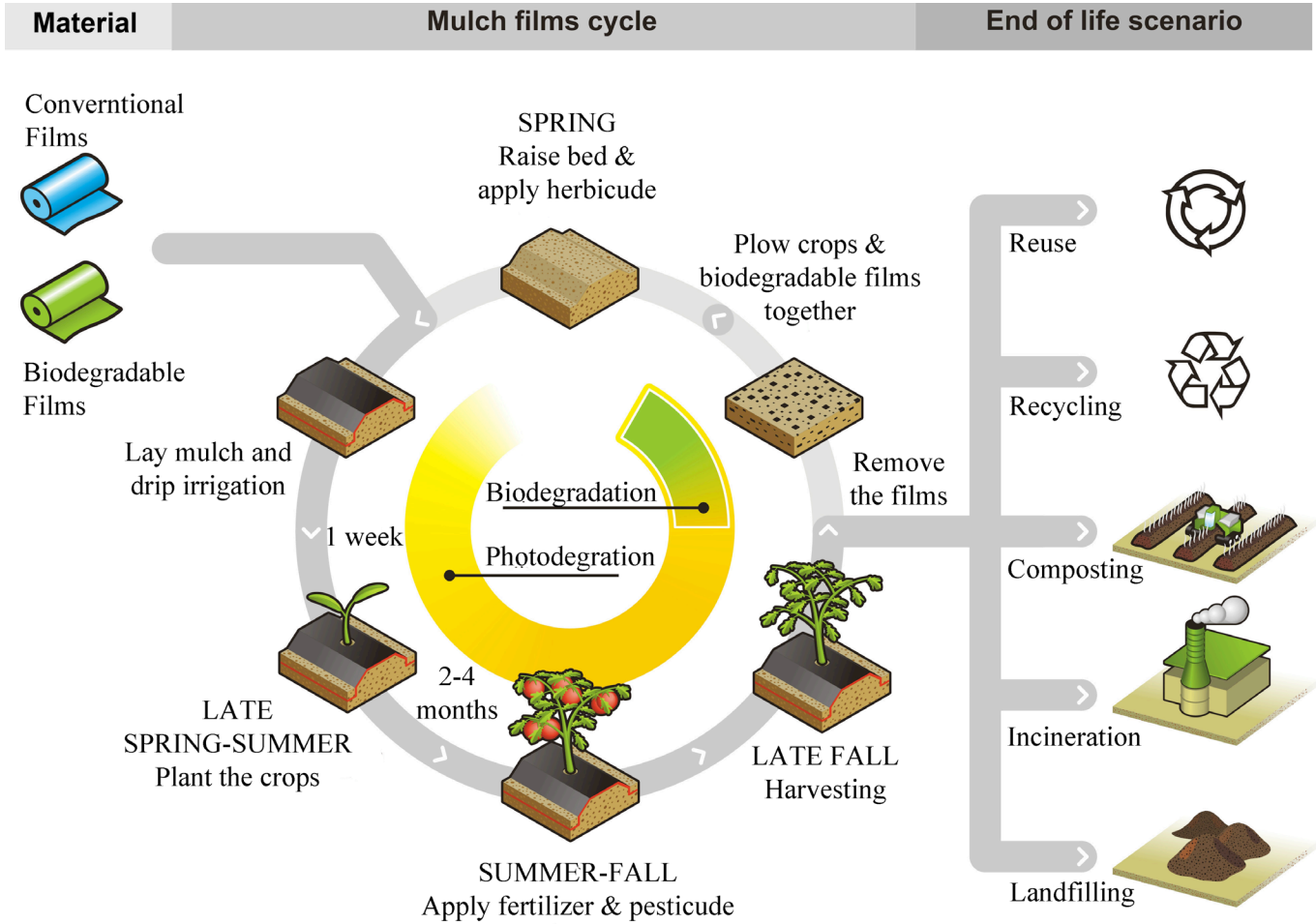

Figure 2-3. Mulch film cycle of conventional LDPE and biodegradable films for single cropping and their end-of-life scenarios; conventional LDPE mulch films can be reused in the next season or disposed of by recycling, incineration, landfilling, or open burning. Two more disposal options, composting and on-field biodegradation, are applicable for biodegradable films.

2.2.1 Benefits of using mulch films

Mulch films create or alter the microclimate around plants by modifying the effect of radiation on the soil surface and decreasing soil water loss (Lamont 2004a). Some mulch film benefits are:[1]

(a) Soil temperature modification and moisture maintenance

(b) Soil structure maintenance

(c) Reduced seed germination time

(d) Earlier crop production or faster crop development (1-3 weeks earlier) for better market prices

(e) Higher marketable yield per acre. Jensen (2004) reported that using plastic mulch with drip irrigation helped increase the yield of eggplant from 27,353 kg/acre in unmulched plot to 46,716 kg/acre.

(f) Improved produce quality

(g) Reduced plant losses from diseases and weeds

(h) Reduced needs for irrigation and agrochemicals used, such as herbicides, pesticides, and fertilizers

(i) Reduced leaching of fertilizers to the environment

---

[1] Mulch film benefits, items a-i, were summarized from Jensen (2004), Lamont (2004b), Espi *et al.* (2006), and Olson (2007)

Wu *et al.* (2001) reported that use of plastic mulch films in rice production could save 75% of irrigation water, 50% of nitrogen fertilizer, 80-100% of herbicides, 30% of pesticides and 40% of seeds compared to the continuous flooding system. Haraguchi *et al.* (2004) demonstrated that subsurface leaching of nitrate nitrogen (NO_3-N) was effectively reduced by using plastic mulch films.

As mentioned earlier, mulch films can affect the microclimate of the plant by altering the effect of solar radiation. Therefore, optical properties or color of the films is definitely important for produce production in different climates and geographical locations. Generally, mulch films can be divided into 4 types: black, clear, white, and wavelength selective or colored mulch (Lamont 2004a).

Black mulch is the most widely used. It absorbs most UV, visible, and infrared (IR) wavelengths and transfers the absorbed energy back to the soil in the form of heat (since soil has higher thermal conductivity than the air). Therefore, soil temperature under black mulch is usually 5°F (3°C) higher than that of bare soil (Lamont 2004a). Another advantage of black mulch is its ability to suppress weed growth because there is no light with photosynthetically active radiation (PAR) wavelength for weeds to photosynthesize, while desired plants can grow through the pre-punctured holes.

Clear mulch, on the other hand, does not absorb as much radiation as black mulch since it allows 85-95% transmission of light but creates a greenhouse effect on the soil surface (Lamont 2004a). Condensed water on the inside of the film surface blocks the low energy IR wavelength from radiating back to the atmosphere. Therefore, daytime soil temperature is generally 8-14°F (5-8 °C) higher than bare soil, since most of the heat

is retained under the clear mulch like a greenhouse. Clear mulch is usually used in very cold areas in the U.S. such as the New England states (Lamont 2004a). Herbicides and soil fumigation need to be applied when clear mulch is used since it cannot suppress weed growth.

White or white on black mulch is usually used to lower soil temperatures in hot areas since the white color reflects light back to the plant canopy resulting in 1-2°F (0.5-1°C) lower soil temperature than bare soil (Lamont 2004a). Herbicides and soil fumigation may or may not need to be applied depending on the opacity of the film.

Wavelength-selective mulch absorbs most of the PAR wavelength and allows only selected wavelengths to pass through (Lamont 2004a; Ngouajio and Ernest 2004; Taber 2004). It is commercially available in different colors, such as red, green, dark blue and brown. There are specific plant responses to each film color. For example, tomato yield was highest when red mulch film is used (Lamont 2004a). In several crops, wavelength-selective mulches are able to increase marketable yield by 12-35% compared to black plastic mulch (Lamont 2004a).

2.2.2 Disadvantages of mulch films

Despite all the advantages, there are a few important drawbacks of using plastic mulch films, such as environmental issues and financial investment. Since mulch film does not degrade, the main problem of plastic mulch films is their removal and disposal after the produce harvesting is completed. Removal and disposal of mulch film create both environmental and financial disadvantages. Regarding the financial aspects, using plastic mulch films not only increases the initial cost for vegetable production due to

material costs of $160-250 per acre for normal black plastic mulch film (Lamont 2004b; Olson 2007), and due to machines and labor for film application and removal, but also material hauling and landfill tipping fees (if landfilling). The use of machines to pull up the mulch films from the beds requires that the crops must be removed and the bed must be clean (Olson 2007).

Environmental issues of using plastic mulch films include pesticide runoff and, most importantly, film disposal. According to Durham (2003) and Rice *et al.* (2001), plastic mulch films increase the runoff of water after rainfall or irrigation, which means that more of the pesticides and other chemicals applied over the plastic mulch films run off the field to surface waters, such as nearby river or lake, or ground water.

Environmental and economic issues of removal and disposal of used agricultural plastic vary depending on the modes of disposal, such as landfilling, open burning, onsite dumping, recycling, or incineration.

2.3 Disposal of agricultural plastics

Currently, the majority of the used agricultural plastics in New York and Pennsylvania are managed by landfilling, on-site dumping or burying, on-site stock piling, or on-site burning (Lawrence 2007; Levitan and Barro 2003; Parish *et al.* 2000; Rollo 1997). According to a survey of Pennsylvania vegetable growers, 66% of participating growers said they disposed of used agricultural plastics by on-site burning, 27% by landfilling, and 25% by burying, dumping, or piling on-site (Garthe 2004).

2.3.1 Landfilling

Landfilling is accepted by society as proper disposal (Garthe 2004). Landfill tipping fees for agricultural plastics range typically from $38 to $120 per ton depending on the level of contamination of the plastics (EPC 2006). Some landfill operators do not accept any dirty agricultural plastics or even any types of agricultural plastics, but some do with additional surcharges. Many landfill operators reject plastic mulch film as unsuitable landfill material due to its level of contamination (Olson 2007).

One of the main criticisms of landfilling is the fact that wastes in the landfills, including plastics, do not degrade or degrade at a very slow rate. Once the plastic product is used and disposed of, if it ends up in the landfill, then it will slowly degrade, due to the design of the landfill to prevent material decomposition (Narayan 2001). In the landfill, once it is capped, moisture and air inside are minimized to prevent contamination of groundwater from decomposed substances (Lee and Jones-Lee 2007).

Local availability of landfill space is also an issue. The number of landfills in the U.S. decreased substantially from 7,924 in 1988 to 1,754 in 2006 (EPA 2008). However,

the capacity has remained relatively constant at the national level, since the new landfills are much larger than those in the past, but the availability and capacity at the local or regional level has changed substantially due to regional centralization. This may increases the transportation costs, and hence disposal expense for growers.

2.3.2 On-site burning or open burning

On-site burning without energy recovery or open burning is a very common way for disposing of agricultural plastic wastes. Because of high transportation cost and landfill tipping fees, farmers consider on-site burning to be economically more favorable (Lawrence 2007). In 2003, it was estimated that more than 50% of agricultural plastics in New York and Pennsylvania were burned on-site (Levitan and Barro 2003).

Due to low the burning temperature of 400-600°F (200-315°C) or less and incomplete combustion of hydrocarbons, on-site burning of mulch films contaminated with fertilizers and pesticides usually generates air pollutants, especially dioxins (EPA 2006; Garthe 2004; Lawrence 2007; Levitan and Barro 2003). Dioxins are known as endocrine disruptors and carcinogens (Levitan and Barro 2003; NTP 2005). Besides dioxins and related compounds, exposure to fine particles (diameter < 2.5 μm) from open burning has been associated with many health effects, such as increased risk of stroke, asthmatic attacks, decreased lung function, respiratory diseases, and premature death (Dockery and Pope III 1994; Hong *et al.* 2002; Seaton *et al.* 1995). Therefore, several states in the U.S. such as Florida, Idaho, Michigan, Oregon, and Wyoming prohibit open burning of several materials including plastics (FLDEP 2005; IDDEQ 2007; MDEQ 1994; ORDEQ 2006; WDEQ 2005). On the other hand, the state of New York only bans

open burning within city or village limits, and open burning of agricultural plastics is still allowed in the state of Pennsylvania (NYDEC 2008).

2.3.3 On-site dumping

Disposal of agricultural plastics by on-site dumping is not recommended since seepage of water that has been in contact with buried agricultural plastics caused by irrigation or rainfall can contaminate groundwater with various agrochemicals (Clarke 1996).

2.3.4 Recycling

In 1994, Amidon Recycling estimated that less than 5% of agricultural plastics was recycled and about the same amount was incinerated for energy recovery (Amidon 1994; Levitan and Barro 2003). Between 1992 and 2008, 95 million pounds of HDPE pesticide containers were recycled in the U.S. while only 1% of agricultural plastic film and nursery container was recycled (ACRC 2008a; Kotrba 2008). The recycled HDPE is then used for pesticide containers, pallets, construction site mats, truck liners, recycled plastic lumber (RPL), and hazardous material (hazmat) drums (ACRC 2008b).

Dirtiness of agricultural plastics is always a difficulty for recycling processes. Plastic films with more than 5% contaminants by weight will not be accepted for recycling (Clarke 1996). In reality contaminants in agricultural plastics can be up to 40-50% by weight from pesticides, fertilizers, soil and debris, moist vegetation, silage juice, water, and UV additives (Amidon 1994; Hussain and Hamid 2003; Levitan and Barro 2003; Rollo 1997), especially in mulch film and drip irrigation tape, which are by far the most difficult components to be recycled (Lamont 2004b). Brook (1996) found that the

contamination level (moisture and soil content) of uncleaned plastic mulch film was 36%. Furthermore, most of the agricultural plastics may be photodegraded due to exposure to UV light, which make them unacceptable as recyclable feedstocks (Levitan and Barro 2003). Currently the most viable application for dirty agricultural plastics is to produce RPL (Levitan and Barro 2003).

In 1997, the New Jersey Department of Agriculture (NJDA) created the New Jersey Agricultural Recycling Program, a collection program for used agricultural plastics (NJDA 2008). At first, the program collected only 'clean' plastics, such as greenhouse film and pesticide containers. In the first 5 years of this programs, 1.8 million pound of greenhouse film were collected from 100-125 growers and recycled (Levitan and Barro 2003; Levitan *et al.* 2005). This number represents a third of the greenhouse film used in the state of New Jersey, where an estimated 1 million pounds are used annually (Levitan and Barro 2003; Levitan *et al.* 2005). In 2005, this program was expanded to accept drip irrigation tape for recycling (NJDA 2008).

2.3.5 Energy-recovery incineration

Plastics, which generally have inherently high heating-energy (more than that of coal but less than that of fuel oil), can be used as fuel for energy-recovery incineration to generate electricity (Table 2-2). High-efficiency incinerators capable of burning at 1,800-2,200°F (1000-1200°C) or higher are recommended to ensure complete combustion and less pollutant emissions (Garthe 2004). The downside of this technology is the cost of the initial investment because an incinerator with steam turbines, generators and a scrubber system, which reduces pollutant emissions, often costs several million dollars.

Table 2-2. Energy yield of various materials (after Garthe (2004) and Lawrence (2007))

Material	Heat of combustion (Btu/lb)
Fuel oil	20,900
Polyethylene	19,900
Polypropylene	19,850
Polystyrene	17,800
Tires	13,000
Bituminous coal	11,700
Pine wood	9,600
Oak wood	8,300
Newspaper	8,000
Textiles	6,900
Average municipal solid waste (MSW)	4,500
Yard waste	3,000
Food waste	2,600

Note: 1 Btu = 1.055 kJ

2.4 Plastics for mulch film applications

LDPE is the dominant plastic in mulch film applications, while ethylene vinyl acetate (EVA), ethylene butyl acrylate (EBA), and their copolymers or blends are used for special purposes in crops with high market values, such as strawberry and asparagus (Espi *et al.* 2006). Due to increases in economic and environmental concerns over removal and disposal of mulch films, much research has been focused on using biodegradable materials, such as poly(lactic acid) (PLA), poly(butylene adipate-*co*-terephthalate) (PBAT), copolymers of poly(hydroxybutyrate) (PHB) and starch based polymers, as mulch films. Table 2-3 shows polymeric mulch materials that are commercially available and currently under research.

Table 2-3 Polymeric materials commercially available (CA) or under research (UR) to be used as mulch film

Types of plastic mulch	CA or UR	Biodegradable	References
LDPE	CA	No	Rollo (1997), Lamont (1999), Hussain and Hamid (2003)
LLDPE	CA	No	Espi *et al.* (2006)
EVA	CA	No	Espi *et al.* (2006)
EBA	CA	No	Espi *et al.* (2006)
Blends of LDPE or LLDPE with EVA	CA	No	Amin (2001)
PBAT	UR	Yes	Kijchavengkul *et al.* (2008a; 2008b)
PLA	UR	Yes	Anonymous (2008)
PHB copolymers	UR	Yes	Kelly (2008), Krishnaswamy (2008)
Copolymer of PCL and starch	UR	Yes	Rangarajan and Ingall (2006)
Starch based polymer	UR	Yes	Halley *et al.* (2001)
Vegetable oil coated kraft paper	UR	Yes	Shogren and David (2006)

LDPE = Low density polyethylene

LLDPE = Linear low density polyethylene

EVA = Ethylene vinyl acetate

EBA = Ethylene butyl acrylate

PLA = Poly(lactide) or poly(lactic acid)

PBAT = Poly(butylene adipate-*co*-terephthalate)

PHB = Poly(hydroxylbutyrate)

PCL = Poly(ε-caprolactone)

2.4.1 Low density polyethylene (LDPE)

LDPE is the most widely used plastic as mulch film because of its low cost and retention of mechanical and optical properties over time.

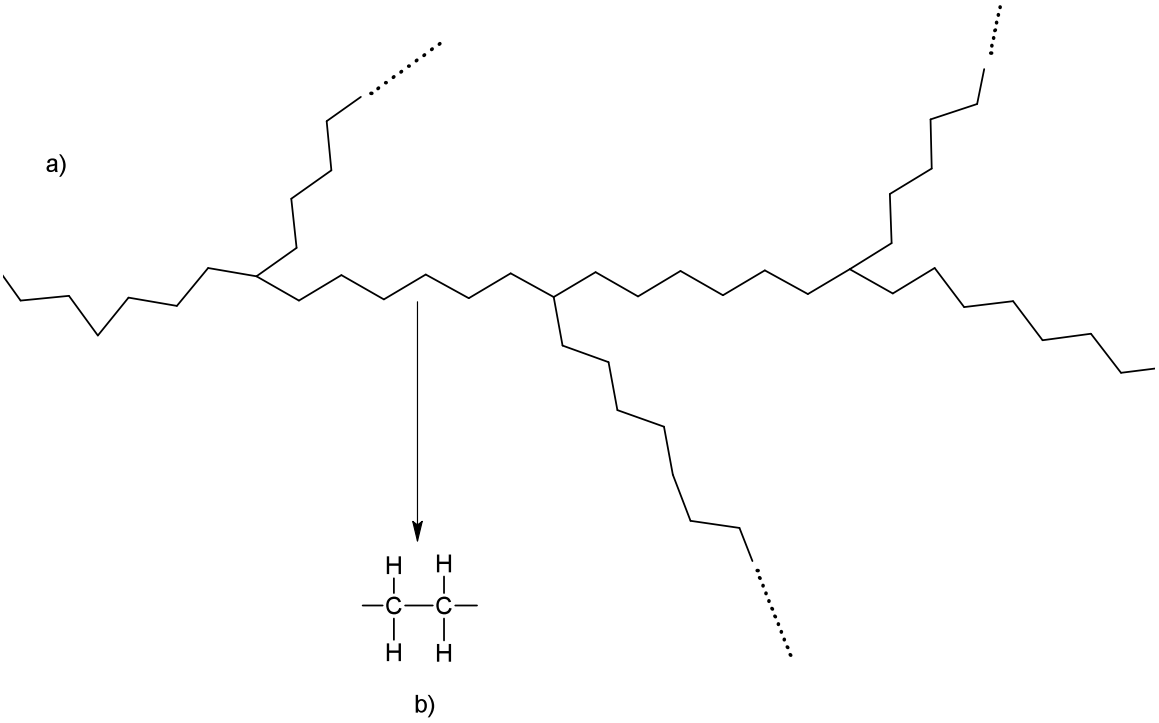

Figure 2-4. Low density polyethylene (LDPE) (a) branched polymer with (b) repetitive units

LDPE is a branched homopolymer, which has ethylene (Figure 2-4) as a repetitive constituent unit (monomer). LDPE mulch film can be as inexpensive as $160 per acre, but the cost also depends on the bed layout (Lamont 2004b). Plastic resin prices on September 22, 2010 are shown in Table 2-4. Moderate tensile strength and high elongation of LDPE are other reasons for its popular use as mulch film (Table 2-5). LDPE has good resistance to photodegradation and excellent retention of optical and mechanical properties. After 15 weeks exposure to outdoor sunlight at total radiant exposure level of 2.18×10^9 J/m^2, LDPE mulch film retains its tensile strength (3.19 kpsi

at week 0 and 3.24 kpsi at week 15), percent elongation at break (516% at week 0 and 626% at week 15), and tensile modulus (30.75 kpsi at week 0 and 33.79 kpsi at week 15) (Kijchavengkul *et al.* 2008a).

Table 2-4. Plastic resin prices per pound on September 22, 2010 (IDES 2010)

Plastic	Price per pound (US$)
LDPE	0.63
LLDPE	0.62
HDPE	0.61
PP	0.71
EVA	0.87
PS	0.81
PET	0.74

Note: Prices are based on average price of purchase order greater than 40,000 lbs except EVA, for which price is based on purchase order less than 40,000 lbs

LDPE = Low density polyethylene

LLDPE = Linear low density polyethylene

HDPE = High density polyethylene

PP = Polypropylene

PS = Polystyrene

EVA = Ethylene vinyl acetate

PET = Polyethylene terephthalate

Table 2-5. Mechanical properties of LDPE (Osswald and Menges 2003)

Mechanical properties	Range
Tensile strength	1.14-3.27 kpsi (7.86-22.6 MPa)
Elongation at break (%)	300-1000
Tensile modulus	28.4-71.1 kpsi (196-490 MPa)

2.4.2 Biodegradable aliphatic aromatic copolyester

Poly(butylene adipate-*co*-terephthalate) or PBAT, also known by the trade name of Ecoflex®, is one of the biodegradable plastics produced from petroleum based resources (Figure 2-5). PBAT was certified as compostable by the Biodegradable Products Institute (BPI) according to ASTM D6400 specification (ASTM 2004; BPI 2008).

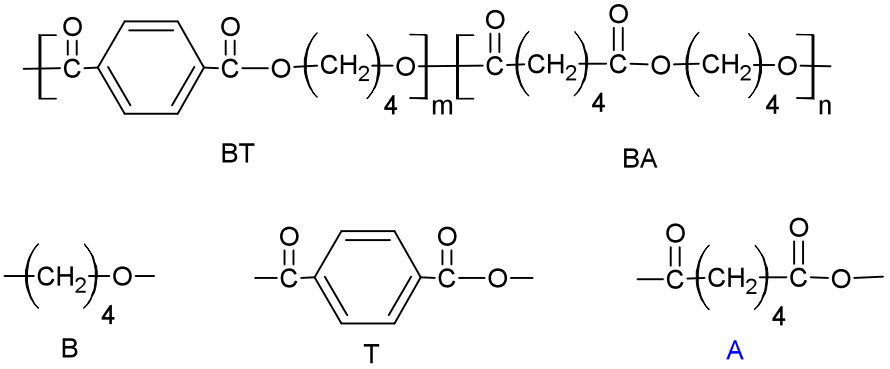

Figure 2-5. Structure of poly(butylene adipate-*co*-terephthalate) (PBAT) and 1,4 butanediol (B), terephthalic acid (T), and adipic acid (A) components

PBAT is a linear random copolyester consisting of two types of dimer (a chemical entity consisting of two monomers). The rigid section BT is an ester repeat unit consisting of 1,4 butanediol (B) and terephthalic acid (T) monomers, while the flexible section BA consists of 1,4 butanediol (B) and adipic acid (A) monomers. Molar masses

for B, A, and T monomers are 72.105, 128.123, and 148.114 g/mol, respectively. Each monomer is readily identified in proton nuclear magnetic resonance (^{1}H-NMR) spectra (Figure 2-6), where $CDCl_3$ is a peak of deuterated chloroform (chloroform-D) solvent and TMS is a group of peaks from tetramethylsilane (TMS) internal standard. There are two sets of peaks for monomer B, one for monomer B in dimer BA called "B1" and the other for monomer B in dimer BT called "B2" (Herrera *et al.* 2002).

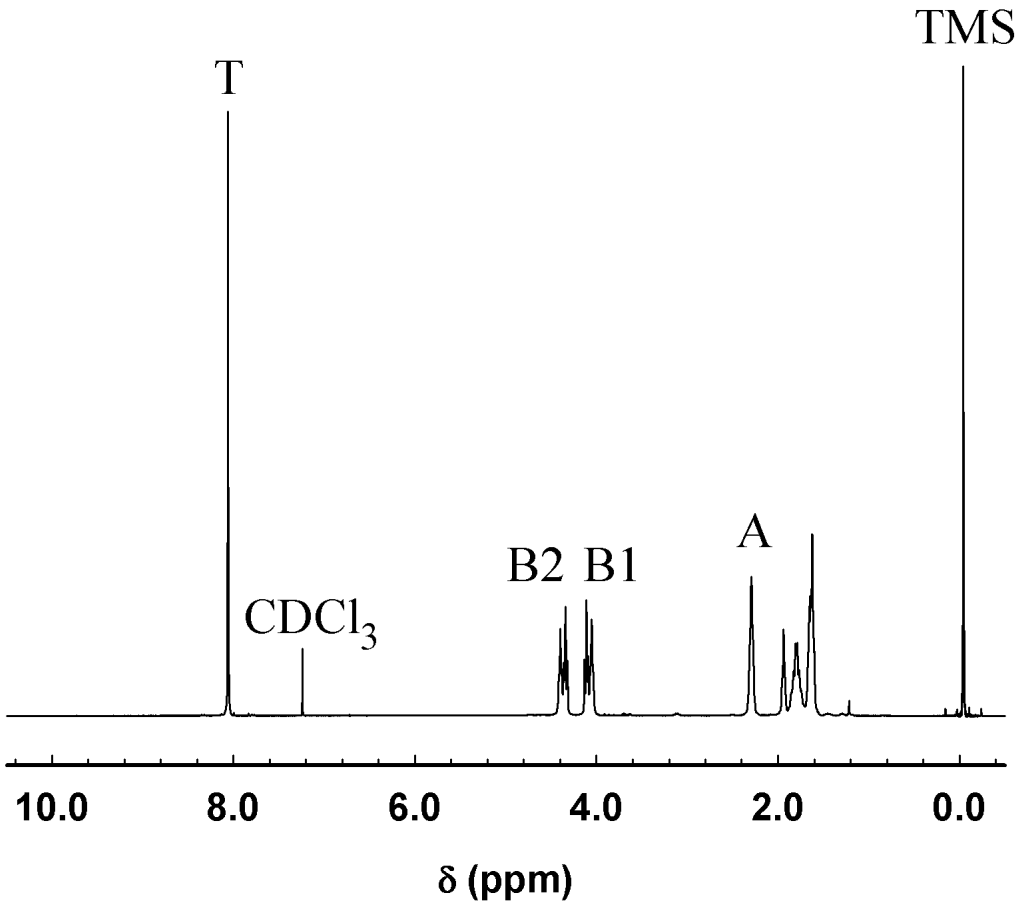

Figure 2-6. ^{1}H-NMR spectrum of PBAT; published in (Kijchavengkul *et al.* 2010)

In PBAT, there are two different types of photosensitive groups, the benzene ring in the T monomer, and the carbonyl groups (C=O) in the A and T monomers. The

benzene ring absorbs UV energy and acts as an energy sink to dissipate the UV energy via electron delocalization (Schnabel 1992). On the other hand, the presence of carbonyl groups makes PBAT more susceptible to photodegradation and results in chain scission by either Norrish I or Norrish II reactions. Furthermore, the hydrolytic reaction of hydrolyzable ester linkages in PBAT causes reduction in molecular weight and thereby facilitates the biodegradation process (see section 2.5.2.4 for more detail). Therefore, carbonyl groups in ester linkages make PBAT susceptible not only to photodegradation but also to biodegradation.

2.5 Degradation of mulch films

Degradation of plastic is defined as an irreversible process leading to structural change of plastic as characterized by changes in appearance or properties, such as mechanical strength, molecular weight, and thermal behavior, under the influence of one or more environmental factors, such as heat, UV light, and moisture (ASTM 2004; Kyrikou and Briassoulis 2007; Rodriguez *et al.* 2003). Degradation of plastic, including mulch films, can be classified into two categories based on the plastics useful lifetime as degradation: the useful lifetime and degradation after the useful lifetime.

2.5.1 Photodegradation during the useful lifetime

Plastic mulch films used outdoors degrade because of long-term exposure to sunlight (for at least 2-3 months) especially at UV wavelengths (190-400 nm). Polyolefins, such as LDPE, tends to undergo both chain scission and crosslinking as a result of photodegradation. Crosslinking is predominant in the absence of oxygen (Osawa 1992; Schnabel 1992).

Chain scission is a process that breaks bonds in the plastic main chain randomly. For each bond that is broken, another molecule is created. As a result, chain scission decreases the molecular weight of the plastic molecules, as well as the strength and modulus of the plastic.

Crosslinking is a process that links two or more main chains of the polymer together to form a network-like structure. Crosslinking in rubbery plastics, in which the glass transition temperature (T_g) is lower than the use temperature, generally increases

the modulus but when mechanical load is applied, the energy-absorbing capacity reaches a maximum and then decreases. As a result, the crosslinked plastic becomes more brittle (Rodriguez *et al.* 2003). Degradation of mulch films during their useful lifetime is generally not a desirable change, since it results in losses of integrity and mechanical strength. Those losses in properties can compromise the ability of mulch films to suppress weed growth, maintain bed structure and moisture, and alter soil temperature.

For mulch films, factors affecting photodegradation, and hence both the chain scission and crosslinking processes, include formulation and quality of the film; temperature; area of exposure, including plot layout and crop canopy; and amount of total solar radiation, which is dependant on season and geographical location (Giacomell *et al.* 2000).

2.5.2 Degradation after the useful lifetime

The degradation process after the useful lifetime of mulch films is similar to that during the useful lifetime, but the intention is different. Further degradation of aged plastic mulch films (after their useful lifetime) is intended as a disposal method either by photodegradation with photo-oxidation, or by biodegradation in order to eliminate the complication and expenses of removal and disposal of those materials.

2.5.2.1 Photodegradable mulch film

The idea of using photodegradation or controlled degradation as a method of mulch film disposal began 20-30 years ago (Ennis 1987; Kyrikou and Briassoulis 2007). The objective of this process is to design plastics to degrade at a specific time under specific environmental conditions. To make the film degradable, the approach was to

modify the LDPE resins to promote photodegradation by incorporating promoters into the polymer main chain. There are two common promoters: metal complexes and photosensitive functional groups (chromophoric groups or chromophores), such as carbonyl groups (C=O) (Kyrikou and Briassoulis 2007).

The carbonyl groups absorb UV radiation energy and cause chain scission via Norrish I and/or Norrish II reactions depending on environmental conditions and polymer structure (Albertsson 1992). In Norrish I, the chain splits at the carbonyl group location and gives off two free radicals (R•), molecular fragments each containing an unpaired electron (radicals 1 and 2 in Scheme 2-1). These free radicals are highly mobile and reactive and subsequently attack weak polymer bonds (Schnabel 1992; Selke *et al.* 2004). In Norrish II, an intermolecular rearrangement occurs and, instead of two free radicals, a terminal double bond and a methyl ketone (compounds 3 and 4 in Scheme 2-1, respectively) are created as a result of chain scission. As the photodegradation continues, this chain scission occurs in more locations. As a result, the plastic film is fragmented and eventually disintegrates into a friable powder (Kyrikou and Briassoulis 2007). The disintegrated plastic fragments may or may not be assimilated by microorganisms depending on the structure of the fragments. If they are not assimilated, these small fragments become pollutants to the environment.

Norrish I reaction

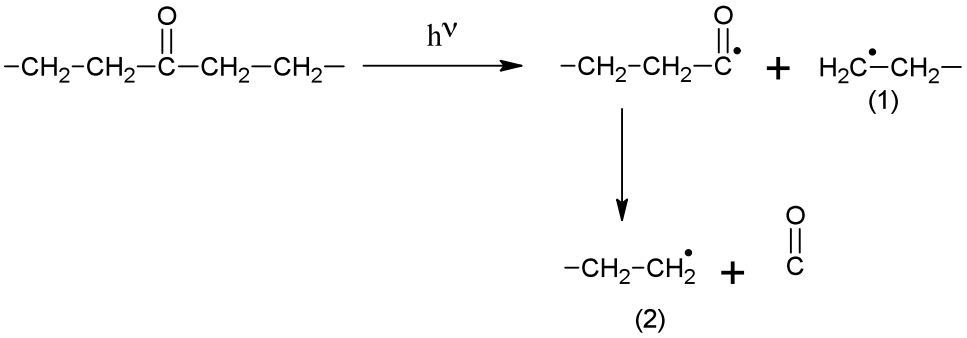

Norrish II reaction

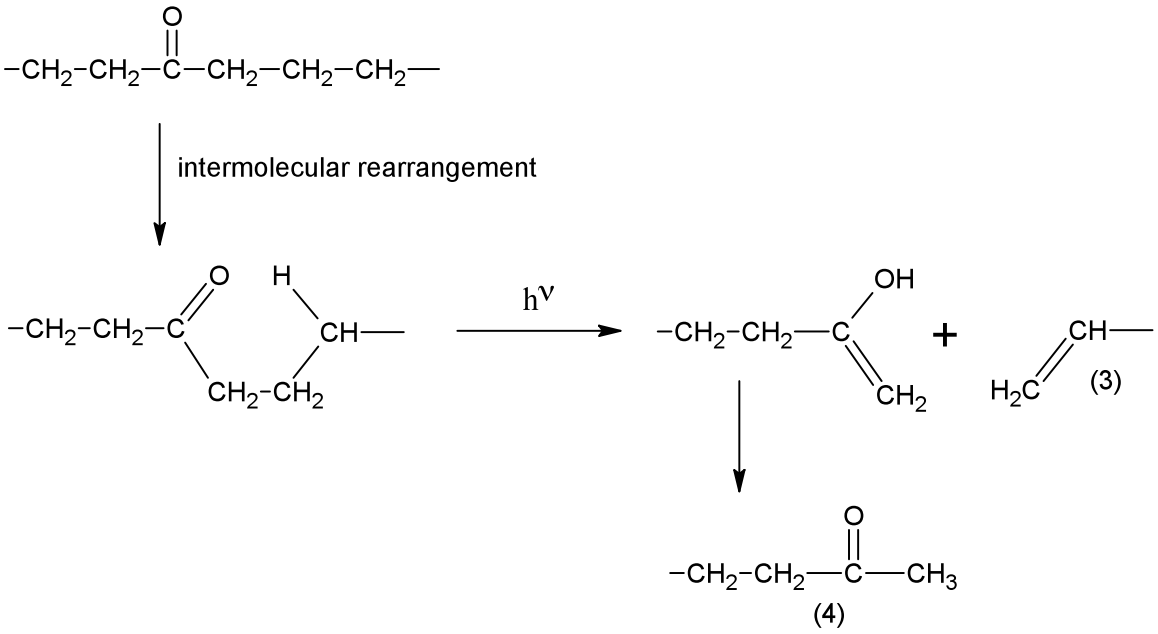

Scheme 2-1. Norrish I and II reactions: (1) and (2) = free radicals generated from Norrish I, (3) = terminal double bond compound, and (4) = methyl ketone compound

Another approach to manufacture photodegradable plastic is to incorporate metal complexes or salts of transition metals, such as iron, copper, and titanium based complexes, into plastic (Ennis 1992; Omichi 1992). Metal complexes can be classified into two groups: accelerators, which promote photodegradation, and retarders, which inhibit photodegradation (Osawa 1992). Theoretically, accelerator metal complexes allow the film to break down even without UV radiation, such as in a landfill or after burial,

since they absorb and store energy from UV radiation prior to burial (Kyrikou and Briassoulis 2007). There are five possible modes in which metal complexes serve as accelerator (Osawa 1992). Schnabel (1992) published most of the relevant equations:

1. Catalytic decomposition of hydroperoxides (R-O-O-H) and acceleration of free radical generation

$$R-O-O\bullet + RH \xrightarrow{M^{n+}} R-O-O-H+R\bullet \qquad (2\text{-}1)$$

2. Direct reaction of excited metal complexes (S*) with polymer (Eq. 2-2)

$$S^* + RH \rightarrow HS\bullet + R\bullet \qquad (2\text{-}2)$$

3. Activation of oxygen leading to electronic charge transfer (Eq. 2-3). The reaction of excited singlet state oxygen with unsaturated hydrocarbons results in formation of hydroperoxides.

$$^3S^* + {}^3O_2 \rightarrow {}^1S + {}^1O_2 \qquad (2\text{-}3)$$

4. Decomposition of excited metal complexes resulting in generation of free radicals (Eq. 2-4)

$$S^* \rightarrow S_1\bullet + S_2\bullet \qquad (2\text{-}4)$$

5. Photosensitizing action, transfer of energy from excited metal complexes to polymer molecules (Eq. 2-5) leading to the chain reaction of free radical formation (Eq. 2-6).

$$S^* + R_1 - R_2 \rightarrow S + R_1 - R_2^* \qquad (2\text{-}5)$$

$$R_1 - R_2^* \rightarrow R_1\bullet + R_2\bullet \qquad (2\text{-}6)$$

There are several concerns about these metal complexes, such as toxicity of the heavy metal residues after photodegradation and fragmentation takes place (Ennis 1992; Kyrikou and Briassoulis 2007).

In reality, the photodegradable mulch films break down unpredictably. This unpredictable breakdown is categorized into two types: premature breakdown when the films disintegrate before the harvest, and postmature breakdown when the films degrade more slowly than expected (Jensen 2004; Lamont 1999).

Fragmentation does not mean total degradation because the plastic fragments may not be easily degraded, especially by microorganisms. Theoretically, the fragments of polymer chain are susceptible to various types of degradation including biodegradation. However, biodegradation of these fragments has not yet been confirmed beyond a reasonable doubt, and the environmental fate of these materials in soils is highly disputed (Chandra and Rustgi 1998; Dřímal *et al.* 2007; Jensen 2004; Kyrikou and Briassoulis 2007).

2.5.2.2 Photooxidation

In the previous section, the initiation of photodegradation and the reaction in the absence of oxygen (photolysis) were described. The second part of photodegradation is propagation, which includes the oxidation process. In photolysis, the quantum yields for chemical reactions, such as generation of free radicals, are relatively low (Schnabel 1992). Oxygen readily reacts with either free radicals from photolysis or embedded free radicals generated from thermal degradation, decomposition of plastic molecules due to

high temperature from extrusion processes (Kyrikou and Briassoulis 2007; Rodriguez *et al.* 2003; Selke *et al.* 2004) and peroxyl radicals are formed (Schnabel 1992).

Photooxidation starts from generation of free radicals from photolysis (Eq. 2-7), reaction of free radicals with oxygen and formation of peroxyl radicals (Eq. 2-8), and formation of hydroperoxides (R-O-O-H) and other free radicals (Eq. 2-9). Equations 2-7 to 2-12 for photooxidation were published in Shlyapintokh (1984) and Schnabel (1992).

$$R_1 - R_2 \xrightarrow{h\nu} R_1 \bullet + R_2 \bullet \quad (2\text{-}7)$$

$$R \bullet + O_2 \rightarrow R - O - O \bullet \quad (2\text{-}8)$$

$$R - O - O \bullet + RH \rightarrow R - O - O - H + R \bullet \quad (2\text{-}9)$$

$$R - O - O - H \rightarrow RO \bullet + \bullet OH \quad (2\text{-}10)$$

$$RH + \bullet OH \rightarrow R \bullet + H_2O \quad (2\text{-}11)$$

$$2R - O - O - H \xrightarrow{h\nu} RO \bullet + H_2O + R - O - O \bullet \quad (2\text{-}12)$$

Hydroperoxide is highly unstable and easily decomposes at relatively low temperatures (Eq. 2-10). The hydroxyl radical (•OH) is very reactive and can react with polymers and generate other free radicals (Eq. 2-11). Then reactions Eq. 2-8 to 2-11 keep repeating and the propagation of photodegradation or oxidation is called an autoxidative process. When the local concentration of R-O-O-H is high, bimolecular decomposition of R-O-O-H (Eq. 2-12) can be found.

2.5.2.3 Photodegradation of aromatic polyesters and generation of phenyl radicals

Since the late 1960s, many research groups have reported formation of benzene free radicals (compound 1 in Figure 2-7) in aromatic polyesters after exposure to UV (Buxbaum 1968; Fechine *et al.* 2004; Grossetete *et al.* 2000; Marcotte *et al.* 1967; Rivaton and Gardette 1998; Tabankia and Gardette 1986; Tabankia and Gardette 1987; Tabankia *et al.* 1985; Valk *et al.* 1970). The early research was focused on the use of PET and poly(butylene terephthalate) (PBT) as electronic components and their photo-stability. Marcotte *et al.* (1967) confirmed the presence of phenyl radicals in PET after exposure to UV at 313 nm using electron spin resonance (ESR) and reported that the combination of these phenyl radicals accounted for the crosslinking in PET (compound 2 in Figure 2-7). Although the actual mechanism of formation of phenyl radicals is still unknown, it was suggested that the phenyl radicals are formed by hydrogen abstraction at the most labile hydrogen atom by the neighboring molecules or free radicals (Scheme 2-2), especially those generated via the Norrish I mechanism, such as •OH (Eq. 2-10) (Buxbaum 1968; Fechine *et al.* 2004; Grossetete *et al.* 2000; Marcotte *et al.* 1967; Rivaton and Gardette 1998; Tabankia and Gardette 1986; Tabankia and Gardette 1987; Tabankia *et al.* 1985; Valk *et al.* 1970).

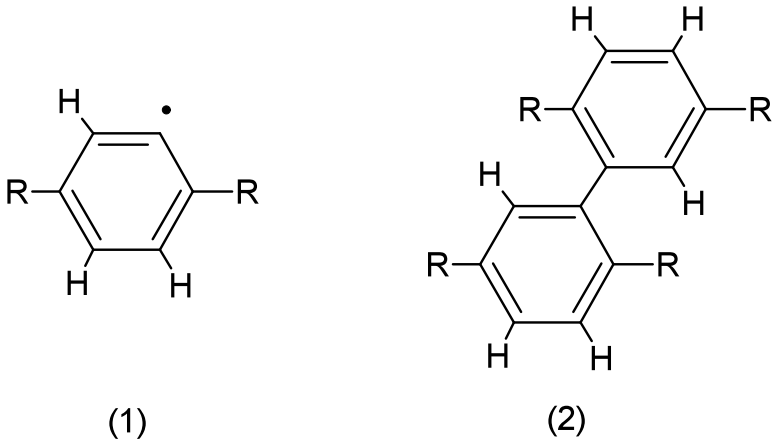

Figure 2-7. Phenyl radical (1) and crosslinked structure from recombination of phenyl radicals (2)

In photo-oxidative conditions, changes in the color or UV spectrum of the aromatic polyester result from the formation of mono- and dihydroxylated compounds (compounds 1 and 2 in Figure 2-8). Those two compounds cause yellowing in the aromatic polyester (Tabankia and Gardette 1986; Tabankia and Gardette 1987). There are two possible routes resulting in formation of type A and type B hydroperoxide compounds from oxidation at two different locations in the aromatic polymer main chain (compounds 3 and 4 in Figure 2-8): 1) formation of types A and B hydroperoxides as shown in Scheme 2-2, and 2) formation of mono- and dihydroxylated compounds from types A and B hydroperoxides as shown in Schemes 2-3 and 2-4, respectively.

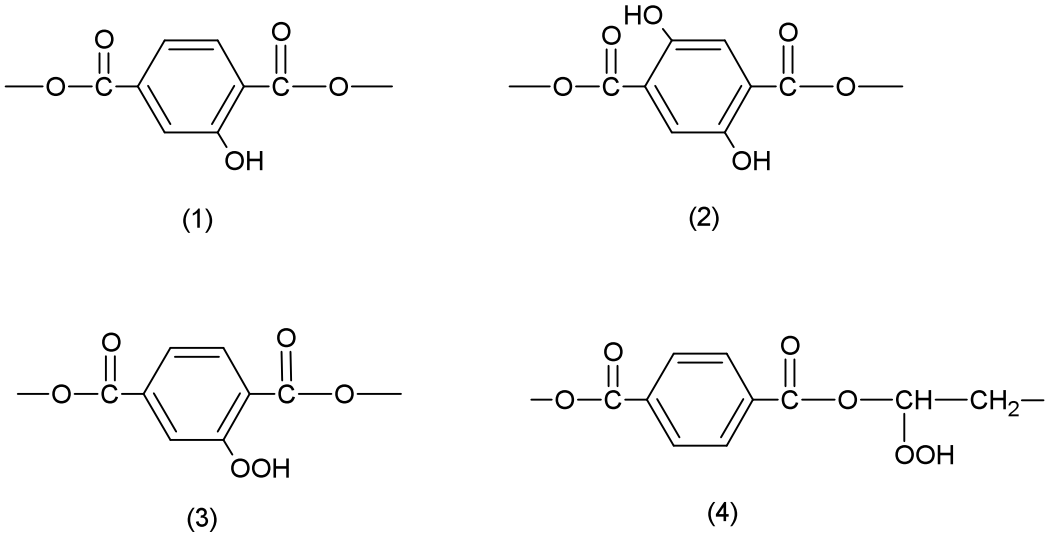

Figure 2-8. Monohydroxylated (1) and dihydroxylated (2) compounds; type A (3) and type B (4) hydroperoxides

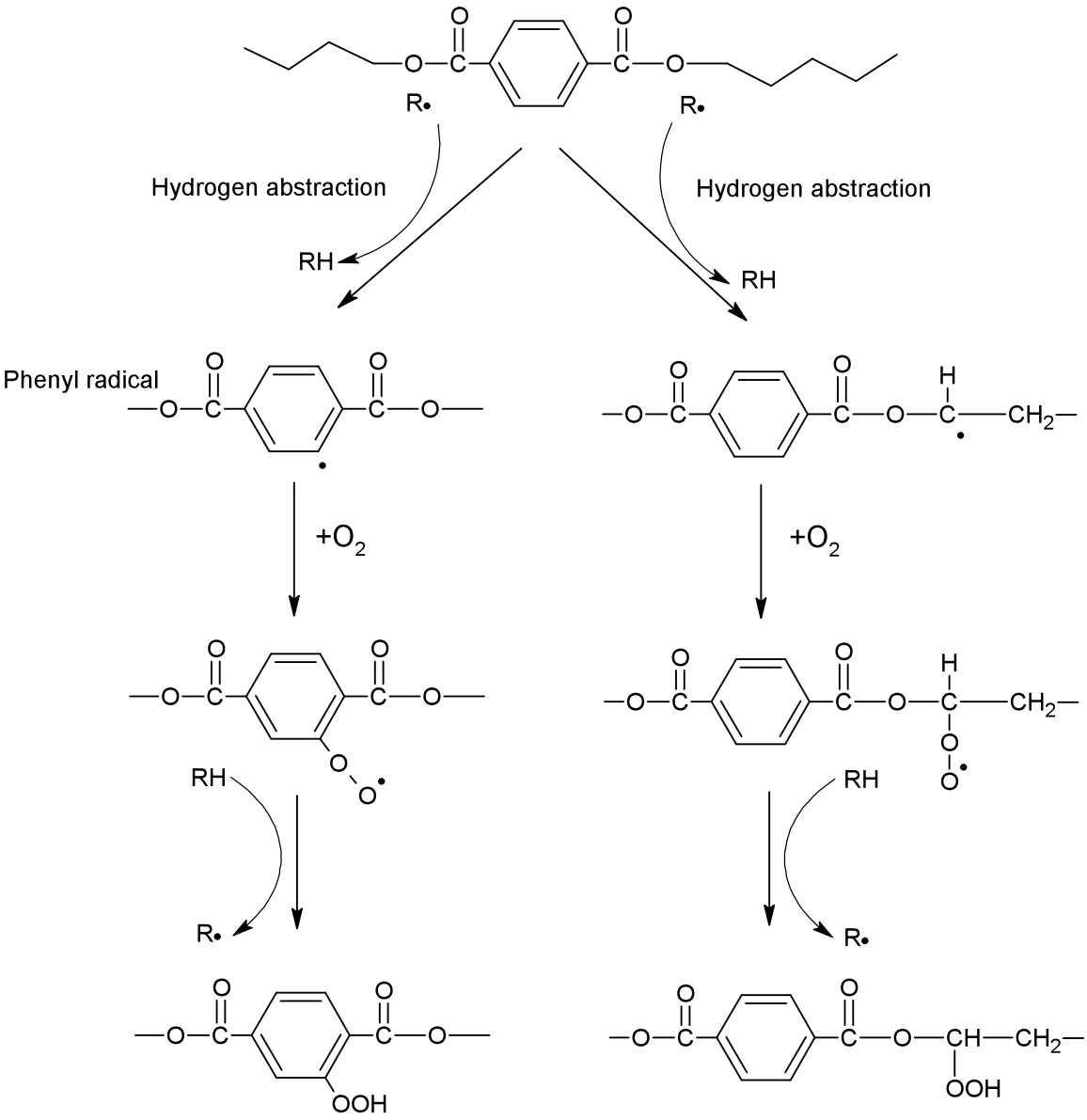

Scheme 2-2. Formation of type A and type B hydroperoxides; adapted from Tabankia and Gardette (1986), Buxbaum (1968), and Rivaton and Gardette (1998)

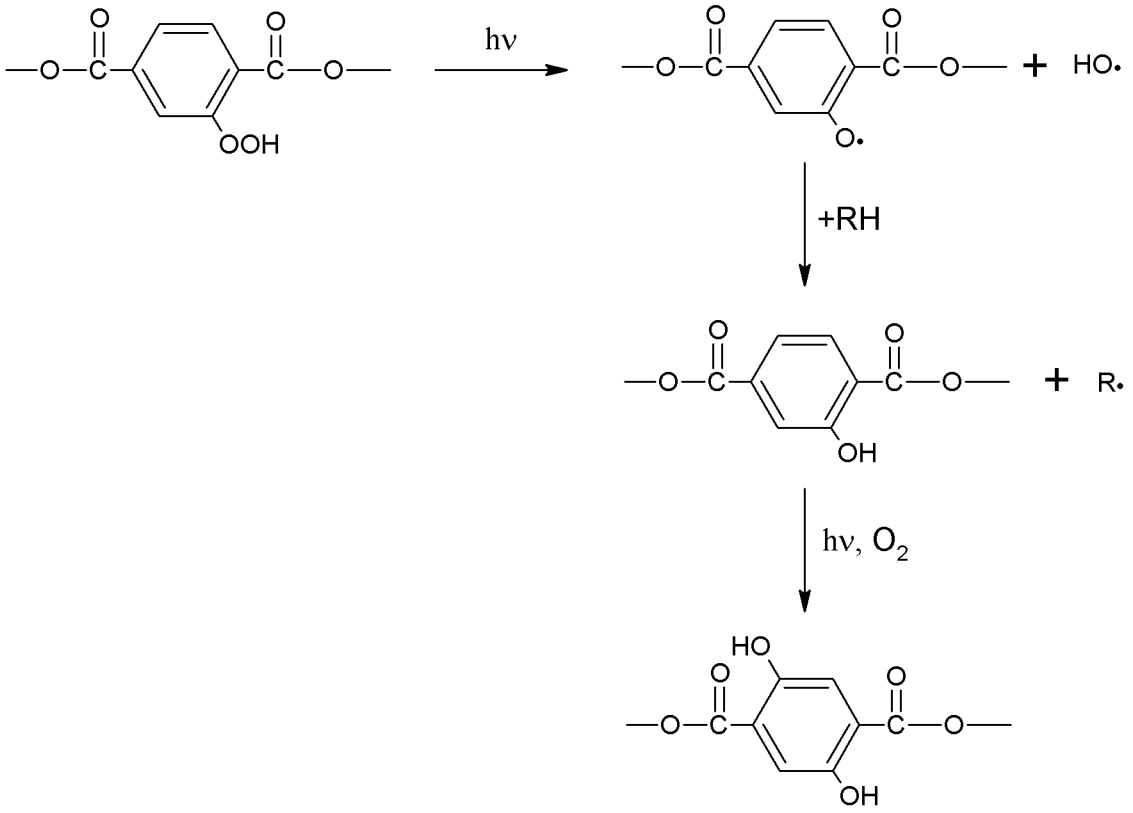

Scheme 2-3. Formation of mono- and dihydroxylated compounds from type A hydroperoxide; adapted from Tabankia and Gardette (1986)

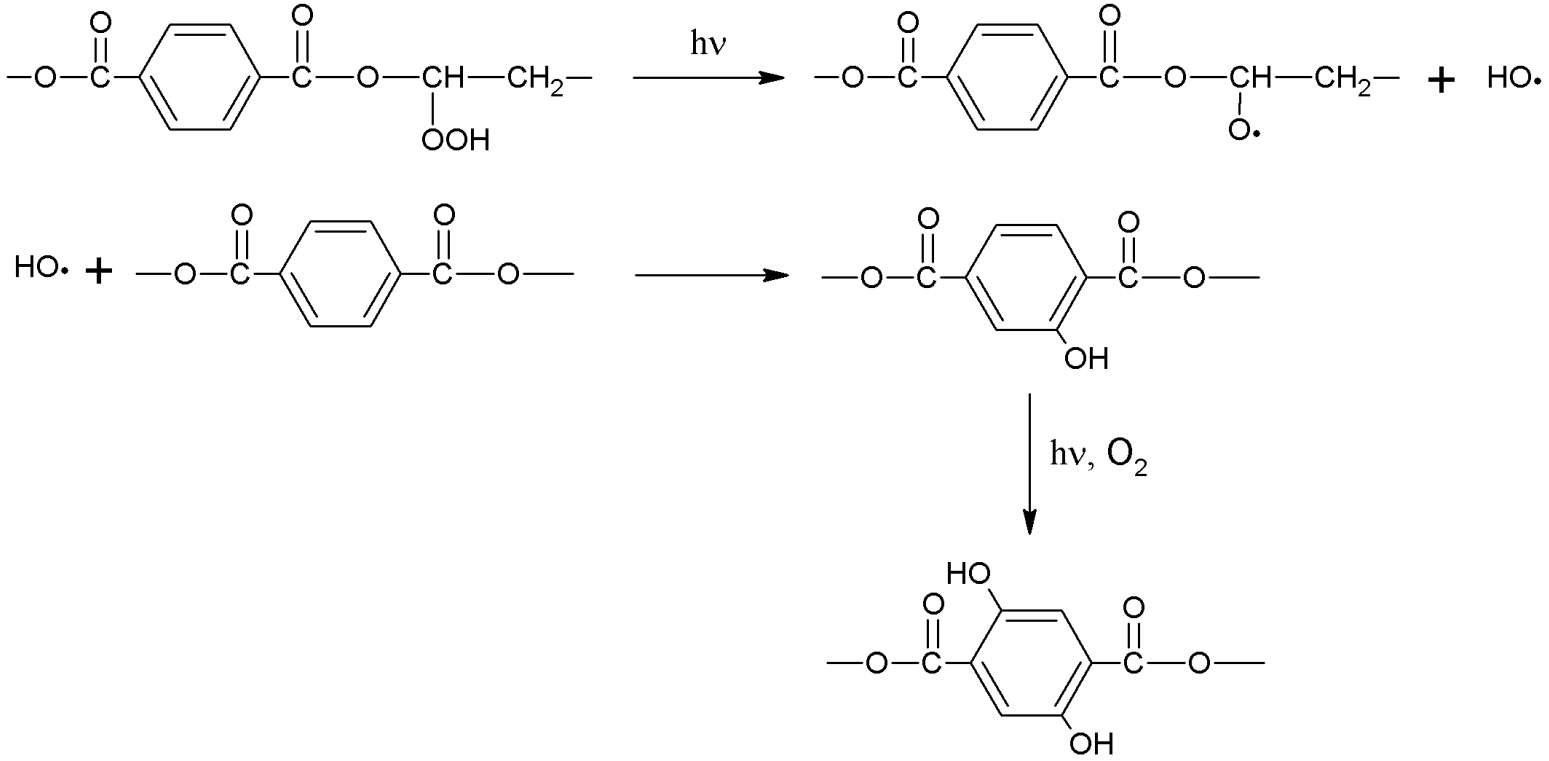

Scheme 2-4. Formation of mono- and dihydroxylated compounds from type B hydroperoxide; adapted from Tabankia and Gardette (1986)

In addition to crosslinking, main chain scission can occur in aromatic polyesters, such as PBAT and PBT. Due to the presence of C=O group in the polymer main chain, Tabankia and Gardette (1986) found that there are 3 Norrish I main chain scission processes depending on the locations of bond cleavages that created free radicals (Scheme 2-5). In absence of O_2, aliphatic radicals (compound 1 in Scheme 2-5) are likely to decompose through decarbonylation and decarboxylation, where carbon monoxide (CO) and carbon dioxide (CO_2) gases are formed, respectively (Marcotte *et al.* 1967; Tabankia and Gardette 1986). Free radicals generated in these processes can then recombine or can react further with labile hydrogen atoms in the main chain, causing hydrogen abstraction.

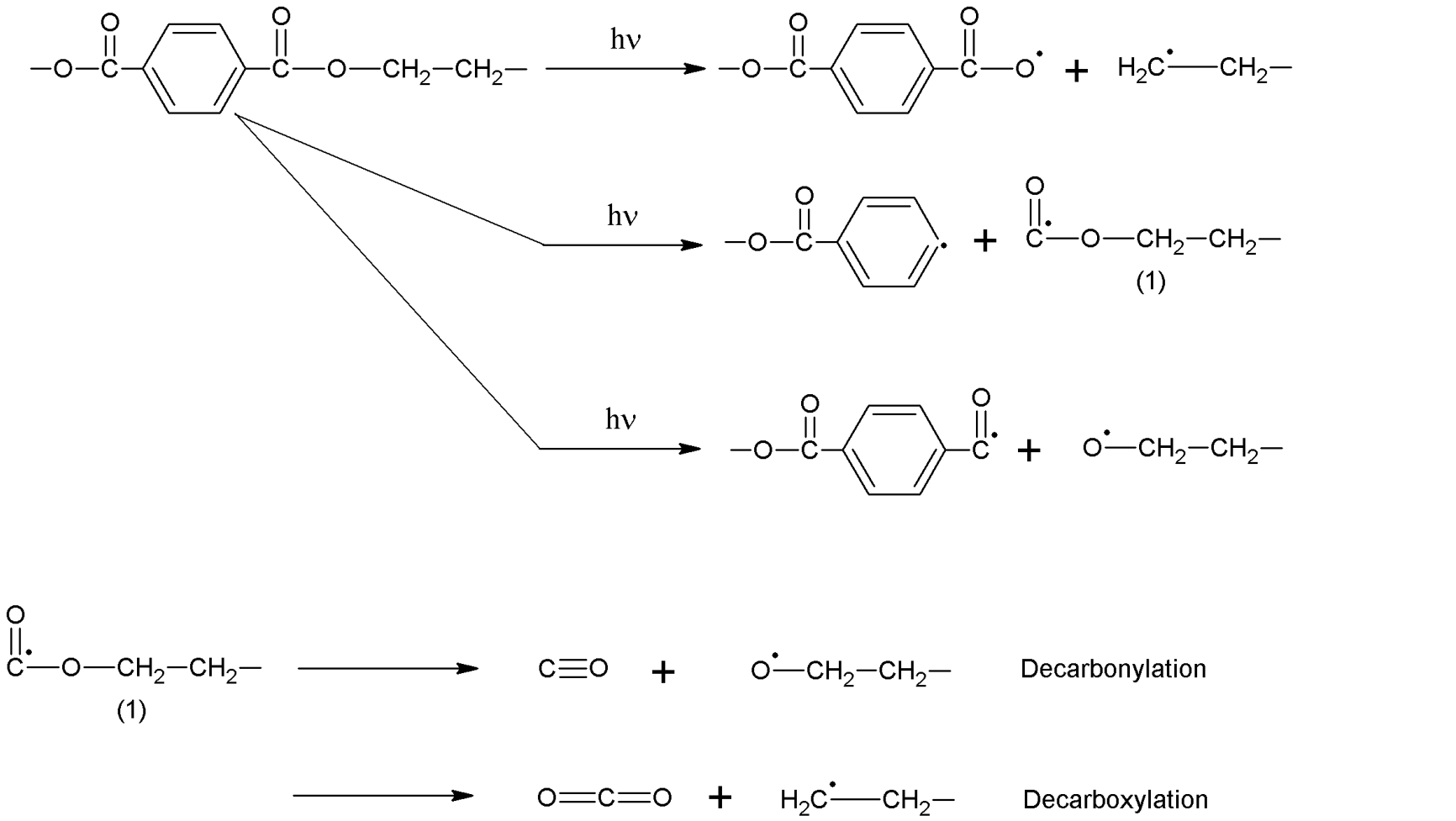

Scheme 2-5. Three Norrish I main chain scission routes that generate free radicals and decomposition of aliphatic radicals via decarbonylation and decarboxylation to form CO and CO_2 gas; adapted from Tabankia and Gardette (1986)

2.5.2.4 Antioxidant

In order to reduce the effect of photooxidation on polymers, various types of chemicals are incorporated into the polymer matrix. To reduce the effect of photodegradation (initiation process), pigments, such as carbon black or titanium dioxide (rutile), are used as UV absorbers to reduce the photon energy (hν) absorbed by the polymer (Chirinos-Padron and Allen 1992).

For the oxidative reaction (propagation process), besides metal deactivators, which trap the metal ions that can accelerate the oxidation, there are two types of antioxidants inhibiting oxidative degradation in plastics: primary antioxidants or chain-breaking antioxidants, and secondary antioxidants or peroxide-decomposing antioxidants (Chirinos-Padron and Allen 1992).

2.5.2.4.1 Primary antioxidants or chain-breaking antioxidants

Chain breaking antioxidants (CB) work by trapping free radicals by two main mechanisms: chain-breaking (electron) donor (CB-D) and chain-breaking (electron) acceptor (CB-A) (Al-Malaika 1989; Chirinos-Padron and Allen 1992). More specifically, CB interrupts the oxidation by removing the main propagating alkyl and alkyl peroxide radicals (R• and ROO•), see equations 2-7 to 2-9. Examples of chain-breaking antioxidants are hindered phenols, such as 2,6-di-tert-butyl-4-methyl phenol or butylated hydroxytoluene (BHT) (Figure 2-9) and alkylarylamines. CB-D reduces ROO• to ROOH according to equation 2-13. The phenoxyl radical from CB (A• (2) in equation 2-13 and Figure 2-9) is more stable than typical free radicals (R• as in equation 2-9) (van Krevelen and Nijenhuis 2009). CB-A, on the other hand, removes R• in an oxidation process. Both

CB activities occur in the overall process (Scheme 2-6). The hindered phenolic antioxidants can be regenerated from the reaction of two radicals (Scheme 2-6). The carbonyl derivative of hindered phenol antioxidant ((3) in Figure 2-9) still has CB-A capability.

$$ROO\bullet + AH_{(1)} \rightarrow ROOH + A\bullet_{(2)} \qquad (2\text{-}13)$$

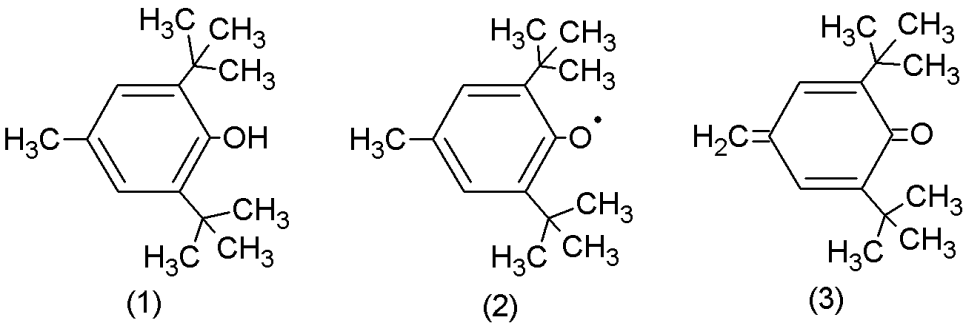

Figure 2-9. (1) 2,6-di-tert-butyl-4-methyl phenol or butylated hydroxytoluene (BHT), (2) phenoxyl radical, and (3) carbonyl derivative

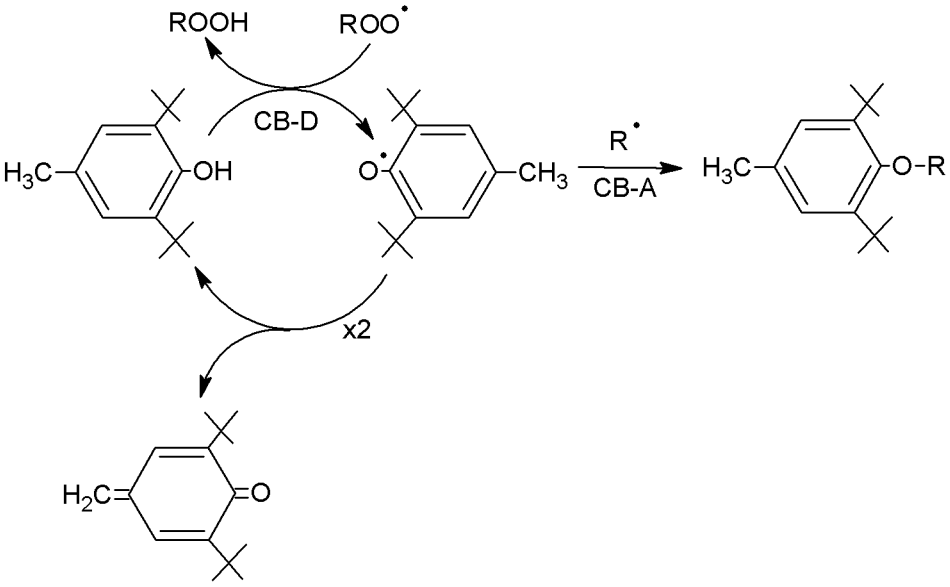

Scheme 2-6. Chain-breaking donor and chain-breaking activities of BHT; adapted from Chirinos-Padron and Allen (1992)

Factors such as the interaction rate of the antioxidant with the radicals, fate of phenoxyl radicals, volatility, solubility, and the size of antioxidant molecule and its derivatives, govern the effectiveness of hindered phenolic antioxidants (Chirinos-Padron and Allen 1992). For example, antioxidants with high molecular weight may cause some difficulty, such as lower compatibility and mobility, which decreases the antioxidant capacity.

2.5.2.4.2 Secondary antioxidants or peroxide-decomposing antioxidants

As mentioned earlier, ROOH is thermally and photolytic unstable, and when it breaks down, the highly reactive hydroxyl radical (•OH) is formed. The hydroxyl radical then react with a polymer (RH) and generate an alkyl radical (R•) and the process keeps repeating (autooxidation). Peroxide-decomposing (PD) antioxidants operate by decomposing hydroperoxide (ROOH) in a way that does not generate more free radicals. There are two types of PD antioxidants: stoichiometric peroxide decomposer (PD-S), and catalytic peroxide decomposer (PD-C) (Chirinos-Padron and Allen 1992).

The PD-S antioxidant decompose hydroperoxide (ROOH) by reducing it to a more inert product, such as an alcohol (ROH) (equation 2-14). Examples of PD-S antioxidants are phosphite esters (Al-Malaika 1989). PD-C antioxidants, which mostly are sulfur-containing compounds, decompose hydroperoxides via oxidation, of which the inorganic sulfur acids SO_2 and H_2SO_4 are the end products (Scheme 2-7) (Chirinos-Padron and Allen 1992).

$$P(OR')_3 \xrightarrow{ROOH} RO^- + HO - P^+(OR')_3 \rightarrow ROH + O = P(OR') \qquad (2\text{-}14)$$

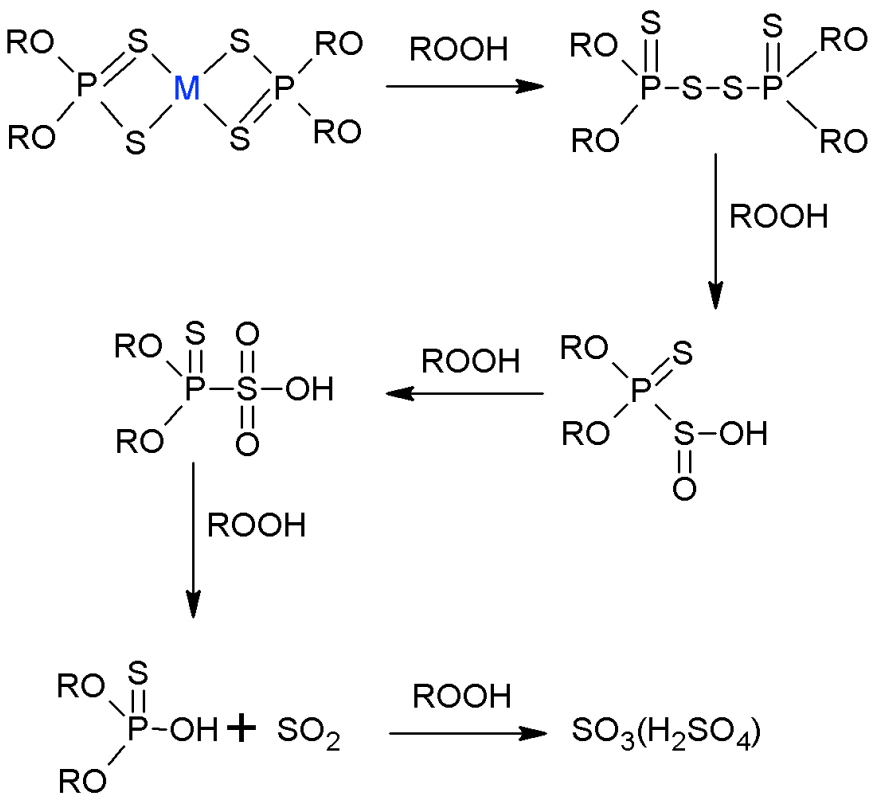

Scheme 2-7. Antioxidant mechanism of catalytic peroxide decomposer; adapted from Chirinos-Padron and Allen (1992)

2.5.2.5 Biodegradation

Partially published in Kijchavengkul, T and Auras, R (2008). "Perspective: Compostability of polymers." Polymer International **57**(6): 793-804.

Biodegradation is a degradation process resulting from the action of naturally occurring microorganisms such as bacteria, fungi, and algae (ASTM 2004). It is the intrinsic chemical structure of the polymer that makes it biodegradable. To be biodegradable, some parts of the polymer main chain must be similar to naturally occurring substances; therefore, microbes can use their existing enzymes to break the polymer chain at those specific locations and use them as a source of energy. For example, microorganisms break down starch to use the glucose, which is broken down to

two molecules of pyruvic acid, which can be further fermented into lactic acid or aerobically converted into CO_2 to generate energy. Portions of polymers that are small enough are transferred into microbial cells and consumed as a food source. Chemical structures of pyruvic acid and lactic acid are similar to that of PLA (Figure 2-10).

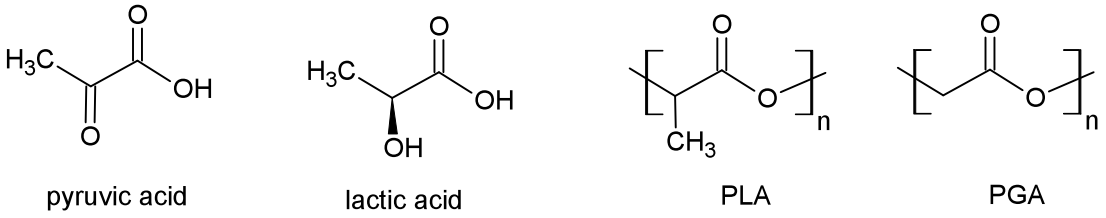

Figure 2-10. Chemical structures of pyruvic acid, lactic acid, PLA, and PGA

Weak links present in the chain also can facilitate attack by particular microorganisms. In the case of the polyolefin and vinyl families, the main chain of the polymer consists of carbon atoms which makes the polymer very stable to degradation or biodegradation. On the other hand, ester bonds in biodegradable polyesters, such as PBAT, PLA, and poly(hydroxyalkanoates) (PHA), make those polymers susceptible to chemical degradation involving water, hydrolysis. Hydrolysis creates random main chain scission, which causes rapid molecular weight reduction. This reaction accelerates the biodegradation since smaller molecules are more susceptible to enzymatic reactions. Therefore, the chemical structure of the polymer is the main factor determining whether the polymer can or cannot biodegrade and its biodegradation or erosion mechanism.

Generally, there are two modes of erosion for biodegradable polymers, surface erosion and bulk erosion (Chandra and Rustgi 1998). In surface erosion, microorganisms start consuming polymers enzymatically from the surface in, thereby causing early slow

reduction in molecular weight due to solely enzymatic reaction. In bulk erosion, a polymer starts to degrade throughout its cross section, since water can diffuse through the polymer in the amorphous regions and cause hydrolysis reactions that cleave the polymer main chain and reduce the size of the polymer molecule, causing rapid reduction in molecular weight in an early stage (Auras *et al.* 2004). The low molecular weight oligomers can diffuse out of the polymer bulk to its surface and then are consumed by the microbes. Bulk erosion can occur only in polymers with hydrolyzable functional groups in the main chain, such as PLA and PBAT.

Biodegradability of these biodegradable polymers in composting conditions and soil burial conditions is affected by two factors, exposure conditions (biotic or abiotic) and polymer characteristics (see Figure 2-11) (Dřímal *et al.* 2007; Kale *et al.* 2007a; Kale *et al.* 2007b; Stevens 2003).

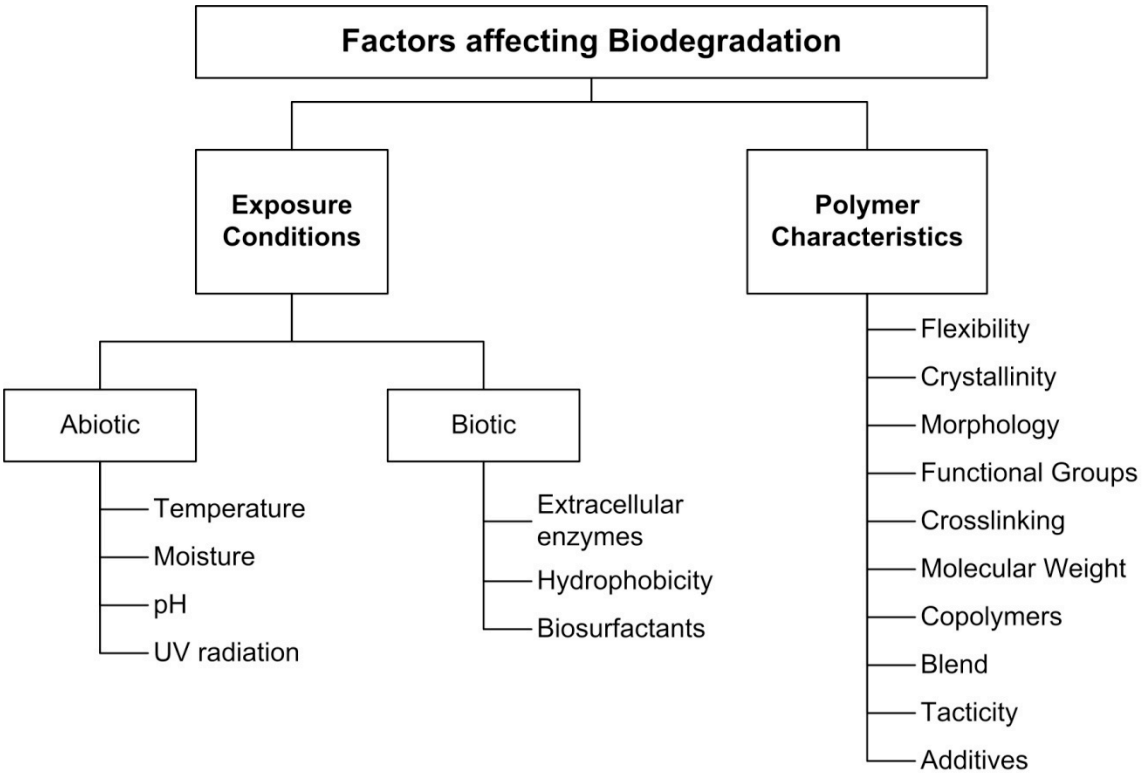

Figure 2-11. Factors affecting biodegradation; published in Kijchavengkul and Auras (2008)

Abiotic exposure factors, such as temperature, pH, and moisture in the compost pile, can affect the biodegradation and hydrolysis reaction rates. Both hydrolysis reaction and microbial activity increase with increasing moisture and temperature, especially above the T_g of the polymers (Henton *et al.* 2005), where the polymer changes its behavior from glassy to rubbery and gains more flexibility. However, if the temperature is too high, microbial activity decreases or even stops (Ho *et al.* 1999a; Ho *et al.* 1999b). Lotto *et al.* (2004) incubated 3 biodegradable polymers (PCL, PHB, and poly(hydroxybutyrate-*co*-valerate) or PHBV) in compost mixtures at 24 and 46°C, and found that the biodegradation of all three polymers at 46°C was higher. In high moisture environments, hydrolysis reactions should increase and produce more chain scission, which will increase the available sites for microorganisms to attack the polymer chains,

causing faster degradation. pH can also affect the rate of hydrolysis, which is important for hydrolyzable polymers such as PLA, since reactions can be either acid or base catalyzed. For example, the hydrolysis rate of PLA capsules in solution was slowest at a pH of 5.0 and increased in more acidic and more alkaline solutions (Auras *et al.* 2004; Henton *et al.* 2005).

UV radiation has mixed effects on the biodegradation of polymers since it can cause main chain scission, crosslinking, or both in the polymer structure. If main chain scission is predominant the biodegradation will be faster since the polymer molecules available will be smaller and more easily consumed by microbes. On the other hand, crosslinking of the polymer chains makes the molecules larger and more stable, making them more difficult to be consumed by microorganisms.

Among biotic factors, extracellular enzymes produced by different microorganisms may have active sites with different specificity, such as complementary shape, charge, and hydrophilicity/hydrophobicity (Miller and Agard 1999), and hence have more capability to biodegrade certain polymers. For example, *Aspergillus niger* and *Aspergillus flavus* fungi, presented in soil and crops, respectively, produce enzymes that more easily digest aliphatic polyesters derived from 6-12 carbon di-acid monomers than those produced from other monomers (Chandra and Rustgi 1998). This enzymatic specificity may contribute to different degradation rates of biodegradable polyesters in differing compost environments.

For the polymer characteristics aspect, the biodegradation rate depends on the accessibility of microbes and water to polymer chains. Conformational flexibility,

energy required to rotate molecules around bonds or to move atoms closer to or further away from others, plays an important role in the biodegradation of polymers. The more flexibility a polymer has, the more accessible to microbes and water it will be. Two factors that affect the conformational flexibility of polymers are bulky side groups that limit polymer chain movement and certain types of linkages in the polymer main chain, such as carbon double bonds that increases polymer flexibility by easing rotation around the adjacent single bonds. This is the case for poly(glycolic acid) or PGA (Figure 2-10), which degrades faster than PLA, since PLA contains methyl ($-CH_3$) side group that inhibit chain movement and hence have less flexibility.

Crystallinity can also limit the accessibility of water to the polymer chain since water cannot diffuse through crystalline regions in the polymer. Amorphous regions are more flexible and accessible to water and microorganisms; therefore, amorphous regions are more susceptible to both hydrolysis and biodegradation than crystalline region (Gopferich 1998). According to Gan *et al.* (2005), morphology of the crystals also plays a major role in degradation. They found that poly(butylene adipate) (PBA) films with an α crystal structure (helical shape) biodegraded faster than PBA with a β crystal structure (zigzag shape), possibly because the spherulites formed with α crystals are larger and contain fewer nuclei than those formed with β crystals, hence having more accessibility.

Functional groups in the polymer chains that are hydrolyzable such as amide, carbonates, esters, and ethers also increase the susceptibility of the polymers to biodegradation, not only by providing the sites for hydrolysis but also by increasing the flexibility of the polymer main chain (Albertsson 1992; Gopferich 1998; Stevens 2003).

Molecular weight of the polymers affects biodegradation by reducing accessibility to water and microbes in two different ways. As the molecular weight increases T_g also increases and the polymer becomes glassier and less flexible. Furthermore, a higher molecular weight polymer also has a longer chain length, which means that there are more bonds to be cleaved in order to reduce it to water soluble oligomers which are small enough to be transferred into cells and consumed by microorganisms (Gopferich 1998). Microorganisms can digest only low molecular weight portions, which are taken into the cells and then converted into metabolites (Chandra and Rustgi 1998). Therefore, smaller molecules are more accessible to microbes and water than the larger ones.

Addition of comonomers into a polymer structure will increase irregularity of the polymer chains which reduces the polymer's crystallinity and might increase accessibility to microbes and water and, hence, biodegradability. However, the biodegradability of the copolymer also depends on the types of the introduced comonomers (Gopferich 1998). Adding comonomers containing hydrolyzable groups, as mentioned earlier, should increase the biodegradability, while adding comonomers with aromatic structures, or other groups that increase rigidity of the polymer chain, and/or with no hydrolyzable groups, will lower biodegradability or even make the final copolymer not biodegradable. For example, PHBV, the copolymer of PHB poly(hydroxybutyrate) and PHV poly(hydroxyvalerate), biodegrades in natural marine environments much faster than pure PHB (Volova *et al.* 2004).

Tacticity affects biodegradability of the polymer mainly by altering the regularity and hence the crystallinity. Ikejima *et al.* (1999) also found that the biodegradability of

the blend depends greatly on the tacticity of the PVOH. Biodegradability of the blends was highest for the blend with atactic PVOH, followed by the blend with syndiotactic PVOH, and the blend with isotactic PVOH had the lowest biodegradability possibly because atacticity of the PVOH suppresses the formation of the PHB crystals. In addition, Ikejima *et al.* (1999) found that the biodegradability of blends of PHB with poly(vinyl alcohol) (PVOH) decreased with increasing amount of PVOH content.

Addition of additives can either accelerate or prevent biodegradation. Yoshie *et al.* (2000) reported that adding low molecular weight additives, such as tributyrin and trilaurin at 1% w/w, can accelerate the biodegradation of PHB by increasing the molecular mobility in the amorphous phase of the PHB. On the other hand, with a larger amount of additives at 9% w/w in the PHB mixtures, those additives act as an inhibitor since the additives on the surface prevent the attack of microorganisms on the PHB molecules (Yoshie *et al.* 2000).

REFERENCES

REFERENCES

ACRC. (2008a). "ACRC in the news." Retrieved Sep 11, 2008, from http://www.biomassmagazine.com/article-print.jsp?article_id=1532.

ACRC. (2008b). "End-use products." Retrieved Sep 11, 2008, from http://www.acrecycle.org/end_products.html.

Al-Malaika, S (1989). Antioxidants and stabilizers for hydro carbon polymers: Past, present, and future. Handbook of Polymer Science and Technology. N P Cheremisinoff ed. New York, NY, Marcel Dekker.

Albertsson, A-C (1992). Biodegradation of polymers. Handbook of Polymer Degradation. S H Hamid, M B Amin and A G Maadhah ed. New York, NY, Marcel Dekker**:** 345-363.

Amidon (1994) Use and disposal of plastics in agriculture, Prepared by Amidon Recycling for the American Plastics Council.

Amin, A-R (2001). "LDPE/EPDM multilayer films containing recycled ldpe for greenhouse applications." Journal of Polymers and the Environment **9**(1): 25-30.

Anderson, RG (1994). Dr. Emery Myers Emmert "the father of plastic greenhouses". The 25th National Agricultural Plastics Congress.

Anonymous. (2008). "Compostable mulch films made of PLA blends." Retrieved Sep 5, 2008, from http://www.interpack.com/cipp/md_interpack/custom/pub/content,lang,2/oid,7483/ticket,g_u_e_s_t/local_lang,2/~/Compostable_mulch_films_made_of_PLA_blends.html.

ASTM (2004) D 6400-04 standard specification for compostable plastics. West Conshohocken, PA, ASTM International.

Auras, R, Harte, B and Selke, S (2004). "An overview of polylactides as packaging materials." Macromolecular Bioscience **4**: 835-864.

BPI. (2008). "Approved products — resins." Retrieved Oct 17, 2008, from http://www.bpiworld.org/BPI-Public/Approved/3.html.

Brooks, TW (1996) Method and apparatus for recycling previously used agricultural plastic film mulch. U.S. Patent no. 5510076.

Buxbaum, LH (1968). "The degradation of poly(ethylene terephthalate)." Angewandte Chemie-International Edition **7**(3): 182-190.

Chandra, R and Rustgi, R (1998). "Biodegradable polymers." Progress in Polymer Science **23**: 1273-1335.

Chirinos-Padron, AJ and Allen, NS (1992). Aspects of polymer stabilization. Handbook of Polymer Degradation. S H Hamid, M B Amin and A G Maadhah ed. New York, NY, Marcel Dekker**:** 261-303.

Clarke, SP. (1996). "Recycling farm plastic films fact sheet." Retrieved Sep 11, 2008, from http://www.omafra.gov.on.ca/english/engineer/facts/95-019.htm.

Dockery, DW and Pope III, CA (1994). "Acute respiratory effects of particulate air pollution." Annual Review of Public Health **15**: 107-132.

Dřímal, P, Hoffmann, J and Družbík, M (2007). "Evaluating the aerobic biodegradability of plastics in soil environments through gc and ir analysis of gaseous phase." Polymer Testing **26**: 727-741.

Durham, S (2003) Plastic mulch: Harmful or helpful? Agricultural Research. July 2003. Retrieved Sep 22, 2010, from http://www.ars.usda.gov/is/AR/archive/jul03/mulch0703.pdf

Ennis, R (1987). Plastigone-a new, time-controlled photodegradable plastic mulch film. The 20th National Agricultural Plastics Congress.

Ennis, R (1992). Controlled degradation of plastics: Environmental toxicity. Handbook of Polymer Degradation. S H Hamid, M B Amin and A G Maadhah ed. New York, NY, Marcel Dekker**:** 383-408.

EPA (2006) An inventory of sources and environmental releases of dioxin-like compounds in the United States for the years 1987, 1995, and 2000. Washington, DC, National Center for Environmental Assessment.

EPA. (2008). "Municipal solid waste generation, recycling and disposal in the United States: 2006 facts and figures." Retrieved April 15, 2008, from http://www.epa.gov/epaoswer/non-hw/muncpl/pubs/msw06.pdf.

EPC (2006) An inventory of agricultural film plastics for the central coast recycling market development zone San Jose, CA, Environmental Planning Consultant.

Espi, E, Salmeron, A, Fontecha, A, Garcia, Y and Real, AI (2006). "Plastic films for agricultural applications." Journal of Plastic Film and Sheeting **22**: 85-102.

Fechine, GJM, Rabello, MS, Souto Maior, RM and Catalani, LH (2004). "Surface characterization of photodegraded poly(ethylene terephthalate). The effect of ultraviolet absorbers." Polymer **45**(7): 2303-2308.

FLDEP (2005) Open burning, Florida Department of Environmental Protection. Chapter 62-256 of Florida Administrative Code.

Gan, Z, Kuwabara, K, Abe, H, Iwata, T and Doi, Y (2005). "The role of polymorphic crystal structure and morphology in enzymatic degradation of melt-crystallized poly(butylene adipate) films." Polymer Degradation and Stability **87**(2005): 191-199.

Garthe, J (2004). Managing used agricultural plastics. Production of Vegetables, Strawberries, and Cut Flowers Using Plasticulture. W Lamont ed. Ithaca, NY, Natural Resource, Agriculture, and Engineering Service (NRAES).

Giacomell, GA, Garrison, SA, Jensen, M, Mears, DR, Paterson, JW, Roberts, WJ and Wells, OS (2000). Advances of plasticulture technologies 1977 – 2000. The 15th International Congress for Plastics in Agriculture, Hershey, PA.

Gopferich, A (1998). Mechanisms of polymer degradation and elimination. Handbook of Biodegradable Polymers. A J Domb, J Kost and D Wiseman ed. Boca Raton, FL, CRC**:** 451-471.

Grossetete, T, Rivaton, A, Gardette, JL, Hoyle, CE, Ziemer, M, Fagerburg, DR and Clauberg, H (2000). "Photochemical degradation of poly(ethylene terephthalate)-modified copolymer." Polymer **41**(10): 3541-3554.

Halley, P, Rutgers, R, Coombs, S, Kettels, J, Gralton, J, Christie, G, Jenkins, M, Beh, H, Griffin, K, Jayasekara, R and Lonergan, G (2001). "Developing biodegradable mulch films from starch-based polymers." Starch **53**((2001)): 362-367.

Haraguchi, T, Marui, A, Yuge, K, Nakano, Y and Mori, K (2004). "Effect of plastic-film mulching on leaching of nitrate nitrogen in an upland field converted from paddy." Paddy and Water Environment **2**(2): 67–72.

Henton, DE, Gruber, P, Lunt, J and Randall, J (2005). Polylactic acid technology. Natural Fibers, Biopolymers, and Biocomposites. A K Mohanty, M Misra and L T Drzal**:** 527-577.

Herrera, R, Franco, L, Rodriguez-Galan, A and Puiggali, J (2002). "Characterization and degradation behavior of poly(butylene adipate-co-terephthalate)." Journal of Polymer Science Part A-Polymer Chemistry **40**(23): 4141–4157.

Ho, K-LG, Pometto, AL, Gadea-Rivas, A, Briceno, JA and Rojas, A (1999a). "Degradation of polylactic acid (PLA) plastics in costa rican soil and iowa state university compost rows " Journal of Environmental Polymer Degradation **7**(4): 173-177.

Ho, K-LG, Pometto, AL and Hinz, PN (1999b). "Effects of temperature and relative humidity on polylactic acid plastic degradation." Journal of Environmental Polymer Degradation **7**(2): 83-92.

Hong, Y-C, Lee, J-T, Kim, H, Ha, E-H, Schwartz, J and Christiani, DC (2002). "Effects of air pollutants on acute stroke mortality." Environmental Health Perspectives **110**(2): 187-191.

Hussain, I and Hamid, H (2003). Plastics in agriculture. Plastics and the Environment. A L Andrady ed. Hoboken, NJ, John Wiley & Sons, Inc**:** 185-209.

IDDEQ. (2007). "Open "Outdoor" Burning guidelines." Retrieved Sep 12, 2008, from http://www.deq.state.id.us/air/prog_issues/burning/open_burning_overview.cfm.

IDES. (2010). "Street plastic prices report." Retrieved Sep 22, 2010, from http://www.ides.com/resinprice/resinpricingreport.asp.

Ikejima, T, Yoshie, N and Inoue, Y (1999). "Influence of tacticity and molecular weight of poly(vinyl alcohol) on crystallization and biodegradation of poly(3-hydroxybutyric acid)/poly(vinyl alcohol) blend." Polymer Degradation and Stability **66**(1999): 263-270.

Jensen, MH. (2004). "Plasticulture in the global community - View of the past and future." Retrieved Nov 20, 2006, from http://www.plasticulture.org/history_global_community.htm.

Kale, G, Auras, R, Singh, SP and Narayan, R (2007a). "Biodegradability of polylactide bottles in real and simulated composting conditions." Polymer Testing **26**(8): 1049-1061.

Kale, G, Kijchavengkul, T, Auras, R, Rubino, M, Selke, SE and Singh, SP (2007b). "Compostability of bioplastic packaging materials: An overview." Macromolecular Bioscience **7**(3): 255-277.

Kaplan, JK. (2003). "Dress-for-success mulch." Retrieved Aug 8, 2008, from http://plasticulture.cas.psu.edu/default.html.

Kelly, P (2008). Mirel: Compostable biobased plastics for a sustainable future. The 34th National Agricultural Plastics Congress, Tampa, FL, American Society for Plasticulture.

Kijchavengkul, T and Auras, R (2008). "Perspective: Compostability of polymers." Polymer International **57**(6): 793-804.

Kijchavengkul, T, Auras, R, Rubino, M, Alvarado, E, Camacho Montero, JR and Rosales, JM (2010). "Atmospheric and soil degradation of aliphatic-aromatic polyester films." Polymer Degradation and Stability **95**(2): 99-107.

Kijchavengkul, T, Auras, R, Rubino, M, Ngouajio, M and Fernandez, RT (2008a). "Assessment of aliphatic-aromatic copolyester biodegradable mulch films. Part I: Field study." Chemosphere **71**(5): 942-953.

Kijchavengkul, T, Auras, R, Rubino, M, Ngouajio, M and Fernandez, RT (2008b). "Assessment of aliphatic-aromatic copolyester biodegradable mulch films. Part II: Laboratory simulated conditions." Chemosphere **71**(9): 1607-1616.

Kotrba, R (2008) "What to do with the remnants of a plastic culture." Biomass April 2008. Retrieved Sep 22, 2010, from http://www.biomassmagazine.com/article.jsp?article_id=1532

Krishnaswamy, RK (2008). The effectiveness of biodegradable poly(hydroxy butanoic acid) copolymers in agricultural mulch film applications. Best of ANTEC™ 2008 e-Live® Presentation.

Kyrikou, I and Briassoulis, D (2007). "Biodegradation of agricultural plastic films: A critical review." Journal of Polymers and the Environment **15**(2): 125-150.

Lamont, W. (1999). "Vegetable production using plasticulture." Retrieved Nov 18, 2006, from http://www.agnet.org/library/eb/476/.

Lamont, W (2004a). Plastic mulches. Production of Vegetables, Strawberries, and Cut Flowers using Plasticulture. W Lamont ed. Ithaca, NY, Natural Resource, Agriculture, and Engineering Service (NRAES).

Lamont, W (2004b). Plasticulture-an overview. Production of Vegetables, Strawberries, and Cut Flowers using Plasticulture. W Lamont ed. Ithaca, NY, Natural Resource, Agriculture, and Engineering Service (NRAES).

Lawrence, MJ (2007) A novel machine to produce fuel nuggets from non-recyclable plastics. Agricultural and Biological Engineering. University Park, PA, The Pennsylvania State University. Doctor of Philosophy Dissertation.

Lee, GF and Jones-Lee, A. (2007). "Flawed technology of subtitle D landfilling of municipal solid waste." Retrieved April 24, 2007, from http://www.members.aol.com/apple27298/SubtitleDFlawedTechnPap.pdf.

Levitan, L and Barro, A (2003) Recycling agricultural plastics in New York state. Ithaca, NY, Environmental Risk Analysis Program, Cornell Center for the Environment, Cornell University. Retrieved Sep 22, 2010, from http://cwmi.css.cornell.edu/recycling%20ag%20plastics.pdf

Levitan, L, Cox, DG and Clarvoe, MB (2005) Agricultural plastic film recycling: Feasibility and options in the central leatherstocking-upper catskill region of New York state. Ithaca, NY, College of Agriculture and Life Sciences, Cornell University. Retrieved Sep 22, 2010, from http://www.p2pays.org/ref/47/46055.pdf

Lotto, NT, Calil, MR, Guedes, CGF and Rosa, DS (2004). "The effect of temperature on the biodegradation test." Materials Science and Engineering **24**(2004): 659–662.

Marcotte, FB, Campbell, D and Cleaveland, JA (1967). "Photolysis of poly(ethylene terephthalate)." Journal of Polymer Science: Part A: Polymer Chemistry **5**(3): 481-501.

MDEQ (1994) Michigan open burning guide. Lansing, MI, Michigan Department of Environmental Quality.

Miller, DW and Agard, DA (1999). "Enzyme specificity under dynamic control: A normal mode analysis of [alpha]-lytic protease." Journal of Molecular Biology **286**(1): 267-278.

Narayan, R (2001). Drivers for Biodegradable/compostable Plastics & Role of Composting Waste Management & Sustainable Agriculture. ORBIT 2001 Conference, Seville, Spain, Spanish waste club.

Ngouajio, M and Ernest, J (2004). "Light transmission through colored polyehtylene mulches affects weed populations." Hortscience **39**(6): 1302-1304.

NJDA. (2008). "New jersey agricultural recycling programs." Retrieved Sep 9, 2008, from http://www.state.nj.us/agriculture/divisions/md/prog/recycling.html#1.

NTP (2005) Report on carcinogens, 11th edition. Washington, DC, U.S. Department of Health and Human Services, Public Health Service, National Toxicology Program.

NYDEC. (2008). "Dangers of open burning." Retrieved Sep 12, 2008, from http://www.dec.ny.gov/chemical/32064.html.

Olson, SM (2007). Mulching. Vegetable Production Handbook for Florida 2007-2008. S M Olson and E Simonne ed. Gainesville, FL, The Institute of Food and Agricultural Sciences, University of Florida.

Omichi, H (1992). Degradable plastics. Handbook of Polymer Degradation. S H Hamid, M B Amin and A G Maadhah ed. New York, NY, Marcel Dekker**:** 335-344.

ORDEQ (2006) Oregon open burning guide. Portland, OR, States of Oregon Department of Environmental Quality

Orzolek, MD. (2004). "An introduction to plasticulture." Retrieved Sep 8, 2008, from http://www.plasticulture.org/what_description.htm.

Osawa, Z (1992). Photoinduced degradation of polymers. Handbook of Polymer Degradation. S H Hamid, M B Amin and A G Maadhah ed. New York, NY, Marcel Dekker**:** 169-217.

Osswald, TA and Menges, G (2003). Materials Science of Polymers for Engineers. Cincinnati, OH, Hanser Gardner.

Parish, RL, Bracy, RP and McCoy, JE (2000). "Evaluation of field incineration of plastic mulch." Journal of Vegetable Crop Production **6**(1): 17-24.

Rangarajan, A and Ingall, B (2006) Biodegradable mulch product testing 2006. Ithaca, NY, Department of Horticulture, Cornell University.

Rice, PJ, McConnell, LL, Heighton, LP, Sadeghi, AM, Isensee, AR, Teasdale, JR, Abdul-Baki, AA, Harman-Fetcho, JA and Hapeman, CJ (2001). "Runoff loss of pesticides and soil: A comparison between vegetative mulch and plastic mulch in vegetable production systems." Journal of Environmental Quality **30**(5): 1808–1821.

Rivaton, A and Gardette, JL (1998). "Photo-oxidation of aromatic polymers." Angewandte Makromolekulare Chemie **261/262**(1): 173-188.

Rodriguez, F, Cohen, C, Ober, C and Archer, L (2003). Principles of Polymer Systems. New York, NY, Taylor & Francis.

Rollo, KL. (1997). "Agricultural plastics - boon or bane?" Retrieved Sep 4, 2008, from http://cwmi.css.cornell.edu/WastRed/AgWaste.html.

Ross, DS (2004). Drip irrigation and water management. Production of Vegetables, Strawberries, and Cut Flowers Using Plasticulture. W Lamont ed. Ithaca, NY, Natural Resource, Agriculture, and Engineering Service (NRAES).

Schnabel, W (1992). Polymer Degradation: Principles and Practical Applications. New York, NY, Hanser.

Seaton, A, MacNee, W, Donaldson, K and Godden, D (1995). "Particulate air pollution and acute health effects." Lancet **345**: 176-178.

Selke, SEM, Culter, JD and Hernandez, RJ (2004). Plastics Packaging. Cincinnati, OH, Hanser Gardner.

Shlyapintokh, V (1984). Photochemical Conversion and Stabilization of Polymers. New York, NY, Hanser.

Shogren, RL and David, M (2006). "Biodegradable paper/polymerized vegetable oil mulches for tomato and pepper production." Journal of Applied Horticulture **8**(1): 12-14.

Stevens, ES (2003). "What makes green plastics green?" Biocycle **24**: 24-27.

Tabankia, M and Gardette, JL (1986). "Photo-chemical degradation of polybutyleneterephthalate: Part 1-photo-oxidation and photolysis at long wavelengths." Polymer Degradation and Stability **14**(4): 351-365.

Tabankia, M and Gardette, JL (1987). "Photo-oxidation of block copoly(ether-ester) thermoplastic elastomers: Part 2-origins of the photo-yellowing." Polymer Degradation and Stability **19**(2): 113-123.

Tabankia, M, Philippart, JL and Gardette, JL (1985). "Photo-oxidation of block copoly(ether-ester) thermoplastic elastomers." Polymer Degradation and Stability **12**(4): 349-362.

Taber, HG. (2004). "Wavelength selective and/or colored plastic ag films." Retrieved Sep 11, 2008, from http://www.plasticulture.org/fg_wavelength.htm.

Valk, VG, Kehren, ML and Daamen, I (1970). "Photooxidation of poly(ethyleneglycol terephthalate)." Angewandte Makromolekulare Chemie **13**(1): 97-107.

van Krevelen, DW and Nijenhuis, Kt (2009). Properties of Polymers. Oxford, UK, Elsevier.

Volova, TG, Gladyshev, MI, Trusova, MY, Zhila, NO and Kartushinskaya, MV (2004). "Degradation of bioplastics in natural environment." Doklady Akademii Nauk **397**: 330–332.

WDEQ (2005) Smoke management. Air Quality Division Standards and Regulations. Cheyenne, WY, Wyoming Department of Environmental Quality.

Wu, L, Zhu, Z, Liang, Y and Zhang, F (2001). Plastic film mulching cultivation: A new technology for resource saving water n fertiliser and reduced environmental pollution. Plant Nutrition – Food Security and Sustainability of Agro-ecosystems. W J Horst ed. Norwell, MA, Kluwer Academic Publishers.

Yoshie, N, Nakasato, K, Fujiwara, M, Kasuya, K, Abe, H, Doi, Y and Inoue, Y (2000). "Effect of low molecular weight additives on enzymatic degradation of poly(3-hydroxybutyrate)." Polymer **41**(2000): 3227–3234.

Chapter 3 Respirometric System

During aerobic biodegradation, carbon in polymer molecules is converted by microorganisms into biomass or humus, water, carbon residues, and carbon dioxide gas as defined by equation 3-1 (Grima *et al.* 2000).

$$C_{polymer} + O_2 \quad \rightarrow \quad CO_2 + H_2O + C_{residue} + C_{biomass} \tag{3-1}$$

Therefore, the degree of aerobic biodegradation can be determined by measuring the total amount of CO_2 evolved from the polymer. The degradation of biopolymers is generally defined as percentage of mineralization. This is the proportion of cumulative CO_2 gas actually generated by the sample tested to the theoretical CO_2 content of the material, which can be determined by either elemental analysis, or calculation from chemical composition according to standards ASTM D5338 (ASTM 2003) and ISO 14855 (ISO 2005).

A respirometric system or respirometer is a device used for monitoring and/or measuring the respiration activity of living organisms by either focusing on oxygen (O_2) consumption, CO_2 evolution or both. It consists of 3 major components: (1) an air supply, (2) an air-tight closed vessel called the "bioreactor", which contains the living test organisms, and (3) a measuring device, to quantify the amount of O_2 uptake or CO_2 release. The respirometric system can be used to measure the amount of CO_2 gas evolved from biopolymers during aerobic biodegradation (equation 3-1).

Based on ASTM D 5338, ISO 14855-1 and ISO 14855-2 standards (ASTM 2003; ISO 2005; ISO 2006), there are three methods of measuring biodegradation, categorized by the methodology used to quantify CO_2 from the exhaust of the bioreactor. These methods are: (1) cumulative measurement respirometric system (CMR), (2) direct measurement respirometric system (DMR), and (3) gravimetric measurement respirometric system (GMR). In the CMR, the CO_2 from the exhaust is trapped in a basic solution, such as sodium hydroxide (NaOH) or barium hydroxide [$Ba(OH)_2$], and then is titrated at a predetermined time to measure the amount of the trapped CO_2 (Figure 3-1). In the DMR (Figure 3-2), the concentration of CO_2 is directly measured from the exhaust of the bioreactor using gas chromatography (GC), or an in-line infrared gas analyzer, such as a non-dispersive infrared (NDIR) gas analyzer. According to ASTM D5338 (ASTM 2003), for this method, the CO_2 concentration of the exhaust gas of each bioreactor has to be measured at least once every six hours. Finally, in the GMR (Figure 3-3), the CO_2 from the exhaust is captured in CO_2 absorbing columns, and the amount of evolved CO_2 is measured by the weight increase of the columns (Funabashi *et al.* 2007; Kunioka *et al.* 2006).

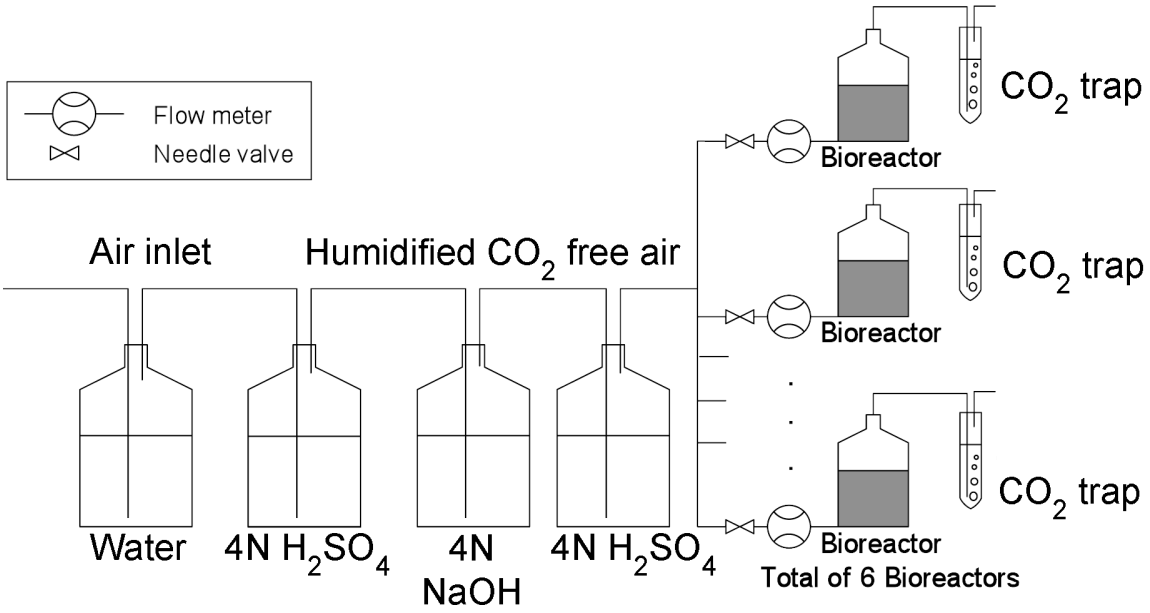

Figure 3-1. Schematic drawing of cumulative measurement respirometric system; published in Kijchavengkul *et al.* (2006)

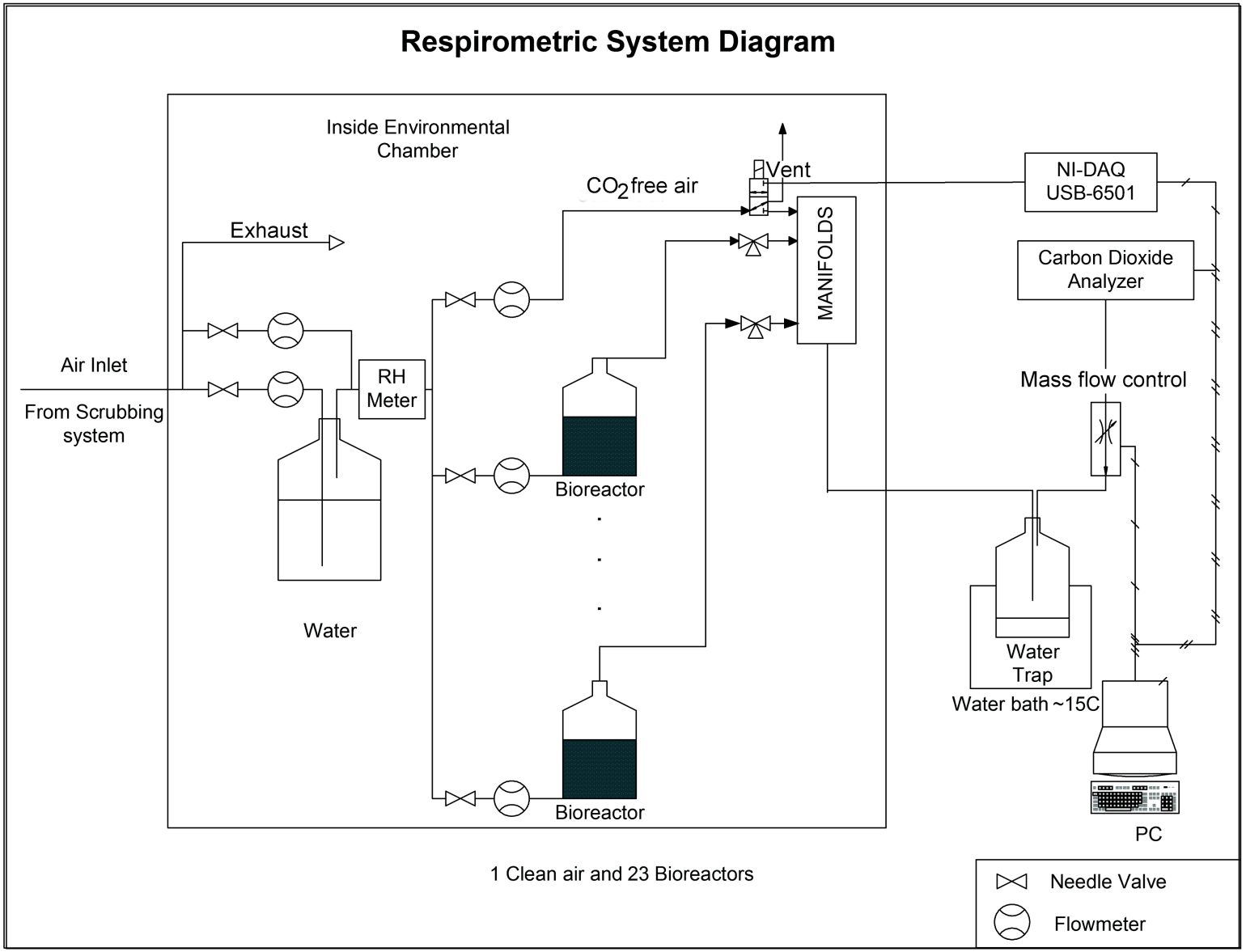

Figure 3-2. Schematic drawing of direct measurement respirometric (DMR) system; published in Kijchavengkul *et al.* (2006)

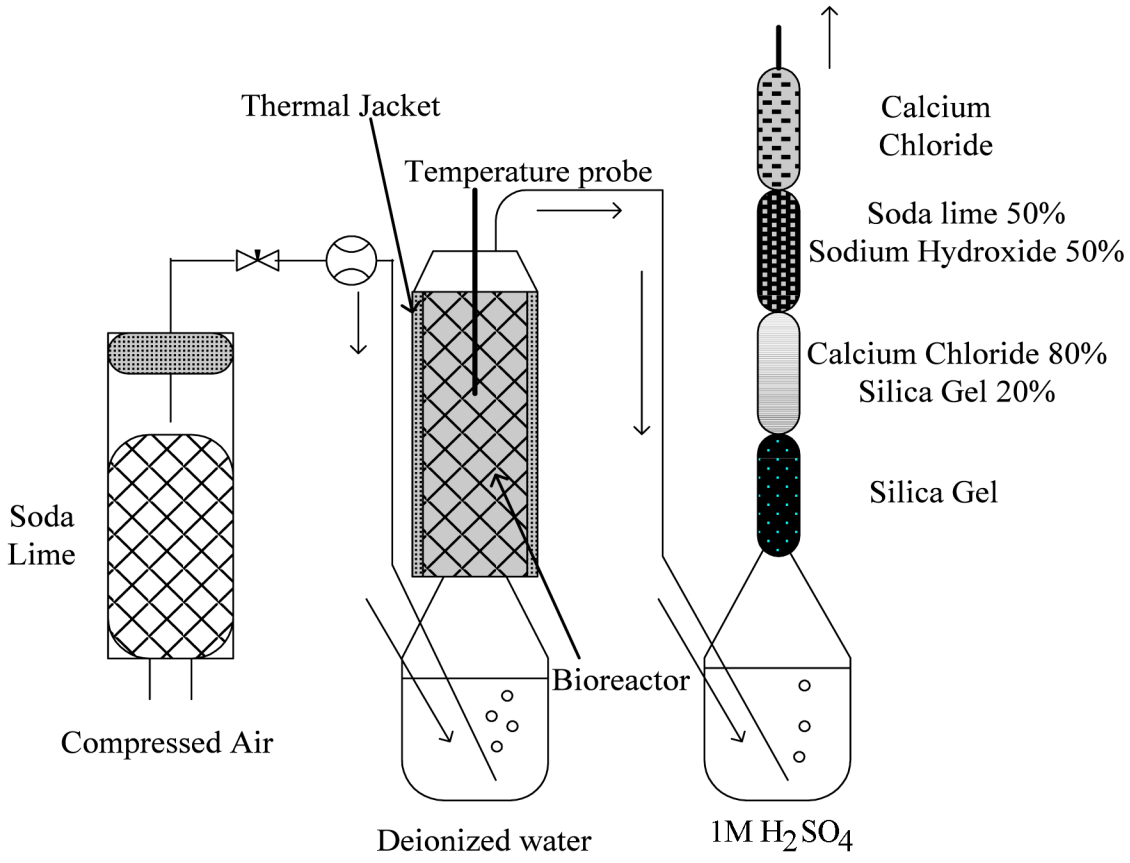

Figure 3-3. Schematic drawing of gravimetric measurement respirometric (GMR) system; published in Kale *et al.* (2007)

3.1 Description of the developed respirometric system apparatus

This instrument has the capability to simulate various testing conditions, from 0°C to an elevated thermophilic phase temperature (70°C), and can be supplied with either dry or humidified air. The system was designed to operate with up to 23 bioreactors of varying volumes (i.e. 1, 2, 3, 5 liters) at the same time, with the exhaust air cycled (diverted to a detector by a switching system) for measurement. The control software can be set to monitor the CO_2 evolved from each bioreactor independently or simultaneously. It is also possible to measure CO_2 evolved by setting the software in an automatic mode where each bioreactor will be tested at predetermined intervals throughout the duration of the experiment.

The DMR instrument can be divided into 7 major components: (1) CO_2 scrubber system, (2) relative humidity generator, (3) environmental chamber, (4) bioreactors, (5) electronic manifold valves and switching system, (6) measurement devices, and (7) control software.

3.1.1 Carbon dioxide scrubber

The ambient CO_2 present in the inlet air from an in-house compressor is removed by passing air through a parallel series of 3 cylinders, each filled with 1 lb of sodalime (total of 6 cylinders). According to calibration experiments, this scrubbing system reduces the CO_2 concentration from the 400 ppm present in the air, to approximately 0 ppm. Normal air (without CO_2 scrubbing) can be used; however, when the exhaust air

from the bioreactors is directly measured, as is the case here, the near zero baseline (from the scrubbing system) should improve the accuracy of the measurements because CO_2 free air is used to purge the detector in every measuring sequence.

3.1.2 Relative humidity (RH) generator

After the CO_2 free air enters the environmental chamber, it is separated into 2 lines. The air in the first line is humidified by bubbling through a water bottle, while that in the other line is not. Then, the air from both lines is combined, and the RH is measured by an RH sensor probe. The desired humidity can be set between 15 and 90% RH by adjusting two high precision flowmeters with needle valves (capacity of 1 L/min from Cole-Parmer, Vernon Hills, IL).

3.1.3 Environmental chamber

An environmental chamber (CARON, Marietta, OH) was used to control the temperature of the bioreactors. The chamber is capable of generating the temperature of the thermophilic phase, and also can provide a programmable temperature profile. The operating temperature range is 0-70°C, and temperature logging data was acquired by Labview software via an RS-485 interface.

3.1.4 Bioreactors

Each bioreactor (Figure 3-4) was made from a glass jar size of 0.5 gallon with an air-tight closure. A hole was drilled 1 inch from the jar bottom, and a plastic barb lure was inserted to create an air inlet port. Two aluminum screens (18 meshes) were aligned at 45° angles to form a double screen. This screen was supported by a grid (4x4 uniform

mesh of copper alloy steel). A T-shape brass fitting was installed on the lid. A rubber septum was placed on the upper end for the purpose of water, gas, or other injections. The middle end of 1/8 inches is the outlet port that was connected to an electronic manifold.

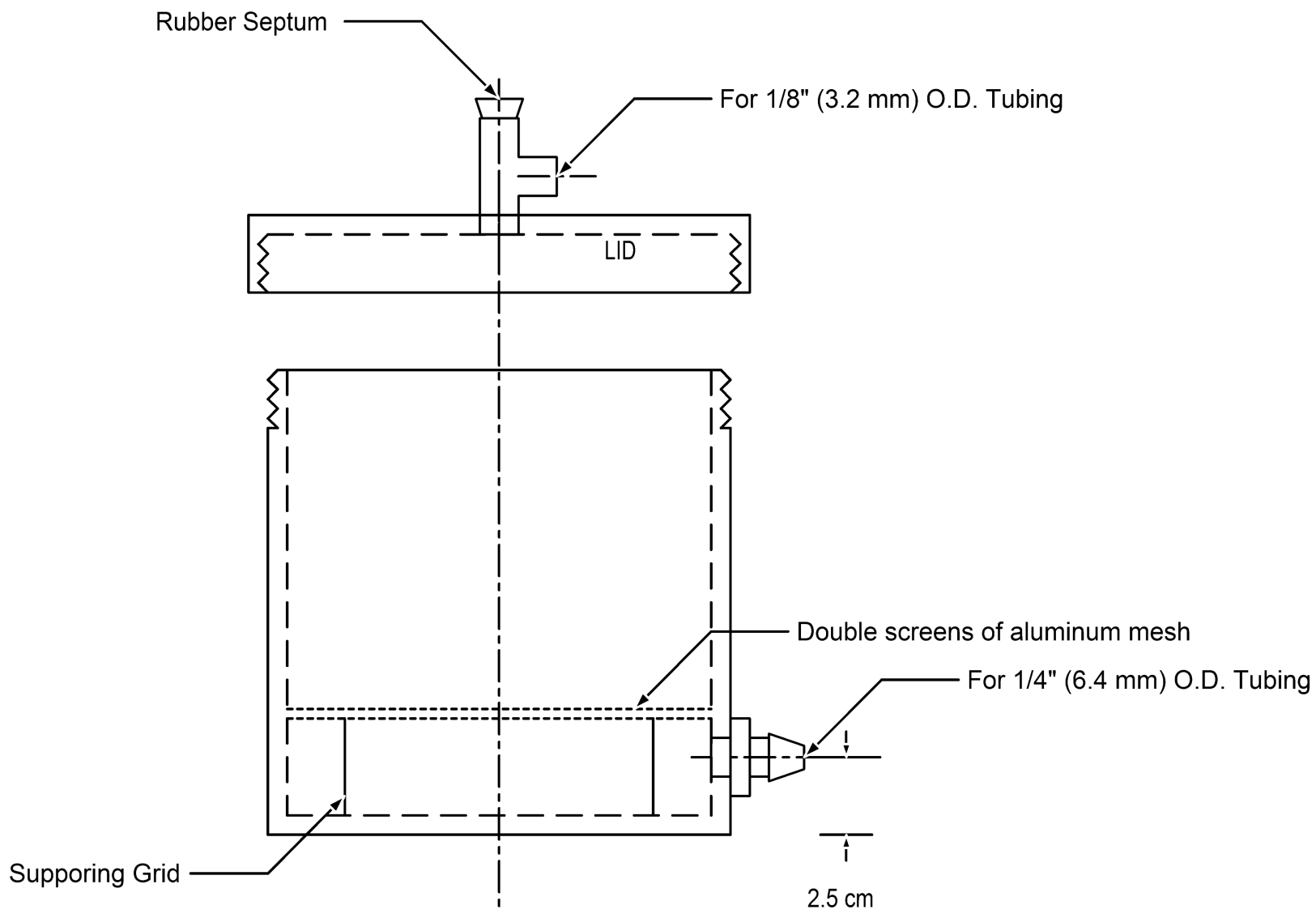

Figure 3-4. Drawing of bioreactor; published in Kijchavengkul et al. (2006)

3.1.5 Electronic manifold valves and switching system

All twenty three bioreactors and one clean air line were connected to two sets of manifolds with solenoid valves from Clippard Minimatics (Cincinnati, OH). The solenoid valves switch and direct the exhaust air from the selected bioreactor to the detector for measurement of the CO_2 concentration. The manifolds are controlled by a personal computer using a data acquisition (DAQ) device connected as an interface. These solenoid valves operate either as totally opened or closed using a digital input/output (I/O) device with 24 output channels, model NI-DAQ USB 6501 from National Instruments (Austin, TX). All the 24 solenoid valves for the 23 bioreactors and 1 clean air line via an in-house made program were controlled using Labview software, from National Instruments.

The output signal from each channel of the NI-DAQ device (5V and 8.5mA) did not have enough power to operate the solenoid valve, which requires a voltage of 6 V and power of 0.67 W. Therefore, a Negative-Positive-Negative (NPN) transistor switching circuit was introduced. Each valve is connected to a 6V external power supply and to a collector of the NPN transistor (Figure 3-5). The output signal from the NI-DAQ channel is connected to the base of the transistor via a 2200 Ω resistor (R_b). Finally, an emitter of the transistor was connected to ground (GND). To open the solenoid valve, the "1" signal or 5V DC signal (Ib) from the digital output channel of the DAQ device is sent to the transistor in order to trigger it and to allow the current from the external power supply (Ic) to pass through the solenoid valve to complete the circuit. The circuit remains incomplete or open during the "0" signal, or when no signal was sent from the NI-DAQ

device to the transistor. A total of 24 circuits were needed for this instrument. The signal sending (i.e., "1" or "0") from the NI-DAQ device to the NPN transistors was also controlled by the Labview software.

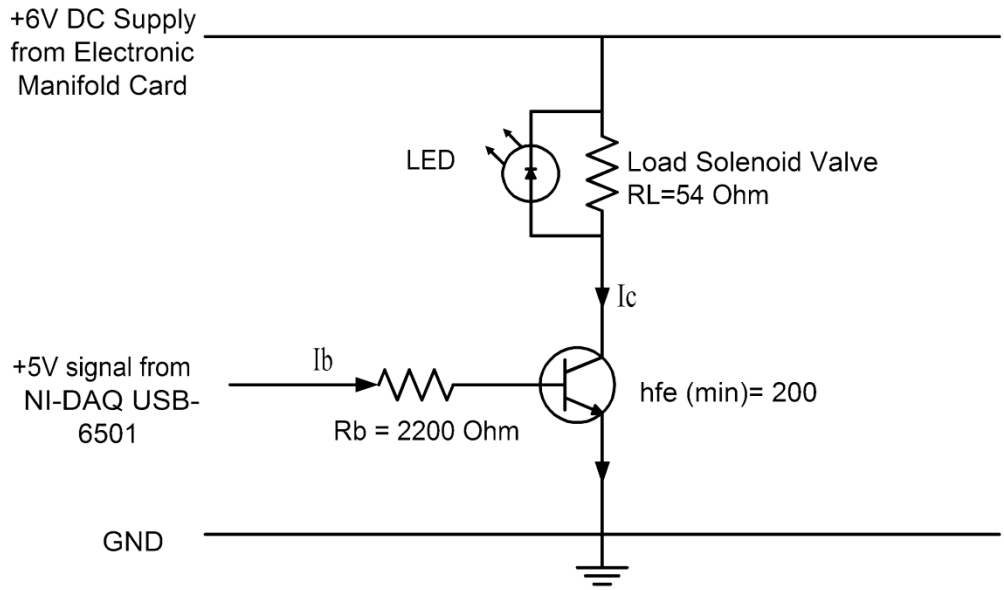

Figure 3-5. NPN switching circuit; published in Kijchavengkul *et al.* (2006)

3.1.6 Measurement devices

After the air from the selected bioreactor exits the environmental chamber, water starts to condense due to changes in the temperature of the air. For example, moisture in the air with a temperature of 58°C and 60% RH will condense if the temperature drops below 47.5°C. Water can cause damages to the detector; therefore, it was trapped in an oil-bubbler device over a water bath, model RTE-100 from Neslab Instruments Inc. (Newington, NH), operated at 15°C in order to remove any condensed water present in the air.

After passing through the oil-bubbler, the air flow rate before entering the detector was controlled by a mass flow controller (MFC) from Aalborg (Orangeburg, NY), which was connected to the computer using an RS-485 interface via the Labview program. An accurate and precise flow rate is needed for calculating the amount of carbon dioxide evolution. The amount of CO_2 dissolved in the water bath was calculated using Henry's law, and was found to be negligible compared to the CO_2 produced from the biodegradable material. The RS-485 interface allows more than one MFC to operate at the same time, providing for possible instrument expansion in the future. A non-dispersive infrared gas analyzer (NDIR), model LI-840 from LI-COR (Lincoln, NE), was used as the CO_2 detector, with measuring range of 0-3000 ppm. The detector is programmed to send the readings of CO_2, water concentration, temperature and pressure of the sensor to the computer every 2 seconds through an RS-232 interface.

3.1.7 Software

Labview software version 7.1 from National Instruments was used to control the entire instrument. Two Labview programs were written and integrated. The first program was for controlling the instrument, such as setting the measuring sequence, selecting the bioreactors to test, controlling the switching of the electronic manifold valves, controlling the flow of the gas analyzer, and acquiring the data from the gas analyzer (Figure 3-6). Another program was written for calculation purposes, such as plotting the data points (CO_2, water, and temperature) versus time, to convert the

concentration of CO_2 gas into mass, to record all the data, and to export the calculated values into spreadsheet format (Figure 3-7).

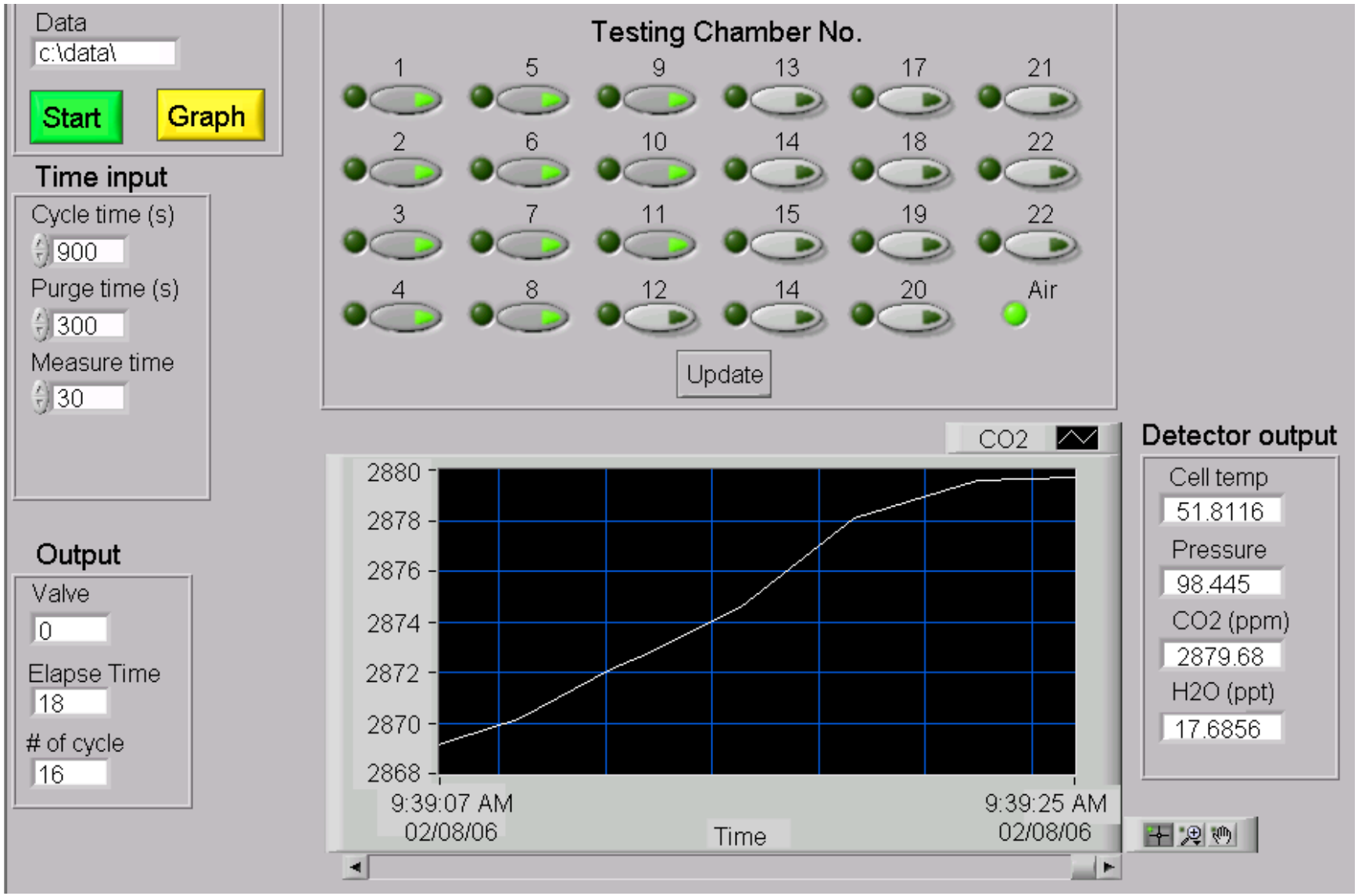

Figure 3-6. Respirometric system control program (chambercontrol.vi); published in Kijchavengkul *et al.* (2006)

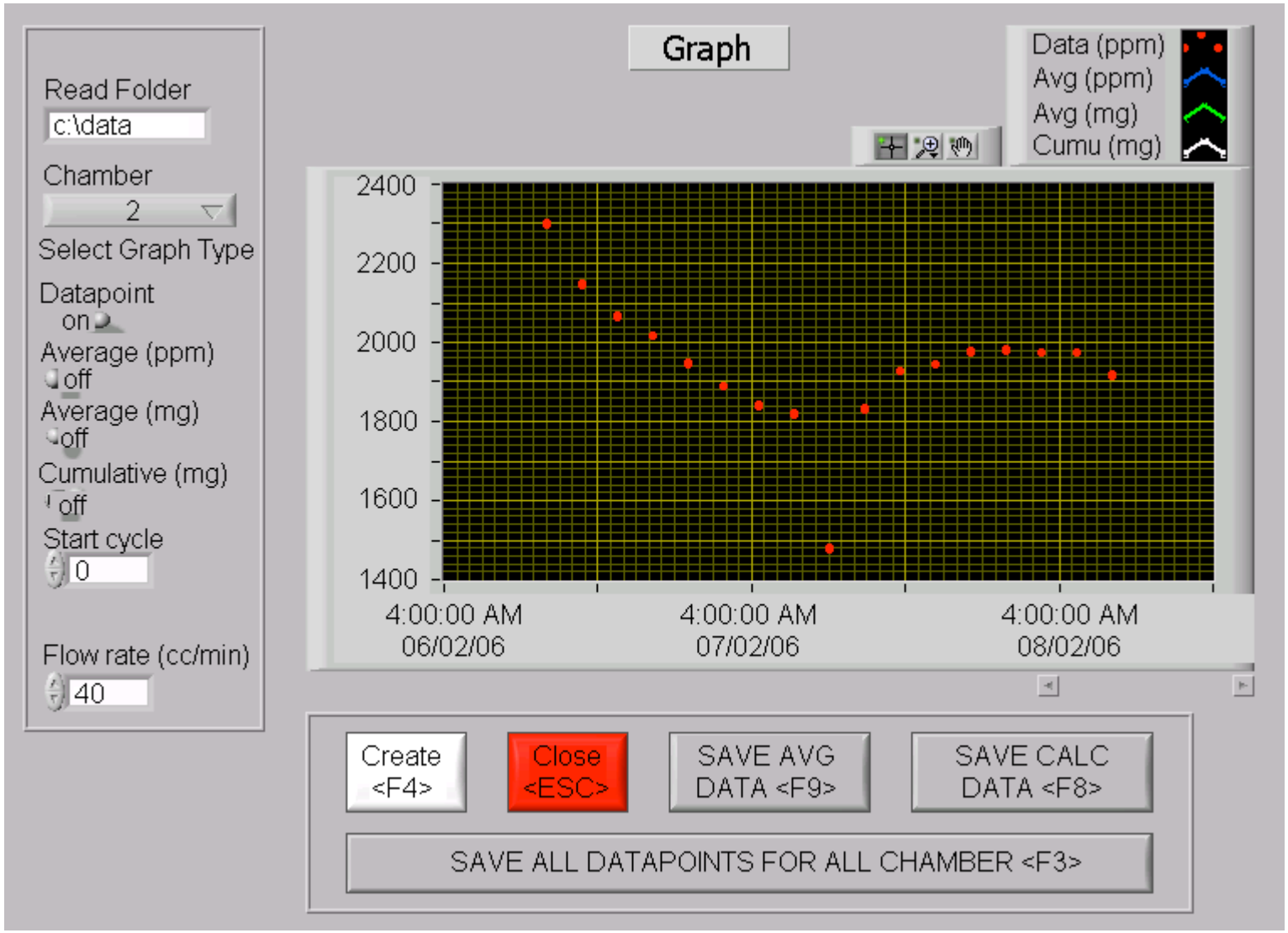

Figure 3-7. Respirometric system calculation program (graph.vi); published in Kijchavengkul *et al.* (2006)

3.2 Instrument Calibration

Although all the equipment, such as flowmeters, mass flow controller, and NDIR gas analyzer were already calibrated by their manufacturers, the complete system was calibrated as response of the detector to CO_2 can be affected by noise generated by components. To calibrate the detector, known amounts of pure CO_2 gas (0.5, 1, 2, 3, 4, 5 mL) were injected to empty reactors via septum at 58°C.

The calibration procedure was as follows:

1. Both the needle valve and solenoid valve of the injected bioreactor were closed
2. The predetermined amount of CO_2 gas was injected into the reactor via the rubber septum (Figure 3-4), and there was no air flow at this time
3. The injected CO_2 gas mixed with CO_2-free air inside the bioreactor. Therefore, the actual concentration of CO_2 in the bioreactor depended on the injection volume. Each CO_2 gas concentration was run by triplicate.
4. Next, both valves were opened, allowing air to flow through the detector at a flow rate of 40 scc/min (standard cc/min), and the time and concentration were recorded automatically by Labview (Figure 3-8). The response and peak concentration detected depended on the volume of CO_2 injected.

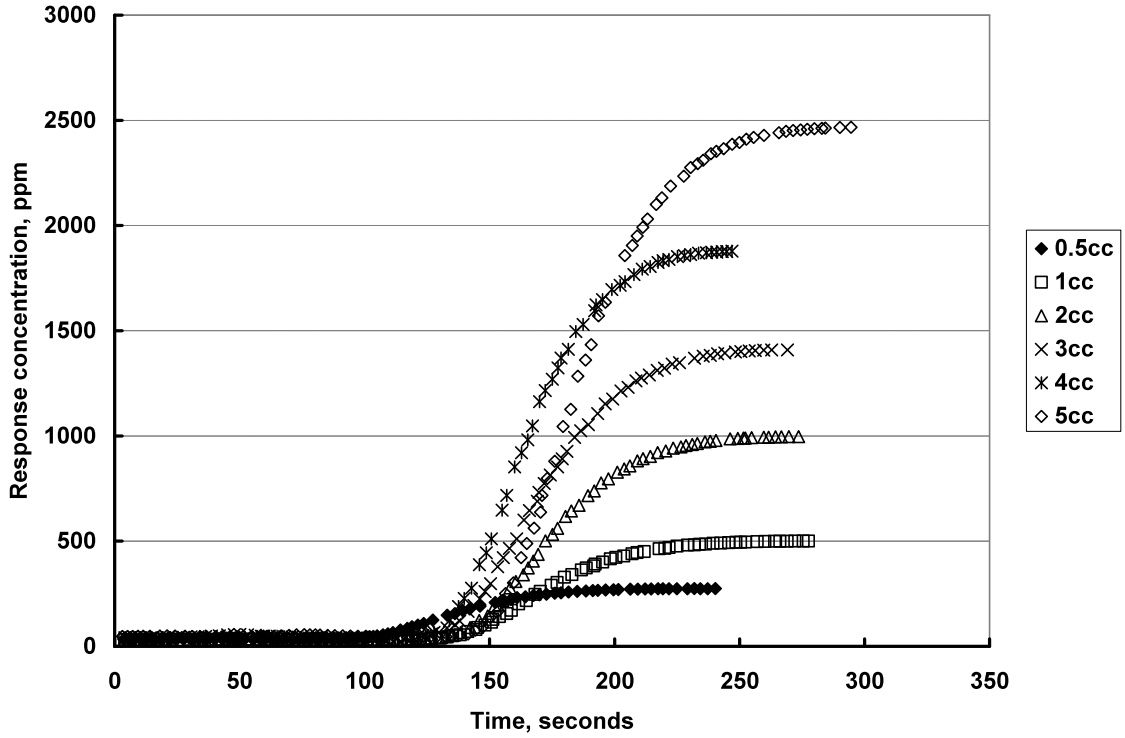

Figure 3-8. Response concentration and time required to reach the peak concentration for each injection volume; published in Kijchavengkul *et al.* (2006)

5. After the reading reached the peak value, the reactor was purged with clean air to prepare for the next injection. This cycle was repeated for each replicate and concentration.
6. Finally, the peak concentrations were plotted against the actual concentrations, which were calculated by dividing the injection volume by the total volume of the reactor. As a result, a calibration curve was generated (Figure 3-9).

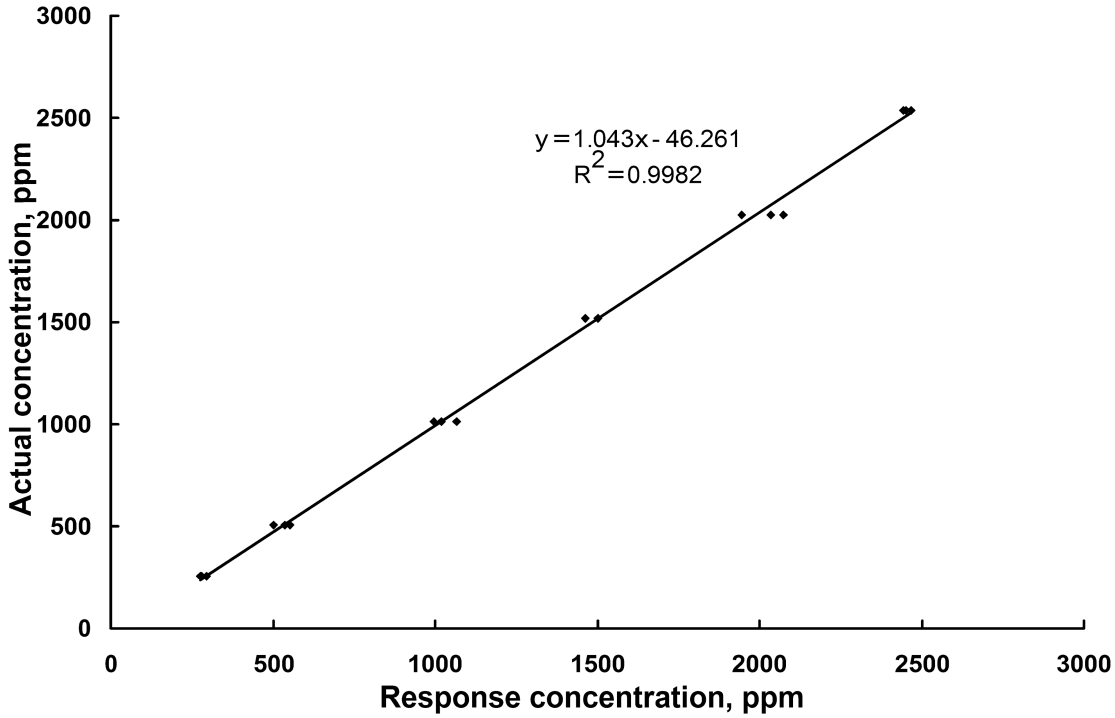

Figure 3-9. Calibration curve of actual concentration vs. response concentration at 58±2°C and flow rate of 40 scc/min; published in Kijchavengkul *et al.* (2006)

3.3 Instrument Operation

To accurately measure the CO_2 concentration of the exhaust air, the switching and measuring sequence of the bioreactor was defined as follows:

1. Each switching and measuring sequence is 15 minutes long.
2. In the first 5 minutes, the clean air valve opens, and the detector is purged with carbon dioxide free air.
3. Then, the valve for the selected chamber opens (clean air valve closed) for 10 minutes; therefore, the exhaust air of that bioreactor enters the gas analyzer, and a steady state measurement is reached.
4. In the last 30 seconds of this period after concentration reaching steady state, the readings from the gas analyzer are recorded every 2 seconds. Then, this sequence is repeated for the other bioreactors.

In order to convert concentration of CO_2 to mass, equation 3-2 is embedded in the Labview program, and the mass values are calculated automatically.

$$gCO_2 = \frac{C \cdot F \cdot t \cdot 44}{22414 \times 10^6} \tag{3-2}$$

Where gCO_2 = Mass of evolved CO_2 (g)

C = CO_2 concentration determined and corrected by the calibration curve (ppm)

F = Flow rate (scc/min)

t = Time between each measuring sequence (min)

22414 = Volume of 1 mol of gas in cc at STP

44 = Molecular weight of carbon dioxide (g/mol)

10^6 = ppm conversion factor

The values of carbon dioxide evolution for all the reactors were calculated by the Labview program were exported to Microsoft® Office Excel®, and the CO_2 evolution was plotted against time. Then, the percent mineralization was calculated using equation 3-3, based on the carbon content of each material measured by CHN analysis.

$$\%Mineralization = \frac{gCO_2 - gCO_2b}{g_{mat} \cdot \frac{\%C_{mat}}{100} \frac{44}{12}} \times 100 \qquad (3\text{-}3)$$

where %Mineralization = percent carbon molecules converted to CO_2

gCO_2-gCO_2b = mass of total evolved CO_2 minus blank CO_2(g)

g_{mat} = mass of test material (g)

$\%C_{mat}$ = % carbon content of test material

44 = molecular weight of carbon dioxide

12 = molecular weight of carbon

The standard error (S_e) of percent mineralization for each material was calculated using equation 3-4 (ASTM 2003).

$$S_e = \frac{\sqrt{\frac{s_{test}^2}{n_1} + \frac{s_{blank}^2}{n_2}}}{g_{mat}} \times 100 \quad (3\text{-}4)$$

Where S_e = Standard error (%)

s = Standard deviation of total CO_2 evolution of each material (g)

n_1, n_2 = numbers of replicate for each test material and blank

95% confident limits were calculated using equation 3-5 (ASTM 2003)

$$95\%CL = \%Mineralization \pm \left(t \times S_e\right) \quad (3\text{-}5)$$

Where t = t-distribution value for 95% probability with n_1+n_2-2 degree of freedom

3.4 Measurement of biodegradation of PLA bottles

To validate that the developed DMR was capable of producing appropriate microbial active environment and measuring biodegradation of polymer, PLA bottles were selected as the test material for the first run. PLA is certified by BPI as compostable (BPI 2008) by satisfying disintegration, biodegradation of at least 60% mineralization, and toxicity requirements.

The percentages of carbon content of corn starch, PLA, and PET, measured from their chemical structures using CHN analysis, were 44.44, 50.0, and 61.86%, respectively. The theoretical carbon dioxide evolution for each sample is shown in Table 3-1.

Table 3-1. Material weights and amount of theoretical carbon dioxide evolution for each bioreactor: CS, PLA, and PET denote corn starch, poly(lactide), and poly(ethylene terephthalate) respectively. Bioreactors No. 2, 4, and 9 contained only compost. (published in Kijchavengkul *et al.* (2006))

Bioreactor No.	Materials	Material weight (g)	Average (g)	Theoretical CO_2 content (g)
3	CS	18.1983		
6	CS	18.3959	18.5184	8.2296
8	CS	18.9610		
1	PLA	18.7650		
10	PLA	18.9055	18.8693	9.4346
11	PLA	18.9373		
5	PET	18.0518	18.2906	11.3138
7	PET	18.5294		

Since the carbon dioxide evolution of both the corn starch and the PLA samples did not reach the plateau stage after 45 days, the incubation period was extended to 63 days. At the end of the test, the mean amount of cumulative carbon dioxide of each

material was calculated and is shown in Figure 3-10. During the first 50 days, the mean carbon dioxide evolution of the corn starch sample was higher than that of PLA. After that the carbon dioxide evolution of both samples was comparable.

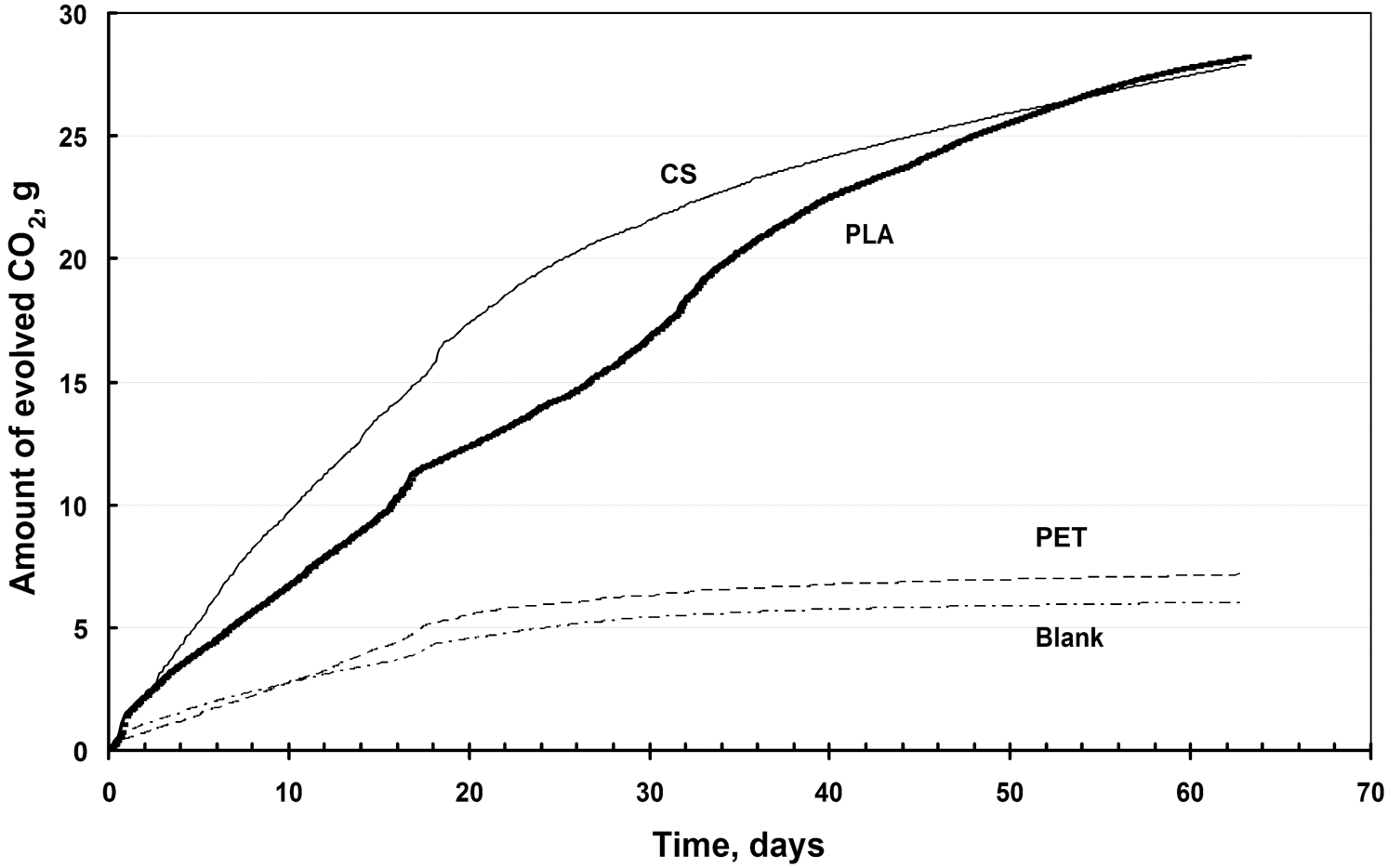

Figure 3-10. Amount of cumulative carbon dioxide evolution of PLA, PET, corn starch, and blank compost at 58±2°C and approximately 55±5% RH in yard waste compost; published in Kijchavengkul et al. (2006)

Delayed PLA biodegradation occurred because PLA has to undergo hydrolytic chain scission prior to the biodegradation process. This process was previously described by Snook (1994) as a two-stage biodegradation mechanism. In the first stage, the PLA polymer undergoes a hydrolytic degradation process, which is mainly a non-enzymatic chain scission of the ester bonds in the polymer backbone, causing a decrease in molecular weight. In the second stage, portions of the polymer chains are broken down into small fractions (or oligomers) with low molecular weight. The oligomers that diffuse out of the bulk polymer are used as food sources by microorganisms and consequently CO_2 is generated.

PET samples emitted slightly more carbon dioxide gas than the blank compost, but the difference was statistically significant with P-value < 0.05. This low emission of CO_2 may happen because PET contained ester bonds which are hydrolyzable.

The percentage of mineralization at 63 days with 95% confidence limit of PLA, corn starch, and PET were 64.2±0.5, 72.4±0.7, and 2.7±0.2%, with standard errors of 6.75, 10.56, and 3.42%, respectively, calculated from equations 3-4 and 3-5 (Figure 3-11). Based on ASTM D6400, the PLA bottle satisfied the biodegradation criterion since the % mineralization was greater than 60% and that of the positive control (corn starch) was also greater than 70%.

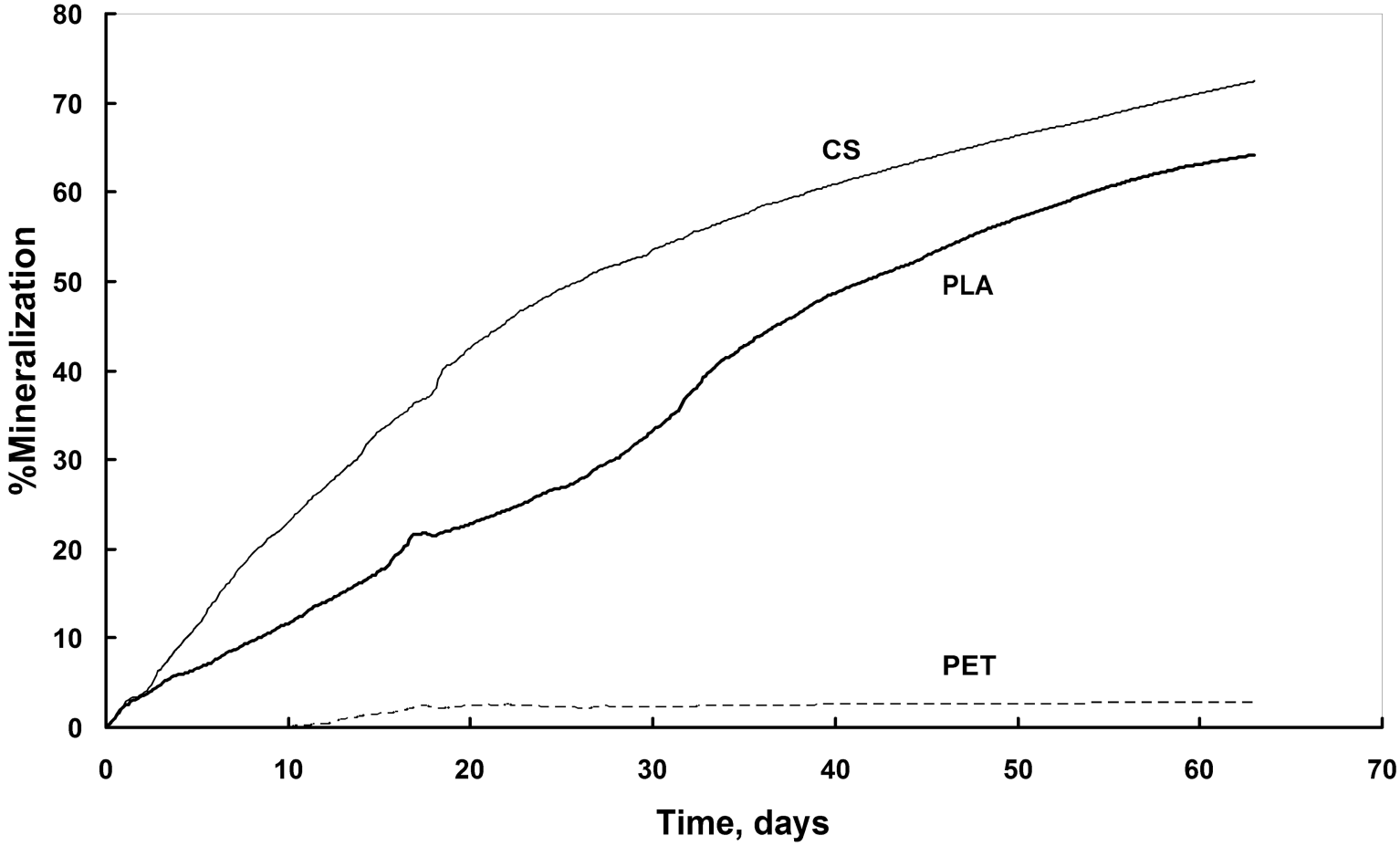

Figure 3-11. Percentage of mineralization of PLA, PET, and corn starch at 58±2°C and approximately 55±5% RH in yard waste compost; published in Kijchavengkul *et al.* (2006)

The in-house DMR system was capable of measuring polymer biodegradability by quantifying the amount of carbon dioxide evolved during biodegradation. This system facilitates biodegradation testing by eliminating human intervention and errors especially from titration. The data were easily interpreted since they were already converted from concentration to mass of carbon dioxide evolution and mineralization by the Labview programs, and there was no further conversion and calculation required, unlike the CMR that requires a titration method. The main drawbacks of this system were the higher initial cost and the time-consuming process of programming Labview.

REFERENCES

REFERENCES

ASTM (2003) D 5338-98(2003) standard test method for determining aerobic biodegradation of plastic materials under controlled composting conditions. West Conshohocken, PA, ASTM International.

BPI. (2008). "Approved products — resins." Retrieved Oct 17, 2008, from http://www.bpiworld.org/BPI-Public/Approved/3.html.

Funabashi, M, Nimomiya, F and Kunioka, M (2007). "Biodegradation of polycaprolactone powders proposed as reference test materials for international standard of biodegradation evaluation method." Journal of Polymers and the Environment **15**: 7-17.

Grima, S, Bellon-Maurel, V, Feuilloley, P and Silvestre, F (2000). "Aerobic biodegradation of polymers in solid state conditions: A review of environmental and physiochemical parameter settings in laboratory simulations." Journal of Polymers and the Environment **8**(4): 183-195.

ISO (2005) 14855-1 determination of the ultimate aerobic biodegradabilty and disintergration of plastic materials under controlled composting conditions-method by analysis of evolved carbon dioxide. Geneva, Switzerland, International Organization for Standardization.

ISO (2006) 14855-2 determination of the ultimate aerobic biodegradability of plastic materials under controlled composting conditions - method by analysis of evolved carbon dioxide. Part 2: Gravimetric measurement of carbon dioxide evolved in a laboratory scale test. (under development). Geneva, Switzerland, International Organization for Standardization.

Kale, G, Kijchavengkul, T and Auras, R (2007). New trends in assessment of compostability of biodegradable polymeric packages. Leading-edge Environmental Biodegradation Research. L E Pawley ed. Hauppauge, NY, Nova Science Publishers**:** 297-315.

Kijchavengkul, T, Auras, R, Rubino, M, Ngouajio, M and Fernandez, RT (2006). "Development of an automatic laboratory-scale respirometric system to measure polymer biodegradability." Polymer Testing **25**(8): 1006-1016.

Kunioka, M, Nimomiya, F and Funabashi, M (2006). "Biodegradation of poly (lactic acid) powders proposed as the reference test material for the international standard of biodegradation evaluation methods." Polymer Degradation and Stability **91**: 1919-1928.

Snook, JB (1994) Biodegradability of polylactide film in simulated composting environments. Department of Chemical Engineering. East Lansing, Michigan State University. Master thesis.

Chapter 4 Techniques of differential scanning calorimetry (DSC) and Fourier transform infrared (FTIR) spectroscopy to measure degree of crosslinking in polymer structure

Polymers with chromophoric groups, such as carbonyl group in ester, are highly susceptible to photodegradation, causing chain scission and resulting in generation of free radicals. Under UV exposure associated with temperature, the degradation of aromatic polyesters, such as PBAT can happen from chain scission and crosslinking due to the recombination of the free radicals at the aromatic structures. This photodegradation promotes a reduction on mechanical properties of the polymer. For agricultural applications, such mulch films, a decrease in mechanical properties means inferior performance by compromising the strength and integrity of the material.

Currently, gel content (X_g), which is a ratio of the portion of polymer that not dissolved in solvent or 'gel', while the portion of the polymer that dissolved in solvent is called 'sol', to the total weight of polymer excluding the filler, is used as one of the tools in measuring the degree of crosslinking within the polymer films. Typically, the gel content is measured according ASTM D 2765 (ASTM 2006), but the disadvantages of this test method are that the testing procedure is a time-consuming process and the solvents used in the standard test method, such as xylene, are dangerous to work with. Therefore, new techniques to measure and detect crosslinking are highly desirable.

Crosslinking of films cause non-uniformity of the crystal lattices, making them melt at different temperature (Ioan *et al.* 2001). The DSC thermogram of polymer with higher degree of crosslinking should indicate a broader melting peak and a lower onset temperature than sample with lower degree of crosslinking (Hullihen 2006). Furthermore, the kinetic of the crosslinked films can be studied using the Avrami equation by observing the changes in gel content and the changes in onset temperature of the melting peak.

On the other hand, crosslinked samples tested with FTIR spectrophotometer should show changes of the absorbance intensities of the functional groups that related to the crosslinking, such as esters and substitutes of benzene. Any changes occurred in those functional groups and their structure could be detected by FTIR. Therefore, the crosslinking of the samples could be monitored by the changes in the polymer functional groups. For example, in aromatic polyesters such as PBAT crosslinking might be caused by a recombination of the generated phenyl radicals of the 1, 3 meta disubstitute benzene and the 1, 2, 4 trisubstitute benzene (Figure 2-7) from hydrogen abstraction induced by other free radicals created from photodegradation via Norrish I process (Buxbaum 1968; Rivaton and Gardette 1998; Schnabel 1992). Therefore, the objective of the study in this chapter was to use and to compare two new methods in measuring the gel content of aromatic polyester films using differential scanning calorimetry (DSC) and Fourier transform infrared spectrophotometry (FTIR).

4.1 Film treatments

PBAT film samples used in this experiment were provided by Northern Technologies International, Inc. (Circle Pines, MN). The film samples (9.8 cm x 6.5 cm) with different degree of crosslinking (gel contents of 0, 10, 30, 50, and 70%) were produced at by being exposed to UV-A light using 8 UVA-340 lamps (wavelength of 340 nm) from Q-Panel Lab (Cleveland, OH) in the QUV Accelerated Weathering Tester(Q-Panel Lab, Cleveland, OH) at an irradiance level of 1.40 $W/m^2/nm$ for different predetermined times (0, 2.5, 6, 10, and 12 hrs) An UV-A lamp was used instead of UV-B since it had UV spectrum closer to the UV spectrum from solar radiation than that of UV-B.

4.2 Actual gel content measurement

The gel content of the film samples were measured according to the standard ASTM D 2765 using tetrahydrofuran (THF) as the solvent. The gel content was calculated using equations 4-1 to 4-3. The actual gel contents from UV exposed PBAT samples are shown in Table 4-1.

$$\%Extract = \frac{W_s - W_d}{f \cdot W_s} \times 100 = \frac{W_s - W_d}{(1 - F) \cdot W_s} \times 100 \quad (4\text{-}1)$$

$$f = 1\text{-}F = \frac{Total\ Sample Weight - Filler Weight}{Total\ Sample Weight} \quad (4\text{-}2)$$

$$\%Gel\ content = 100 - \%Extract \quad (4\text{-}3)$$

where

W_s = Weight of the specimen being tested

W_d = Weight of dried gel

f = Polymer fraction (the ratio of the weight of the polymer in the formulation to the total weight of the formulation)

F = Fraction of filler

Table 4-1. Gel contents of the film samples exposed to UV-A at different predetermined times measured by ASTM D 2765; published in Kijchavengkul *et al.* (2008).

Exposure Time, hours	Gel content, %
0	0.00 ± 0.00^{a}
2.5	9.56 ± 2.80^{b}
6	33.71 ± 1.89^{c}
10	51.68 ± 5.60^{d}
12	66.95 ± 2.56^{e}

Note: Numbers followed by the same letter within a column are not statistical significantly different at $P\leq0.05$ (t-test with Fisher LSD)

4.3 Fourier Transform Infrared Spectrophotometry (FTIR)

For each film, three samples were scanned using a Shimadzu IR-Prestige 21 (Columbia, MD) with an Attenuated Total Reflectance (ATR) attachment from PIKE Technologies (Madison, WI) from wave number of 4000 to 650 cm^{-1} to measure any changes in the spectra intensities which correlated to the formation and destruction of functional groups in the films.

Figure 4-1 represents the FTIR spectra of the PBAT samples with different gel contents. The main functional groups of PBAT can be described as: peaks at 3000 cm^{-1} represented C-H stretching in aliphatic and aromatic portions; peak at 1710 cm^{-1} represented carbonyl group (C=O) in the ester linkage; peak at 1267cm^{-1} represented C-O in the ester linkage; sharp peak at 720 cm^{-1} represented four or more adjacent methylene ($-CH_2-$) groups. Bending peaks of the benzene substitutes are located at wave number between 700 and 900 cm^{-1}.

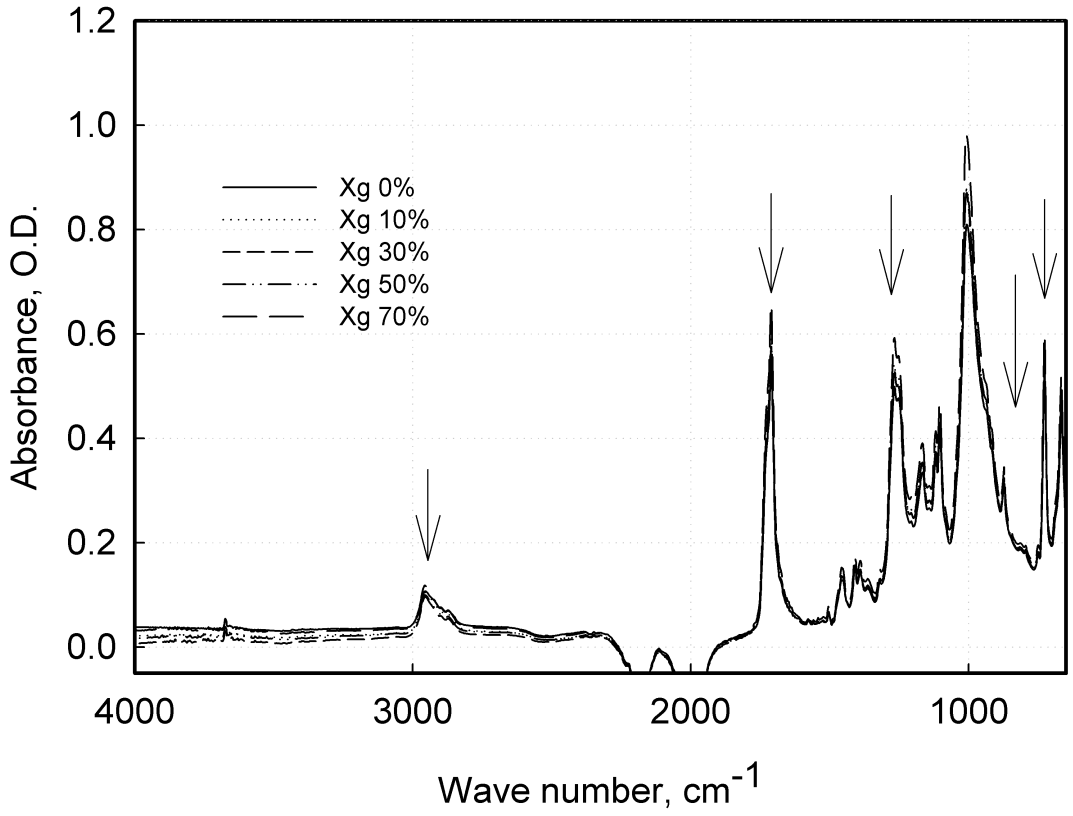

Figure 4-1. Full FTIR spectra of the samples with 0, 10, 30, 50, and 70% gel contents; published in Kijchavengkul *et al.* (2008).

In the case of PBAT, crosslinking happened due to the recombination of the generated free radicals of the 1, 3 meta disubstitute benzene and the 1, 2, 4 trisubstitute benzene (more detail in section 2.5.2.3). FTIR spectra at wave number of 780-820 cm^{-1} indicated the increasing in absorbance of the 796 cm^{-1} peak (correspond to 1,2,4 trisubstitute benzene) with the increasing level of gel contents in the samples (Figure 4-2). Then, the gel contents of the samples were plotted against the absorbance at 796 cm^{-1} and a sigmoid relationship between gel content and absorbance was observed (Figure 4-3). An empirical fitted equation with R^2-value of 0.9913 is shown in equation 4-4.

$$X_g = \frac{67.27}{1+\left(\frac{A}{A_O}\right)^{-231.0}} \quad (4\text{-}4)$$

Where

X_g = Gel content (%)

A = Absorbance of the tested sample

A_o = Absorbance of the sample with 0% gel content

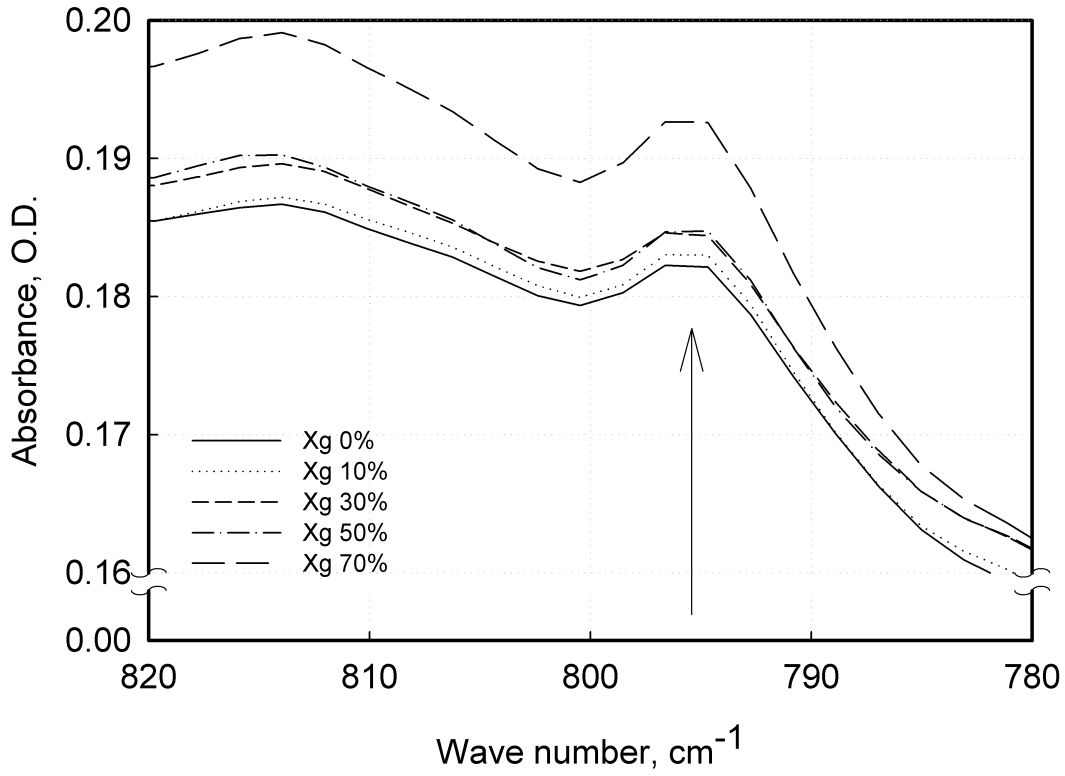

Figure 4-2. FTIR spectra showing the increasing in absorbance at 796 cm^{-1} with increasing gel contents; published in Kijchavengkul *et al.* (2008).

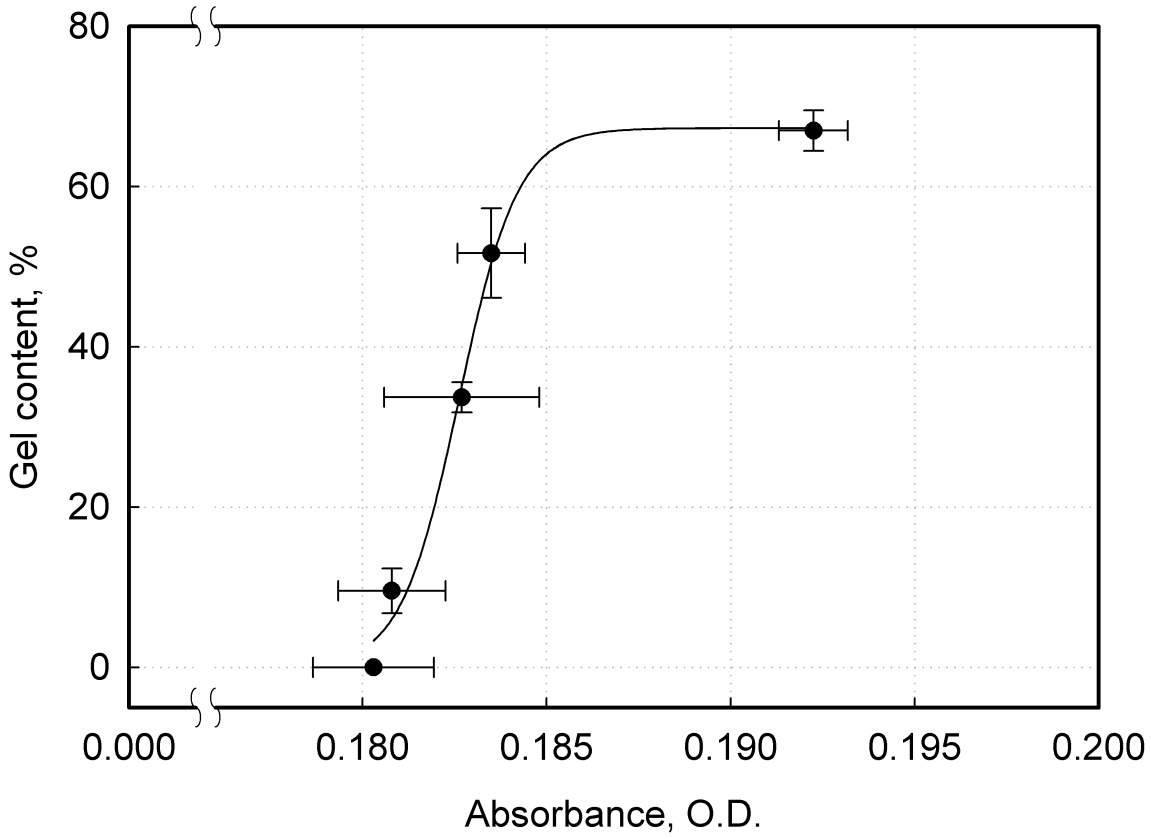

Figure 4-3. Plot of gel contents vs. absorbance at 796 cm^{-1}; Error bars represents standard deviations of the gel content and the absorbance from the 3 replicates; published in Kijchavengkul *et al.* (2008).

4.4 Differential scanning Calorimetry (DSC)

Glass transition (T_g) and melting (T_m) temperatures of the PBAT films were measured using a Differential Scanning Calorimeter (DSC) model Q 100 from Thermal Analysis Inc (New Castle, DE). The sample size used was approximately 5-10 mg. The testing temperature was from -60 to 160°C with a ramping rate of 10°C/min, according to ASTM D 3418 (ASTM 2003). Three samples were used for each gel content sample.

The relationship between the difference in the onset time of the melting peak (between the unexposed and the exposed samples) and the gel content of the film at different time was fitted by the Avrami equation 4-5.

$$-\ln(1 - X_g) = k\Delta t^n \qquad (4\text{-}5)$$

Where

X_g = Gel content

k = Rate constant

Δt = Difference of the onset time of the melting peak between the unexposed and the exposed samples

n = Avrami exponent

From DSC thermogram, the onset melting time is the time at the onset melting temperature, where a change in the slope of the melting peak occurred, which is defined as the temperature at the intersection of an initial tangent line (horizontal baseline) with a

final tangent line (Figure 4-4). If the melting temperature were the same, the sample with lower onset time will have broader melting peak. The onset time and the onset time difference (Δt) between exposed and unexposed samples are shown in Figure 4-4. Then, the $-ln(1-X_g)$ is plotted against the onset time difference (Δt) and the Avrami equation is used to fit the data points from Table 4-2 (Figure 4-5). Equation 4-6 represented the Avrami fitted equation with R^2-value of 0.9980.

$$-\ln(1-X_g) = 0.5415\Delta t^{0.7058} \tag{4-6}$$

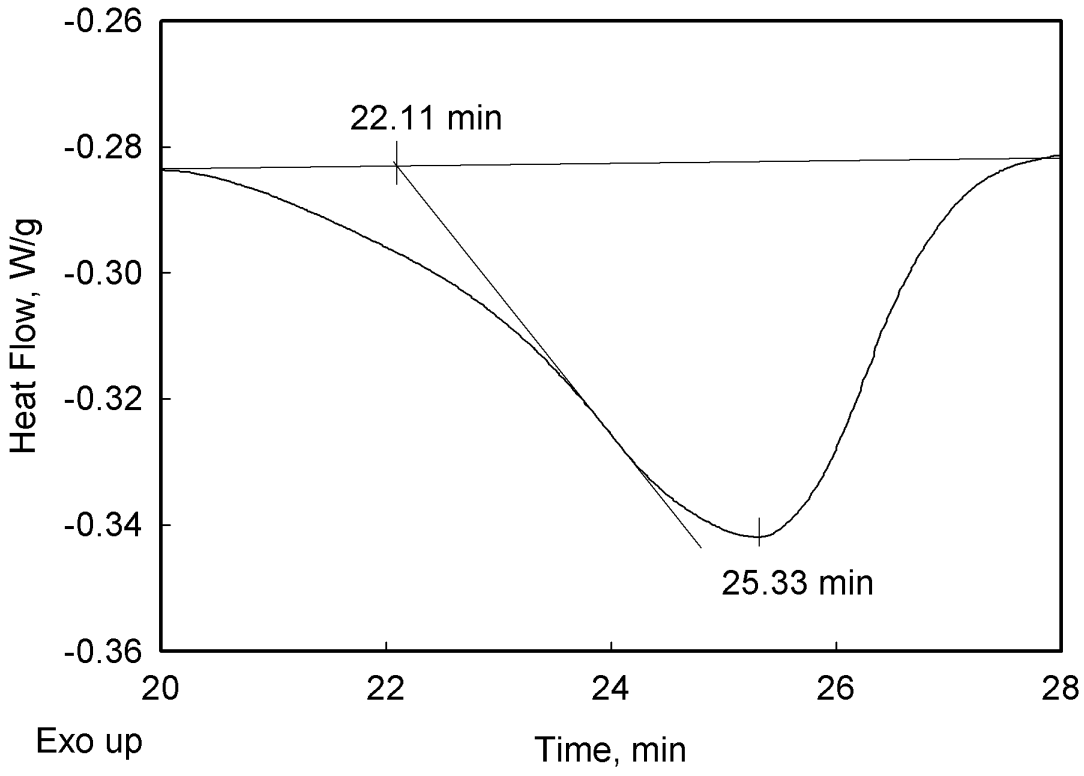

Figure 4-4. Onset time of the melting peak in DSC thermogram for samples with 0% gel content. In this case, onset time equals 22.11 min; published in Kijchavengkul *et al.* (2008).

Table 4-2. Onset time of the melting peak and the difference between the unexposed and the exposed samples; published in Kijchavengkul *et al.* (2008).

Gel content, %	Onset time, min	*Δt*, min *
0	22.1056	0.0012
0	22.0984	0.0084
0	22.1100	-0.0032**
9.56	22.0274	0.0794
9.56	22.0223	0.0845
9.56	22.0186	0.0882
33.71	21.4126	0.6942
33.71	21.4830	0.6238
33.71	21.3619	0.7449
51.68	20.6436	1.4632
51.68	20.5243	1.5825
51.68	20.5997	1.5071
66.97	19.2699	2.8369
66.97	19.3327	2.7741
66.97	19.4683	2.6385

Note: *Δt values were calculated by subtracting the onset time with the average of three onset times at 0% gel content, which was 22.1047 min.

** This negative value was discarded for the Avrami calculation.

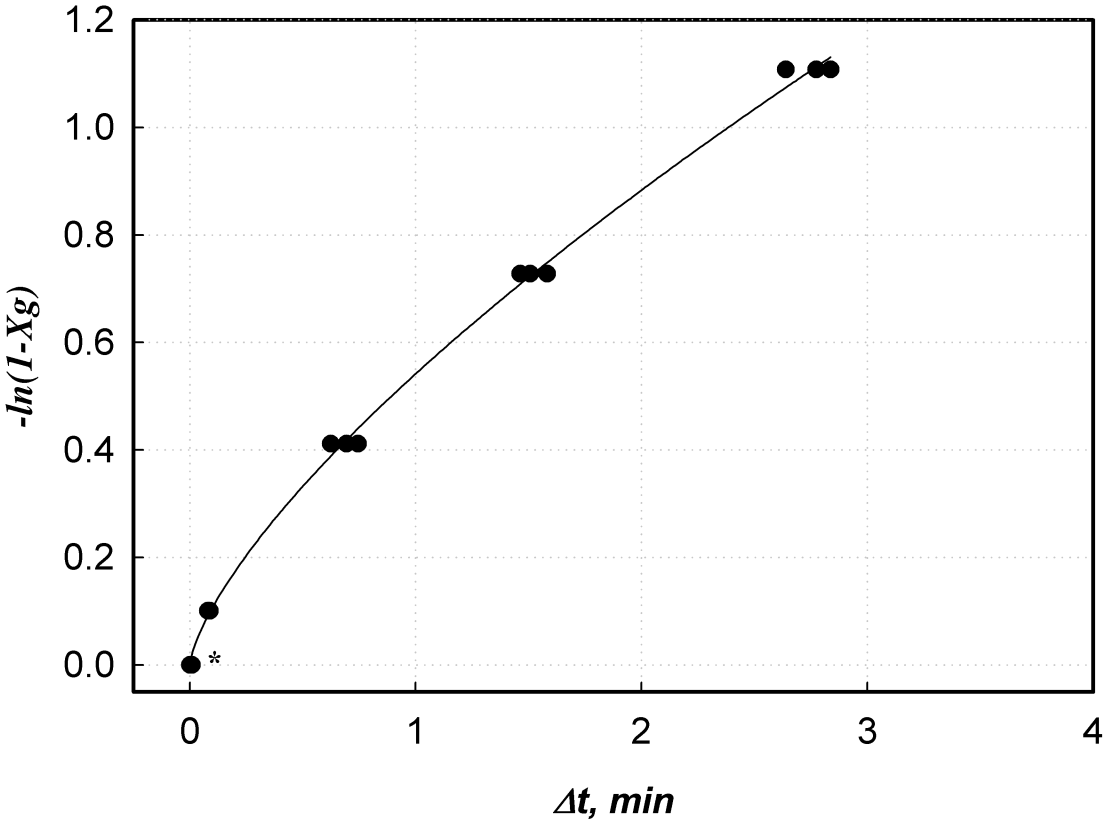

Figure 4-5. Avrami Plot and fitted line of $-ln(1-X_g)$ versus onset time differences (Δt) between the unexposed and the exposed samples. * Represented only 2 data points, since one onset time difference with negative value was discarded; published in Kijchavengkul *et al.* (2008)

The predicted gel contents calculated from the empirical FTIR equation (equation 4-4) and from the DSC Avrami equation (equation 4-6) are shown in Table 4-3 along with the actual values measured by ASTM D 2765. The Avrami model seems to be a better model, since its predicted values were closer to the actual ones with less variability than those of empirical FTIR model based on absorbance at 796 cm^{-1} peak. The empirical FTIR was likely to mispredict at low gel contents (X_g < 30%), while both models were accurately predicted at high gel contents (X_g > 30%). In addition, there were

large variability in the absorbance from the samples with gel contents of 30% and lower (Figure 4-3), possibly due to the fact that FTIR with ATR attachment only measured the functional groups in small areas of non-homogeneity of the film samples from crosslinking, which may cause the misprediction in the FTIR model.

Table 4-3. Comparison between predicted gel content values from empirical FTIR and DSC Avrami methods and actual gel contents measured according ASTM D 2765; published in Kijchavengkul *et al.* (2008).

Actual gel content, %	**FTIR predicted gel content, %***	**DSC Avrami predicted gel content, %****
0.00 ± 0.00^{a}	3.42 ± 1.29^{b}	0.70 ± 0.97^{a}
9.56 ± 2.80^{a}	6.19 ± 2.15^{a}	9.00 ± 0.32^{a}
33.71 ± 1.89^{a}	35.76 ± 4.55^{a}	34.01 ± 1.72^{a}
51.68 ± 5.60^{a}	50.92 ± 3.19^{a}	51.66 ± 0.98^{a}
66.95 ± 2.56^{a}	67.27 ± 0.01^{a}	66.90 ± 0.96^{a}

Note: *Calculated using equation 4-4

**Calculated using equation 4-6

Numbers followed by the same letter within a row are not statistical significantly different at $P \leq 0.05$ (t-test with Tukey adjustment)

REFERENCES

REFERENCES

ASTM (2003) D 3418-03 standard test method for transition temperatures and enthalpies of fusion and crystallization of polymers by differential scanning calorimetry. West Conshohocken, PA, ASTM International.

ASTM (2006) D 2765-01 standard test methods for determination of gel content and swell ratio of crosslinked ethylene plastics. West Conshohocken, PA, ASTM International.

Buxbaum, LH (1968). "The degradation of poly(ethylene terephthalate)." Angewandte Chemie-International Edition **7**(3): 182-190.

Hullihen, K (2006). "Determining gel content of polyethylene using a differential scanning calorimeter." Industrial and Engineering Chemistry Research **45**(18): 6095-6098.

Ioan, S, Grigorescu, G and Stanciu, A (2001). "Dynamic-mechanical and differential scanning calorimetry measurements on crosslinked poly(ester-siloxane)-urethanes." Polymer **42**(2001): 3633-3639.

Kijchavengkul, T, Auras, R and Rubino, M (2008). "Measuring gel content of aromatic polyesters using FTIR spectrophotometry and DSC." Polymer Testing **27**(1): 55-60.

Rivaton, A and Gardette, J-L (1998). "Photo-oxidation of aromatic polymers." Angewandte Makromolekulare Chemie **261/262**(1): 173-188.

Schnabel, W (1992). Polymer Degradation: Principles and Practical Applications. New York, NY, Hanser.

Chapter 5 Determination of the performance of the commercial and biodegradable mulch films under field and laboratory studies

5.1 Field experiment

In a field study, black and white PBAT films with different thickness (25 and 35 μm) were used as biodegradable mulch film for covering the beds of tomato plots in the state of Michigan (42°44' N, 84°29' W) during the months of May through September, 2006 and May through September, 2007. A Latin square plot layout with 4 or 5 blocks were used for statistical analysis (Figure 5-1). The results were compared to that of conventional LDPE mulch film (M). Every week the changes in the physical appearance of the films and tomato plants were visually observed and recorded. Every two weeks, film samples were taken from no-crop plots, from which that the films can be extracted. Mechanical, optical, physical, and thermal properties were characterized and plotted as a function of time. Furthermore, biodegradation tests of the mulch film samples were conducted in laboratory conditions, based on ASTM standards (ASTM 2003; ASTM 2004) using and using a direct measurement respirometric (DMR) system. Detail of the DMR apparatus was described later in Chapter 3.

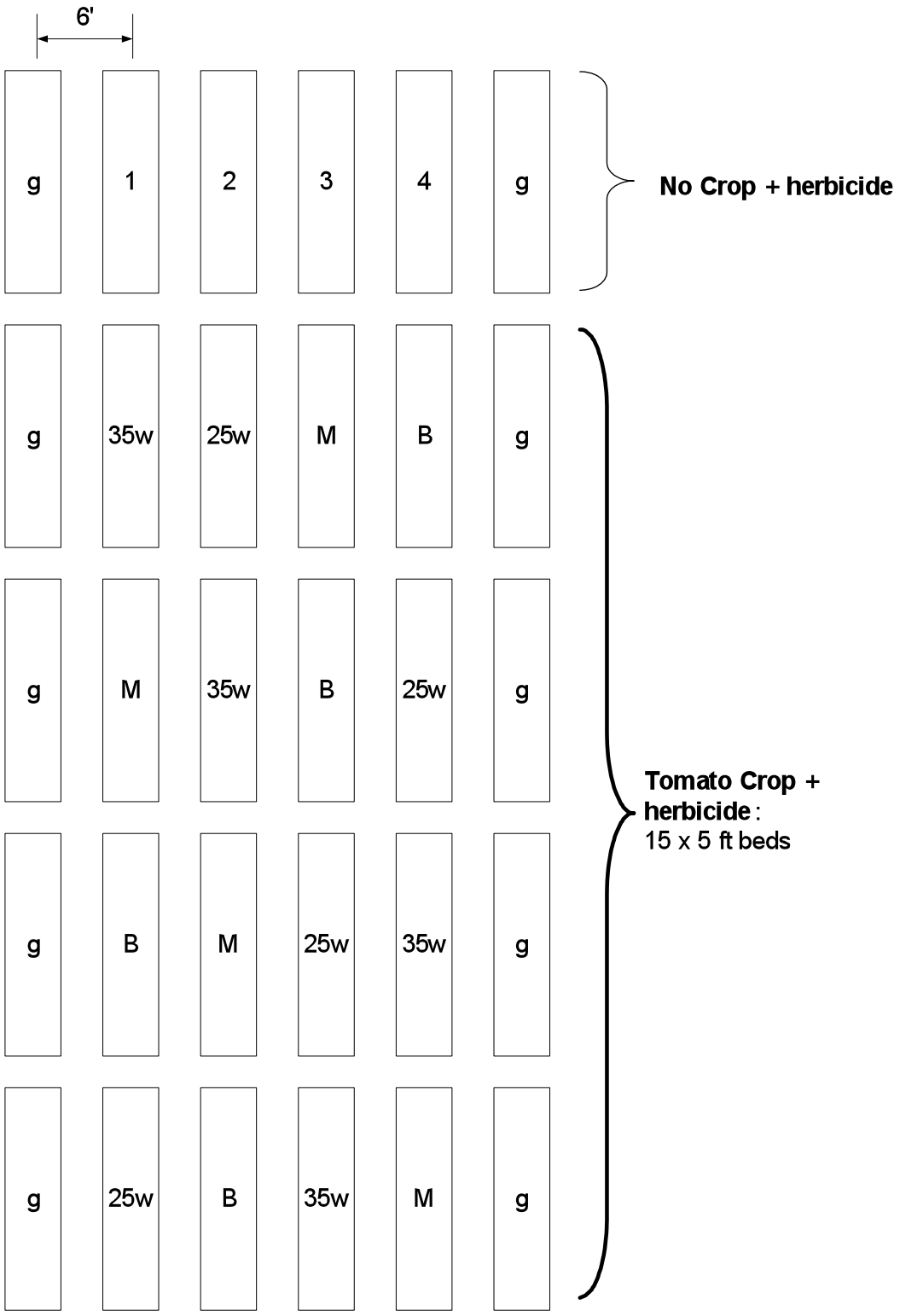

Figure 5-1. Latin square experimental plot layout with four blocks, where g = guard row (data were not collected from these plots); 25w = 25 µm PBAT film; 35w = 35 µm PBAT film; B = black PBAT film; and M = black LDPE film

5.1.1 Visual observation

It was visually observed that both of the white films degraded faster than the black film. The white films started breaking down and forming cracks within the first two weeks of testing (Figure 5-2) while the black biodegradable film started breaking down slowly at around 8th week (Figure 5-3). The LDPE film did not show any visual degradation during the test period.

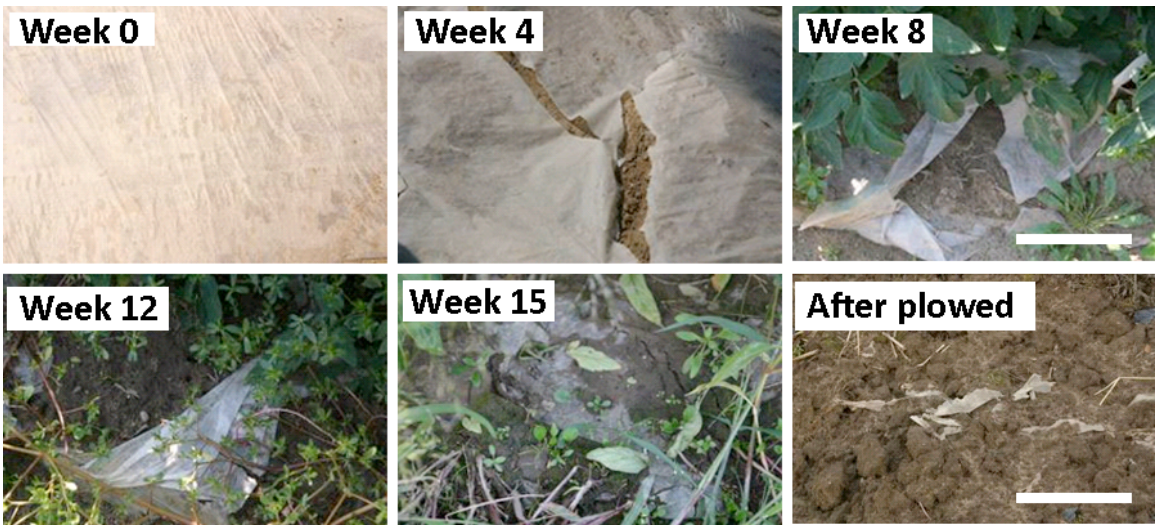

Figure 5-2. Pictures of the white PBAT films during and after the growing season (Bar length equals 5 cm); published in Kijchavengkul *et al.* (2008a)

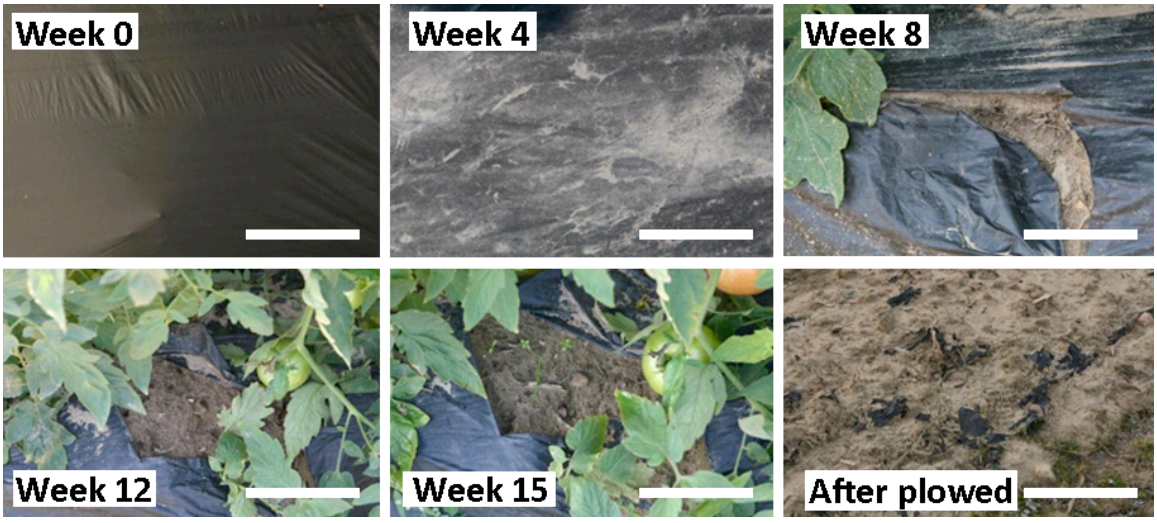

Figure 5-3. Pictures of the white PBAT films during and after the growing season (Bar length equals 5 cm); published in Kijchavengkul *et al.* (2008a)

5.1.2 Light transmission

One of the main requirements for mulch films to perform in the field is the suppression of weed germination through the low transmission of visible light in the ranges of 400 nm to 700 nm wavelengths, which is the Photosynthetically Active Radiation range or PAR range (Ngouajio and Ernest 2004). The percentage of light transmissions of the white PBAT films decreased throughout the experiment from 93% at 0^{th} week to 81% at 8^{th} week, but no change was observed from the black PBAT and LDPE films (Figure 5-4). Percent light transmission within the PAR range for both PBAT and LDPE films were below 5% during the whole field test. The white films could not prevent weed growth, which may contribute to the disintegration of the film since weeds were able to penetrate/protrude the films and create cracks, since white PBAT films still had very high % light transmission rates (all above 80%).

Weed control performance of both black PBAT and LDPE were not statistically different (all above 94%, where 100% means no weed was observed in the plots), while the percent weed control of white PBAT films were less than 35% (Ngouajio *et al.* 2008) (Table 5-1). Ngouajio and Ernest (2004) reported in their study done in the tomato plots at Benton Harbor, MI that the mulch films with higher % light transmission were correlated with the greater weed density and weed biomass. This premature breakdown of the films is a serious drawback for the implementation of mulch films since it allows the visible light to pass through which in turn allows the growth of weeds. Besides, the films lost their ability to cover the soil, to prevent soil moisture loss and to alter soil temperature.

Both black PBAT films (25 and 35 μm) used in the 2007 season had significantly higher % light transmission compared to that used in 2006 (Figure 5-5). The initial % light transmissions of both films were 21.7 and 19.7%, respectively, while that used in 2006 was below 5%. The differences in the % light transmission between the films used in 2006 and 2007 were due to the changes of formulation from the film manufacturer (Northern Technologies International, Inc., Circle Pines, MN). However, both films were able to provide the same level of weed control as the LDPE mulch film with type I error of 0.05 (Table 5-1).

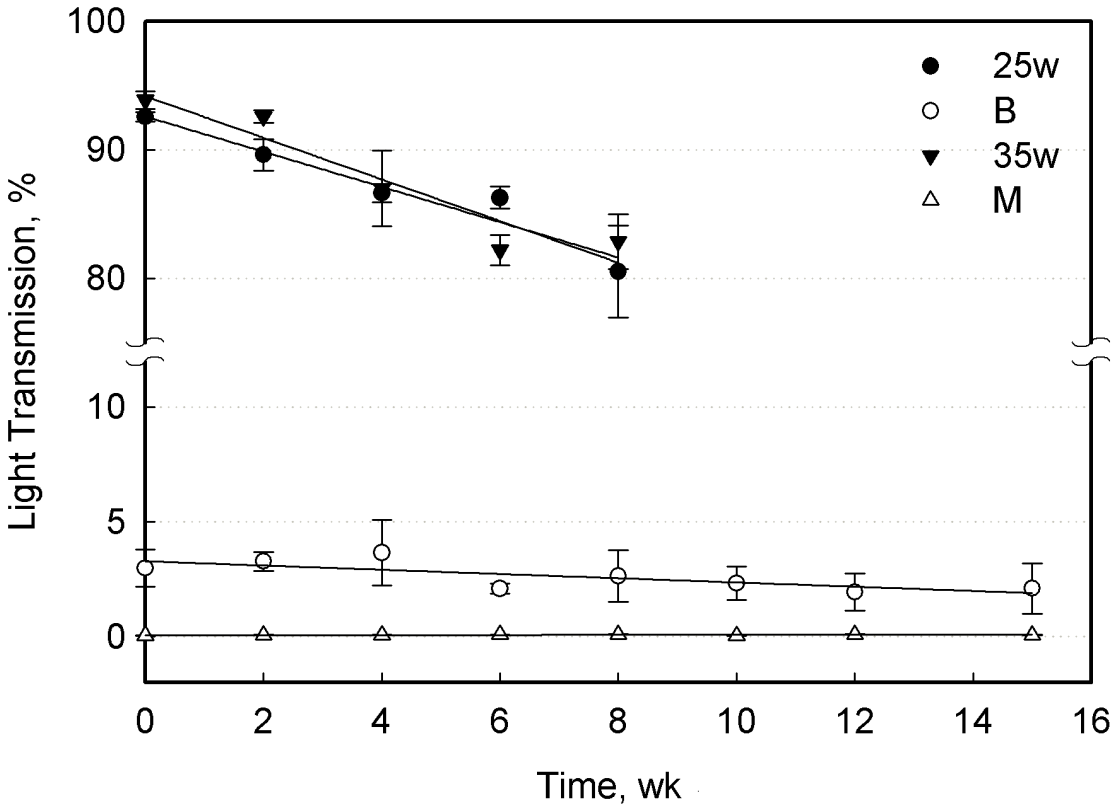

Figure 5-4. Changes in % Light transmission of 25 µm black PBAT (B), 25 µm white PBAT (25w), 35 white black PBAT (35w), and black LDPE films (M); published in Kijchavengkul *et al.* (2008a)

Table 5-1. Effects of biodegradable PBAT and mulches on weed control and weed biomass in tomato in 2006 and 2007; adapted from Ngouajio *et al.* (2008)

Mulch	Weed Control %				Weed Biomass (g)	
	2006		2007		2006	2007
	Jul 7	Aug 21	Jun 28	Jul 23	Jul 26	Jul 23
LDPE	100.0[a]	100.0[a]	100.0[a]	100.0[a]	1.6[a]	0.0[a]
PBAT 25 μm	-	-	100.0[a]	94.5[a]	-	0.0[a]
PBAT 35 μm	98.7[a]	97.5[a]	100.0[a]	98.5[a]	0.0[a]	0.0[a]

Note: Weed control of 100% means there are no weeds observed on the plot, while 0% means the plot is completely filled with weeds. Weed biomass was measured on a 50 x 50 cm^2 area on top of each raised bed. Values within a column followed by the same letter are not significantly different at α of 0.05.

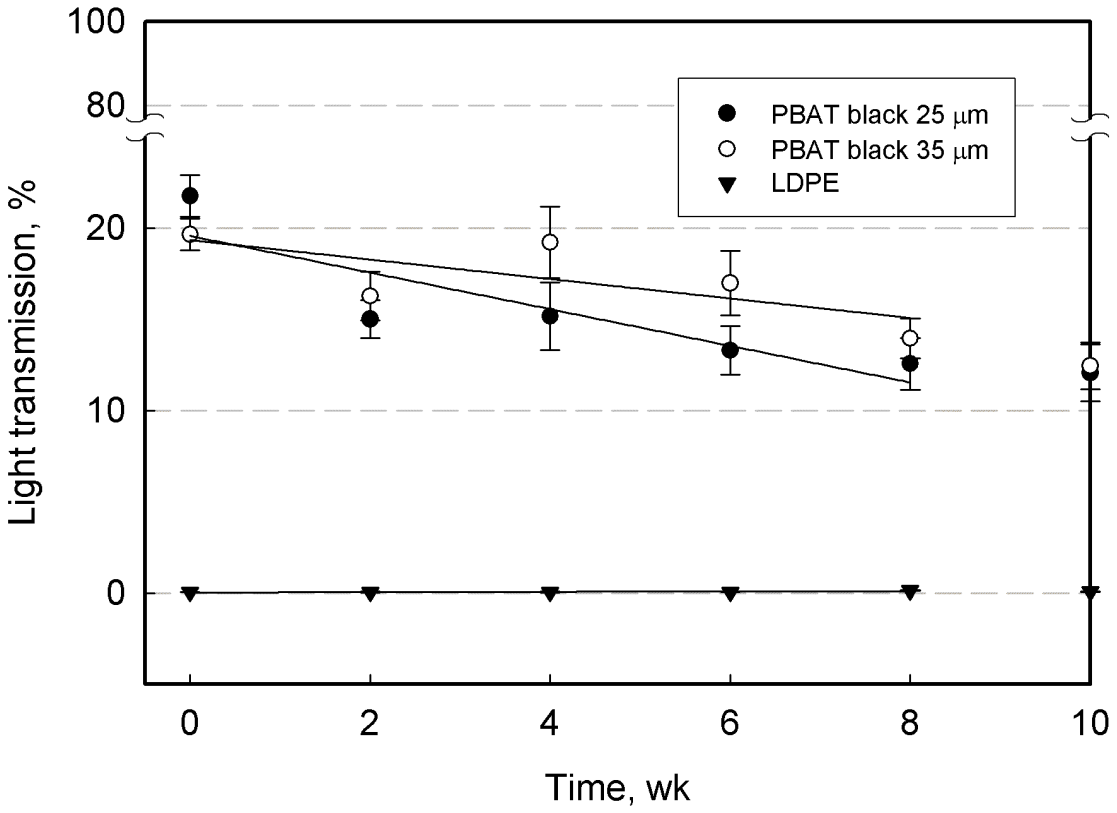

Figure 5-5. % Light transmission of 25 μm black PBAT, 35 μm black PBAT, and black LDPE films used in 2007 growing season

5.1.3 Mechanical properties

Since all the white films started breaking within two weeks, the samples of the white film for mechanical testing could only be retrieved until 2nd week. In the case of the black PBAT films, the sampling continued until 8th week. After two weeks, the white films became very brittle, while the black films were still ductile. Figure 5-6a shows that there were decreases in tensile strength for all the biodegradable films, especially during the first two weeks for the white films. Conversely, there were no changes for the conventional mulch. It can be seen in Figure 5-6b that the % elongation also dropped after the first two weeks for all the PBAT films. The PBAT films were more brittle after exposure in the field; the data coincided with the initial visual evaluation done on site. On the other hand, there was no change in the tensile modulus for the LDPE film.

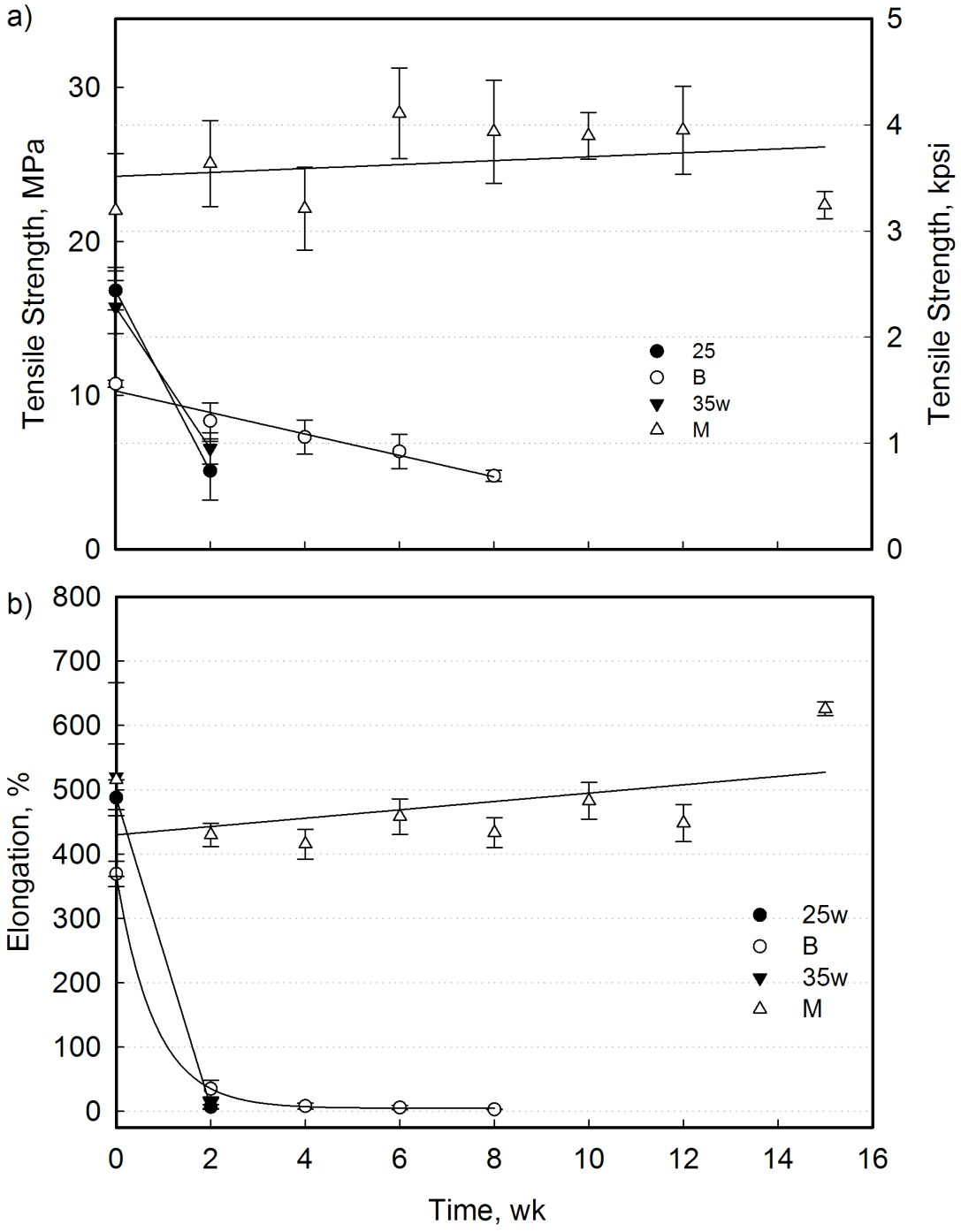

Figure 5-6. Changes in Mechanical properties of all the films against time: (a) Tensile strength and (b) % Elongation; published in Kijchavengkul *et al.* (2008a)

5.1.4 Molecular weight and gel content

Table 5-2 displays the changes in molecular weight of the biodegradable films. Samples of the films obtained from 2nd to 15th week could not be dissolved in tetrahydrofuran (THF), except the black PBAT film sample from 2nd week. This change in THF dissolution from day zero can be attributed to crosslinking that occurred in the films due to UV radiation. The molecular weight of the B film decreased from 84.4 kDa at 0th week to 60.0 kDa at 2nd week. After all the biodegradable mulch films were plowed into the field in November, the molecular weights of 25w, 35w, and B films (only portions that dissolved in THF) were 55.4, 60.5, and 51.0 kDa in December, respectively, 48.5, 50.9, and 43.2 kDa in February, respectively, and 46.7, 54.4, and 45.2 kDa, respectively in April. This is an indication that there were likely main chain scissions occurring in the soil after the films were plowed, but at slow degradation rates because of the low ambient/soil temperatures of below 5°C and the low solar radiation of below 8.4 MJ/d during the winter.

Table 5-2. Changes in molecular weight of the PBAT films; published in Kijchavengkul *et al.* (2008a)

Time span	Week number	Molecular Weight (kDa)		
		25w	35w	B
June 6, 2006	0	86.3±2.2	89.3±1.9	84.4±1.7
June 23, 2006	2	N/A	N/A	60.0±8.5
July 5, 2006	4	N/A	N/A	N/A
July 19, 2006	6	N/A	N/A	N/A
…	…	…	…	…
September 20, 2006	15	N/A	N/A	N/A
After plowed				
December 20, 2006	28	55.4±0.1	60.5±0.5	51.0±0.5
February 21, 2007	37	48.5±0.4	50.9±0.6	43.2±0.3
April 25, 2007	46	46.7±5.5	54.4±2.9	45.2±2.5

Since the samples of field experiment were difficult to dissolve in THF, the gel content of the samples was measured together with the molecular weight. The gel content of the white PBAT films was around 50-60%, while that of black PBAT film was at 20-30% (Figure 5-7). The possible explanation for the increase in gel content is that presence of TiO_2 in the white PBAT films affected the photodegradation rate of these films. The TiO_2 photocatalytic ability could catalyze the photodegradation of the white films and increase their degradation rate (Gesenhues 2000; Irick 1972; Searle and Worsley 2002). On the other hand, the carbon black used as black colorant for the PBAT film stabilized the photodegradation with a screening method, where any light absorbing substance, carbon black in this case, absorbs the light energy and reduces the intensity of the light reacting with the polymer (Schnabel 1992; Shlyapintokh 1984).

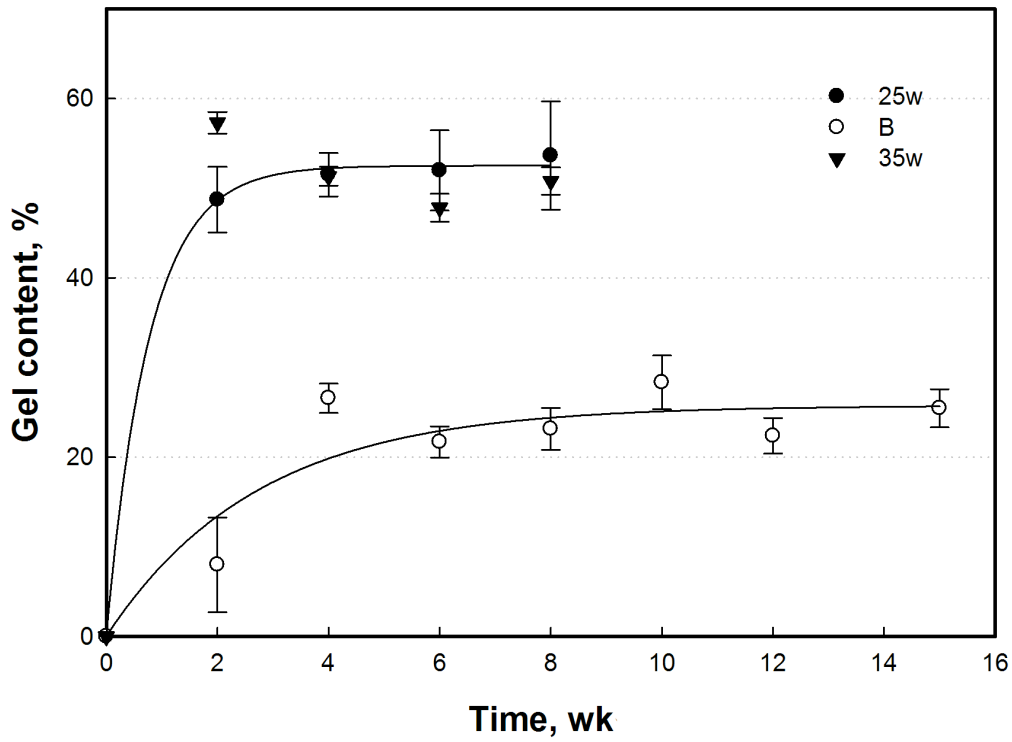

Figure 5-7. Changes in gel content of all the sample films against time; published in Kijchavengkul *et al.* (2008a)

5.1.5 Thermal behavior

The T_g, the amorphous transition temperature, and T_m of the unexposed film were -33.4±1.2, 54.8±0.5, and 121.6±0.3°C, respectively. There was no change in T_g with time, but T_m of all three PBAT films decreased (Figure 5-8a). As the photodegradation proceeded, the melting peaks in the thermograms became broader and the area under these peaks and T_m were more difficult to identify (Figure 5-8b). The broadening of the peak does not mean that the percentage of crystallinity increased since the crosslinked structure of the polymer can disrupt the melting process (Ioan *et al.* 2001). Crosslinking could cause non-uniformity of the crystal lattices, which makes them melt at different temperatures, hence, causing the broader melting peaks in the thermograms.

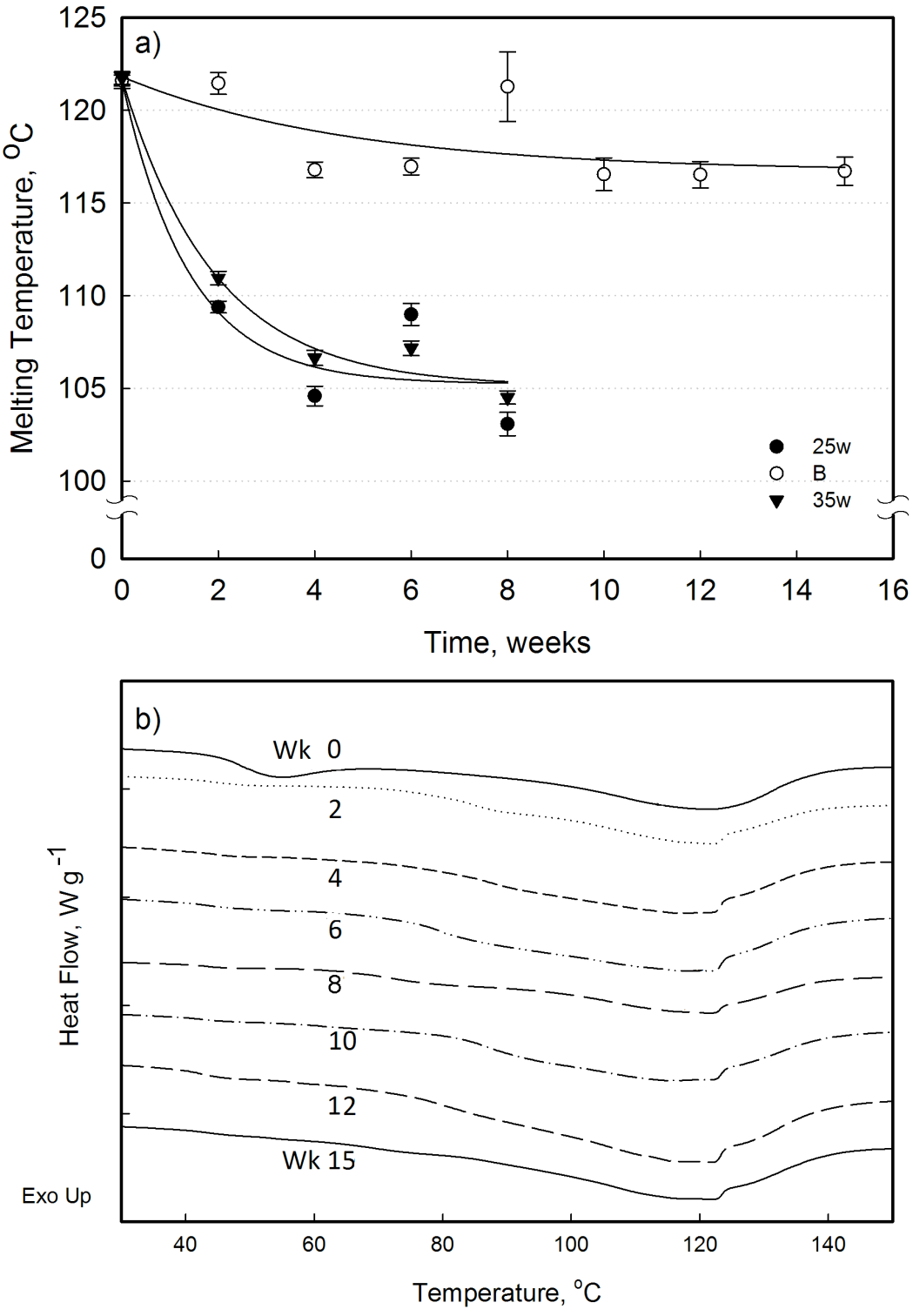

Figure 5-8. (a) Changes in the melting temperatures of all PBAT film over times; (b) DSC thermogram of the changes in the melting temperatures of the black PBAT film; published in Kijchavengkul *et al.* (2008a)

5.1.6 FTIR spectra (functional group determination)

From the data on the visual evaluation, the changes in mechanical properties, and increase in gel content of the samples, it is confirmed that there was crosslinking occurring within the exposed biodegradable films, both black and white. To further understand the mechanism of the crosslinking, FTIR was used to detect any changes in the functional group intensities of the film samples.

There were decreases in the intensities of the C-O bonds (1270 cm^{-1}) and C=O bonds (1710 cm^{-1}) from the ester groups for all the biodegradable films as function of time (Figure 5-9). This could be attributed to the high susceptibility to photodegradation of the carbonyl group (C=O). In addition, there were formations of small amount of hydroxyl groups (-O-H) at 3740 cm^{-1} starting from 2^{nd} week for all the biodegradable films, since the absorbance intensities were slightly higher than the noise level. The intensities of this hydroxyl peak remained the same until the end of the season. The small formation of the hydroxyl attributed to the formation of the alcohol groups caused by the main chain scission at the ester groups.

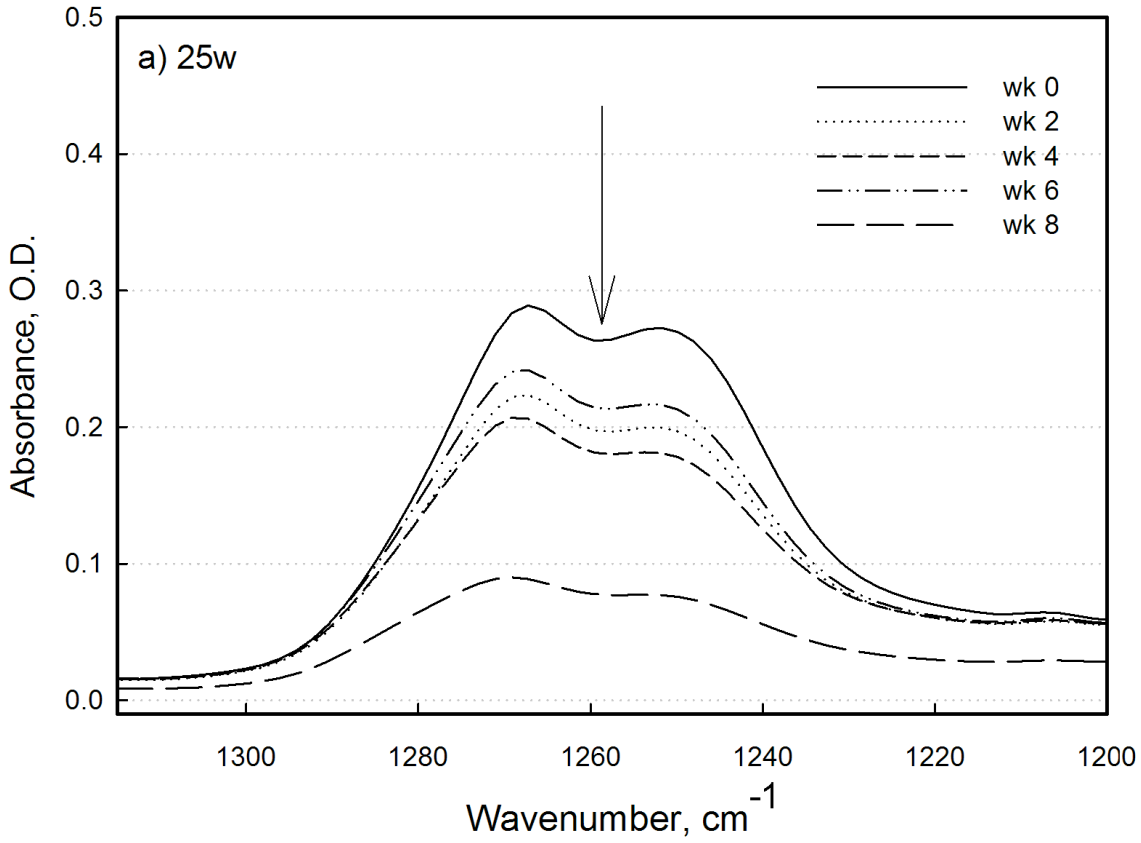

Figure 5-9a. FTIR spectra indicated C-O bond of ester group at 1200-1300 cm^{-1} in 25w samples; published in Kijchavengkul *et al.* (2008a)

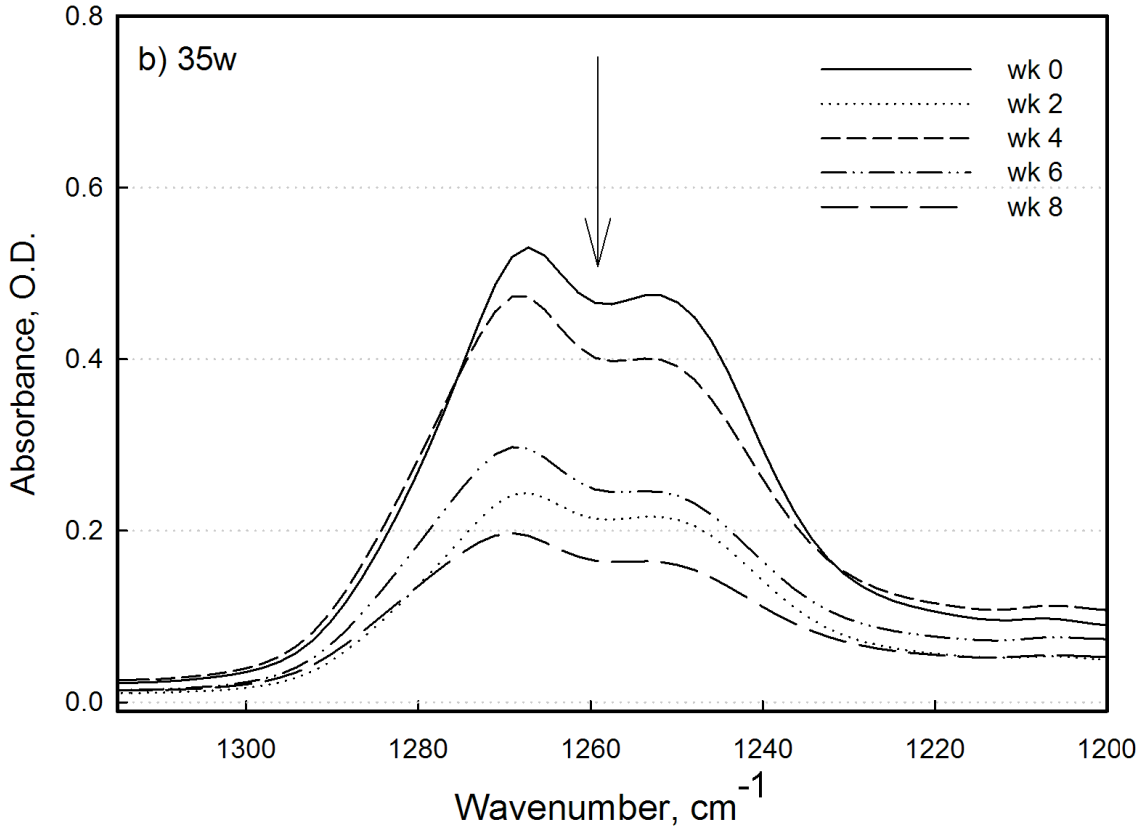

Figure 5-9b. FTIR spectra indicated C-O bond of ester group at 1200-1300 cm^{-1} in 35w samples; published in Kijchavengkul *et al.* (2008a)

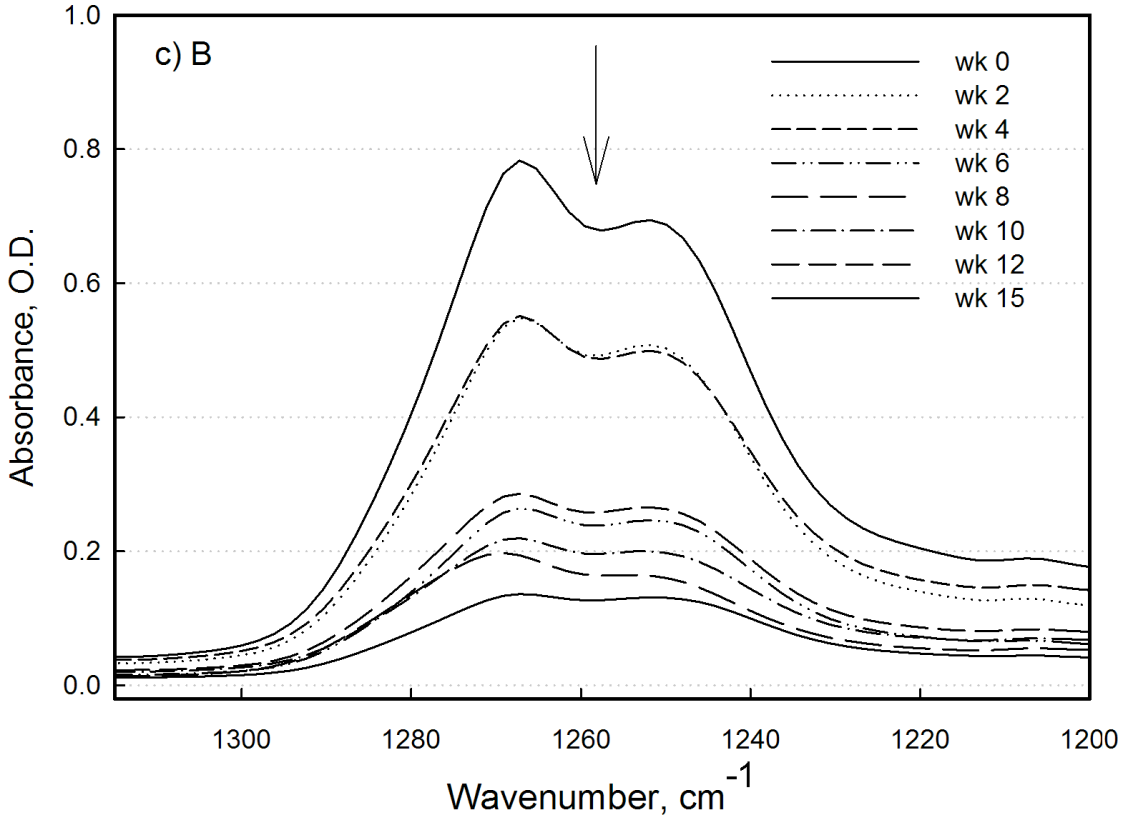

Figure 5-9c. FTIR spectra indicated C-O bond of ester group at 1200-1300 cm^{-1} in B samples; published in Kijchavengkul *et al.* (2008a)

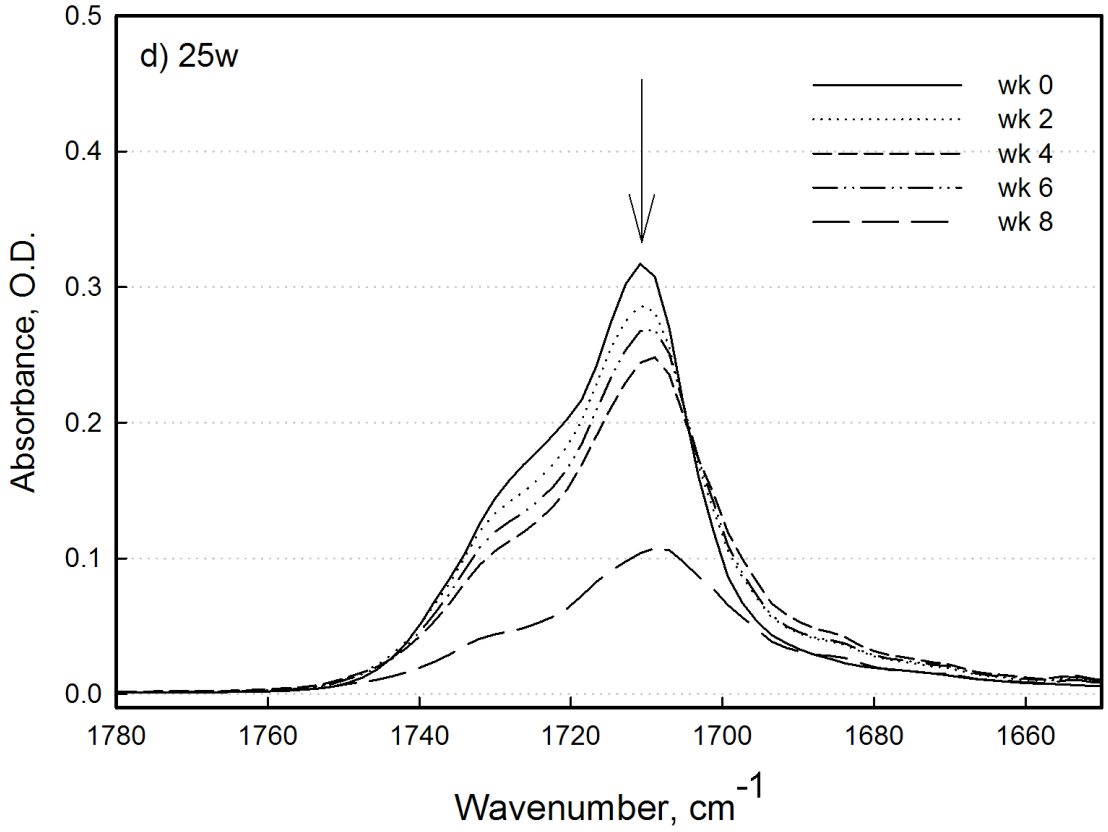

Figure 5-9d. FTIR spectra indicated C=O bond of ester group at 1650-1750 cm^{-1} in 25w samples; published in Kijchavengkul *et al.* (2008a)

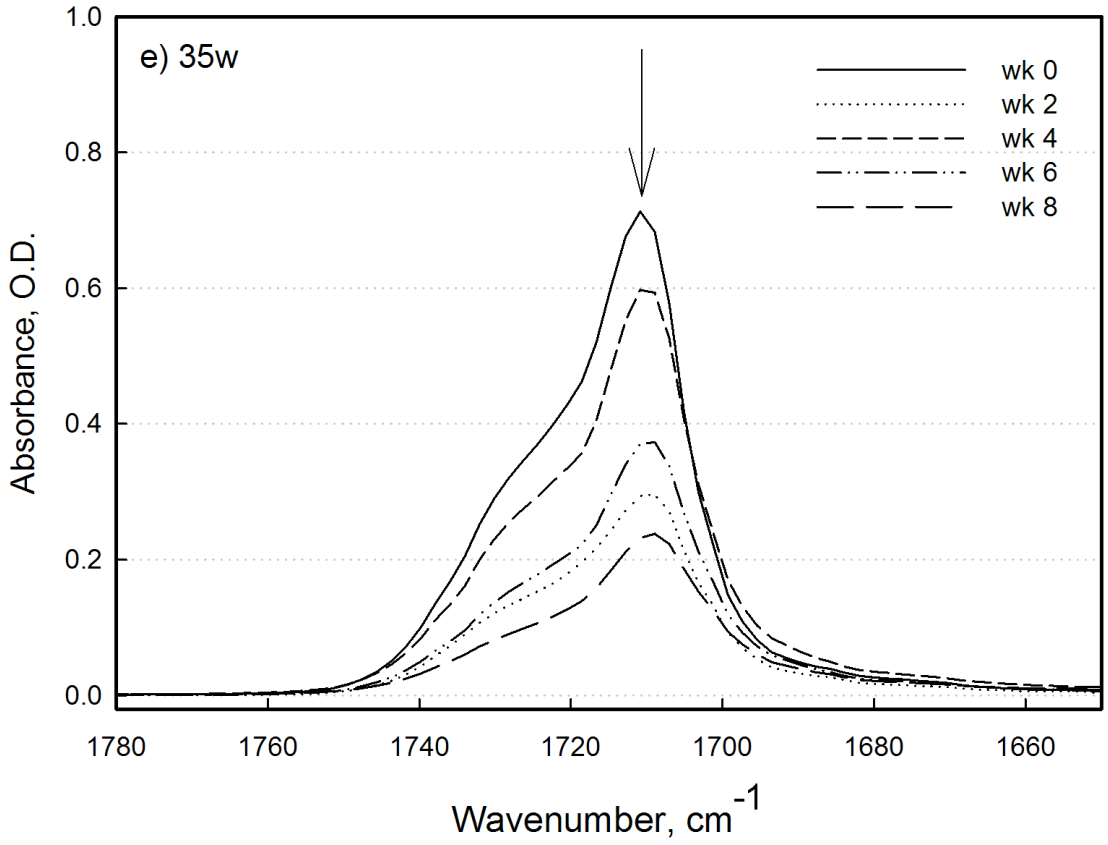

Figure 5-9e. FTIR spectra indicated C=O bond of ester group at 1650-1750 cm^{-1} in 35w samples; published in Kijchavengkul *et al.* (2008a)

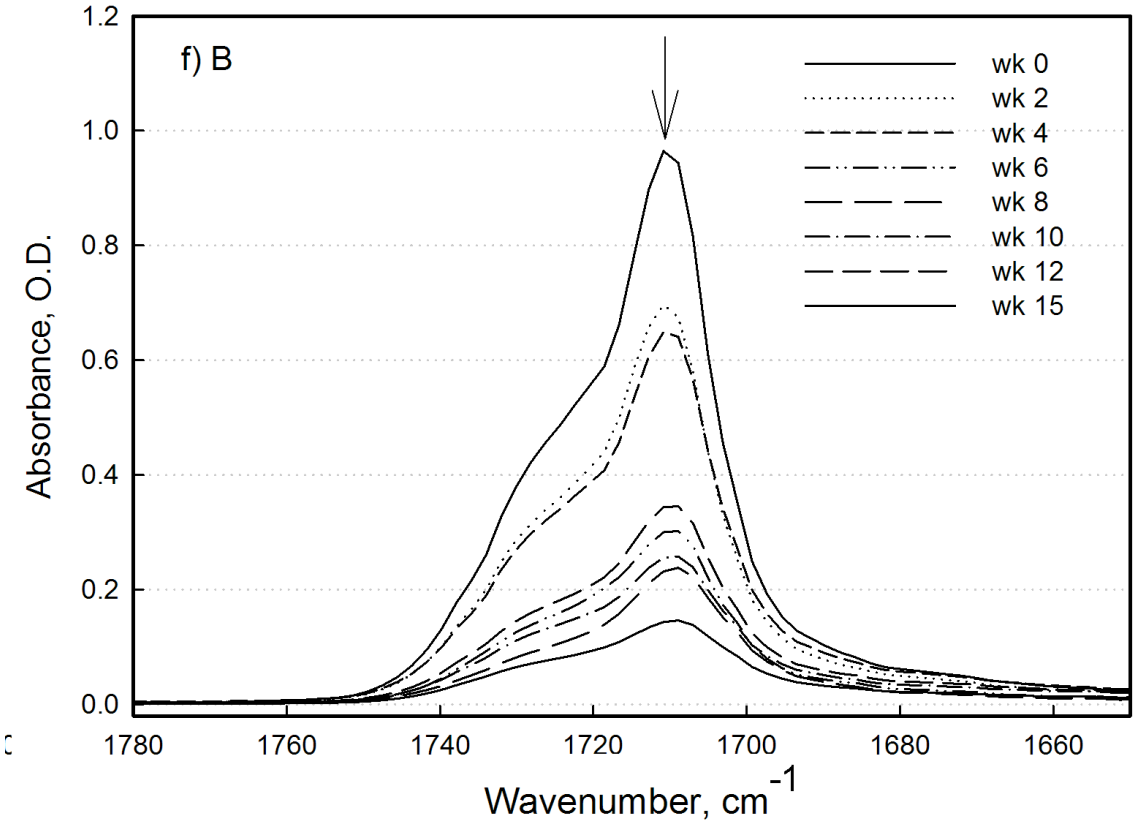

Figure 5-9f. FTIR spectra indicated C=O bond of ester group at 1650-1750 cm^{-1} in B samples; published in Kijchavengkul *et al.* (2008a)

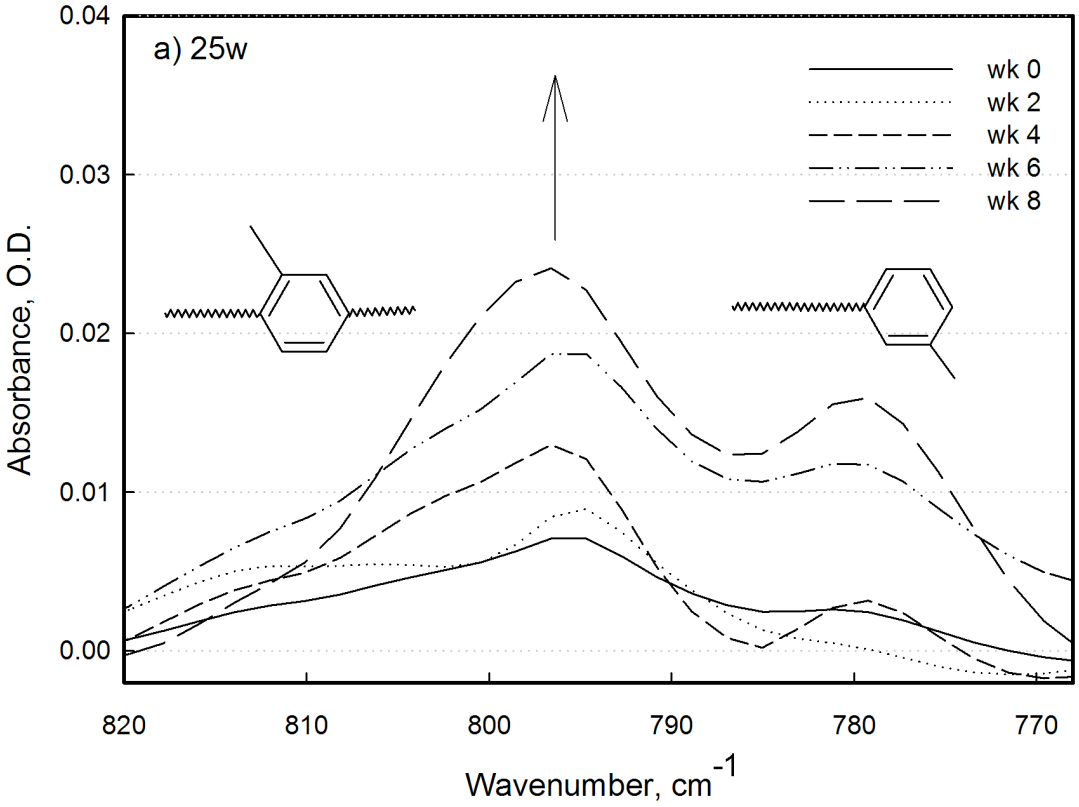

Figure 5-10a. FTIR spectra indicated out-of-plane bending of the benzene ring substitutes at 765-820 cm^{-1} (left peaks at 796 cm^{-1} represent 1, 2, 4 trisubstitution benzene, and right peaks at 780 cm^{-1} represent 1, 3 meta disubstitution benzene) in 25w sample; published in Kijchavengkul *et al.* (2008a)

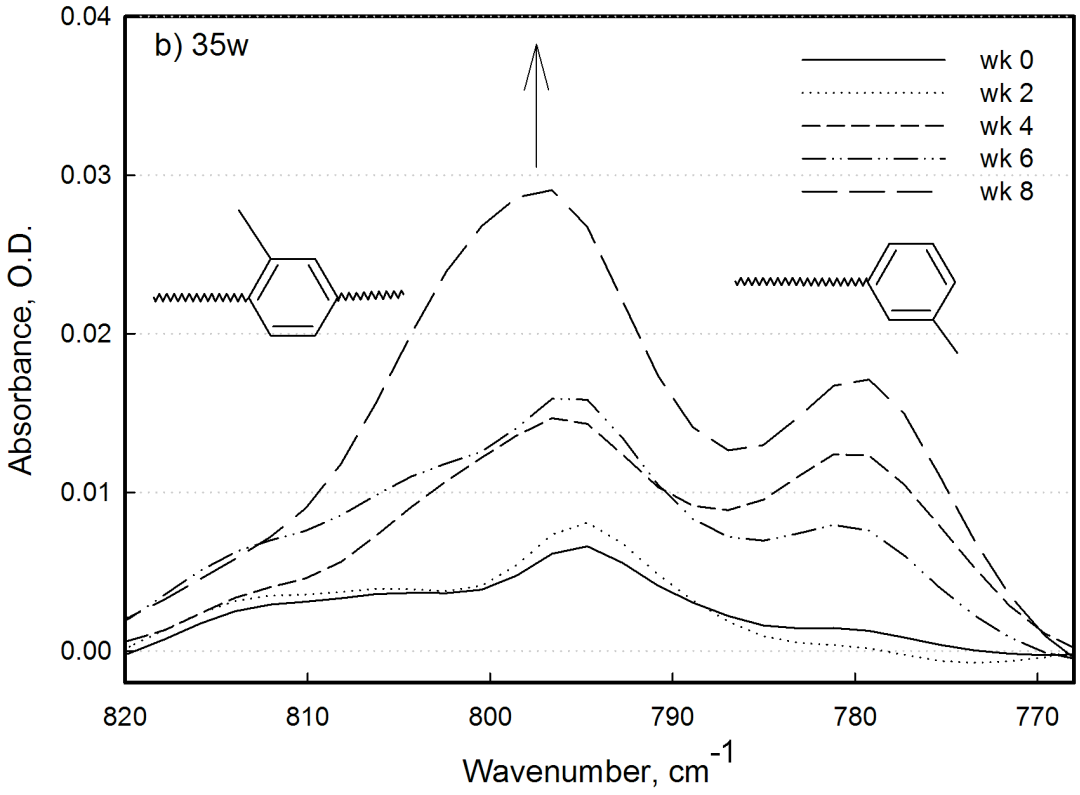

Figure 5-10b. FTIR spectra indicated out-of-plane bending of the benzene ring substitutes at 765-820 cm^{-1} (left peaks at 796 cm^{-1} represent 1, 2, 4 trisubstitution benzene, and right peaks at 780 cm^{-1} represent 1, 3 meta disubstitution benzene) in 35w sample; published in Kijchavengkul *et al.* (2008a)

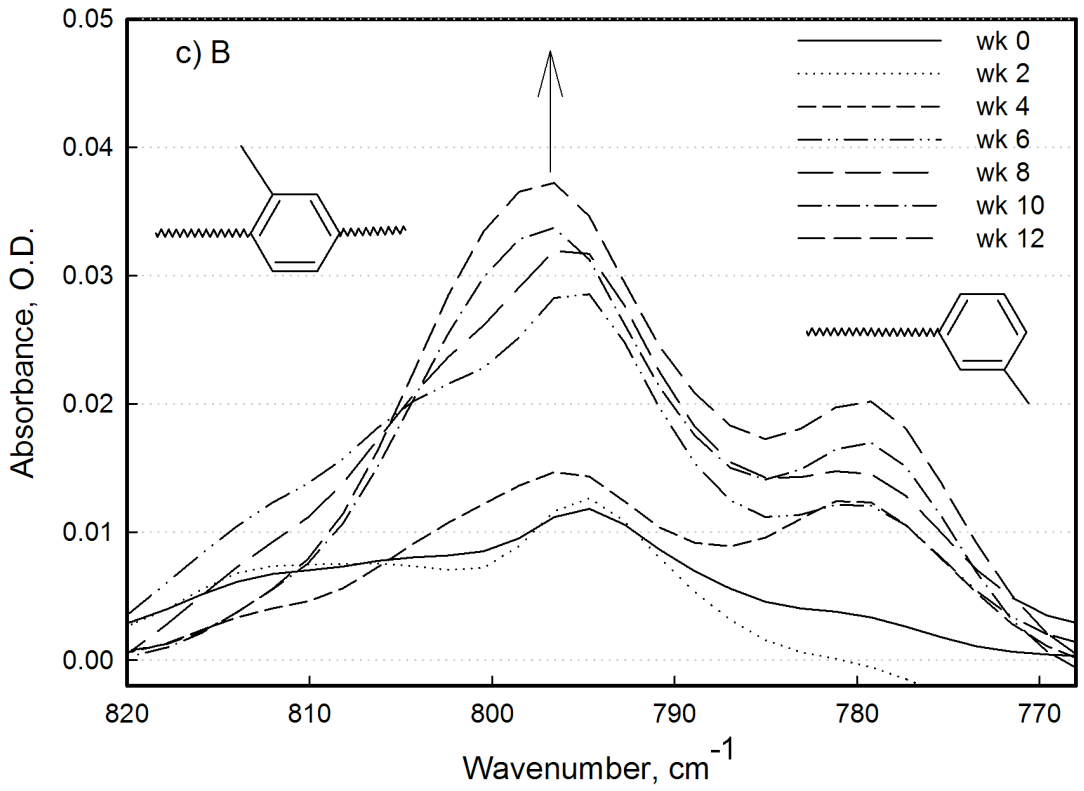

Figure 5-10c. FTIR spectra indicated out-of-plane bending of the benzene ring substitutes at 765-820 cm^{-1} (left peaks at 796 cm^{-1} represent 1, 2, 4 trisubstitution benzene, and right peaks at 780 cm^{-1} represent 1, 3 meta disubstitution benzene) in B sample; published in Kijchavengkul *et al.* (2008a)

The increases in the absorbance of the 'out of plane' bending of benzene groups at 796 and 780 cm^{-1}, with exposure time indicated that there were changes of the benzene ring substitutes due to formations of 1, 3 meta disubstitute benzene, wave number of 780 cm^{-1} (Robinson *et al.* 2005) and 1, 2, 4. trisubstitute benzene, wave number of 796 cm^{-1} (Robinson *et al.* 2005) as photodegradation proceeded (Figure 5-10). Therefore, the crosslink structure could result from a recombination of the generated free radicals of the 1, 3 meta disubstitute benzene and the 1, 2, 4 trisubstitute benzene from hydrogen abstraction induced by other free radicals created from photodegradation via Norrish I

process or from decomposition of hydroperoxides compounds (Buxbaum 1968; Marcotte *et al.* 1967; Rivaton and Gardette 1998; Schnabel 1992).

A tentative crosslinking mechanism previously presented by Rivaton and Gardette (1998) for PBT, which is a homopolymer produced from BT dimer , can be appropriately applied to this finding (Scheme 5-1). In this mechanism, there is hydrogen abstraction of one of the hydrogen atoms by a free radical generated from the Norrish I reaction and a benzene free radical is formed. Detail of generation of phenyl free radical can be found in section 2.5.2.3. Two of those new radicals then recombine to form an H-link structure. This H-link structure is still susceptible to the photodegradation due to the presence of carbonyl in the ester group. Further exposure to UV light causes those structures to breakdown at the carbonyl group and makes them more susceptible to oxidation. Therefore, the H-link structure is reduced into a Y-link structure after further exposed to UV light. These observations showed that all the PBAT films present a high degree of photodegradation which led to crosslinking due to UV light exposure.

5.1.7 Biodegradation

Figure 5-11 represents the amount of CO_2 evolution (percent biodegradation) of the samples measured by the DMR system after an incubation period of 120 days. From the curve, all the PBAT films biodegraded at comparable rates to that of the corn starch (positive control), and the values of percent mineralization of all sample are greater than 60% with that of corn starch is greater than 70%. Therefore, these PBAT films satisfies the biodegradation criterion in ASTM D6400 specification (ASTM 2004) tested according to ASTM D5338 test method (ASTM 2003).

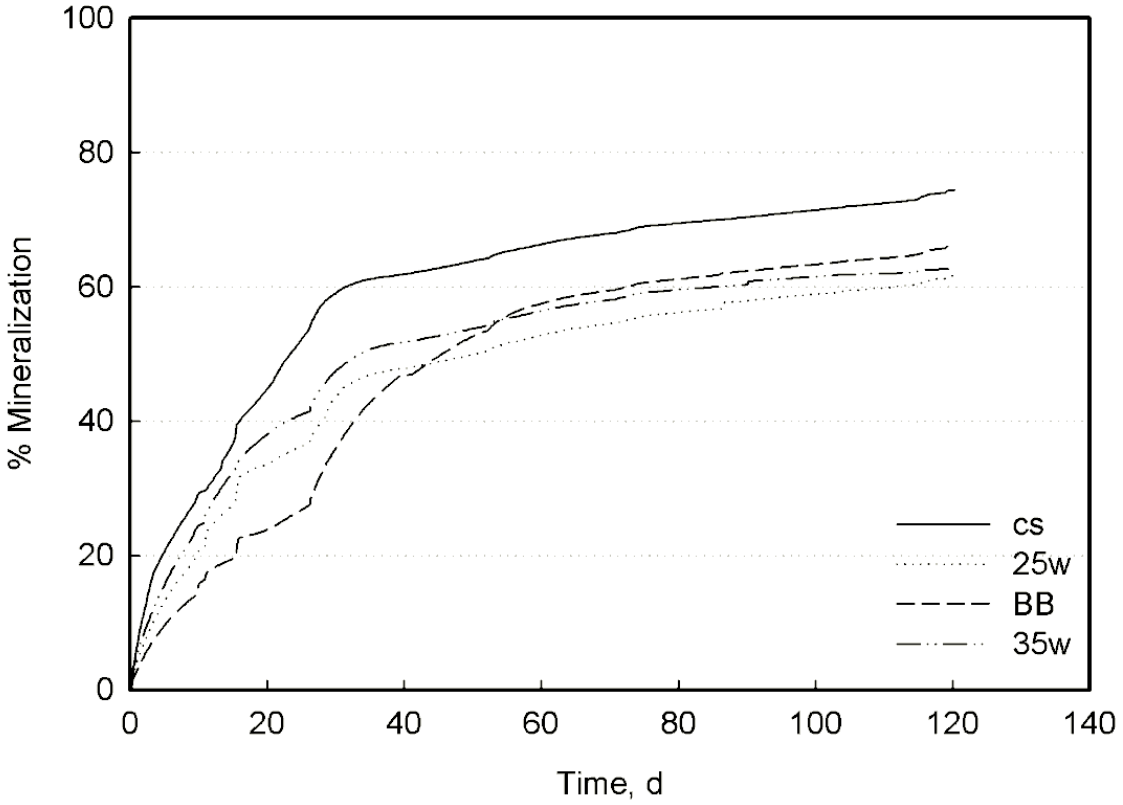

Figure 5-11. Amount of carbon dioxide evolution of all the film samples against incubation time; published in Kijchavengkul *et al.* (2008a)

From this experiment, it is possible to conclude that the main degradation mechanism observed for the biodegradable mulch films was photodegradation. Therefore, as a consequence of exposure of the film to UV light, crosslinking within the films took place as supported by the following facts: (1) the brittleness of the film detected from the visual evaluation and the changes in the mechanical properties, (2) the difficulty in dissolving the films sample in THF after two weeks of exposure, (3) the FTIR spectra that corresponded to the changes of the benzene substitutions and the ester groups, and 4) the broader melting peaks from the DSC thermograms.

In horticulture aspect, Table 5-3 indicates that marketable tomato yields in 2006 and 2007 seasons from plots with black LDPE and PBAT films were not statically different, while the yield in 2007 from the plots with white PBAT films were significantly lower (approximately 58% lower) than that from the plots with black films (Ngouajio *et al.* 2008).

Table 5-3. Tomato yield and fruit as affected by biodegradable PBAT and mulches on weed control and weed biomass in tomato in 2006 and 2007; adapted from Ngouajio *et al.* (2008).

Mulch	**Marketable yield**			
	2006		**2007**	
	No. (fruit/plot)	**Wt. (kg/plot)**	**No. (fruit/plot)**	**Wt. (kg/plot)**
Conventional 25 μm	381[a]	94.1[a]	363[a]	81.7[a]
PBAT 25 μm	-	-	329[a]	75.8[a]
PBAT 35 μm	396[a]	95.5[a]	341[a]	80.4[a]

Note: Each plot consisted of one bed 21 ft long with one row of tomato plants spaced 1.5 ft apart (14 plants/plot, but only the middle 12 plants were harvested). Beds were spaced on 5.5 ft (center-to-center). Values within a column followed by the same letter are not significantly different at α of 0.05.

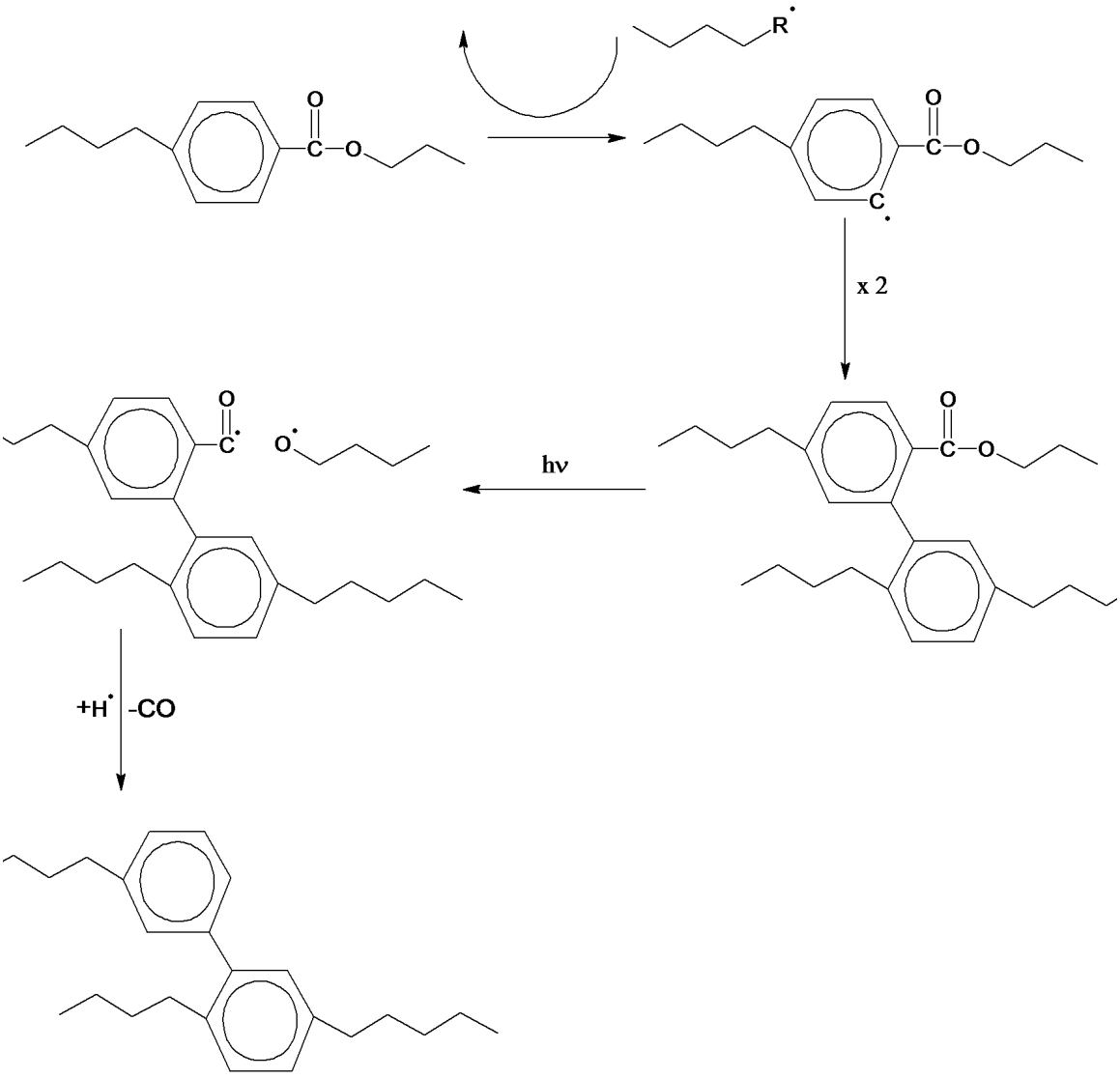

Scheme 5-1. Tentative crosslinking mechanism; published in Kijchavengkul *et al.* (2008a)

5.2 Laboratory simulated experiment

To investigate the development or cause of crosslinking in the films, it is essential to eliminate other uncertainty factors, such as temperatures, day lengths, and irradiances, which vary significantly under field conditions. The use of UV light under laboratory simulated control environments at specific radiation energy irradiance, exposure time, and temperature may improve the assessment of crosslinking effect on polymer as suggested by the field experiments.

In this experiment, PBAT film samples were exposed to UV-A in the QUV Accelerated Weathering Tester for various predetermined times (0, 2.5, 6, 10, and 12 h) to produce films with specific gel contents (0, 10, 30, 50, and 70%). Later the gel contents of the crosslinked films were measured according to ASTM D 2765 method A (ASTM 2006) using THF as solvent to ensure that the samples had the target gel contents. The gel contents and molecular weight of the film samples with different exposure time are summarized in Table 5-4.

Table 5-4. Gel contents and molecular weight of the film samples exposed to UV-A at different predetermined times; published in Kijchavengkul *et al.* (2008b)

Exposure Time (h)	Gel content (%)	Molecular weight (kDa)
0	0.0 ± 0.0^{a}	60.4 ± 1.1^{a}
2.5	9.6 ± 2.8^{b}	71.5 ± 2.6^{b}
6	33.7 ± 1.9^{c}	70.6 ± 1.2^{b}
10	51.7 ± 5.6^{d}	58.4 ± 2.6^{a}
12	67.0 ± 2.6^{e}	34.5 ± 4.3^{c}

Note: Numbers followed by the same letter within a column are not statistical significantly different at $P\leq0.05$ (t-test with Fisher LSD)

Biodegradability of the film samples were measured as percent mineralization, which is the percentage of carbon in the polymer molecules converted into CO_2 by microorganisms using DMR system. The DMR consisted of a total of 21 bioreactors, three for blank (compost only), three for positive control (cellulose), and three for each crosslinked biodegradable film (0, 10, 30, 50, and 70%). In order to accelerate this test, manure compost with greater microbial activity was used instead of yard compost as before.

5.2.1 Biodegradation of UV exposed samples

Percent mineralization is related to crosslinked content of the film samples in the biodegradation (Figure 5-12). After the test period of 45 days, mineralization of cellulose approached 100%, indicating total degradation of the polymer. The non-crosslinked sample plateau at 60%, which, according to ASTM D 6400 (ASTM 2004) indicated that the sample was biodegradable. This is expected, since PBAT is a random copolymer and the mineralization of the positive control (cellulose) was greater than 70%. It was observed that the percent mineralization of the crosslinked samples decreased with increasing gel content. Percent mineralization of 36, 43, 21, and 24% were obtained for the samples with gel content of 10, 30, 50, and 70%, respectively (Figure 5-12). There was no statistical significant difference in the percent mineralization between 10 and 30% gel content samples and between 50 and 70% gel content samples, but the former group showed greater biodegradation than the latter group. The lower and slower biodegradation in the crosslinked samples can be caused by the crosslinked structure itself. The crosslink structures make the film samples much less flexible, as seen in the

reduction in the % elongation and the increase of tensile modulus, and might prevent the accessibility of the microorganisms to the polymer chains (Kale *et al.* 2007).

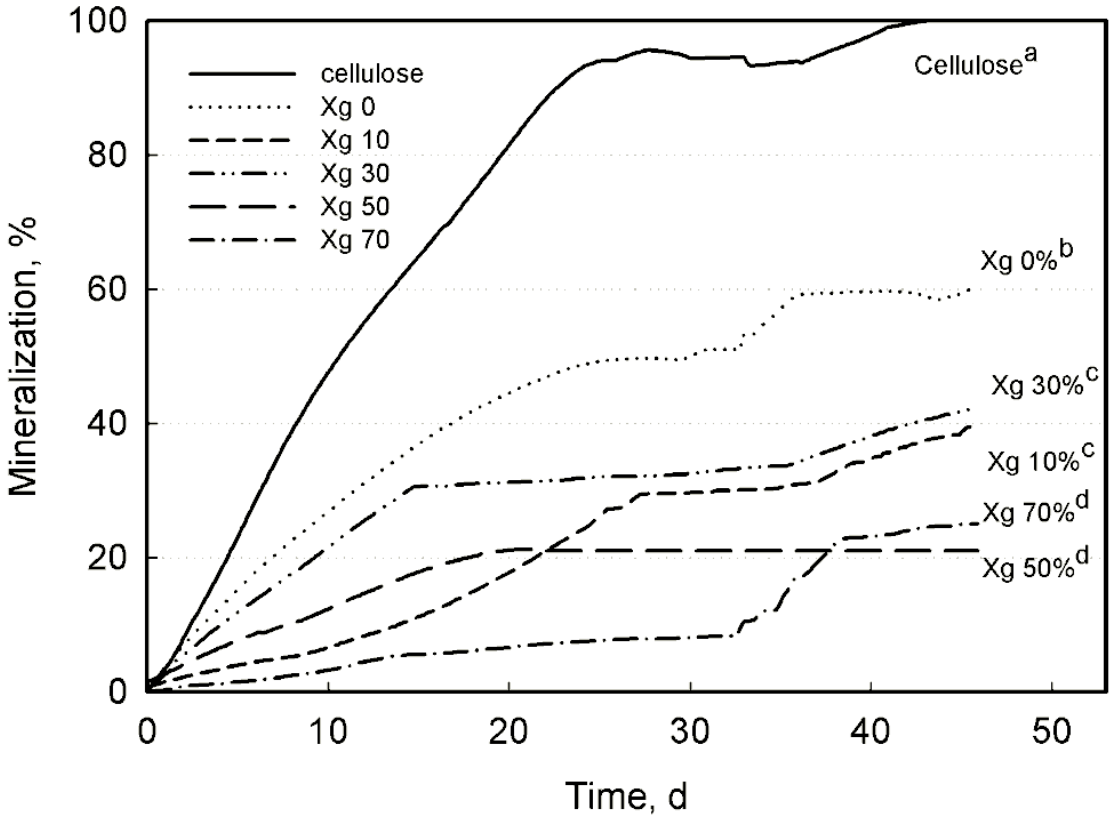

Figure 5-12. Percent mineralization of the crosslinked samples compared to non-crosslinked sample and cellulose after an incubation period of 45 days in manure compost mixture; published in Kijchavengkul *et al.* (2008b)

5.2.2 Molecular weight and X-ray diffraction analyses

Once the PBAT film was exposed to UV light, the molecular weight of the dissolved part of the samples increased initially with the gel content (from 60.4 kDa at 0% gel content to 71.5 kDa at 10% gel content). Thereafter, as the gel content increased, the molecular weight of the dissolved part of the sample started to decline rapidly to 58.4

and 34.5 kDa at gel contents of 50 and 70%, respectively (Table 5-4). This also suggests that both chain scission and crosslinking occurred in the film during exposure to UV. The chain scission caused the reduction in molecular weight, while the crosslinking caused the undissolved portions in the solution of the film samples. X-ray Diffraction (XRD) spectra of the non-crosslinked and crosslinked samples showed that there were no changes in the intensity and no shifting in the 2θ angle (Figure 5-13). This also indicates that there was no change in the crystalline region in the PBAT films. Any changes due to the UV radiation or crosslinking must have occurred in the amorphous region.

At the end of the 45 days biodegradation test, crosslinked samples prior to the DMR test were found to have two different portions of molecular weight; one with low molecular weight that decreased after being incubated in the compost mixture and one with high molecular weight around 230-250 kDa (Figure 5-14). Only the non-crosslinked sample showed one molecular weight portion. These could be caused by the crosslink structures that had really high molecular weight and could not be dissolved in the THF prior to the DMR test have become smaller after the DMR test possibly due to high thermal degradation and hydrolysis they experienced in the DMR system. The portions of the DMR residues that had high molecular weight indicated the presence of these small crosslink structures.

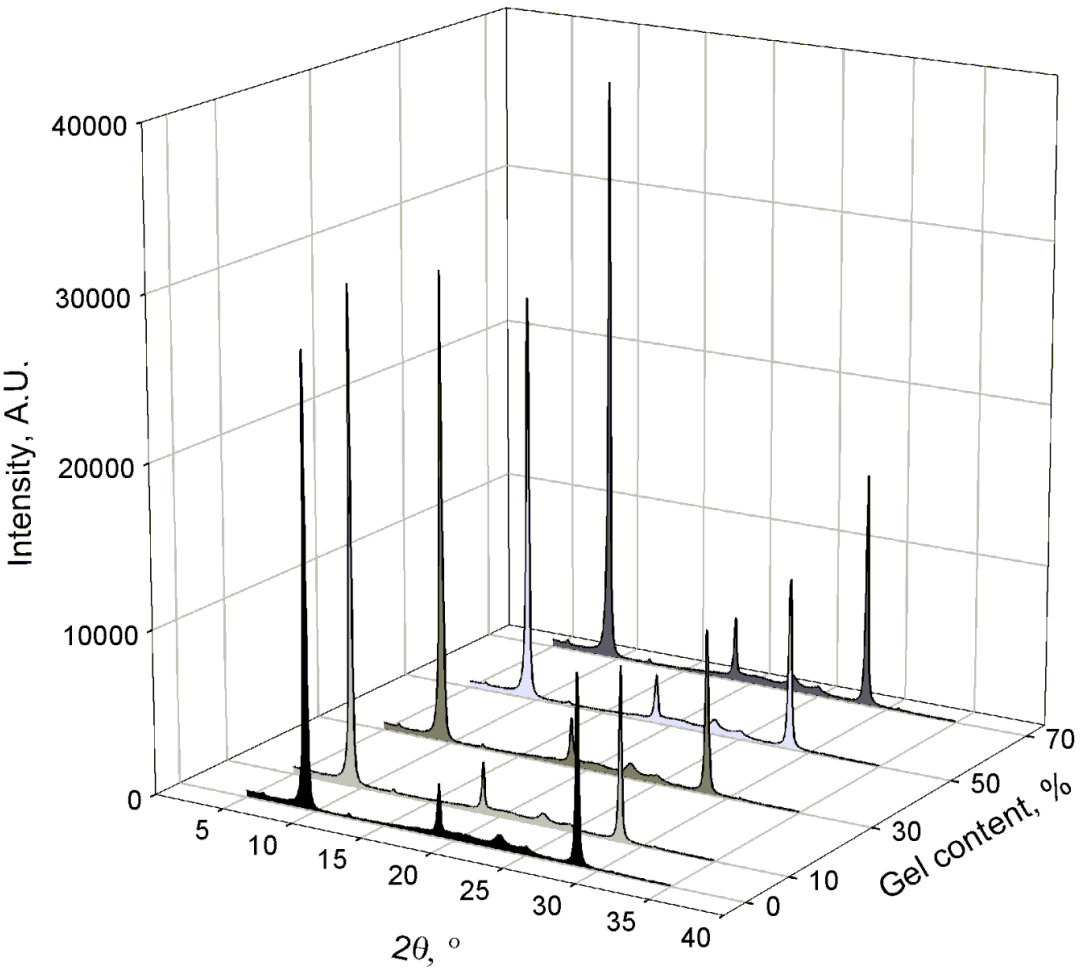

Figure 5-13. XRD spectra of the samples with 0, 10, 30, 50, and 70% gel contents; published in Kijchavengkul *et al.* (2008b)

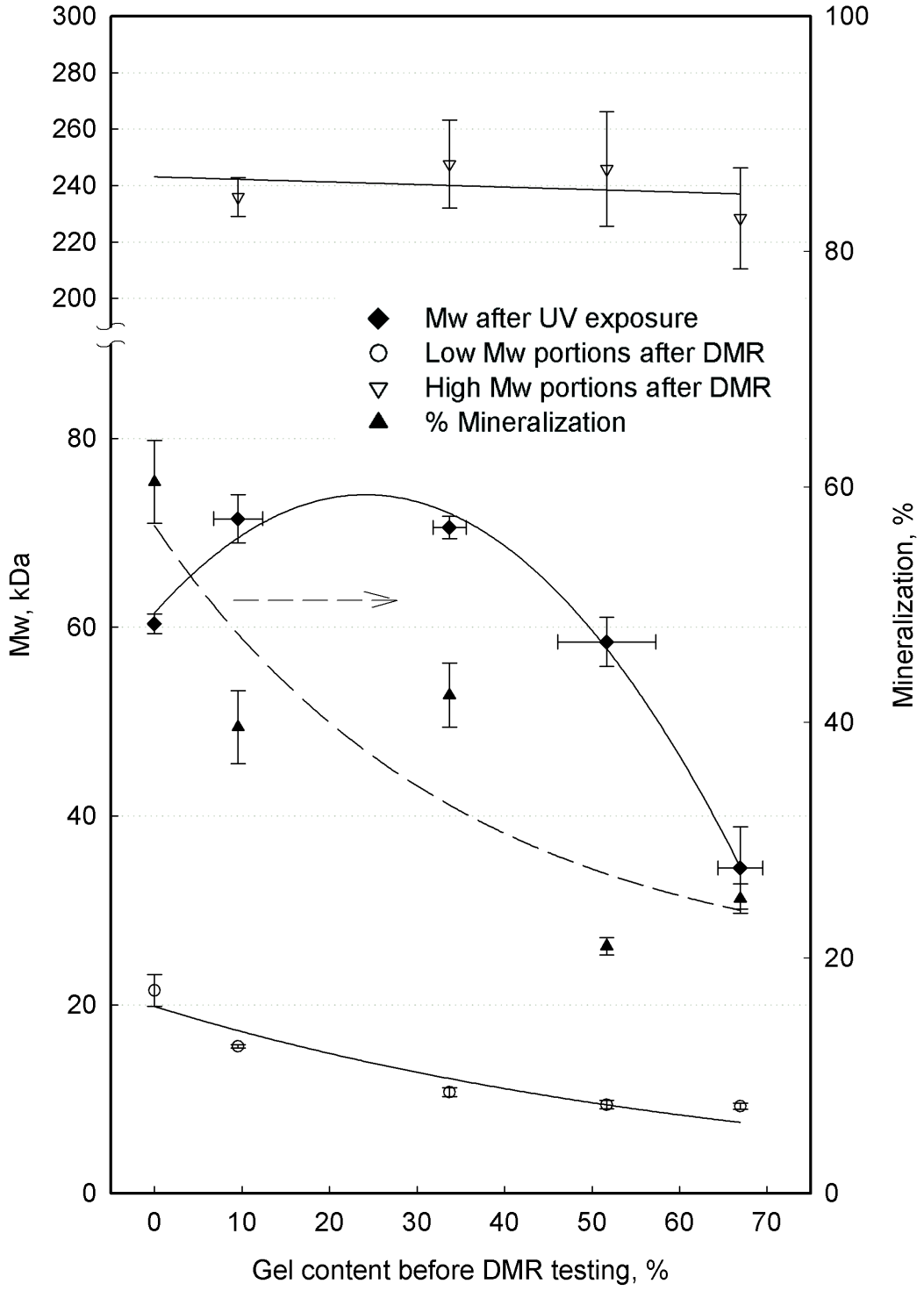

Figure 5-14 Molecular weight of the samples with different gel contents before and after the biodegradation test along with the corresponding percent mineralization; published in Kijchavengkul *et al.* (2008b)

5.2.3 Scanning electron microscopy (SEM)

For samples with 0, 10, and 30% gel contents, SEM micrographs show large amount of microbes and microbe-created cavities (CV) were observed which indicated that PBAT samples were digested by the microorganisms (Figure 5-15e, f, h, i, k, l, n, and o and Figure 5-16d, g, and m). This resulted in the percent mineralization values of greater than the samples with 50 and 70% gel contents, where only small numbers of local surface erosion occurred and most of the surface areas were still intact (Figure 5-16b, c, e, f, h, i, k, n, and o) and no cavities created by microbes were observed. Microbes found on the 70% gel content sample were simply living on the sample and not digesting the sample (Figure 5-16).

Figure 5-15h shows that the microorganisms had consumed and formed cavities around the PBAT crystalline regions (CT), which indicated that the amorphous region is more susceptible to microorganisms attack compared to the crystalline region, where the polymer chains were packed more tightly and orderly; therefore, the accessibility of the microbes to the polymer chains was limited.

Networks of filament-like biofilm (BI) created by microbes to attach themselves to the film surface and formed attached sites for other microorganisms were observed (Figure 5-15e, h, i, l, and o, Figure 5-16d and m, and Figure 5-17a and b). Figure 5-15l also shows the large amount of microorganisms impregnated in the PBAT film surface, digesting the PBAT samples and creating cavities on the film surface. The cracks found in Figure 5-15l and 5-16g were developed by the air-drying process used during samples

preparation for SEM microscope. The edge or side of the film samples has undergone severe microbial attack, as indicated by the numbers of cavities found.

Figure 5-17a presents the surface area of the film being covered with biofilm, which were found only on the surface of the samples with 0, 10, and 30% gel contents. Figure 5-17b shows colonies of microbes on the film surface, where biofilm is being produced and PBAT became food sources and was consumed forming large cavities on the surface of the film. Therefore, it can be seen from the percent mineralization values and SEM micrographs that crosslinking decreased the biodegradability of the PBAT samples.

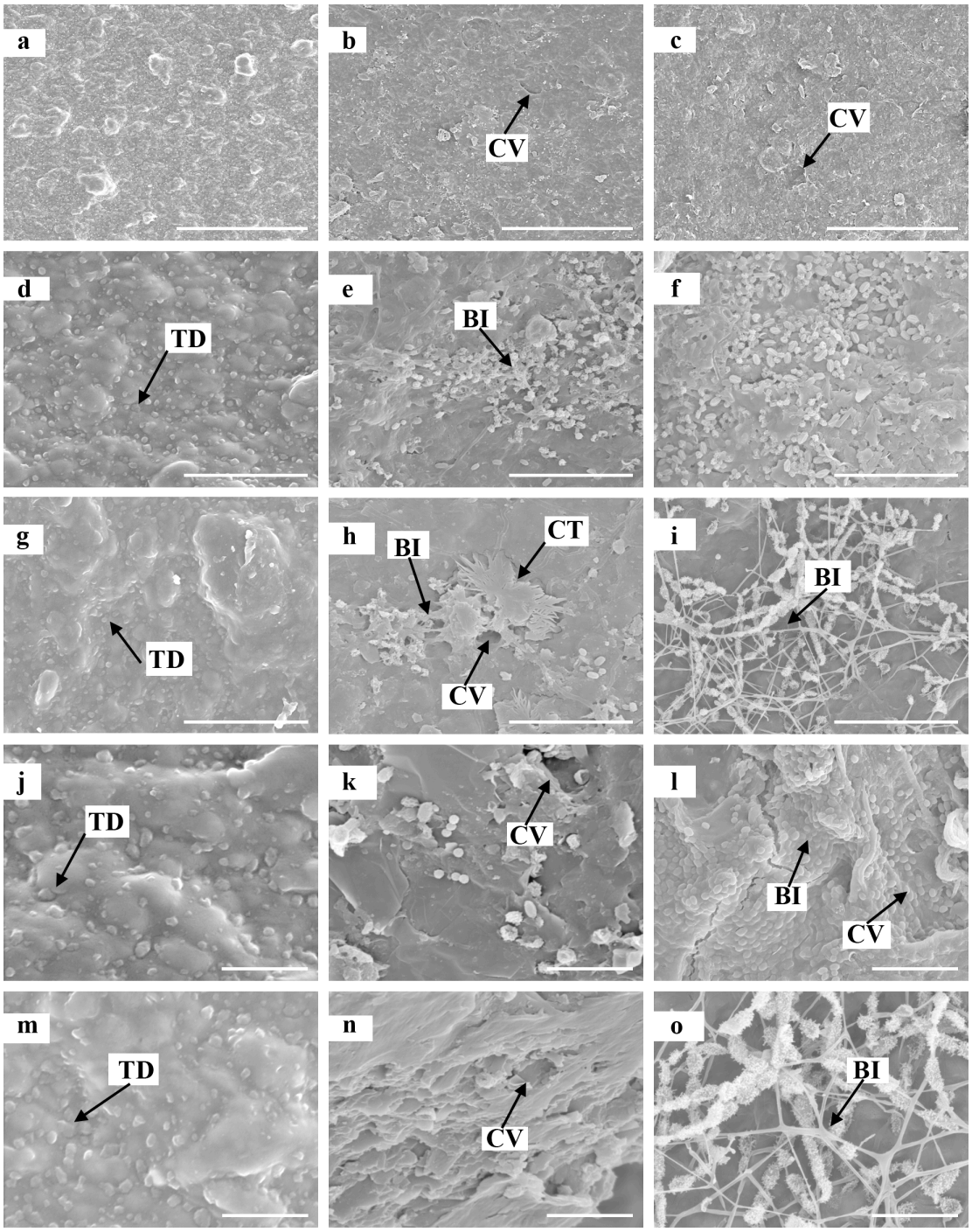

Figure 5-15. SEM micrographs showing the effects of biodegradation on the surface of PBAT sample with 0% (b, e, h, k, and n) and 10% (c, f, i, l, and o) gel contents after 45 d of biodegradation test compared to non-incubated samples (a, d, g, j, and m) at different magnification. (a, b, c) bars = 100 μm; (d, e, f, g, h, i) bars = 20 μm; (j, k, l, m, n, o) bars = 10 μm; BI = Biofilm; CT = Crystal of PBAT; CV = cavity; TD = Titanium dioxide; published in Kijchavengkul *et al.* (2008b)

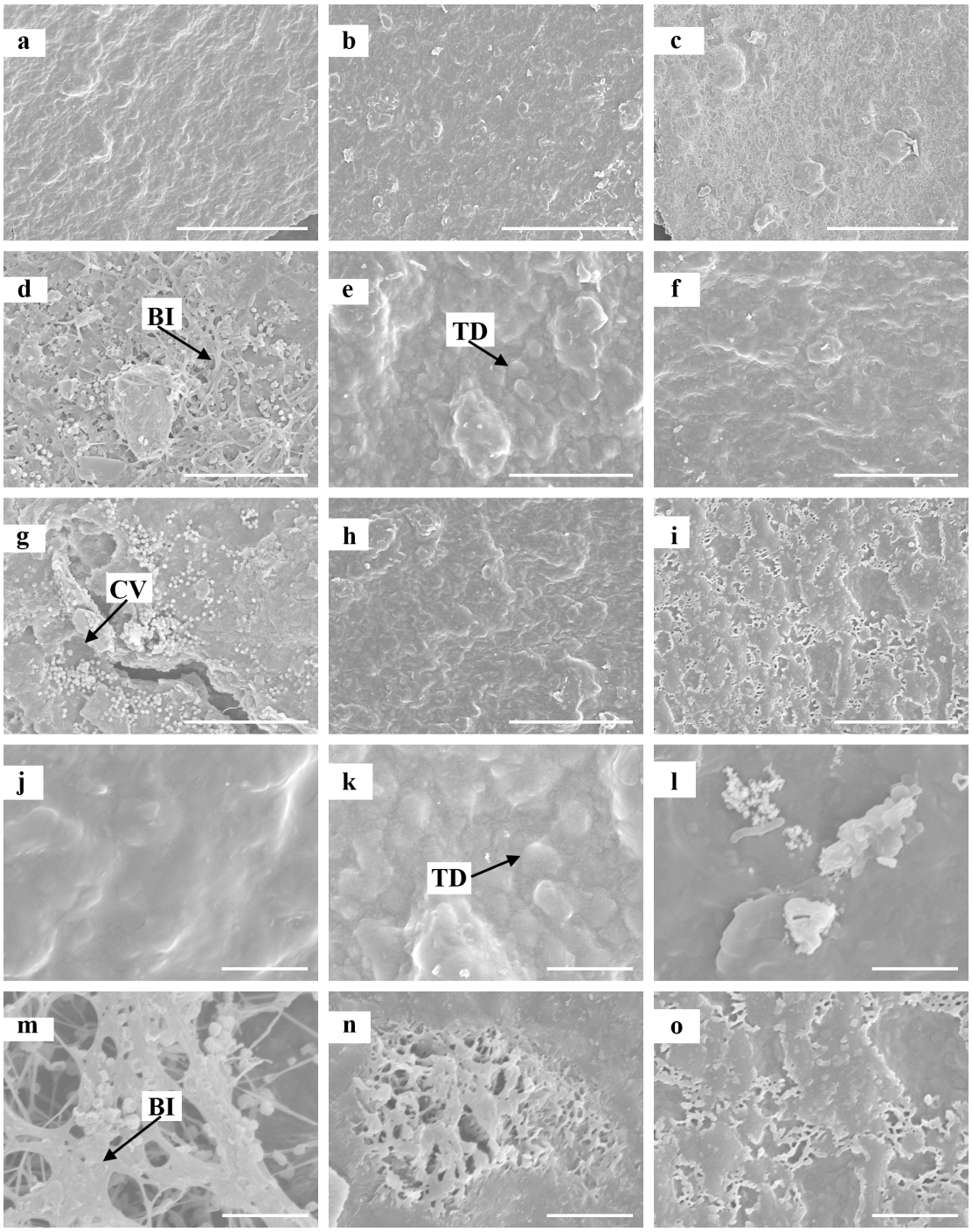

Figure 5-16. SEM micrographs showing the effects of biodegradation on the surface of PBAT sample with 30% (a, d, g, j, and m), 50% (b, e, h, k, and n) and 70% (c, f, i, l, and o) gel contents after 45 days of biodegradation test at different magnification. (a, b, c) bars = 100 μm; (d, e, f, g, h, i) bars = 20 μm; (j, k, m, n, o) bars = 10 μm; (l) bar = 5 μm; BI = Biofilm; CT = Crystal of PBAT; CV = cavity; TD = Titanium dioxide; published in Kijchavengkul *et al.* (2008b)

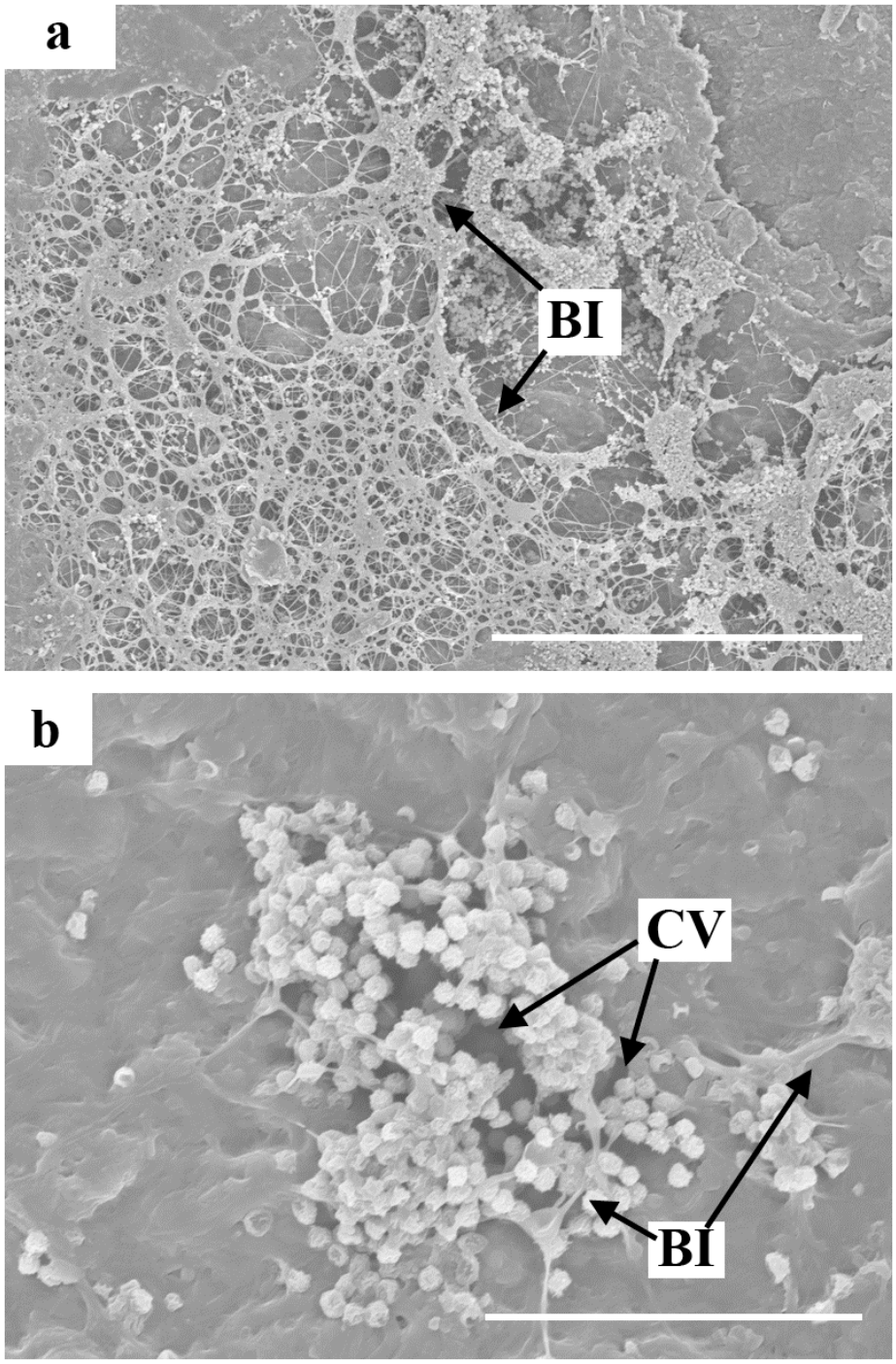

Figure 5-17. (a) SEM micrograph of the PBAT surface covered with biofilm; (b) SEM micrograph of microorganism colonies, biofilm, and cavities on the film surface. (a) bar = 100 μm ; (b) bar = 20 μm; BI = Biofilm; CV = cavity; published in Kijchavengkul *et al.* (2008b)

REFERENCES

REFERENCES

ASTM (2003) D 5338-98(2003) standard test method for determining aerobic biodegradation of plastic materials under controlled composting conditions. West Conshohocken, PA, ASTM International.

ASTM (2004) D 6400-04 standard specification for compostable plastics. West Conshohocken, PA, ASTM International.

ASTM (2006) D 2765-01 standard test methods for determination of gel content and swell ratio of crosslinked ethylene plastics. West Conshohocken, PA, ASTM International.

Buxbaum, LH (1968). "The degradation of poly(ethylene terephthalate)." Angewandte Chemie-International Edition **7**(3): 182-190.

Gesenhues, U (2000). "Influence of titanium dioxide pigments on the photodegradation of poly(vinyl chloride)." Polymer Degradation and Stability **68**(2): 185-196.

Ioan, S, Grigorescu, G and Stanciu, A (2001). "Dynamic-mechanical and differential scanning calorimetry measurements on crosslinked poly(ester-siloxane)-urethanes." Polymer **42**(2001): 3633-3639.

Irick, G (1972). "Determination of the photocatalytic activities of titanium dioxides and other white pigments." Journal of Applied Polymer Science **16**: 2387-2395.

Kale, G, Kijchavengkul, T, Auras, R, Rubino, M, Selke, SE and Singh, SP (2007). "Compostability of bioplastic packaging materials: An overview." Macromolecular Bioscience **7**(3): 255-277.

Kijchavengkul, T, Auras, R, Rubino, M, Ngouajio, M and Fernandez, RT (2008a). "Assessment of aliphatic-aromatic copolyester biodegradable mulch films. Part I: Field study." Chemosphere **71**(5): 942-953.

Kijchavengkul, T, Auras, R, Rubino, M, Ngouajio, M and Fernandez, RT (2008b). "Assessment of aliphatic-aromatic copolyester biodegradable mulch films. Part II: Laboratory simulated conditions." Chemosphere **71**(9): 1607-1616.

Marcotte, FB, Campbell, D and Cleaveland, JA (1967). "Photolysis of poly(ethylene terephthalate)." Journal of Polymer Science: Part A: Polymer Chemistry **5**(3): 481-501.

Ngouajio, M, Auras, R, Fernandez, RT, Rubino, M, Counts, JW and Kijchavengkul, T (2008). "Field performance of aliphatic-aromatic copolyester biodegradable mulch films in a fresh market tomato production system." Horttechnology **18**(4): 605-610.

Ngouajio, M and Ernest, J (2004). "Light transmission through colored polyehtylene mulches affects weed populations." Hortscience **39**(6): 1302-1304.

Rivaton, A and Gardette, JL (1998). "Photo-oxidation of aromatic polymers." Angewandte Makromolekulare Chemie **261/262**(1): 173-188.

Robinson, JW, Skelly-Frame, EM and FrameII, GM (2005). Undergraduate Instrumental Analysis. New York, NY, Marcel Dekker.

Schnabel, W (1992). Polymer Degradation: Principles and Practical Applications. New York, NY, Hanser.

Searle, J and Worsley, D (2002). "Titanium dioxide photocatalysed oxidation of plasticisers in thin poly(vinyl chloride) films." Plastics Rubber and Composite **31**(8): 329-335.

Shlyapintokh, V (1984). Photochemical Conversion and Stabilization of Polymers. New York, NY, Hanser.

Chapter 6 Biodegradation and hydrolysis rate of aliphatic aromatic polyester

6.1. Introduction

Biodegradable and compostable polymers have gained attention from industries, consumers, and governments as a potential way to reduce municipal solid waste since they can be recycled or energy recovered through composting into soil amendment products (Narayan 2001). Therefore, much attention has been given to their production, implementation, and end of life scenario.

One of the biodegradable and compostable polymers that has potential in commercial use is poly(butylene adipate-*co*-terephthalate) or PBAT, due to its ease of processing and similar mechanical properties to polyethylene (Kijchavengkul *et al.* 2008a). PBAT is an aliphatic aromatic copolyester produced from petroleum based resources and certified as compostable by the Biodegradable Products Institute (BPI) according to the ASTM D6400 specification (BPI 2008). PBAT is a linear random copolyester consisting of two types of dimer. The rigid section BT is an ester repeat unit consisting of 1,4 butanediol and terephthalic acid monomers, while the flexible section BA consists of 1,4 butanediol and adipic acid monomers (Figure 6-1).

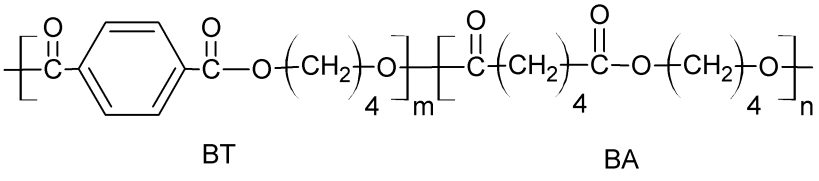

Figure 6-1. Chemical structure of poly(butylene adipate-*co*-terephthalate) or PBAT

As determined by a life cycle inventory (Shen and Patel 2008), PBAT, as well as other biodegradable polyesters, has the greatest environmental benefits when it is recovered through recycling or composting. Composting is a process where biodegradable materials, such as manure and leaves, are decomposed and transformed by microorganisms into a humus-like substance called compost, CO_2, water, and minerals, through a controlled biological process (ASTM 2004). According to ASTM D6400, in order to be compostable, a material must possess three essential qualities: ability to easily disintegrate in a composting environment, inherent biodegradability, which is tested using the ASTM D5338 method, and absence of ecotoxicity or any adverse effects of the final compost after decomposition (ASTM 2004).

According to ASTM D5338, sources of inocula used in biodegradation tests for biodegradable polymers are composts (ASTM 2003c). In general, there are three types of wastes used as compost feedstocks: yard, food and manure wastes (Kale *et al.* 2007b). Any of these can be used if during the first 10 days of the test the compost inoculum produces 50-150 mg of CO_2 per g volatile solids and the C/N ratio is between 10 and 40 (ASTM 2003c). Yard waste is a vegetative waste, such as leaves, grass clippings, tree trunks, and pruning wastes from the maintenance of landscaped areas. Food waste is uneaten food or waste from a food preparation process from residences, commercial, or institutional sources, such as restaurants or cafeterias. Manure waste is fecal and urinal excretion of livestock and is usually rich in nitrogen (Kale *et al.* 2007b).

The author have previously studied the biodegradation of biodegradable polyesters, such as poly(lactic acid) and PBAT, in various composting (Kijchavengkul *et*

al. 2006; Kijchavengkul *et al.* 2008a; Kijchavengkul *et al.* 2008b) and other environments such as soil burial (Kijchavengkul *et al.* 2010). Biodegradability of these biodegradable polymers in composting conditions and soil burial conditions is affected by both biotic or abiotic factors of the environment, such as temperature, moisture, pH, bio-surfactant and enzymes, and by polymer characteristics, such as chain flexibility, crystallinity, regularity and heterogeneity, functional groups, and molecular weight (Dřímal *et al.* 2007; Kale *et al.* 2007b; Stevens 2003).

Among biotic factors, extracellular enzymes produced by different microorganisms may have active sites with different specificity, such as complementary shape, charge, and hydrophilicity/hydrophobicity (Miller and Agard 1999), and hence have more capability to biodegrade certain polymers. For example, *Aspergillus niger* and *Aspergillus flavus,* presented in soil and crop, respectively, fungi produce enzymes that more easily digest aliphatic polyesters derived from 6-12 carbon di-acid monomers than those produced from other monomers (Chandra and Rustgi 1998). This enzymatic specificity may contribute to different degradation rates of biodegradable polyesters in differing compost environments.

Therefore, the objective of this study was to determine the effect of environment on the biodegradation/hydrolysis of aliphatic aromatic polyester (in this case PBAT). The biodegradation rates of aliphatic aromatic polyester under different compost environments was measured and compared with hydrolysis in buffer solution and in vermiculite as an example of an abiotic compost-like material.

6.2. Materials and Methods

6.2.1 Film Production

Poly(butylene adipate-*co*-terephthalate) or PBAT resin was purchased from BASF (Florham Park, N.J., USA). PBAT film was produced using a Killion KLB 100 blown film single screw extruder manufactured by Davis-Standard, LLC, (Pawcatuck, Conn., USA) with a temperature profile of 177-177-177-170-165-165-165°C for zone 1, 2, 3, clamp ring, adaptor, die 1 and 2, respectively. The extruder screw diameter was 25.4 mm (1 in) with L/D ratio of 24:1 and a diameter of the blown die of 50.8 mm (2 in). Screw speed and take up speed were 18.6 rpm and 0.033 m/s. The final thickness of the PBAT film was 38.1±5.1 μm (1.5±0.2 mil).

6.2.2 Biodegradation

Three types of commercial representative compost were used: manure compost from the Michigan State University commercial composting facility, East Lansing, Mich., USA; yard compost purchased from Hammond Farm, East Lansing, Mich., USA; and food waste compost from a local provider (Woodcreek Elementary School, Lansing, Mich., USA). First, film samples were analyzed for carbon content and composts for carbon to nitrogen ratio using a PerkinElmer CHN analyzer (Waltham, Mass., USA). Film carbon content was used for calculation of % mineralization, which is defined as the percentage of carbon in the polymer that is converted into CO_2. The carbon to nitrogen ratio (C/N ratio) was measured to determine suitability of composts for the testing. As previously mentioned, good quality compost should have a C/N ratio between 10 and 40 (ASTM 2003c; Rynk 1992).

An in-house built direct measurement respirometric system (DMR) connected to a CO_2 infrared gas analyzer was used to determine the biodegradation of the PBAT films in compost. Each bioreactor contained 250 g compost (wet basis) as control; a mixture of 250 g compost (wet basis) with 6 g cellulose powder (20 μm grade, Sigma Aldrich, St. Louis, Mo., USA) as positive control; or compost with 6 g of PBAT film cut into 1 cm x 1 cm pieces. Each test was run in triplicate. Details of the apparatus and testing conditions can be found elsewhere (Kale *et al.* 2007a; Kijchavengkul *et al.* 2006). The test was conducted according to ASTM D5338 specifications (ASTM 2003c). The bioreactors were incubated in an environmental chamber at 58°C for 45 days. At 7, 15, 30, and 45 days, film samples were retrieved from the bioreactors and were analyzed for changes in thermal properties, FTIR spectra, and molecular weight reduction. The percent mineralization was calculated using equation 6-1.

$$\%Mineralization = \frac{sCO_2 - bCO_2}{W \times \frac{\%C}{100} \times \frac{44}{12}} \times 100 \qquad (6\text{-}1)$$

where sCO_2 is the amount of CO_2 from the sample or the cellulose reactor, bCO_2 is the amount of CO_2 from the compost reactor, W is the weight of sample or cellulose, and %C is the % carbon in the sample or cellulose obtained from the CHN analyzer.

6.2.3 Hydrolysis

The hydrolysis test was performed using an FDA migration cell consisting of a 40 ml glass amber, a screw cap with a hole, and a sealing polytetrafluoroethylene (PTFE)/silicon septum (ASTM 2003b). For each cell, fourteen circular PBAT disks of 38.1±5.1 μm thickness with a diameter of 0.0254 m were placed in the cells separated in

between by glass beads. The cells were filled with 35 ml of phosphate buffer with a pH of 8.0 (measured using an Oakton pH meter, Vernon Hills, Ill., USA) as a control for hydrolysis, and 35 ml of vermiculite with 50% moisture content (mixed with phosphate buffer) in order to simulate only hydrolysis under composting conditions. Vermiculite was used since it has texture similar to compost and excellent water holding capacity (Bellia *et al.* 1999). Three replicate test cells for each medium were stored in a water bath at 58°C for 45 days. The temperature was monitored using an HOBO® datalogger (Onset Computer, Bourne, Mass., USA). Samples were retrieved at 7, 15, 25, and 45 days for FTIR, molecular weight measurement, and ^{1}H-NMR.

6.2.4 Molecular weight measurement

The retrieved samples were cleaned with laboratory wipe without using water in order to prevent any further degradation. The weight average molecular weight reduction of the samples was determined by dissolving the PBAT sample in tetrahydrofuran (THF), Pharmco-Aaper (Brookfield, Conn., USA), at a concentration of 2 mg/mL. Once the sample was filtered through 0.45 μm PTFE filter, one hundred μL of each sample solution was injected into a Waters® Gel Permeation Chromatograph (GPC) equipped with three-column bank and a refractive index detector (Milford, Mass., USA.). The column bank consisted of three 7.8 mm x 300 mm single pore columns, Waters Styragel® HR4, HR3, and HR2, packed with 5 μm styrene divinylbenzene particles. A flow rate of 1 mL/min, a runtime of 45 min, and a temperature of 35°C were used. A calibration curve of a third-order polynomial equation was conducted using 10 different molecular weight polystyrene standards (range from 1.20×10^{3} to 3.64×10^{6} Da).

6.2.5 FTIR spectra

Film samples were scanned using a Shimadzu IR-Prestige 21 (Columbia, Md., USA) with an Attenuated Total Reflectance (ATR) attachment (PIKE Technologies, Madison, Wis., USA) from 4000 to 650 cm^{-1} to measure any changes in the spectral intensities, which correlate to the formation and destruction of functional groups within the films.

6.2.6 Thermal behavior

A differential scanning calorimeter (DSC) from Thermal Analysis Inc. (model Q100, New Castle, Del., USA) was used to determine changes in crystallinity of PBAT due to biodegradation in different compost media via changes in the heat of fusion. The sample size used was approximately 5-10 mg. The testing temperature was from -60 to 160°C with a ramping rate of 10°C/min, in accordance with ASTM D 3418 (ASTM 2003a).

6.2.7 ^{1}H-NMR spectroscopy

The ^{1}H-NMR spectra of the films in phosphate buffer or vermiculite were collected on a Varian 300 MHz NMR-Spectrometer (Varian Inc., Palo Alto, Calif., USA). Fifty milligrams of PBAT disks were dissolved in 5 mL of deuterated chloroform (δ = 7.24 ppm) from Cambridge Isotope Laboratories Inc. (Andover, Mass., USA). Chemical displacement was corrected as tetramethylsilane (δ = 0 ppm) was used as an internal standard, included in the deuterated chloroform solution.

6.3. Results and Discussion

6.3.1 Biodegradation in three different composts

Total biodegradation of PBAT film at 45 days in manure compost was the highest (67.3±2.8%), followed by those in food compost (44.9±2.6%) and yard compost (33.9±1.5%), respectively (Figure 6-2). The biodegradation of cellulose also shows a similar pattern, highest biodegradation in manure compost, followed by food and yard compost. The higher degradation in manure compost than food and yard compost can be attributed to greater microbial activity in the manure compost. Evidence of the greater activity of the manure compost includes the greater amount of evolved CO_2 gas from compost respiration (Figure 6-3). In this case, the recommended compost activity was 2,430-8,080 mg CO_2, calculated from 50-150mg/g volatile solid of the composts (ASTM 2203c). CO_2 production from yard compost during the first 10 days was just 4.3% below the recommended value, while those from manure and food compost were within the recommended range. Furthermore, the C/N ratio of yard compost (47.1±5.2) was slightly outside the range of suitable compost, which possibly indicates an inactive compost (Rynk 1992), while those of manure (22.9±1.3) and food (36.0±1.7) composts were well within the recommended C/N range of 10 to 40. Therefore, this confirms that microbial activity of the compost and the C/N ratio play a significant role in the total biodegradation of biodegradable plastics as inferred by Ishii and Takii (2003), Ishii *et al.* (2007), and Nakajima-Kambe *et al.* (2009).

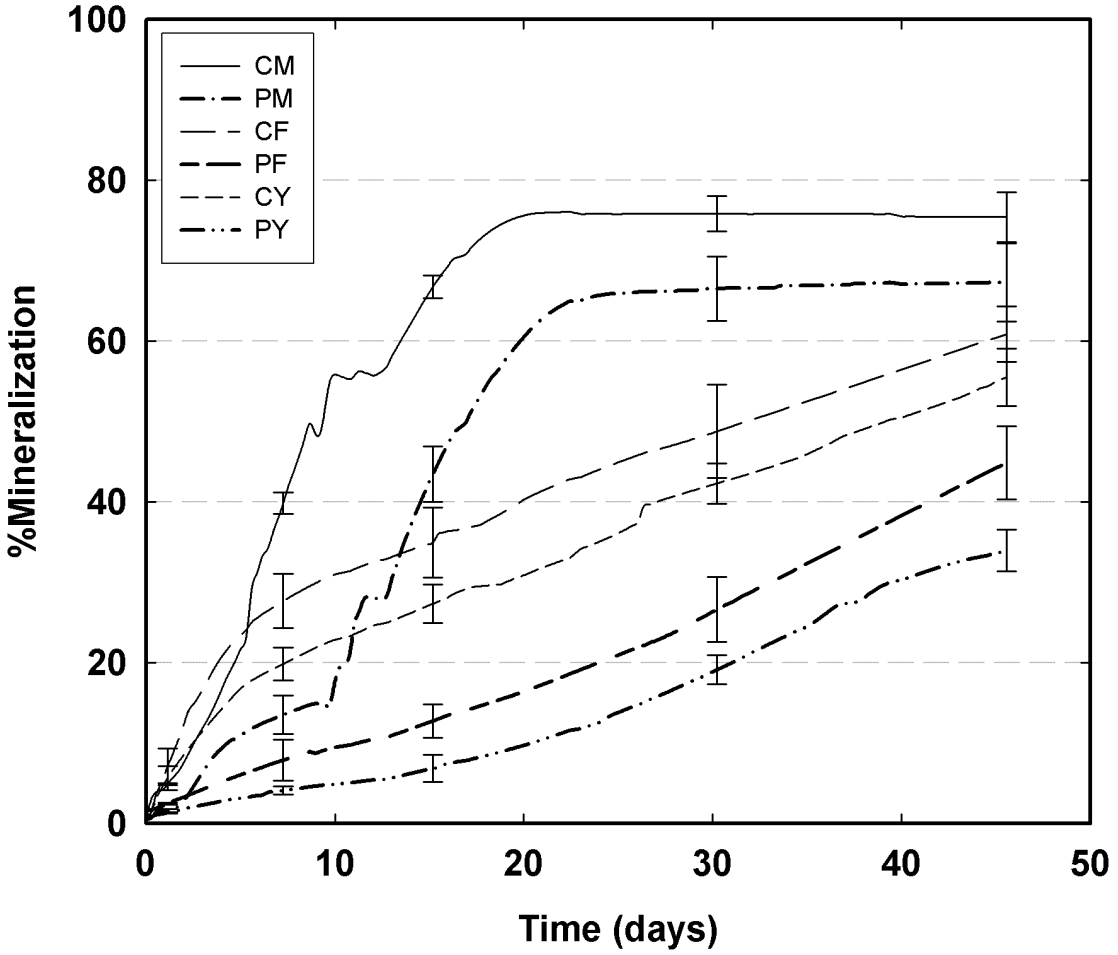

Figure 6-2. Mineralization of PBAT and cellulose positive control in three different composts, where CM is mineralization of cellulose in manure compost, PM is PBAT in manure compost, CF is cellulose in food compost, PF is PBAT in food compost CY is cellulose in yard compost, and PY is PBAT in yard compost. Error bars represent standard deviation at 1, 7, 15, 30, and 45 days.

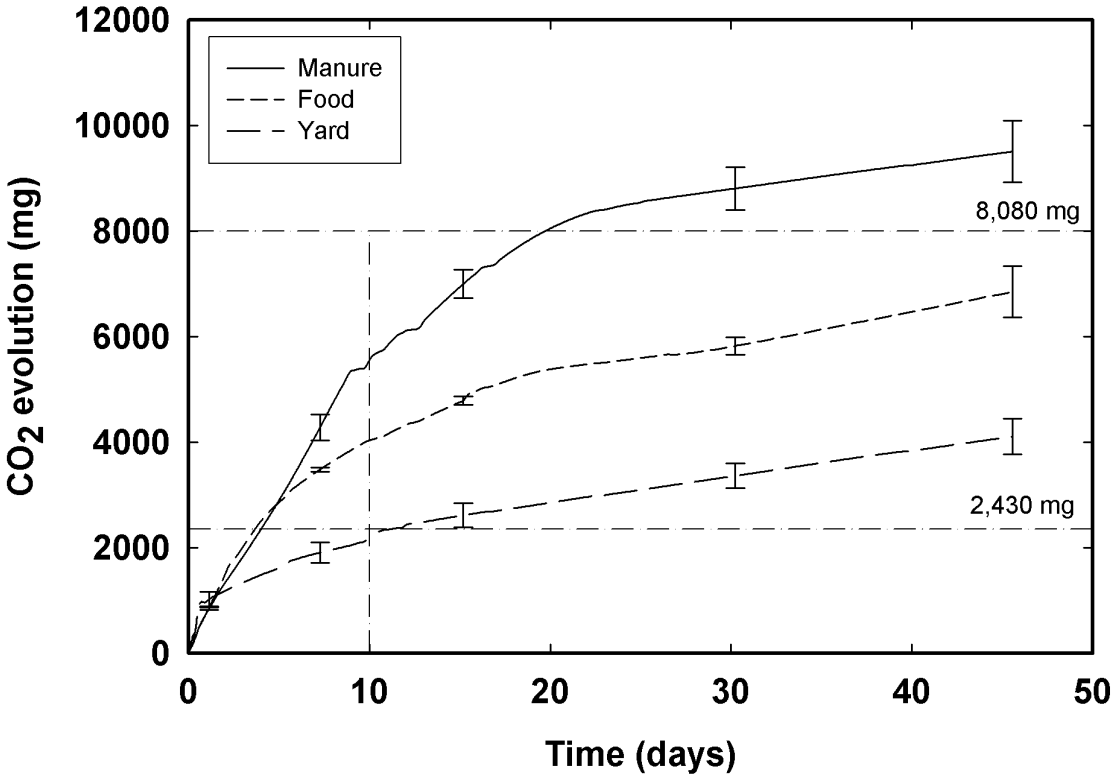

Figure 6-3. Evolution of CO_2 gas from respiration of manure, food, or yard composts as function of time; values of 2,430 and 8,080 mg indicate the window of recommended compost according to ASTM D5338 standard, which was calculated from 50 mg/g and 150 mg/g volatile solid of composts. Error bars represent standard deviation at 1, 7, 15, 30, and 45 days. Each bioreactor contained 250 g of each compost type.

6.3.2 Biodegradation rate and hydrolysis

While the previous biodegradation results indicated that samples in the manure compost environment degraded faster than in the other two composts, it did not determine whether there were differences in the biodegradation and/or hydrolysis rates in these different compost environments. In addition to microbial activity, hydrolysis has a substantial influence on biodegradation and biodegradation rates of biodegradable polyesters such as PBAT, since hydrolysis is one of the initial processes of

biodegradation (Kale *et al.* 2007b; Kasuya *et al.* 2009; Lucas *et al.* 2008; Witt *et al.* 2001). Hydrolytic random chain scission at ester linkages reduces the size of polyester chains into the size range that microorganisms can bio-assimilate. Therefore, it is critical to understand and determine if hydrolysis and/or microbial activity are the main determinants of degradation of PBAT in different compost environments. The same pattern of molecular weight reduction for the PBAT samples in the phosphate buffer solution and vermiculite media are observed in Figure 6-4a and 6-b, indicating the same hydrolysis process for these two environments. The fact that during the first 15 days only slight changed in molecular weight distributions (MWD) was observed indicates that, initially, the hydrolytic main chain scission favored the chain ends because of the increased free volume associated with them. As the hydrolysis proceeds, while the MWD of the hydrolyzed samples become narrower, the main chain scission starts to occur at the middle of the chains, indicated by the significantly shift of MWD towards lower molecular weight. Figure 6-5 shows changes in number average molecular weight (M_n) of PBAT films from biodegradation in the three different compost environments, as well as from hydrolysis in pH 8.0 buffer solution or in vermiculite as a function of time.

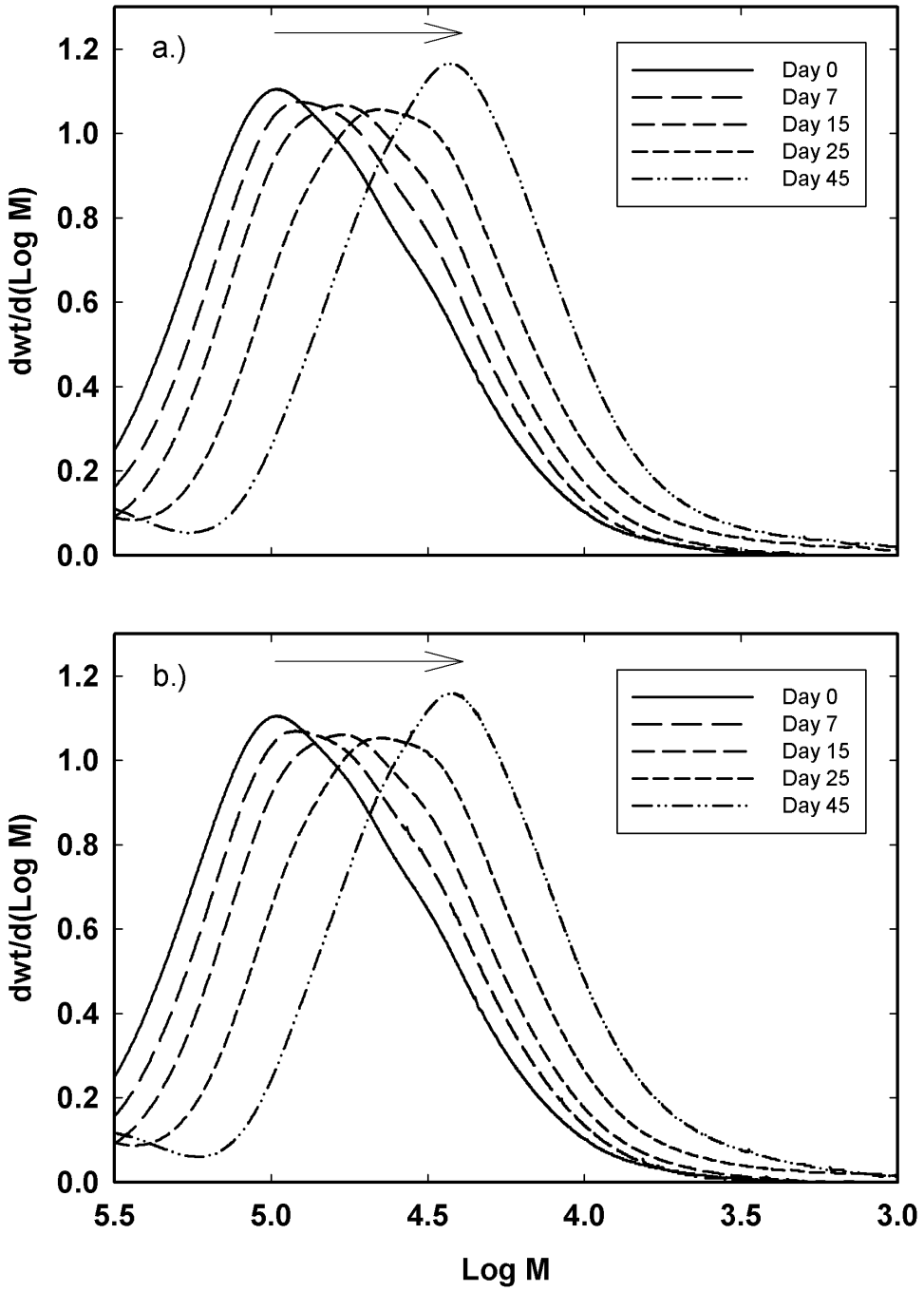

Figure 6-4. Molecular weight distribution (MWD) of hydrolyzed samples in (a) phosphate buffer solution of pH 8.0 and (b) vermiculite for 0, 7, 15, 25, and 45 days at 58°C

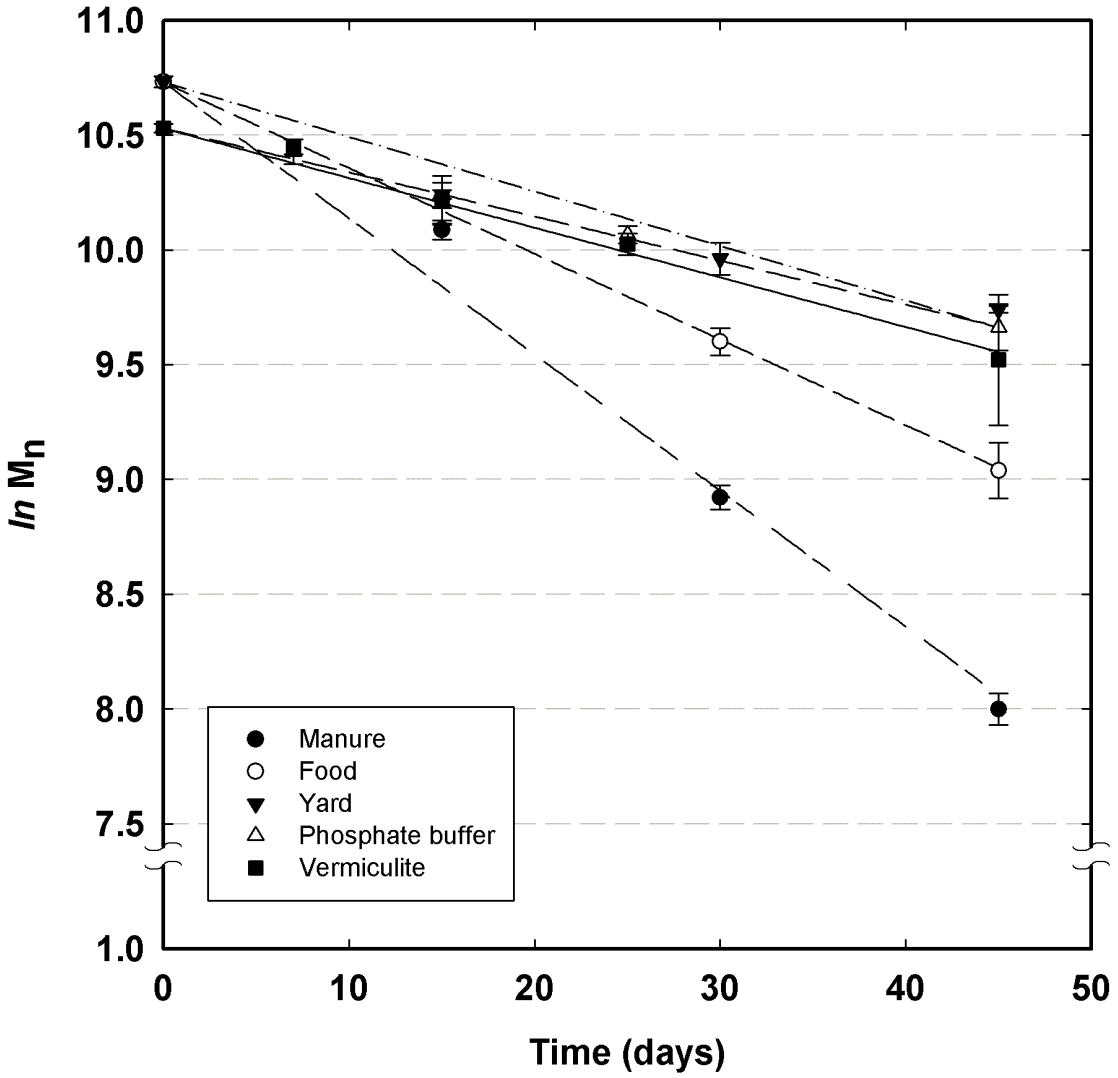

Figure 6-5. Logarithmic reduction of molecular number (M_n) in of PBAT films from hydrolysis in phosphate buffer solution (pH = 8.0) or in vermiculite, or from biodegradation in manure, yard, or food composts as a function of time; the regression are performed using a 1st order reaction. Values are represented as mean ± standard error.

The reduction of M_n from biodegradation in compost and hydrolysis in both media follows a first order reaction, where the rate constants (k) can be obtained from the slopes as shown in Table 6-1. The k value from PBAT biodegradation in manure

compost was the highest (0.0593±0.0025 d^{-1}) and those from biodegradation in yard compost (0.0237±0.0017 d^{-1}), hydrolysis in buffer solution (0.0192±0.0011 d^{-1}) and in vermiculite (0.0216±0.0021 d^{-1}) are among the lowest. The reduction of M_n of PBAT from biodegradation in yard compost was not different from those from hydrolysis due to the low microbial activity of yard compost, as indicated by poor CO_2 emissions and a too high C/N ratio. Although the composts used for testing have all or most of the recommended parameters according to the ASTM and the ISO standards, e.g. C/N ratio and CO_2 production, specification of compost type and the current recommended parameters may not be sufficient as a guideline for testing because of the lack of consistency of microbial composition among different composts and within the same compost (Ishii and Takii 2003). Furthermore, enzymatic preferences of microorganisms for different isomers and number of carbon atoms for polymers are diverse (Maeda *et al.* 2005; Nakajima-Kambe *et al.* 2009; Shah *et al.* 2008). Therefore, relating the biodegradation rate to general compost composition and/or other factors may overlook the specific families of microorganisms presented in the compost that may be more or less successful than others at biodegrading the aliphatic aromatic polyester. Microorganisms in composts and their enzymes responsible for the hydrolytic degradation can be identified in order to solve this issue. This is subject of our current and future research, and it will be further communicated.

Table 6-1. Rate constants (*k*) calculated from reduced molecular number of biodegradation of PBAT films in manure, yard, or food composts or hydrolysis in phosphate buffer solution or in vermiculite

Media	*k* from M_n (d^{-1})
Manure	0.0593 ± 0.0025^{a}
Food	0.0376 ± 0.0012^{b}
Yard	0.0237 ± 0.0017^{c}
Phosphate buffer	0.0192 ± 0.0011^{c}
Vermiculite	0.0216 ± 0.0021^{c}

Note: values are represented as average ± standard error. '*k*' values with a different superscript letter are statistically different at a=0.05 (Tukey – HSD test)

The preference of biodegradation and hydrolysis of amorphous polymeric regions in semi-crystalline biodegradable polymers is well established (Kale *et al.* 2006). DSC thermograms should indicate an increase of the crystalline region of the polymer as a function of time as samples are subjected to hydrolysis and/or biodegradation. Despite the fact that PBAT is a statistical random copolymer with a degree of randomness (*r*) of 0.97 to 1.02 and average block length of 1.6 to 2.6 (Herrera *et al.* 2002), which theoretically cannot crystallize (Rodriguez *et al.* 2003; Shi *et al.* 2005; van Krevelen and Nijenhuis 2009), the lower melting temperature of PBAT (130°C) than PBT (230°C) is evidence that cocrystallization in PBAT can occur since the soft BA sections can adjust its chain conformation to that of the rigid BT units. Furthermore, in order to undergo cocrystallization, the cohesive energies of the two comonomers should be relatively comparable so that the comonomer with greater cohesive energy does not get separated and form crystal lattices of only one copolymer. In this case, the ratio of cohesive energy of BA to BT (E_{BA}/E_{BT}) of PBAT film with f_{BA}/f_{BT} of 0.59/0.41 calculated using the functional group contribution method is 1.15 (cohesive energies of $-CH_2-$, -(C=O)-O-,

and aromatic -C_6H_4- are 4.19, 13.41, and 31.00 kJ/mol, respectively), which indicates that PBAT can cocrystallize (van Krevelen and Nijenhuis 2009). In the case of PBAT, the soft aliphatic BA unit is infused into the BT crystal lattice (Shi *et al.* 2005).

In biodegradation of PBAT in manure, yard, and food composts, increased heat of fusion (ΔH_f) from DSC thermograms was observed in all three composts as biodegradation proceeded (Figure 6-6), indicating increased crystallinity as a result of the amorphous regions being degraded first. The increased crystallinity also confirmed that the amorphous regions are more susceptible to biodegradation than the crystalline regions as reported by Mochizuki and Hirami (1997), Hakkarainen *et al.* (2000), Hayase *et al.* (2004), Gan *et al.* (2005), *Tserki et al.* (2006), Barone and Arikan (2007), and Kijchavengkul *et al.* (2008b) in various biodegradable polymers.

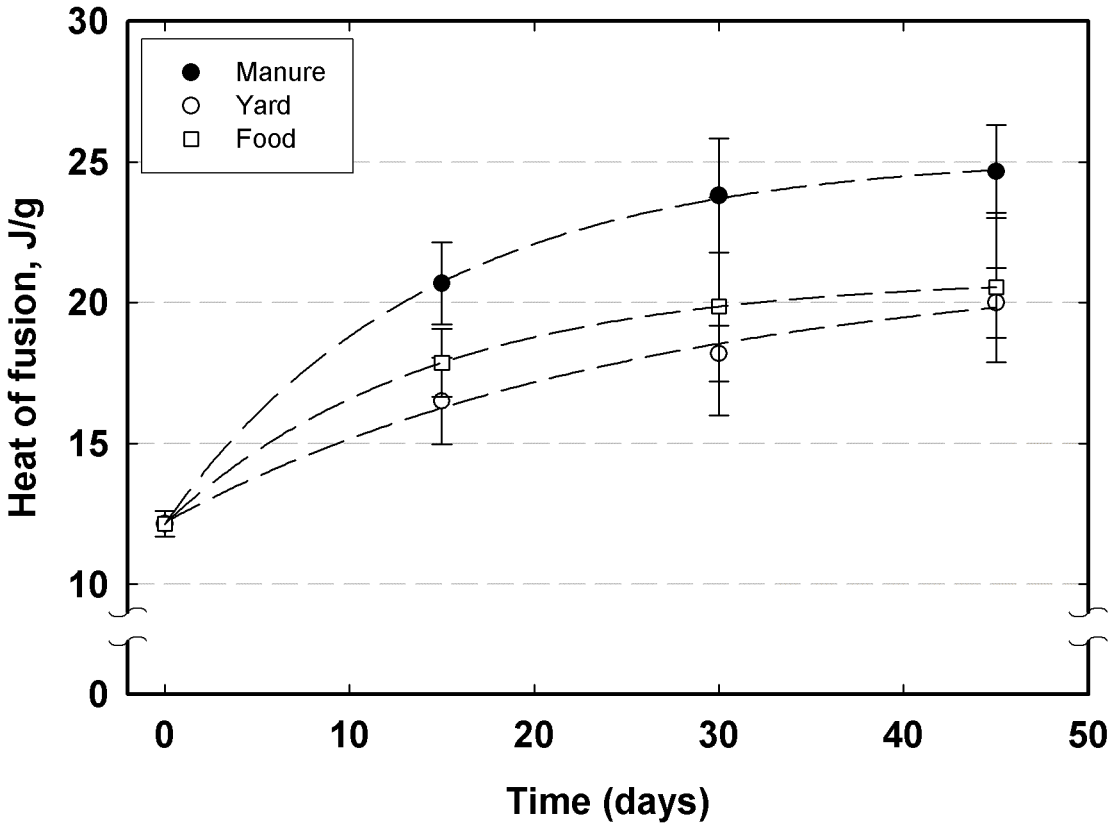

Figure 6-6. Increased heat of fusion (areas under melting peak in DSC thermogram) of PBAT films incubated in manure, yard, or food composts as a function of time. Error bars represent standard deviation. Dashed lines are the fitted curves to represent the increasing trend of heat of fusion.

Based on the structure of PBAT (Figure 6-1), several functional groups, such as hydroxyl (OH) and carbonyl (C=O) groups can be used as tools to study degradation. As a result of main chain scission from hydrolysis at ester linkages, terminal alcohol and carboxylic acid groups are produced, so as hydrolysis progresses, an increase in OH groups should be observed in the FTIR absorbance spectra. An increase in OH groups (3350 cm^{-1}) in all the samples was observed, and was more prominent in the compost samples than in phosphate buffer and vermiculite (Figure 6-7a to 6-7e). However, in the

PBAT samples hydrolyzed in phosphate buffer, an increase in the OH group was only observed during the first week, since compounds with OH terminal groups may dissolve in the phosphate buffer due to the greater polarity of this solution compared to the PBAT matrix.

Hydrolytic main chain scission at multiple locations in the polymer chain produces smaller molecules or oligomers, which can easily permeate out of the polymer matrix. Therefore, reduction of the carbonyl absorbance (1710 cm^{-1}) also results from hydrolysis. Only slight reductions in carbonyl groups were observed in the PBAT samples hydrolyzed in phosphate buffer (Figure 6-7f) and in vermiculite (Figure 6-7g). However, PBAT samples in manure (Figure 6-7h), food (Figure 6-7i), and yard composts (Figure 6-7j) manure showed greater reduction in carbonyl groups possibly due to synergistic effects of enzymatic degradation.

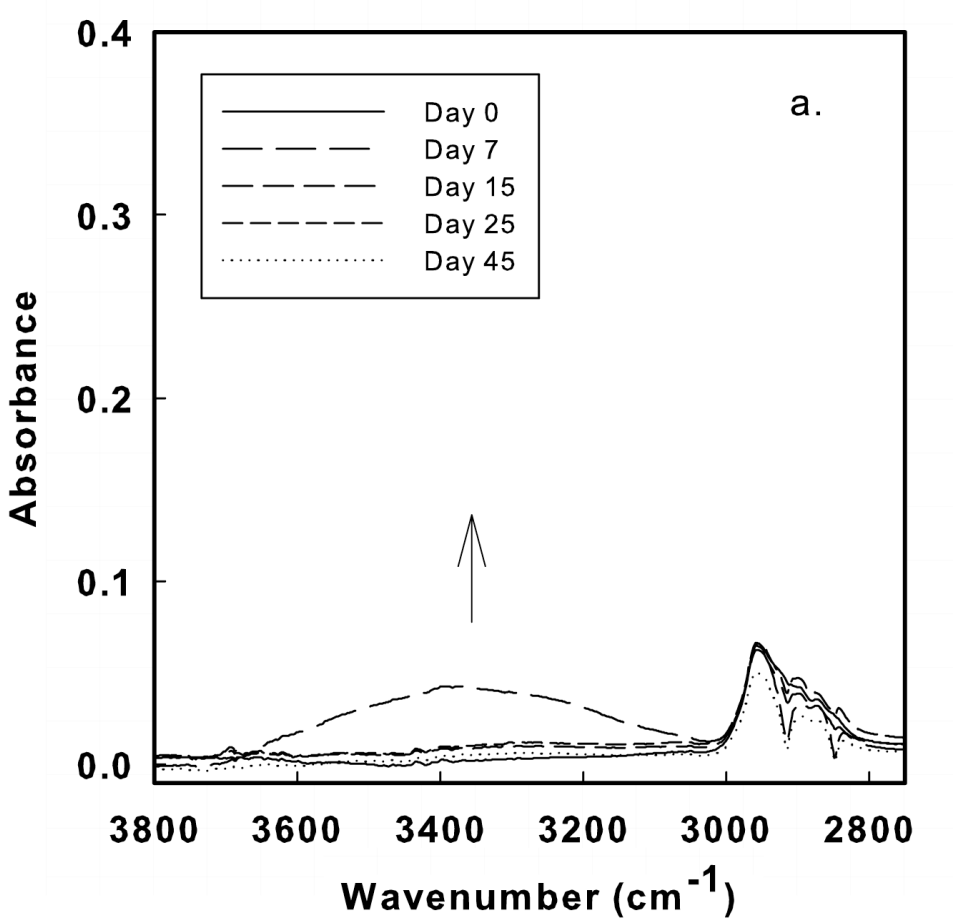

Figure 6-7a. FTIR absorbance spectra in the wavenumber range of 3800-2750 cm^{-1} of PBAT film in phosphate buffer solution

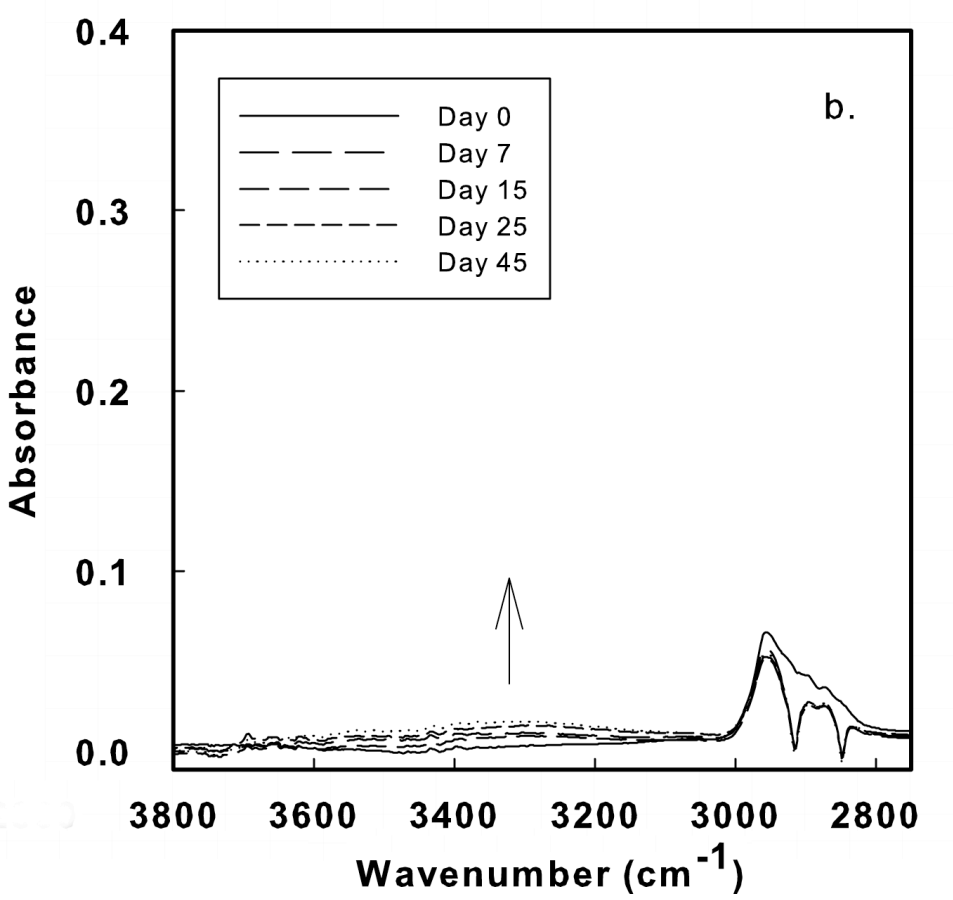

Figure 6-7b. FTIR absorbance spectra in the wavenumber range of 3800-2750 cm^{-1} of PBAT film in vermiculite

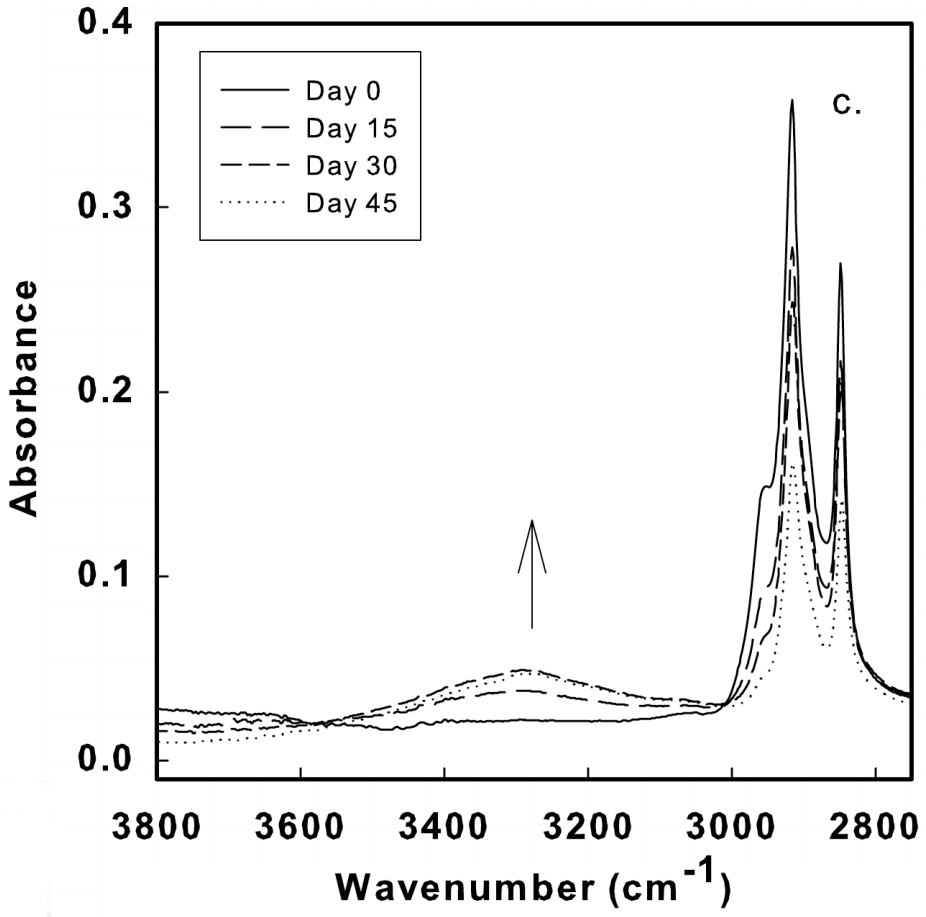

Figure 6-7c. FTIR absorbance spectra in the wavenumber range of 3800-2750 cm^{-1} of PBAT film in manure compost

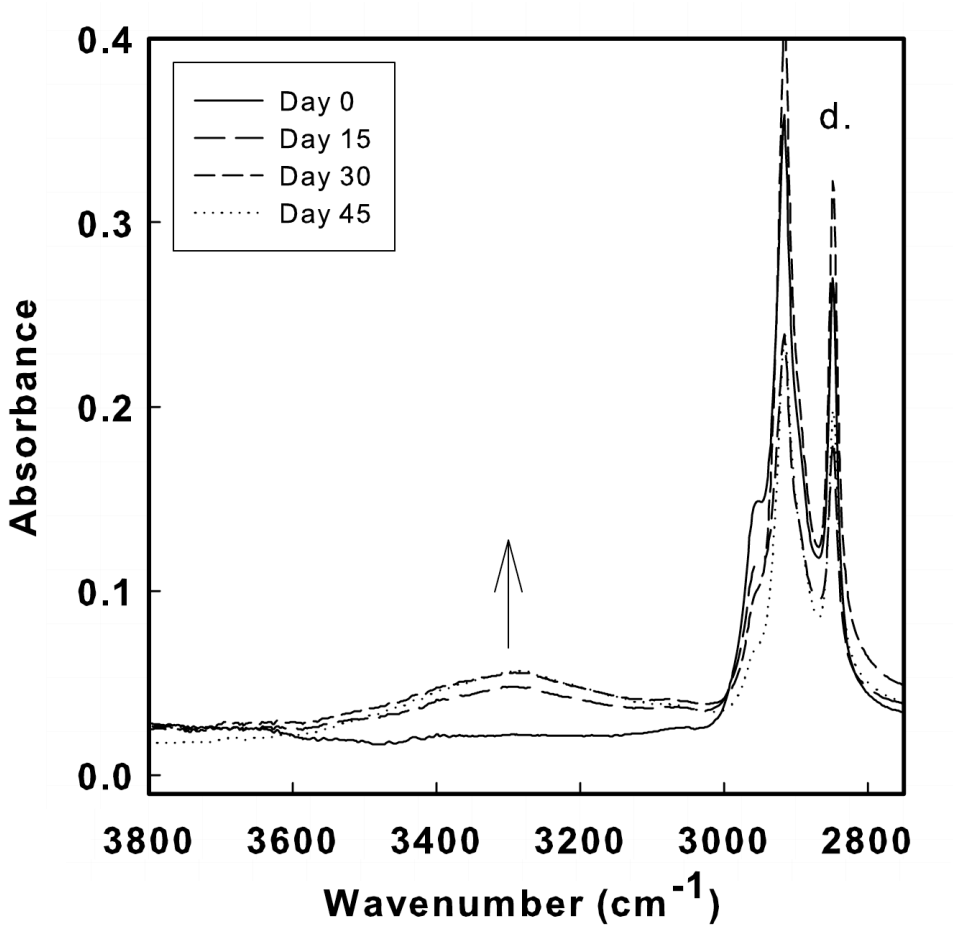

Figure 6-7d. FTIR absorbance spectra in the wavenumber range of 3800-2750 cm^{-1} of PBAT film in food compost

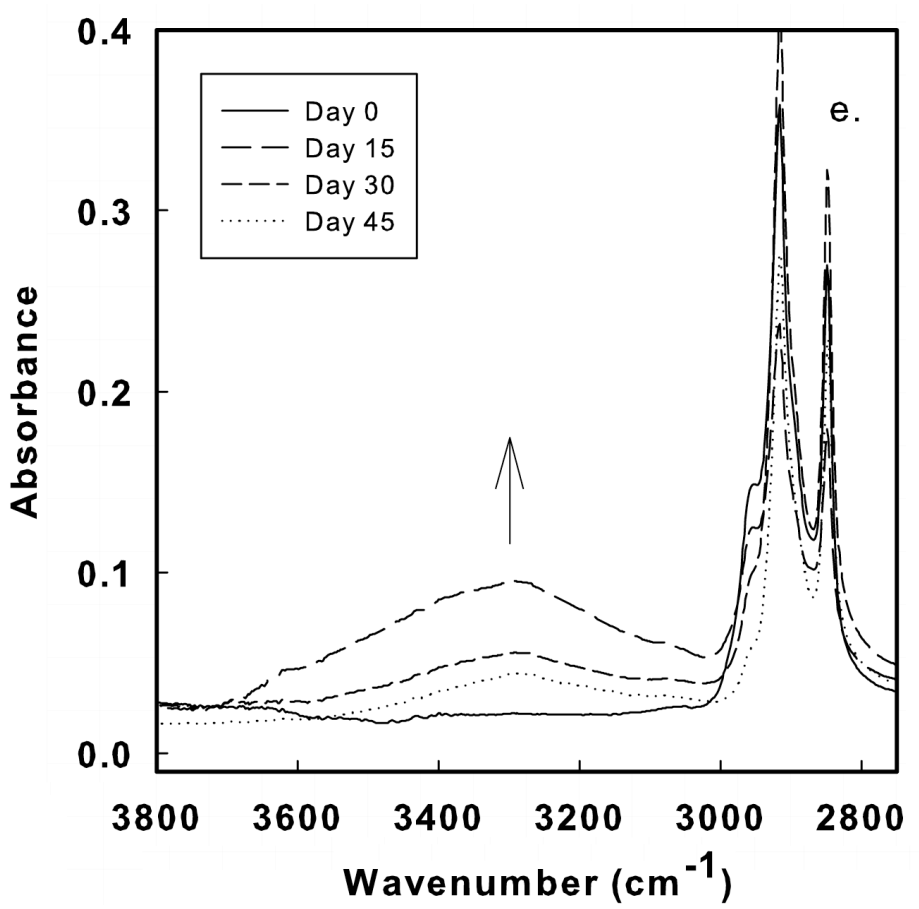

Figure 6-7e. FTIR absorbance spectra in the wavenumber range of 3800-2750 cm^{-1} of PBAT film in yard compost

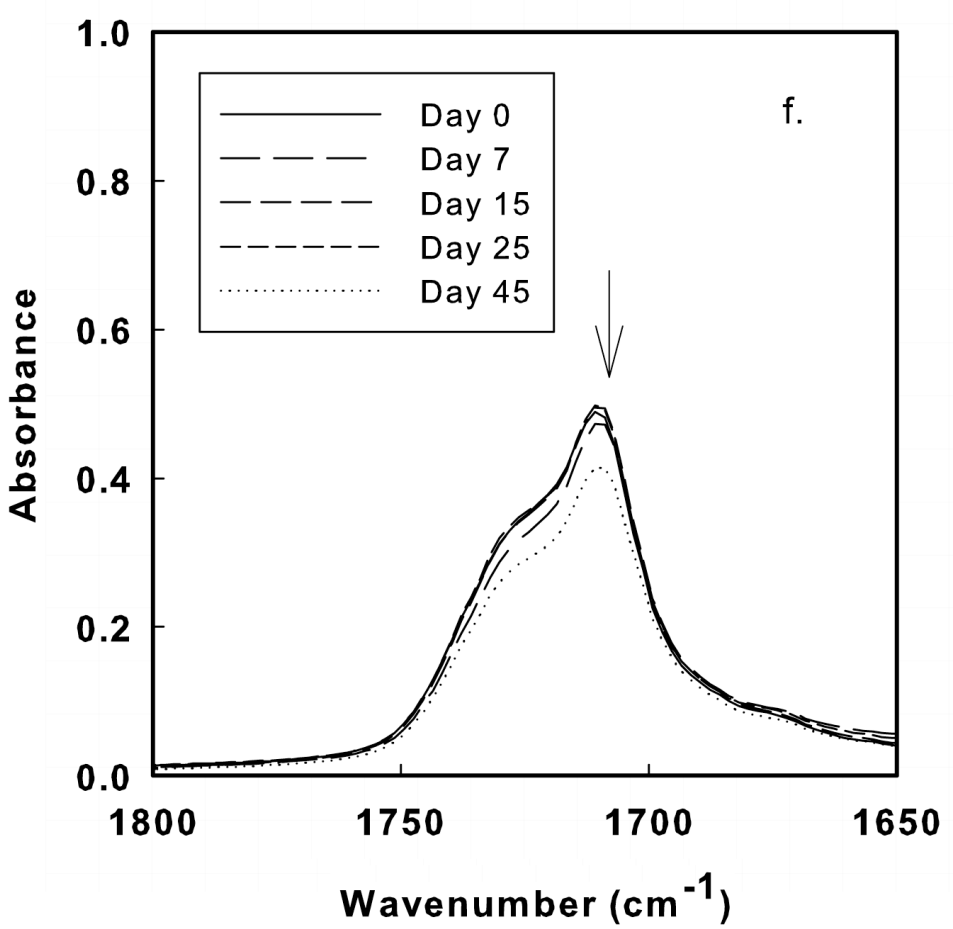

Figure 6-7f. FTIR absorbance spectra in the wavenumber range of 1800-1650 cm^{-1} of PBAT film in phosphate buffer solution

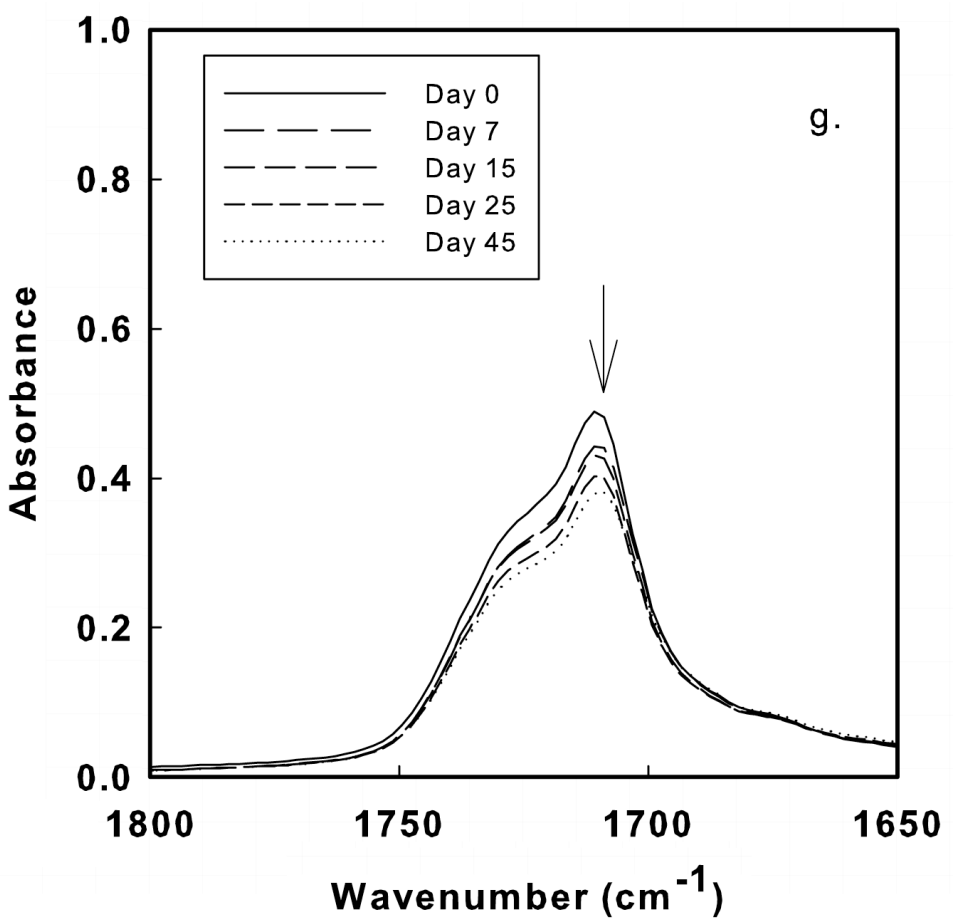

Figure 6-7g. FTIR absorbance spectra in the wavenumber range of 1800-1650 cm^{-1} of PBAT film in vermiculite

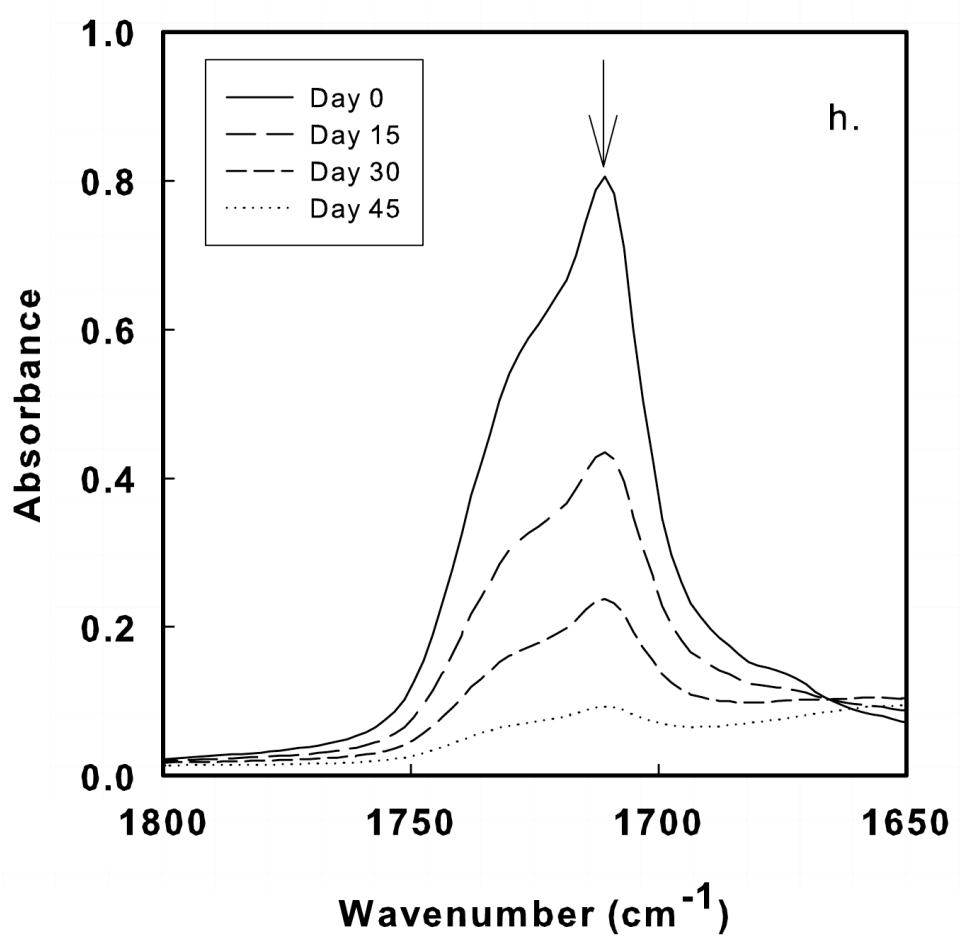

Figure 6-7h. FTIR absorbance spectra in the wavenumber range of 1800-1650 cm^{-1} of PBAT film in manure compost

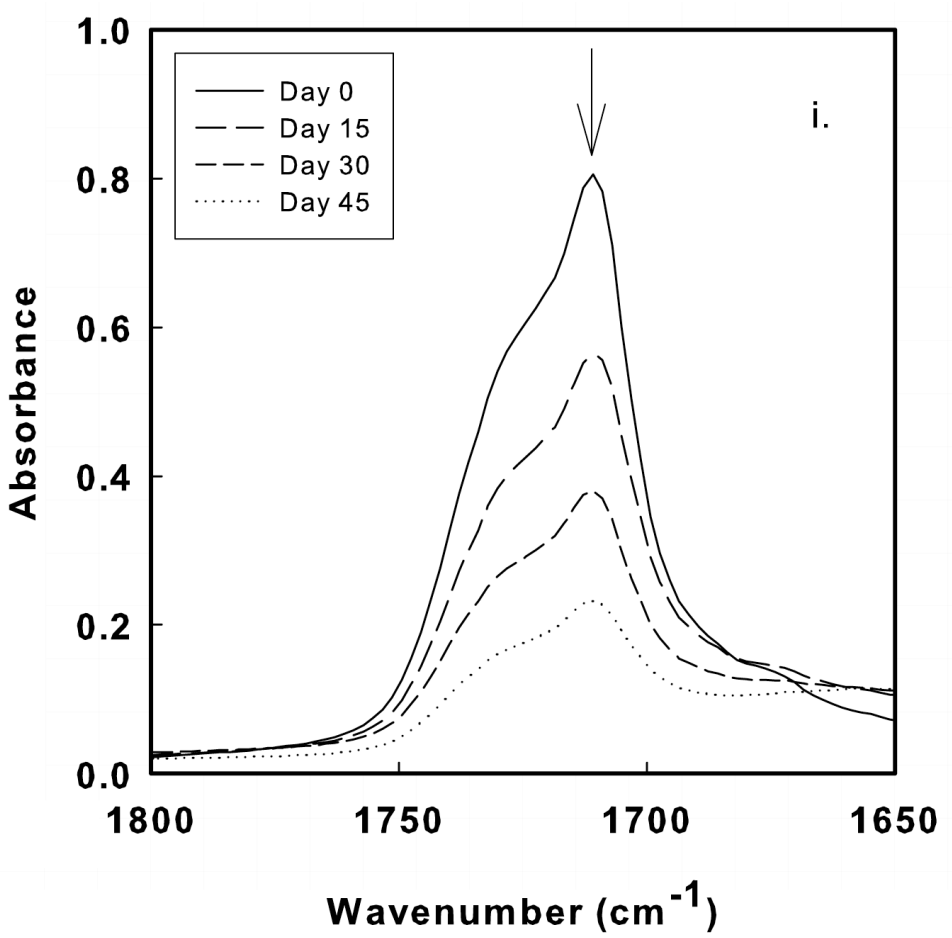

Figure 6-7i. FTIR absorbance spectra in the wavenumber range of 1800-1650 cm^{-1} of PBAT film in food compost

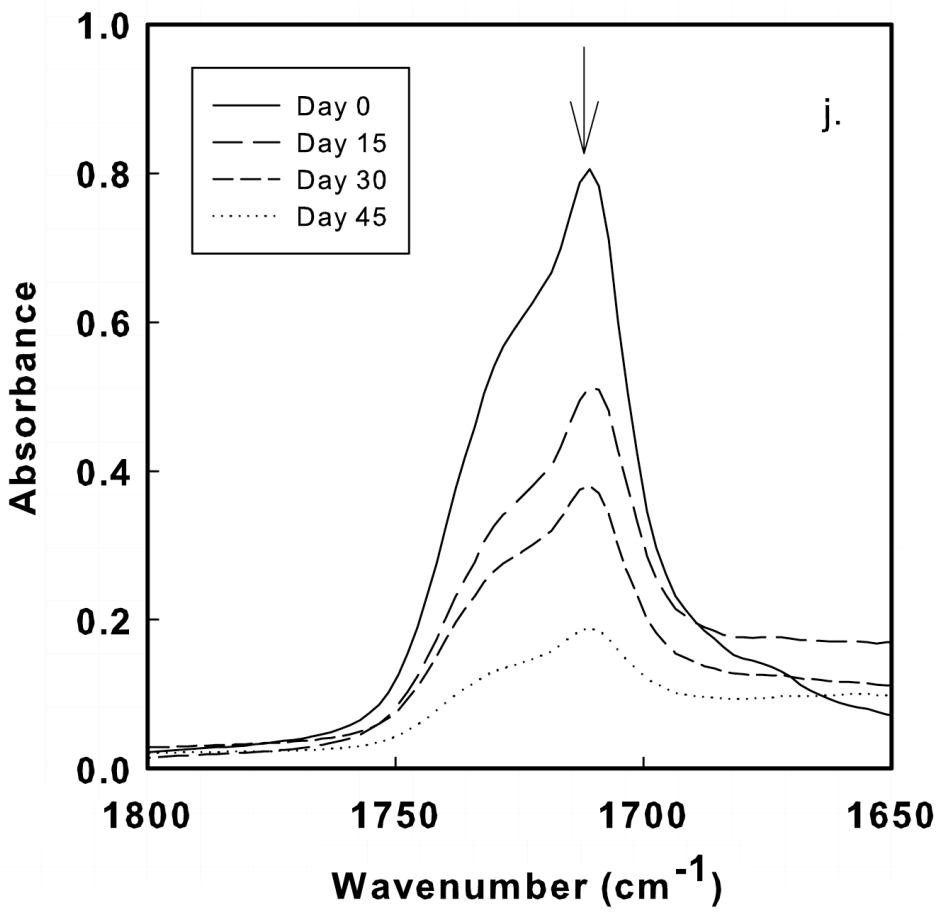

Figure 6-7j. FTIR absorbance spectra in the wavenumber range of 1800-1650 cm^{-1} of PBAT film in yard compost

6.3.3 Comonomers, microstructures, and degradation

PBAT is a random copolymer consisting of soft butylene adipate (BA) sections and hard butylene terephthalate (BT) sections (Figure 6-1). Equations 6-2 and 6-3, as suggested by Herrera *et al.* (2002), were used to determine the composition of the adipate fraction (f_{BA}) and the terephthalate fraction (f_{BT}) using the area of signals at 2.29 ppm (-OCOC**H$_2$**-) and 8.06 ppm (aromatic) (Figure 6-8). Changes in f_{BA} and f_{BT} were used to determine the effects of hydrolysis on each comonomer.

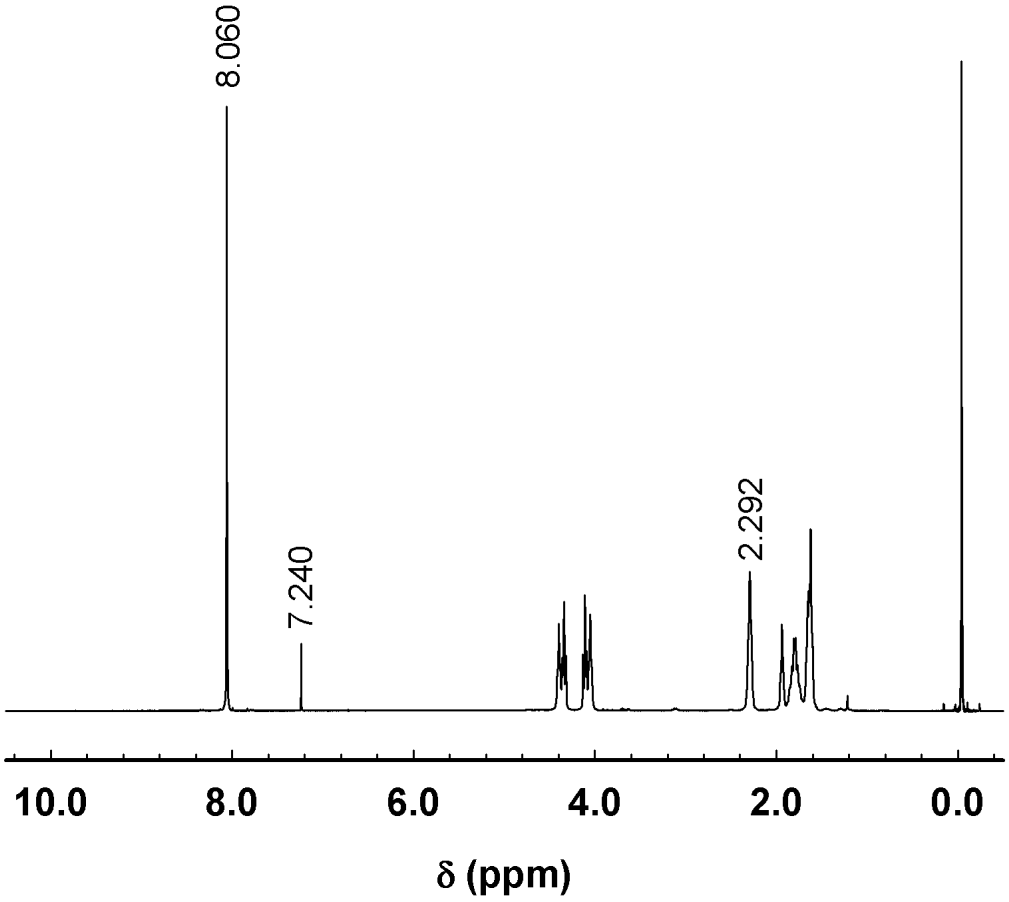

Figure 6-8. ^{1}H-NMR spectrum of PBAT with aromatic peak at δ = 8.06 ppm, deuterated chloroform at δ = 7.24 ppm, and -OCOC**H$_2$**- (adipate fraction) at δ = 2.29 ppm

$$f_{BA} = \frac{A_{2.29}}{A_{2.29} + A_{8.06}} \quad (6\text{-}2)$$

$$f_{BT} = \frac{A_{8.06}}{A_{2.29} + A_{8.06}} \quad (6\text{-}3)$$

Initially, the PBAT film had a f_{BA}/f_{BT} ratio of 0.59/0.41, but as the hydrolysis proceeded and reduction of M_n was observed, the pattern of decreased f_{BA} and increased f_{BT} was observed in both buffer solution and vermiculite, with the change being more gradual in vermiculite than in the buffer solution (Figure 6-9). In the phosphate buffer solution, the pattern of decreased f_{BA} and increased f_{BT} continued until the reverse pattern occurred (increased f_{BA} and decreased f_{BT}), which suggested that at this point the BT domains started undergoing hydrolysis. Therefore, this indicates that the ester groups in the soft aliphatic BA section are more susceptible to hydrolysis, consequently making the BA sections more susceptible to biodegradation than the hard aromatic BT sections, as previously suggested by Kasuya *et al.* (2009), Abou-Zeid *et al.*(2004), and Muller *et al.* (2001). Esterase (hydrolase) enzymes are lipase type and enzymatic degradation rates can be dictated mainly by the mobility of the chain, i.e. the length of aromatic domains not the length of aliphatic counterparts (Hakkarainen and Is 2008; Kuwabara *et al.* 2002; Lucas *et al.* 2008; Marten *et al.* 2005; Mochizuki and Hirami 1997; Mueller 2006).

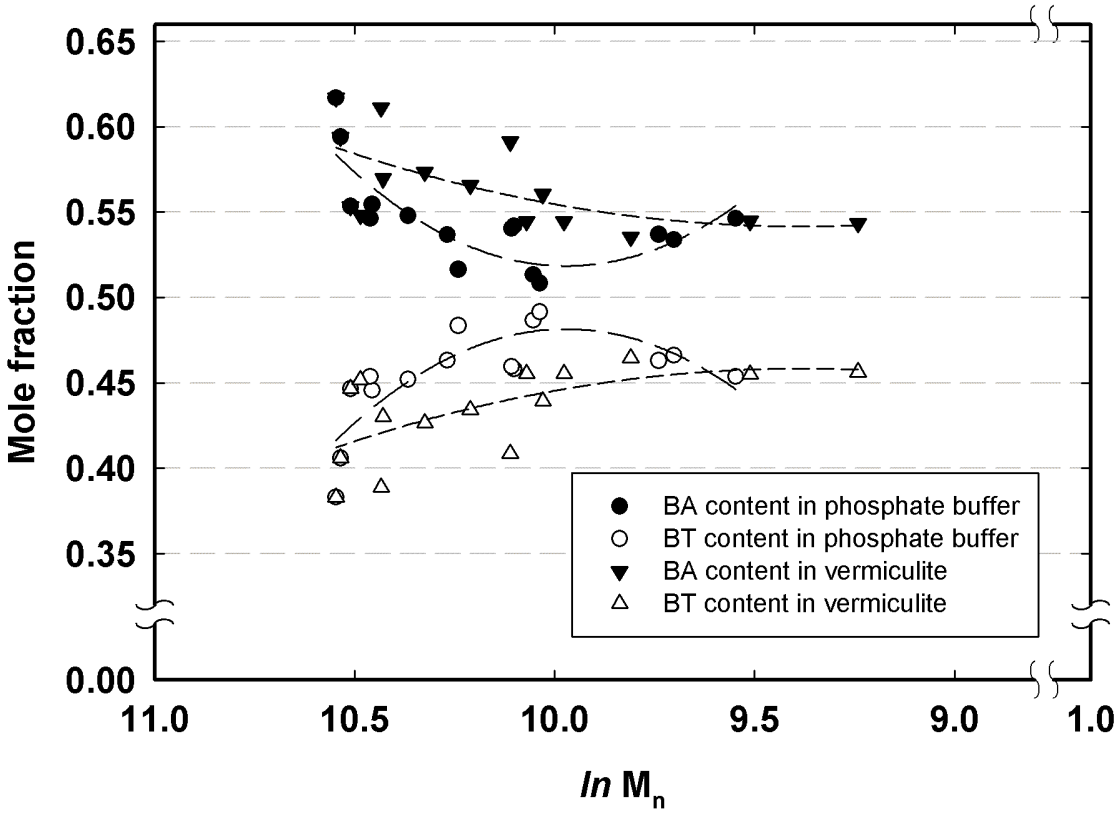

Figure 6-9. Mole fraction of BA and BT content of hydrolyzed PBAT films in phosphate buffer or in vermiculite at 58°C as a function of logarithmic reduction of molecular number (M_n)

Thus, there is a critical need to understand the effect of microbial population, family of microorganisms, and their enzymatic specificity in different microbial environments on the total biodegradation of biodegradable polyesters and their biodegradation rates. Compost with appropriate C/N ratio and CO_2 emission may not directly be a suitable testing media, due to lower total biodegradation of cellulose positive controls and different enzymatic specificity of microorganisms in composts. These results have implications for deployment of biodegradable polymers in commercial composting environments. There is a future need to include guidelines in current testing

methodologies to determine the family and the quantity of microbial populations in the compost environment.

6.4. Conclusions

Biodegradation of biodegradable polyesters such as PBAT were strongly influence by the total microbial activity of the exposure environments, which was monitored by CO_2 emissions or C/N ratio. PBAT degraded more and faster in manure compost than in yard or food waste composts. The ester group in the aliphatic BA unit was more susceptible to hydrolysis than that in the aromatic BT unit. Consequently, the BA unit was more vulnerable to hydrolysis and biodegradation. During biodegradation, increases in PBAT crystallinity were observed, which indicated that the amorphous regions biodegraded faster than the crystalline regions.

REFERENCES

REFERENCES

Abou-Zeid, DM, Muller, RJ and Deckwer, WD (2004). "Biodegradation of aliphatic homopolyesters and aliphatic-aromatic copolyesters by anaerobic microorganisms." Biomacromolecules **5**(5): 1687-1697.

ASTM (2003a) D 3418-03 standard test method for transition temperatures and enthalpies of fusion and crystallization of polymers by differential scanning calorimetry. West Conshohocken, PA, ASTM International.

ASTM (2003b) D 4754-98(2003) standard test method for two-sided liquid extraction of plastic materials using fda migration cell. West Conshohocken, PA, ASTM International.

ASTM (2003c) D 5338-98(2003) standard test method for determining aerobic biodegradation of plastic materials under controlled composting conditions. West Conshohocken, PA, ASTM International.

ASTM (2004) D 6400-04 standard specification for compostable plastics. West Conshohocken, PA, ASTM International.

Barone, J and Arikan, O (2007). "Composting and biodegradation of thermally processed feather keratin polymer." Polymer Degradation and Stability **92**(2007): 859-867.

Bellia, G, Tosin, M, Floridi, G and Degli-Innocenti, F (1999). "Activated vermiculite, a solid bed for testing biodegradability under composting conditions." Polymer Degradation and Stability **66**(1): 65-79.

BPI. (2008). "Approved products — resins." Retrieved Oct 17, 2008, from http://www.bpiworld.org/BPI-Public/Approved/3.html.

Chandra, R and Rustgi, R (1998). "Biodegradable polymers." Progress in Polymer Science **23**: 1273-1335.

Dřímal, P, Hoffmann, J and Družbík, M (2007). "Evaluating the aerobic biodegradability of plastics in soil environments through gc and ir analysis of gaseous phase." Polymer Testing **26**: 727-741.

Gan, Z, Kuwabara, K, Abe, H, Iwata, T and Doi, Y (2005). "The role of polymorphic crystal structure and morphology in enzymatic degradation of melt-crystallized poly(butylene adipate) films." Polymer Degradation and Stability **87**(2005): 191-199.

Hakkarainen, M and Is, A (2008). "Degradation products of aliphatic and aliphatic-aromatic polyesters." Chromatography for Sustainable Polymeric Materials: Renewable, Degradable and Recyclable **211**: 85-116.

Hakkarainen, M, Karlsson, S and Albertsson, A (2000). "Influence of low molecular weight lactic acid derivatives on degradability of polylactide." Journal of Applied Polymer Science **76**: 228-239.

Hayase, N, Yano, H, Kudoh, E and Tsutsumi, C (2004). "Isolation and characterization of poly (butylene succinate-co-butylene adipate)-degrading microorganism." Journal of Bioscience and Bioengineering **97**(2): 131-133.

Herrera, R, Franco, L, Rodriguez-Galan, A and Puiggali, J (2002). "Characterization and degradation behavior of poly(butylene adipate-co-terephthalate)." Journal of Polymer Science Part A-Polymer Chemistry **40**(23): 4141–4157.

Ishii, K and Takii, S (2003). "Comparison of microbial communities in four different composting processes as evaluated by denaturing gradient gel electrophoresis analysis." Journal of Applied Microbiology **95**: 109-119.

Ishii, N, Inoue, Y, Shimada, K, Tezuka, Y, Mitomo, H and Kasuya, K (2007). "Fungal degradation of poly (ethylene succinate)." Polymer Degradation and Stability **92**: 44-52.

Kale, G, Auras, R and Singh, SP (2006). "Comparison of the degradability of poly(lactide) packages in composting and ambient exposure conditions." Packaging Technology and Science **20**(1): 49-70.

Kale, G, Kijchavengkul, T and Auras, R (2007a). New trends in assessment of compostability of biodegradable polymeric packages. Leading-edge Environmental Biodegradation Research. L E Pawley ed. Hauppauge, NY, Nova Science Publishers**:** 297-315.

Kale, G, Kijchavengkul, T, Auras, R, Rubino, M, Selke, SE and Singh, SP (2007b). "Compostability of bioplastic packaging materials: An overview." Macromolecular Bioscience **7**(3): 255-277.

Kasuya, K-i, Ishii, N, Inoue, Y, Yazawa, K, Tagaya, T, Yotsumoto, T, Kazahaya, J-i and Nagai, D (2009). "Characterization of a mesophilic aliphatic-aromatic copolyester-degrading fungus." Polymer Degradation and Stability **94**(8): 1190-1196.

Kijchavengkul, T, Auras, R, Rubino, M, Alvarado, E, Camacho Montero, JR and Rosales, JM (2010). "Atmospheric and soil degradation of aliphatic-aromatic polyester films." Polymer Degradation and Stability **95**(2): 99-107.

Kijchavengkul, T, Auras, R, Rubino, M, Ngouajio, M and Fernandez, RT (2006). "Development of an automatic laboratory-scale respirometric system to measure polymer biodegradability." Polymer Testing **25**(8): 1006-1016.

Kijchavengkul, T, Auras, R, Rubino, M, Ngouajio, M and Fernandez, RT (2008a). "Assessment of aliphatic-aromatic copolyester biodegradable mulch films. Part I: Field study." Chemosphere **71**(5): 942-953.

Kijchavengkul, T, Auras, R, Rubino, M, Ngouajio, M and Fernandez, RT (2008b). "Assessment of aliphatic-aromatic copolyester biodegradable mulch films. Part II: Laboratory simulated conditions." Chemosphere **71**(9): 1607-1616.

Kuwabara, K, Gan, ZH, Nakamura, T, Abe, H and Doi, Y (2002). "Crystalline/amorphous phase structure and molecular mobility of biodegradable poly(butylene adipate-co-butylene terephthalate) and related polyesters." Biomacromolecules **3**: 390-396.

Lucas, N, Bienaime, C, Belloy, C, Queneudec, M, Silvestre, F and Nava-Saucedo, J (2008). "Polymer biodegradation: Mechanisms and estimation techniques." Chemosphere **73**: 429-442.

Maeda, H, Yamagata, Y, Abe, K, Hasegawa, F, Machida, M, Ishioka, R, Gomi, K and Nakajima, T (2005). "Purification and characterization of a biodegradable plastic-degrading enzyme from aspergillus oryzae." Applied Microbiology and Biotechnology **67**(6): 778-788.

Marten, E, Muller, RJ and Deckwer, W (2005). "Studies on the enzymatic hydrolysis of polyesters. Ii. Aliphatic-aromatic copolyesters." Polymer Degradation and Stability **88**: 371-381.

Miller, DW and Agard, DA (1999). "Enzyme specificity under dynamic control: A normal mode analysis of [alpha]-lytic protease." Journal of Molecular Biology **286**(1): 267-278.

Mochizuki, M and Hirami, M (1997). "Structural effects on biodegradation of aliphatic polyesters." Polymers for Advanced Technologies **8**: 203-209.

Mueller, RJ (2006). "Biological degradation of synthetic polyesters - enzymes as potential catalysts for polyester recycling." Process Biochemistry **41**: 2124-2128.

Muller, RJ, Kleeberg, I and Deckwer, WD (2001). "Biodegradation of polyesters containing aromatic constituents." Journal of Biotechnology **86**(2): 87-95.

Nakajima-Kambe, T, Ichihashi, F, Matsuzoe, R, Kato, S and Shintani, N (2009). "Degradation of aliphatic-aromatic copolyesters by bacteria that can degrade aliphatic polyesters." Polymer Degradation and Stability **94**(11): 1901-1905.

Narayan, R (2001). Drivers for Biodegradable/compostable Plastics & Role of Composting Waste Management & Sustainable Agriculture. ORBIT 2001 Conference, Seville, Spain, Spanish waste club.

Rodriguez, F, Cohen, C, Ober, C and Archer, L (2003). Principles of Polymer Systems. New York, NY, Taylor & Francis.

Rynk, R (1992). On-farm Composting Handbook, Natural Resource, Agriculture and Engineering Service (NRAES) Cooperative Extension.

Shah, AA, Hasan, F, Hameed, A and Ahmed, S (2008). "Biological degradation of plastics: A comprehensive review." Biotechnology Advances **26**(3): 246-265.

Shen, L and Patel, M (2008). "Life cycle assessment of polysaccharide materials: A review." Journal of Polymers and the Environment **16**(2): 154-167.

Shi, X, Ito, H and Kikutani, T (2005). "Characterization on mixed-crystal structure and properties of poly(butylene adipate-*co*-terephthalate) biodegradable fibers." Polymer **46**: 11442-11450.

Stevens, ES (2003). "What makes green plastics green?" Biocycle **24**: 24-27.

Tserki, V, Matzinos, P, Pavlidou, E, Vachliotis, D and Panayiotou, C (2006). "Biodegradable aliphatic polyesters. Part i. Properties and biodegradation of poly (butylene succinate-co-butylene adipate)." Polymer Degradation and Stability **91**: 367-376.

van Krevelen, DW and Nijenhuis, Kt (2009). Properties of Polymers. Oxford, UK, Elsevier.

Witt, U, Einig, T, Yamamoto, M, Kleeberg, I, Deckwer, W-D and Muller, R-J (2001). "Biodegradation of aliphatic-aromatic copolyesters: Evaluation of the final biodegradability and ecotoxicological impact of degradation intermediates." Chemosphere **44**(2): 289-299.

Chapter 7 Design of biodegradable film formulation for mulch film using response surface methodology (RSM)

7.1 Introduction

The main drawback for PBAT films to properly perform as biodegradable mulch films, as demonstrated in chapter 5, is the crosslinking reactions happening when they are exposed to UV radiation in term of mechanical performance (section 5.1) and biodegradation (section 5.2). Therefore, understanding the rate of crosslinking, and its paths is essential for successful mulch film design.

As described earlier in chapter 5 scheme 5.1, crosslinking of PBAT occurs because of the recombination of free radicals, especially phenyl radicals. Therefore, one of the solutions to the radical recombination is to minimize the amount of free radicals that are produced during the photooxidation process. Although a substantial amount of the aromatic domain (40-50% mole) in PBAT structure can dissipate photon energy, antioxidants, such as BHT, could be incorporated into the PBAT mulch films to reduce the amount of free radicals produced from UV exposure. Furthermore, carbon black can also be used to inhibit the photodegradation since it can absorb the photon energy and reduce the intensity of the light reacting with the polymer (Shlyapintokh 1984). Since there are multiple factors that need to be designed to affect the overall properties of the PBAT mulch films, a response surface methodology (RSM) is the most appropriate methodology to determine the precise range of concentrations of carbon black and antioxidants that lead to an optimal performance of the biodegradable mulch films.

RSM is a combination of mathematical and statistical techniques for developing, improving, and optimizing processes. Munguia *et al.* (1992) used RSM to study the influence of time, temperature, and the amount of catalyst on weight average molecular weight of PLA, and then use the obtained response to predict the maximum molecular weight, later confirmed by experiment. Guan and Hanna (2005) used RSM to analyze the effect of acetylated starch type, PLA content, barrel temperature, and screw speed on the mechanical energy requirement, radial expansion ratio, and compressibility of extruded foams. Zhong and Xia (2008) studied the effect of cassava starch, gelatin, and glycerol on the mechanical properties, water and oxygen permeability of chitosan based films using RSM. Additional detailed information about how to set up an RSM can be found in Appendix A.

Use of multiple response surfaces allows more than one dependent variable (property) to be considered. In this work, multiple response surfaces of tensile strength, light transmission, molecular weight, and gel content were simultaneously used to determine the overall performance of the PBAT mulch films. The concentration of antioxidant and carbon black that yielded the overall best performance in all the properties were selected as the final formulation for the biodegradable PBAT mulch film.

7.2 Materials and methods

The methods involved in this study are RSM design of experiment, film production and treatment, film characterization, and data analysis.

7.2.1 RSM design of experiment

For this experiment, a 2^2 factorial rotatable central composite design (CCD) with α of $\sqrt{2}$ was selected (Figure 7-1). The two selected factors were the concentrations of carbon black (CB) and antioxidant (AnOx). With this design of experiment, the total number of treatments equals 12. The type of antioxidants used in this experiment was limited to only one compound or one type because if another type of antioxidant, such as peroxide decomposer, were used, the total number of treatments would have increased to 18. The UV chamber in the MSU School of Packaging has only 24 sample holders; therefore, the number of treatments was limited to 12, so that two sets of samples can be exposed to UV simultaneously. The antioxidant selected for the experiment was BHT, a chain-breaking antioxidant. BHT is widely used and easily detected by various instruments, such as liquid chromatography or nuclear magnetic resonance (NMR).

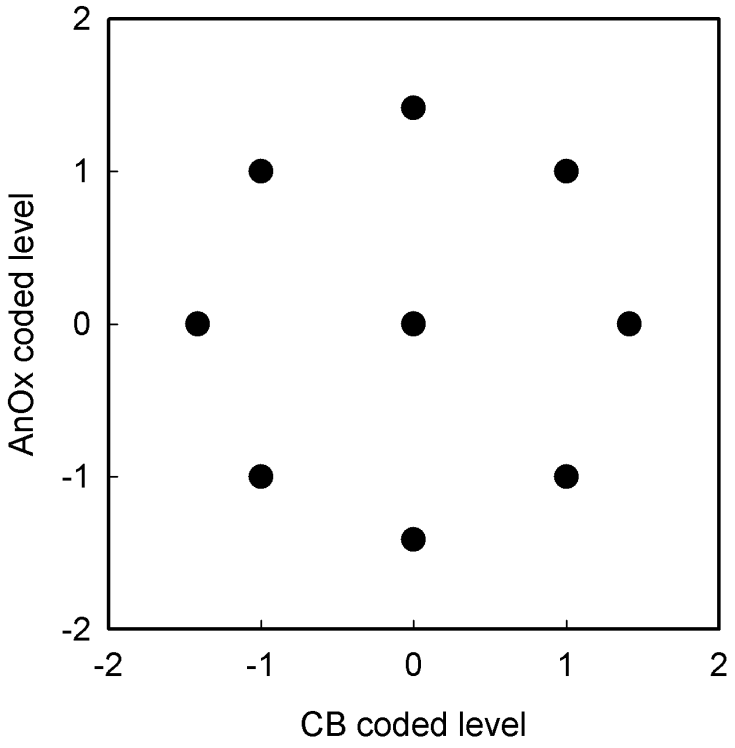

Figure 7-1. Rotatable central composite design (CCD) for RSM used in this experiment ($\alpha=\sqrt{2}$, CB = carbon black, and AnOx = antioxidant)

Table 7-1 summarizes the pattern, actual concentrations, and coded levels of carbon black and antioxidant matching the rotatable central composite design presented in Figure 7-1. Since all 12 treatments of film cannot be produced in one day, an orthogonal block design was used. Block 1, consisting of four corner-point and two center-point treatments, was produced in one day, while Block 2, consisting of four-star point and two-center point treatments, was produced another day. Trial orders within each block were randomized. In this experiment, the amount of each additive was limited to be at most 1% w/w, which is the limit in the ASTM D6400 compostable specification for additives without further biodegradation and toxicity tests (ASTM 2004). The center

point of 0.39% w/w of carbon black was based on the manufacturing specification of the films used in the preliminary tomato production experiment (Chapters 4 & 5).

Table 7-1. Detailed list of all 12 treatments used in this rotatable CCD design

Treatment	Pattern	Block	Actual concentration %(w/w)		Coded level	
			CB	AnOx	CB_C	$AnOx_C$
1	-+	1	0.10	0.85	-1	1
2	00	1	0.39	0.50	0	0
3	00	1	0.39	0.50	0	0
4	--	1	0.10	0.15	-1	-1
5	++	1	0.82	0.85	1	1
6	+-	1	0.82	0.15	1	-1
7	00	2	0.39	0.50	0	0
8	00	2	0.39	0.50	0	0
9	A0	2	1.04	0.50	1.414	0
10	0A	2	0.39	1.00	0	1.414
11	a0	2	0.00	0.50	-1.414	0
12	0a	2	0.39	0.00	0	-1.414

Note: The carbon black levels were coded based on natural log transformation $CB_C = 2\sqrt{2}\ln\left(CB + e^{-0.5}\right)$, where CB_C = coded level of carbon black and CB = uncoded level of carbon black. The antioxidant levels were coded based on linear transformation $AnOx_C = \sqrt{2}\left(2AnOx - 1\right)$, where $AnOx_C$ = coded level of antioxidant and $AnOx$ = uncoded level of antioxidant. In pattern column, - means coded level of -1, + means coded level of +1, 0 means coded level of 0, a means coded level of –α, and A means coded level of α.

7.2.2 Film production

For each trial, specific amounts of PBAT with carbon black master batch (Northern Technologies International Inc., Circle Pines, MN) and BHT (Figure 7-2) (Sigma Aldrich, St. Louis, MO) were added to the PBAT resin (BASF, Florham Park, NJ) (see Table 7-1). The master batch contains 10% w/w of carbon black in PBAT resin. Then the mixture was extruded and blown into film using an in-house Killion KLB 100 blown film extruder (Davis-Standard LLC, Pawcatuck, CT) with a temperature profile of

177-177-177-170-165-165-165°C for zone 1, 2, 3, clamp ring, adaptor, die 1 and 2, respectively. The extruder screw diameter was 25.4 mm (1 in) with L/D ratio of 24:1 and a diameter of the blown die of 50.8 mm (2 in). Screw speed and take up speed were 21.5 rpm and 0.033 m/s. The final thickness of the produced PBAT film was 75.4±10.5 μm (1.9±0.4 mil).

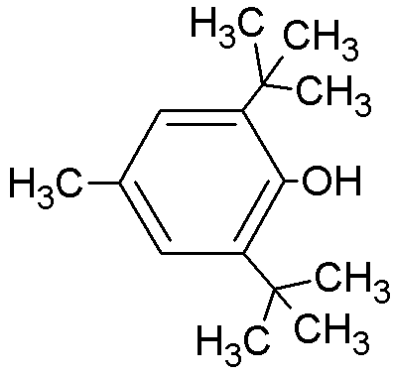

Figure 7-2. Structure of 2,6-di-tert-butyl-4-methyl phenol or butylated hydroxytoluene (BHT)

7.2.3 UV Simulating Cycle (UVSC) film treatment

To simulate field conditions, the three-to-four month use of biodegradable mulch film in Michigan or regions with similar climates, where the films are exposed to 1500-2000 MJ/m^2 of radiation (average solar radiation 14 MJ/m^2/day) in the laboratory, the PBAT film samples were exposed to UV-A light (long wave UV with wavelength range of 320-400 nm) using 8 UVA-340 lamps (wavelength of 340 nm) from Q-Panel Lab (Cleveland, OH), which have an irradiance spectrum close to the sunlight experienced in the field (Figure 7-3). The exposure was carried out in a QUV Accelerated Weathering Tester (Q-Panel Lab, Cleveland, OH). This setting allows for a better control over irradiance or radiation energy levels than samples exposed in an open field. The average

irradiance of the preliminary field experiment was 0.70 W/m^2/nm during the photodegradation period, which started once the mulch films were laid in June through harvesting in September in Michigan. In the laboratory conditions, an irradiance of 1.40 W/m^2/nm can be used to accelerate the simulation. Further information can be found in Chapters 4 and 5. This experiment was conducted under the assumption that the UV-A lamp can perfectly simulate solar radiation and provide the same energy at any wavelength.

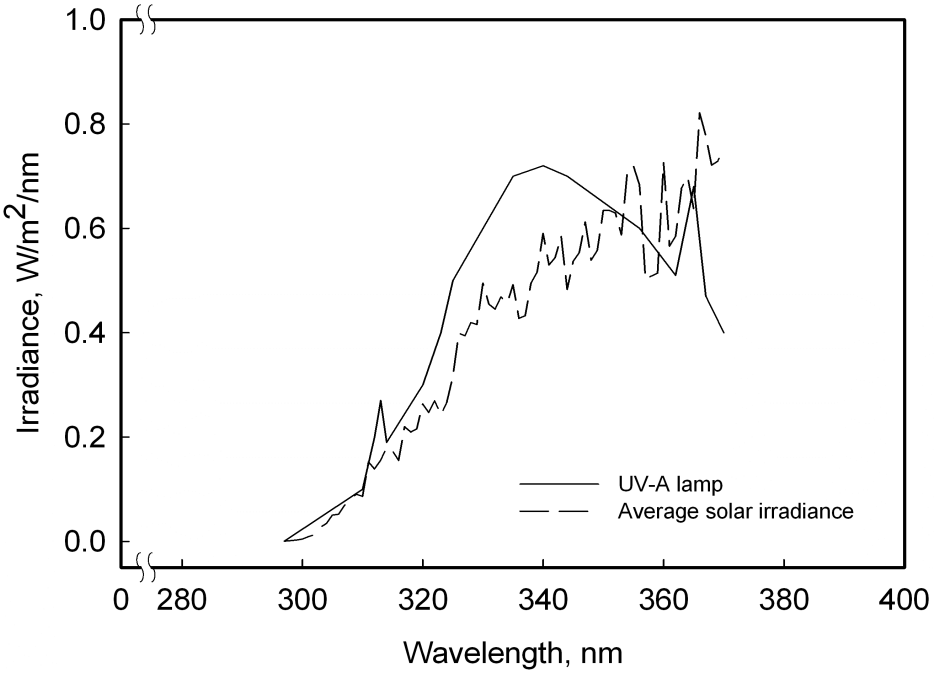

Figure 7-3 Spectrum of sunlight compared to that of UV-A irradiance lamp

Therefore, the UV exposure of the films from the field experiment can be doubled and simulated in a shorter period of time. The simulation includes an 8-hour cycle when the mulch film is exposed to UV light in order to reproduce daylight conditions and a 4-hour dark cycle to replicate night conditions. This light/dark cycle of 12 hours was repeated for 6 weeks to simulate the exposure the films had during the field study of 12

weeks. Multiple sets of PBAT films were exposed for predetermined times, and then the changes in light transmission, molecular weight, gel content, and mechanical properties as a function of time were characterized.

7.2.4 Film characterization

7.2.4.1 Optical properties

Changes in percentage of light transmission rate of the films were determined using a Lambda 25 UV/Visible spectrophotometer from PerkinElmer with integrating sphere (Wellesley, MA). For each film, three samples were scanned from wavelength 400 to 700 nm the PAR region. Light transmission was calculated from an integrated area under the light transmission spectrum divided the bandwidth of 300 nm.

7.2.4.2 Molecular weight

The retrieved samples were cleaned with laboratory wipes without using water, to prevent any further degradation. The weight average molecular weight reduction of the samples was determined using gel permeation chromatography. The methodology for molecular weight measurement can be found in section 6.2.4.

7.2.4.3 Gel Content

The gel content of the film samples was measured according to ASTM D 2765 method A using THF as the solvent. The methodology for gel content measurement can be found in section 4.2.

7.2.4.4 Mechanical properties

A universal tester machine from Instron, Inc. (Norwood, MA) was used to test tensile strength, percentage of elongation, and tensile modulus on three samples for each film in the machine direction (MD) using ASTM standard D 882 (ASTM 1998). An initial grip length set at 1 inch (2.5 cm), and a grip separation rate of 0.1 or 10 in/min (0.25 or 25 cm/min) was used depending on the initial strain of the sample.

7.2.5 Data analysis

The values obtained from various characterization properties such as light transmission, gel content, and mechanical properties of the UV exposed films were used as dependent variables for fitting multiple response surfaces. More specifically, the changes of light transmission, molecular number, gel content, and tensile strength were plotted for all treatments as a function of total UV radiation, which linearly proportional to exposure time.

For each property, changes of all treatments were fitted to one specific mathematical equation, such as the first order reduction ($y = ae^{-bx}$), non-linear first order reduction ($y = y_o + ae^{-bx}$), exponential increase to maximum ($y = a(1 - e^{-bx})$), etc. As a result, there were 12 equations for each property. Every change consisted of multiple parameters and each parameter consisted of 12 coefficients from 12 treatments. Then a second-order response surface with interaction and blocking effect (equation 7-1) was assigned to a particular parameter. Since there were multiple parameters, multiple

second-order response surfaces were analyzed simultaneously using JMP 8.0 software (SAS Institute Inc., Cary, NC).

$$E\{Y\} = \beta_o + \beta_1 CB_C + \beta_2 AnOx_C + \beta_{11} CB_C^2 + \beta_{22} AnOx_C^2 + \beta_{12} CB_C \times AnOx_C + \tau(block) \quad (7\text{-}1)$$

where $E\{Y\}$ = Estimate of interested parameter

CB_C = Coded level of carbon black

$AnOx_C$ = Coded level of antioxidant

β_o = Intercept

β_1 = Linear main effect of carbon black

β_2 = Linear main effect of antioxidant

β_{11} = Quadratic main effect of carbon black

β_{22} = Quadratic main effect of antioxidant

β_{12} = Interaction effect of carbon black and antioxidant

τ = Blocking effect

$block$ = Block number

7.3 Results and discussion

7.3.1 Light transmission

There were no changes in % light transmission except for treatments 1 and 4, which had 0.10% CB_C where reduction of light transmission was observed (Figure 7-4). Since light transmission, especially, the ability of the film to block light in the PAR wavelength is more important during the early growing period of the season and there were few changes in the film light transmission, the initial values of % light transmission of all 12 treatments were used in the second-order RSM model (Table 7-2)

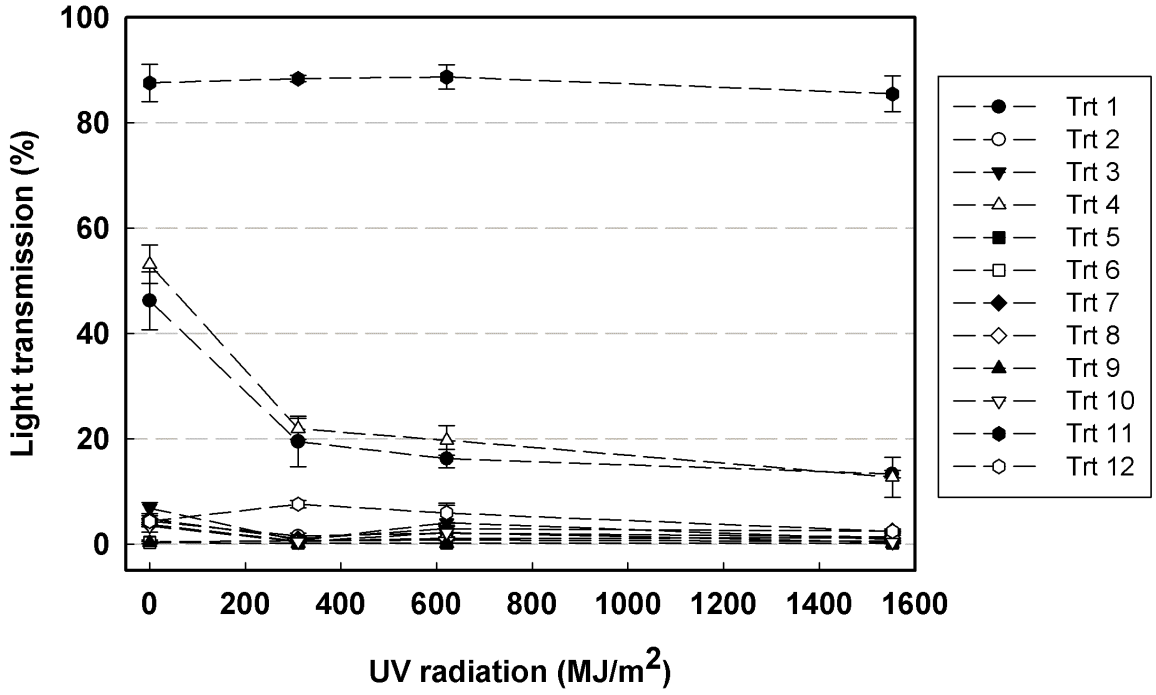

Figure 7-4. Changes of % light transmission of all 12 treatments as a function of UV radiation

Table 7-2. Initial % light transmission of all 12 treatments along with coded carbon black and antioxidant levels and block number

Treatment	Pattern	CB_C	$AnOx_C$	Block	%Light transmission
1	−+	-1	1	1	46.1959
2	0	0	0	1	4.3101
3	0	0	0	1	6.8109
4	−−	-1	-1	1	53.1319
5	++	1	1	1	0.3838
6	+−	1	-1	1	0.2698
7	0	0	0	2	4.7296
8	0	0	0	2	3.6966
9	A0	1.414	0	2	0.2667
10	0A	0	1.414	2	3.4081
11	a0	-1.414	0	2	87.5209
12	0a	0	-1.414	2	4.3212

Note: CB_C = coded level of carbon black and $AnOx_C$ = coded level of antioxidant. In pattern column, - means coded level of -1, + means coded level of +1, 0 means coded level of 0, a means coded level of –α, and A means coded level of α.

From the RSM model, the plot of actual light transmission vs. predicted light transmission using the estimated parameters from Table 7-3 shows a linear relationship (Figure 7-5). The linear relationship, R^2 of 0.99, and P-value of RSM model of <0.0001 indicate that the model is well represented by the experimental data. Detailed statistical results can be found in Table B-1 in Appendix B.

Table 7-3. Parameter estimates of % light transmission RSM model

Term	Estimate	Std Error	t Ratio	Prob>|t|
Intercept	4.8868	2.048366	2.39	0.0627
CB_C	-27.75878	1.448414	-19.16	<.0001*
$AnOx_C$	-1.014165	1.448414	-0.70	0.5150
CB_C x $AnOx_C$	1.7625	2.048366	0.86	0.4289
CB_C x CB_C	19.782531	1.619376	12.22	<.0001*
$AnOx_C$ x $AnOx_C$	-0.232044	1.619376	-0.14	0.8917
Block	0.5966086	1.182625	0.50	0.6354

Note: * indicates statistical significance at type I error (α) of 0.05

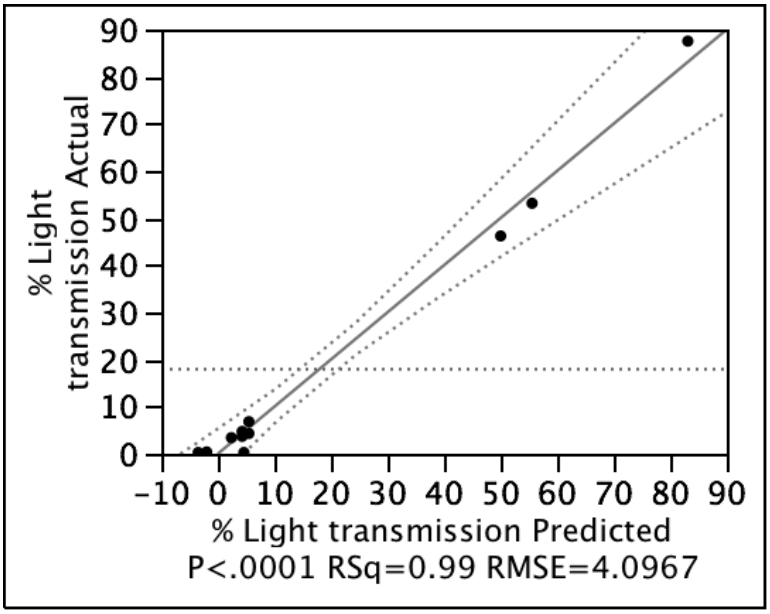

Figure 7-5. Actual light transmission vs. predicted light transmission from RSM model. The horizontal dotted line represents overall mean of 12 treatments. The solid diagonal line is the line of fit. Two curvature dotted lines are 95% confident interval.

Also, from the parameter estimates (Table 7-3), both linear and quadratic main effects of the coded level of carbon black affected the % light transmission of the PBAT samples with P-value < 0.0001. The negative estimated parameter for CB_C indicates that increased concentration of carbon black will decrease the % light transmission. On the other hand, antioxidant concentration did not play any important role in % light transmission with P-value of 0.5150.

Figure 7-6 is a response surface of the % light transmission model with the parameter estimates shown in Table 7-3. The curvilinear line in the contour profile of the RSM model for light transmission was set so that % light transmission of all the points on this line is 20% (Figure 7-6). From the tomato production trial discussed in Chapter 5 section 5.1.2, films with 20% light transmission in the PAR range can provide the same weed control level as LDPE mulch film. Since the fitted response surface has a bowl-

shaped surface, any coded carbon black levels on the right side of this curvilinear line will have % light transmission less than 20% and should have weed suppression ability that is comparable to conventional PE mulch films.

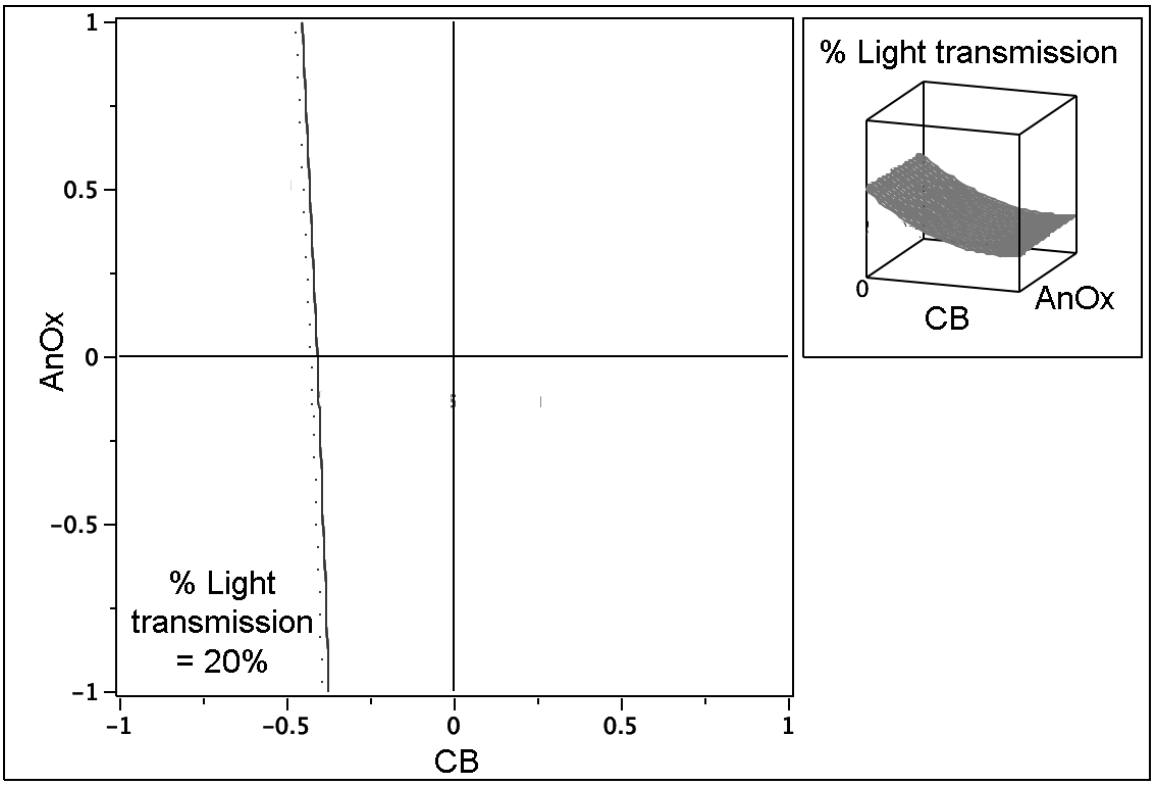

Figure 7-6. The contour profile of RSM model for % light transmission with the curvilinear line representing 20% light transmission

7.3.2 Tensile strength

Tensile strength of all the 12 treatments of PBAT films before the UV exposure was not different (Table 7-4). However, during the 6 weeks of UV exposure, the tensile strength of all the treatments decreased exponentially from 19.82-26.81 MPa to 4.00-7.91 MPa (Table 7-4). Reduction of tensile strength followed a first order exponential reduction (Figure 7-7). As a result, a non-linear first order reduction (equation 7-2) was

used to fit to the tensile strength reduction pattern and the fitted parameters and the R^2-value are reported in Table 7-5.

$$TS = TS_O + TS_a e^{-TS_b x} \quad (7\text{-}2)$$

where TS = Estimated tensile strength of PBAT exposed to x MJ/m^2 of UV radiation

TS_o = Estimated final tensile strength

TS_a = Total amount of tensile strength reduction from the beginning to the end of the exposure

TS_b = Reduction rate

Table 7-4. Initial and final tensile strength of all 12 treatments of PBAT films after the UV exposure sorted from maximum to minimum final tensile strength with mean comparison using Tukey-Kramer

Treatment	Initial tensile strength (MPa)	S.D.	Tukey mean comparison	Final tensile strength (MPa)	S.D.	Tukey mean comparison
6	19.82	1.38	A	7.91	1.12	A
10	25.79	4.29	A	7.49	1.78	A
9	24.98	1.23	A	7.41	0.56	A
5	23.98	4.20	A	7.26	0.55	A
3	21.83	2.32	A	6.98	0.30	A
8	26.81	1.02	A	6.70	0.49	AB
7	24.34	5.49	A	6.56	0.57	AB
2	20.68	0.26	A	6.33	0.75	ABC
12	24.17	0.81	A	5.68	0.88	ABC
4	20.37	2.21	A	4.49	0.99	BC
1	24.31	1.60	A	4.47	0.43	BC
11	25.26	3.02	A	4.00	0.18	C

Note: Levels with different letters are significantly different; S.D. = standard deviation

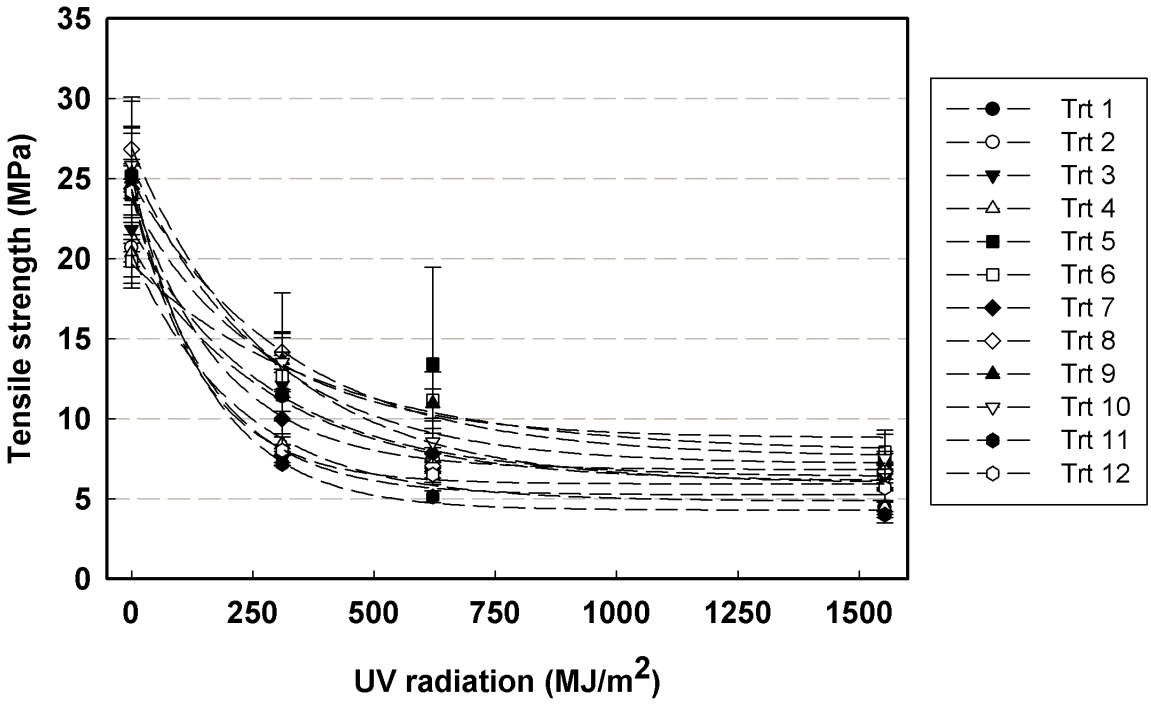

Figure 7-7. Changes of tensile strength of all 12 PBAT film treatments as a function of UV radiation in MJ/m^2; dashed lines represent non-linear first order reduction $TS = TS_O + TS_a e^{-TS_b x}$ trend lines.

Table 7-5. TS_o, TS_a, and TS_b fitted parameters of non-linear first order reduction of tensile strength of all 12 treatments and their R^2-value

Treatment	TS_o	TS_a	TS_b	R^2
1	5.24	19.05	0.00616	0.9780
2	6.09	14.64	0.00343	0.9943
3	6.37	15.57	0.00364	0.9569
4	4.86	15.47	0.00445	0.9862
5	8.79	14.90	0.00378	0.8923
6	7.94	11.74	0.00253	0.9560
7	6.82	17.51	0.00537	0.9964
8	5.96	21.01	0.00342	0.9624
9	7.60	17.27	0.00309	0.9802
10	7.17	18.68	0.00366	0.9934
11	4.30	20.96	0.00628	0.9973
12	5.92	18.24	0.00685	0.9978

The non-linear first order reduction equation can well represent the reduction of tensile strength from UV exposure, since the R^2-values of all the treatments were 0.89 or greater. The estimates parameters TS_o, TS_a, and TS_b were used as variables for the second-order RSM model for tensile strength. In this case, models were generated for TS_a, TS_b, and TS_o.

7.3.2.1 TS_a parameter

The relationship between the actual and predicted values of TS_a is quite linear with R^2-value of 0.85 (Figure 7-8). Besides the blocking effect, only a linear main effect of carbon black significantly affected the total reduction of tensile strength with P-value of 0.0324 (Table 7-6). The negative parameter estimate (of -1.637) indicates that the total reduction of tensile strength can be reduced with higher concentration of carbon black, due to the UV absorbing capability of carbon black. Carbon black inhibits the photodegradation by absorbing the photon energy and reducing the intensity of the light reacting with the polymer (Shlyapintokh 1984). Detailed statistical results can be found in Table B-2 in Appendix B.

Table 7-6. Parameter estimates of RSM model for TS_a parameter

Term	Estimate	Std Error	t Ratio	Prob>|t|
Intercept	17.1811	0.788544	21.79	<.0001*
CB_C	-1.637427	0.557585	-2.94	0.0324*
$AnOx_C$	0.9202123	0.557585	1.65	0.1598
CB_C x $AnOx_C$	-0.10355	0.788544	-0.13	0.9006
CB_C x CB_C	0.0932187	0.623398	0.15	0.8870
$AnOx_C$ x $AnOx_C$	-0.236406	0.623398	-0.38	0.7201
Block[1]	-1.858525	0.455266	-4.08	0.0095*

Note: * indicates a statistical significance at type I error (α) of 0.05

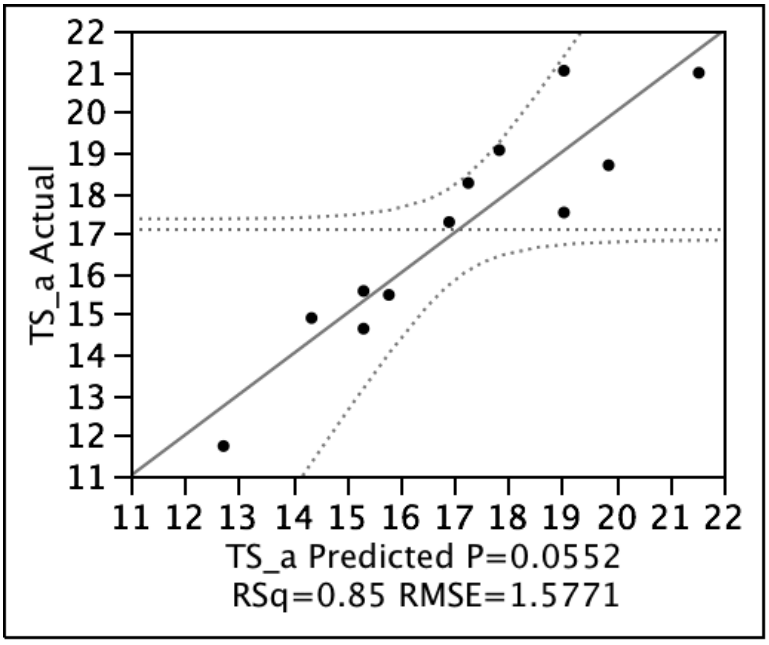

Figure 7-8. Actual vs. predicted TS_a parameters from RSM model. The horizontal dotted line represents overall mean of 12 treatments. The solid diagonal line is the line of fit. Two curvature dotted lines are 95% confident interval.

7.3.2.2 TS_b parameter

The relationship between the actual and predicted values of the TS_b from RSM model (Table 7-7) is not quite linear or clustered along the diagonal line with R^2-value of 0.60 (Figure 7-9). The ANOVA Table B-3 shows that TS_b does not provide a good

representation for the tensile strength reduction (P-value = 0.4149), and that none of the factors affected the reduction rate of the tensile strength at type I error (α) of 0.05 (Table 7-7). Detailed statistical results can be found in Table B-3 in Appendix B.

Table 7-7. Parameter estimates of RSM model for TS_b parameter

Term	Estimate	Std Error	t Ratio	Prob>|t|
Intercept	0.003965	0.000667	5.94	0.0019*
CB_C	-0.001101	0.000472	-2.33	0.0670
$AnOx_C$	-0.000196	0.000472	-0.42	0.6946
CB_C x $AnOx_C$	-0.000115	0.000667	-0.17	0.8703
CB_C x CB_C	0.000175	0.000528	0.33	0.7536
$AnOx_C$ x $AnOx_C$	0.00046	0.000528	0.87	0.4231
Block[1]	-0.000391	0.000385	-1.01	0.3571

Note: * indicates a statistical significance at type I error (α) of 0.05

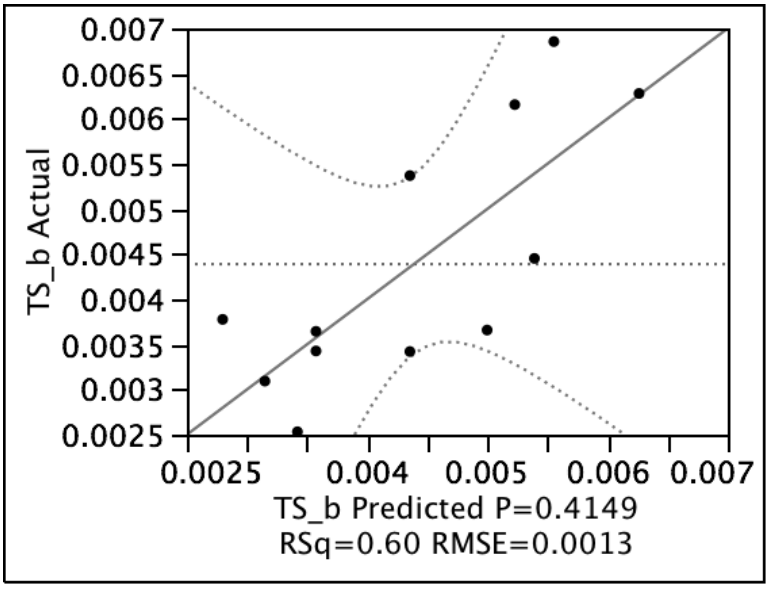

Figure 7-9. Actual vs. predicted TS_b parameters from RSM model. The horizontal dotted line represents overall mean of 12 treatments. The solid diagonal line is the line of fit. Two curvature dotted lines are 95% confident interval.

7.3.2.3 TS_o parameter

The plot of actual vs. predicted TS_o from the RSM model (Table 7-8) shows a linear relationship (Figure 7-10). The R^2 of 0.94 and P-value of 0.0070 indicate the significance of the RSM model (Figure 7-10). The linear main effect of carbon black as the only factor that is significant with P-value of 0.0004 (Table 7-8). The positive parameter estimate (of 1.414) indicates that the PBAT film with higher concentration of carbon black will result in greater final tensile strength after the exposure to UV light. Detailed statistical results can be found in Table B-4 in Appendix B.

Table 7-8. Parameter estimates of RSM model for TS_o parameter

Term	Estimate	Std Error	t Ratio	Prob>|t|
Intercept	6.3102	0.243591	25.90	<.0001*
CB_C	1.4142357	0.172245	8.21	0.0004*
$AnOx_C$	0.375122	0.172245	2.18	0.0813
CB_C x $AnOx_C$	0.116075	0.243591	0.48	0.6538
CB_C x CB_C	-0.065662	0.192576	-0.34	0.7470
$AnOx_C$ x $AnOx_C$	0.2337625	0.192576	1.21	0.2790
Block[1]	0.1273167	0.140637	0.91	0.4068

Note: * indicates a statistical significance at type I error (α) of 0.05

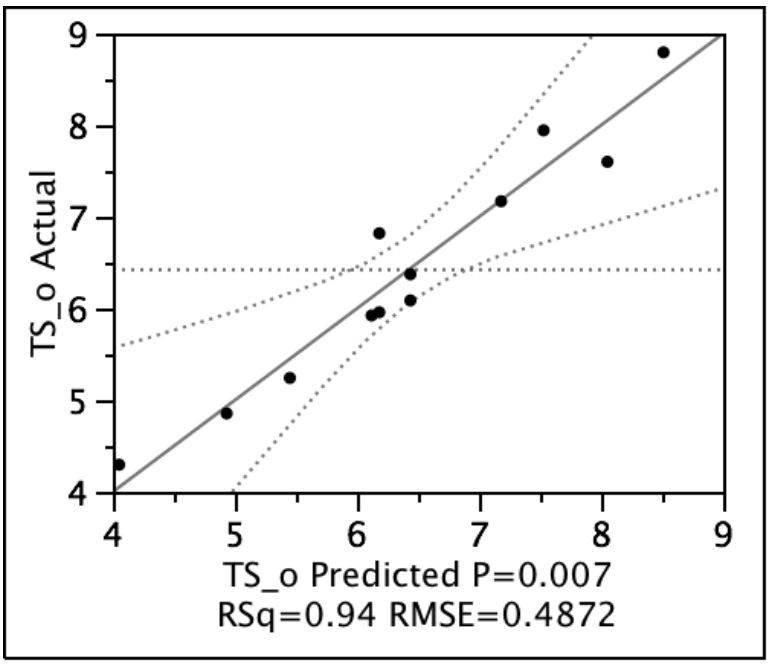

Figure 7-10. Actual vs. predicted TS_O parameters from RSM model. The horizontal dotted line represents overall mean of 12 treatments. The solid diagonal line is the line of fit. Two curvature dotted lines are 95% confident interval.

In the tomato production trial presented in Chapter 5 sections 5.1.2 and 5.1.3 using biodegradable mulch film, the black PBAT film provided adequate weed suppression throughout the whole season and the marketable yields from the plots using this film were comparable to those from the plots using conventional PE mulch film. From Figure 5-5a in Chapter 5, the tensile strength of the black PBAT film prior to week 8, when it started to disintegrate, was 6.35 MPa. Figure 7-11 is a response surface of the TS_O model with the parameter estimates shown in Table 7-8. The curvilinear line in the contour profile of the RSM model for TS_O was set so that final tensile strength of all the points on this line is 6.35 MPa (Figure 7-11). Since the fitted response surface is an incline flat surface, any combination of carbon black and BHT on the right side of this curvilinear line will have final tensile strength greater than 6.35 MPa and should satisfy

the mechanical properties requirement for tomato production in Michigan or regions with similar radiation.

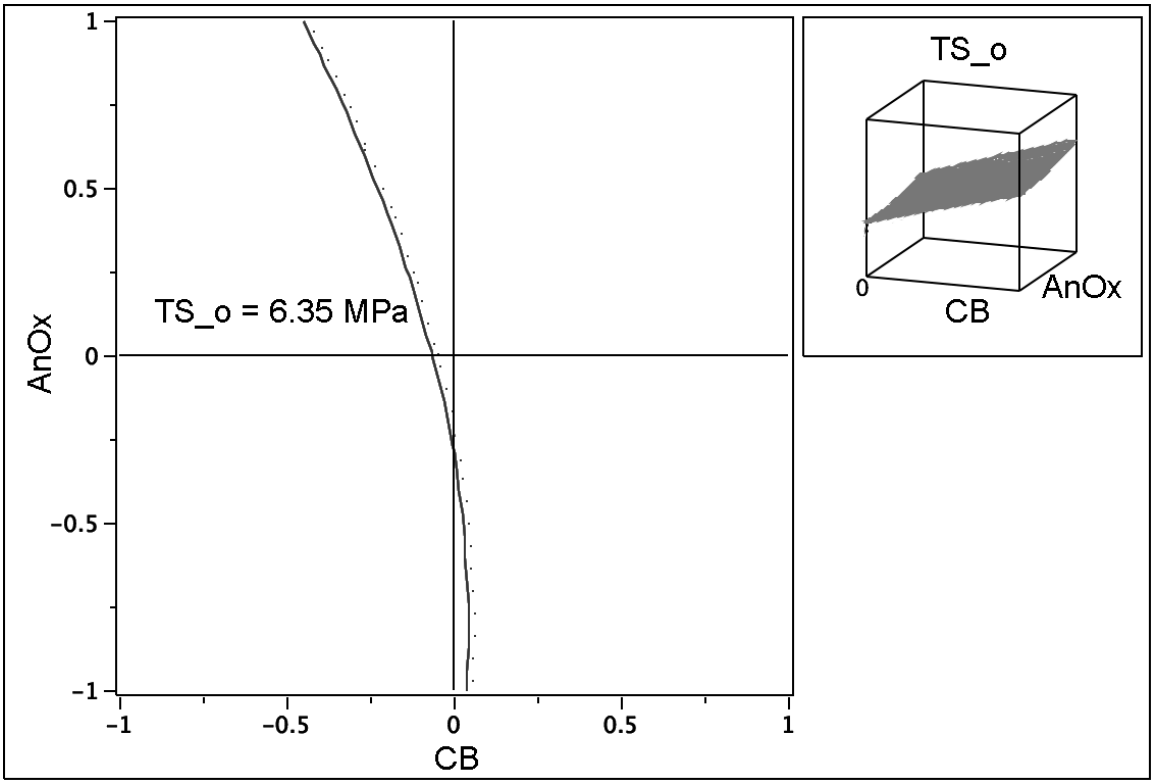

Figure 7-11. The contour profile of RSM model for final tensile strength with the curvilinear line representing tensile strength of 6.35 MPa

7.3.3 Gel content

During exposure to the UV radiation, PBAT film samples developed gel from 0 g gel/g polymer at the beginning of the test to 0.23-0.64 g gel/g polymer (Table 7-9) due to crosslinking and recombination of free radicals, as mentioned in Chapters 2 and 5. The patterns of the increase in gel content were similar among all the 12 treatments. Initially the gel content developed rapidly, but then reached a plateau stage as time proceeded (Figure 7-12). The development of gel content as a function of time follows an exponential increase to a maximum. Equation 7-3 was used to fit the gel content as a

function of UV radiation for each PBAT treatment and the Gel_a, Gel_b, and R^2-values are shown in Table 7-10.

$$Gel = Gel_a(1 - e^{-Gel_b x}) \tag{7-3}$$

where Gel = Estimated gel content of PBAT exposed to x MJ/m^2 of UV radiation

Gel_a = Estimated maximum gel content of PBAT sample

Gel_b = Gel-forming rate

Table 7-9. Final gel content of all 12 treatments of PBAT films after the UV exposure sorted from maximum to minimum with mean comparison using Tukey-Kramer

Treatment	Gel content (g gel/g polymer)	S.D.	Tukey mean comparison
11	0.6402	0.0010	A
1	0.5907	0.0337	AB
12	0.4708	0.0149	BC
4	0.4157	0.1158	CD
9	0.3779	0.0113	CDE
7	0.3464	0.0346	CDEF
10	0.3341	0.0271	CDEF
8	0.3307	0.0260	DEF
2	0.3155	0.0358	DEF
3	0.2968	0.0794	DEF
5	0.2684	0.0060	EF
6	0.2279	0.0282	F

Note: Levels with different letters are significantly different; S.D. = standard deviation

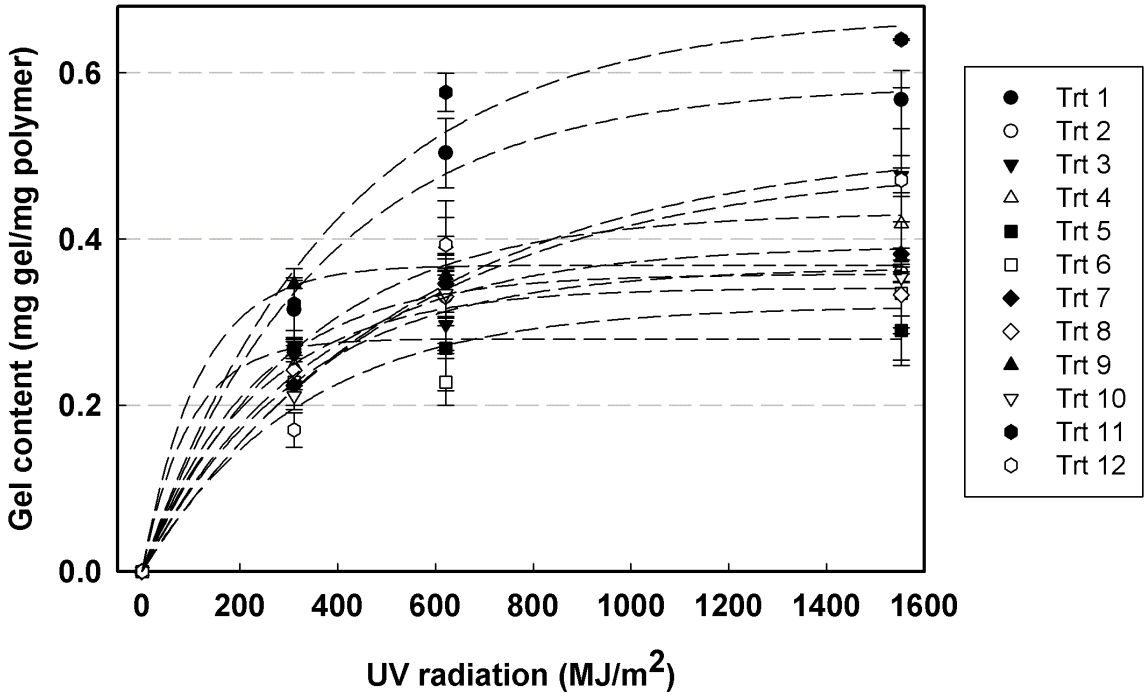

Figure 7-12. Changes of gel contents of all 12 PBAT film treatments as a function of UV radiation in MJ/m^2; dashed lines represent $Gel = Gel_a(1 - e^{-Gel_b x})$ trend lines

Table 7-10. Gel_a and Gel_b fitted parameters of $Gel = Gel_a(1 - e^{-Gel_b x})$ for gel content of all 12 treatments and their R^2-value

Treatment	Gel_a	Gel_b	R^2
1	0.5855	0.00274	0.9913
2	0.3578	0.00436	0.9997
3	0.4909	0.00189	0.9528
4	0.4323	0.00308	0.9849
5	0.2798	0.01030	0.9942
6	0.3194	0.00306	0.9180
7	0.3922	0.00297	0.9923
8	0.3411	0.00424	0.9936
9	0.3685	0.00871	0.9968
10	0.3655	0.00312	0.9855
11	0.6702	0.00251	0.9752
12	0.5157	0.00178	0.9471

The R^2 values in Table 7-10 indicate that equation 7-3 well represents the development pattern of gel content in the exposed PBAT films, since all the treatments have R^2-values greater than 0.9180. The estimate parameters Gel_a and Gel_b were used as variables for the second-order RSM model for gel content. In this case, two response surface model were developed.

7.3.3.1 Gel_a parameter

From Figure 7-13, the relationship between the actual and predicted Gel_a parameter from the RSM is somewhat linear and indicates that the Gel_a parameter may not be a good response surface model variable, due to R^2-value and adjusted R^2-value of 0.76 and 0.48, respectively (Table B-5). The P-value of 0.147 also indicates that the RSM model for Gel_a parameter is not significant at $\alpha = 0.05$.

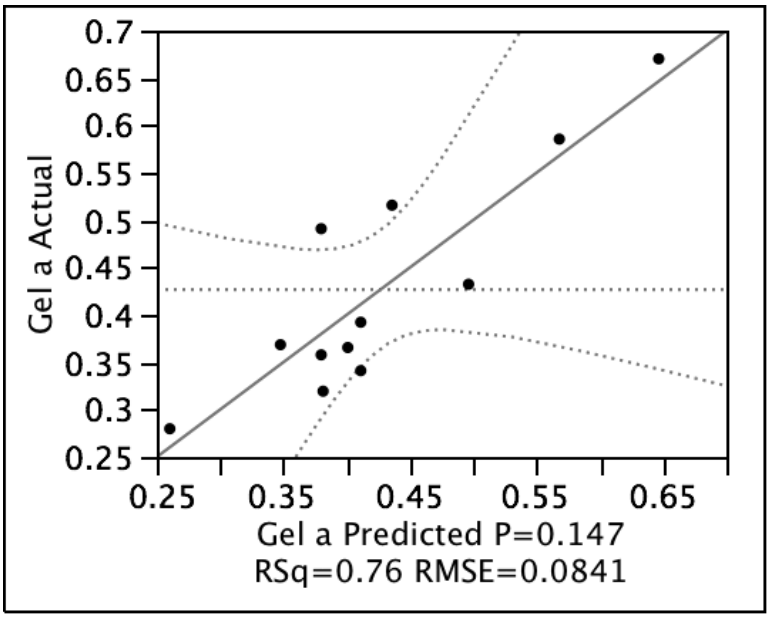

Figure 7-13. Actual vs. predicted Gel_a parameters from RSM model. The horizontal dotted line represents overall mean of 12 treatments. The solid diagonal line is the line of fit. Two curvature dotted lines are 95% confident interval.

7.3.3.1 Gel_b parameter

From Figure 7-14, the relationship between the actual and predicted Gel_b parameter from the RSM parameter estimates (Table 7-11) is linear and indicates that the Gel_b parameter is an excellent response surface model variable, due to R^2-value and adjusted R^2-value of 0.8959 and 0.7709, respectively (Table B-6). The P-value of 0.0236 also indicates that the RSM model for Gel_b parameter is significant (Figure 7-14).

Table 7-11. Parameter estimates of RSM model for Gel_b parameter

Term	Estimate	Std Error	t Ratio	Prob>|t|
Intercept	0.0033625	0.00064	5.25	0.0033*
CB_C	0.00204	0.000453	4.50	0.0064*
$AnOx_C$	0.0010977	0.000453	2.42	0.0598
CB_C x $AnOx_C$	0.0018952	0.00064	2.96	0.0315*
CB_C x CB_C	0.0013138	0.000506	2.59	0.0485*
$AnOx_C$ x $AnOx_C$	-0.000265	0.000506	-0.52	0.6226
Block[1]	0.0001759	0.00037	0.48	0.6544

Note: * indicates a statistical significance at type I error (α) of 0.05

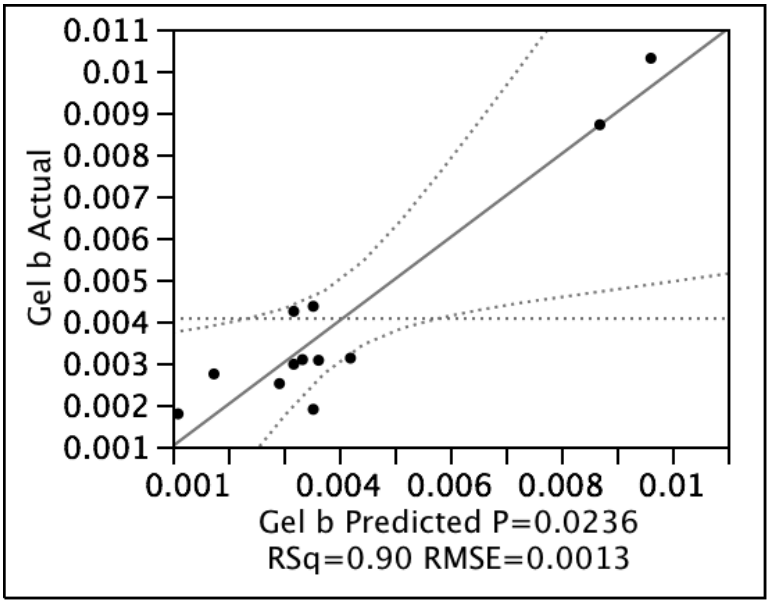

Figure 7-14. Actual vs. predicted Gel_b parameters from RSM model. The horizontal dotted line represents overall mean of 12 treatments. The solid diagonal line is the line of fit. Two curvature dotted lines are 95% confident interval.

From the parameter estimates, both linear and quadratic main effects of the coded level of carbon black affected the Gel_b parameter with P-values of 0.0064 and 0.0485. The positive estimated for CB_C indicates that a greater carbon black concentration will result in greater gel-forming rate. This can be seen from Figure 7-12, as the PBAT treatments with higher amount of carbon black concentrations developed gel more

quickly than those with lower concentrations in the initial phase, while later the treatments with higher concentrations reached the plateau stage faster at a lower amount of gel content. In addition, there is a significant interaction term of CB_C x $AnOx_C$ with the estimated parameter of 0.0018952 and P-value of 0.0315. Therefore, the increased concentration of antioxidant will increase the gel-forming rate more in the treatments with higher concentrations of carbon black than in those with lower concentrations. Kovács and Wolkober (1976) reported that the mutual effect of carbon black and phenolic antioxidants, such as BHT, on photooxidation is usually antagonistic, with a few cases of synergism depending on the interactions between the function groups on the carbon black surface and the functional groups on the phenolic antioxidants.

7.3.3.2 Final gel content

In Chapter 5 section 5.2.1, it was found that increased gel content resulted in lower biodegradability of the PBAT film. Percent mineralization of the films with 10, 30, 50, and 70% gel content were 36, 43, 21, and 24%, respectively, during the 45-day test under composting environments. Therefore, the actual final gel contents of all 12 treatments (Table 7-9) were used in the RSM model, since the estimated final gel content (Gel_a) parameter was not suitable as the RSM variable.

The actual final gel content is a much better RSM variable than parameter Gel_a, due to greater R^2, a more linear relationship between actual and predicted final gel content from the RSM parameter estimates (Table 7-12), and P-value of 0.0488 (Figure 7-15). Detailed statistical results can be found in Table B-7 in Appendix B.

From the parameter estimates, again, only linear and quadratic main effects significantly affected the final gel contents of the PBAT treatments. The negative estimated parameter for CB_C of -0.107596 indicates that greater carbon black concentration will result in lower gel content development. The UV absorbing ability of carbon black may contribute to this finding, since greater carbon black concentration results in less photon energy to interact with polymer chains.

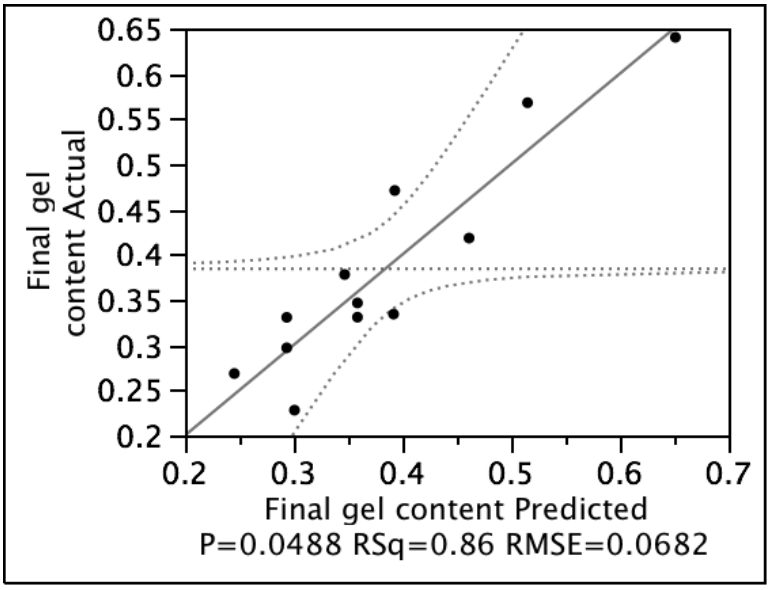

Figure 7-15. Actual vs. predicted final gel content from RSM model. The horizontal dotted line represents overall mean of 12 treatments. The solid diagonal line is the line of fit. Two curvature dotted lines are 95% confident interval.

Table 7-12. Parameter estimates of RSM model for final gel content

Term	Estimate	Std Error	t Ratio	Prob>|t|
Intercept	0.3260891	0.034103	9.56	0.0002*
CB_C	-0.107596	0.024115	-4.46	0.0066*
$AnOx_C$	-0.00039	0.024115	-0.02	0.9877
CB_C x $AnOx_C$	-0.027298	0.034103	-0.80	0.4598
CB_C x CB_C	0.0701789	0.026961	2.60	0.0481*
$AnOx_C$ x $AnOx_C$	0.0168773	0.026961	0.63	0.5588
Block[1]	-0.032538	0.019689	-1.65	0.1593

Note: * indicates a statistical significance at type I error (α) of 0.05

It was expected that after UV exposure, the films with 0% were not achievable. In Chapter 5 section 5.2.1, the % biodegradations of PBAT films with 0.10 and 0.30 g gel/g polymer in manure compost for 45 days were 36 and 43%, respectively, which were not statistically different. Therefore, gel content of 0.30 g gel/g polymer was selected as target criterion. Figure 7-16 is the contour plot created from the RSM model with the parameter estimates shown in Table 7-12. The curvilinear line in the contour profile was set so that gel content of all the points on this line is 0.30 g gel/g polymer, for which percent mineralization under a composting environment for 45 days is approximately 43%. Since the fitted response surface has a bowl-shaped surface, any combination of carbon black and antioxidant on the right side of this curvilinear line, having gel content less than 0.30 g gel/ g polymer should satisfy the biodegradation requirement for tomato production in Michigan.

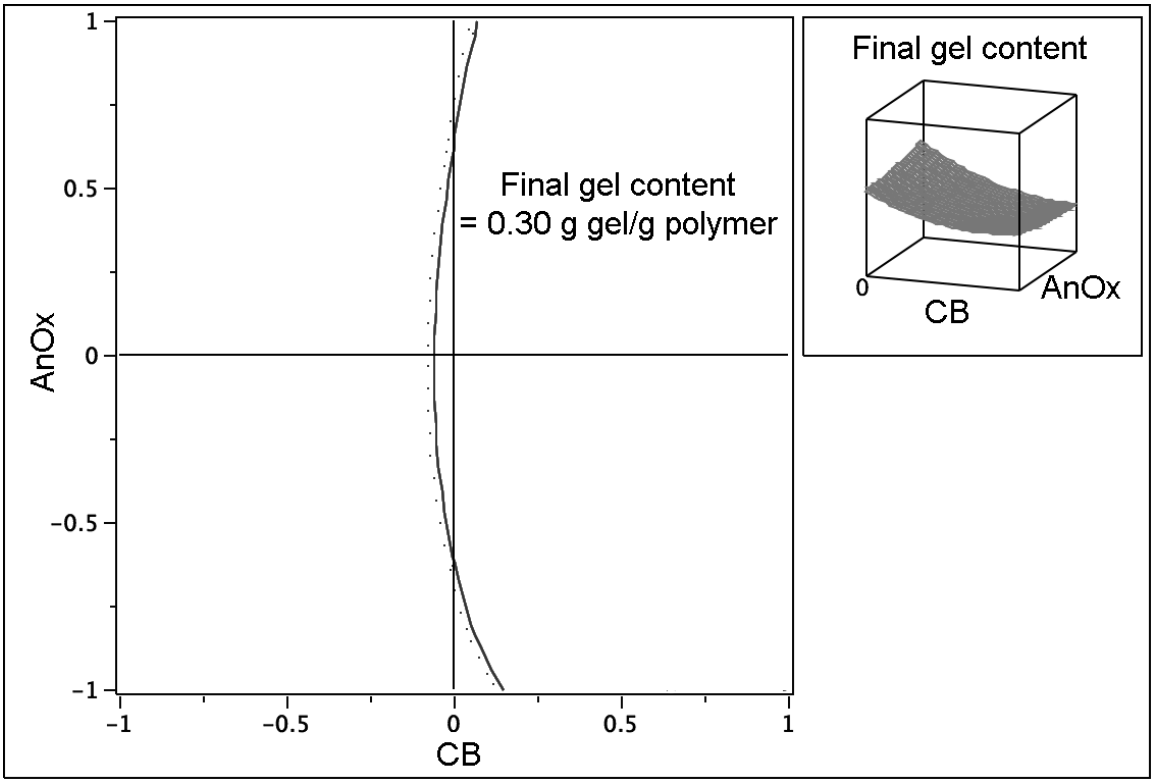

Figure 7-16. The contour profile of RSM model for final gel content with the curvilinear line representing gel content of 0.30 g gel/g polymer

7.3.4 Reduction of number average molecular weight (M_n)

As the PBAT films were exposed to UV radiation, the number average molecular weight (M_n) of treatments decreased differently (Figure 7-17). The reduction patterns varied among the treatments. Therefore, it is challenging to find a single equation that can represent the reduction pattern for all the treatments. As a result, a non-linear exponential equation (equation 7-4) was selected, since this equation can define a variety of reduction patterns (Figure 7-18).

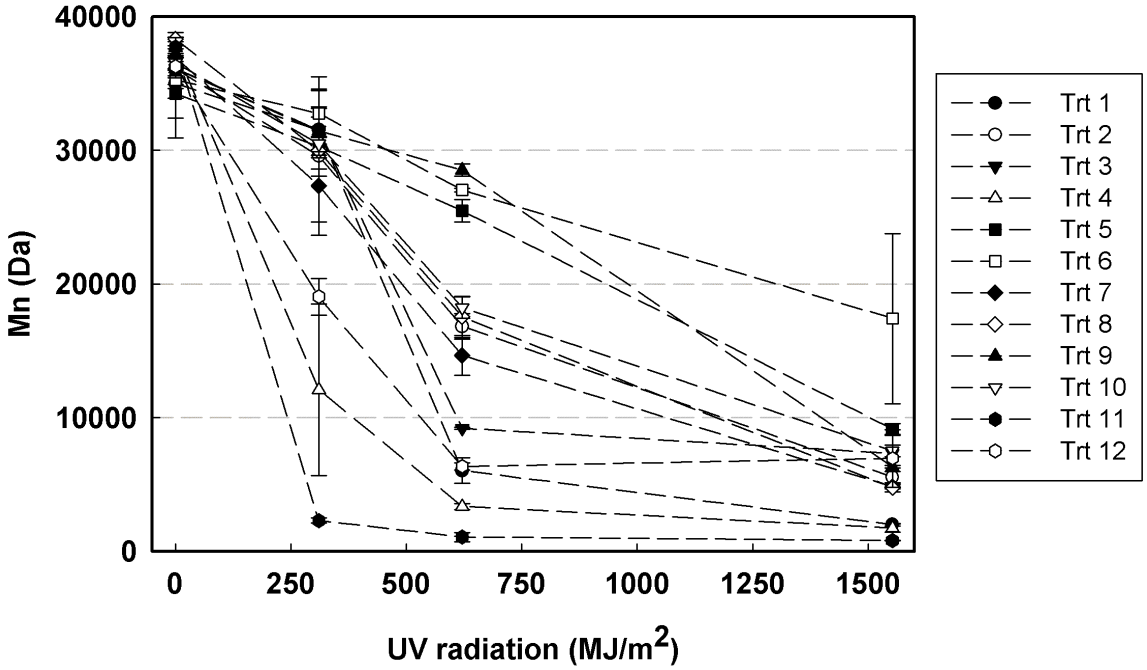

Figure 7-17. Reduction of M_n of all 12 treatments of PBAT films as function of time

$$M_n = y_O + ae^{bx} \quad (7\text{-}4)$$

where M_n = Number average molecular weight of PBAT film exposed to x MJ/m^2 of UV radiation

y_O, a = Adjusted parameters, where $y_o + a$ equals the initial M_n at x = 0 MJ/m^2

b = Reduction rate

With this equation, there are three possible cases of M_n reduction (Figure 7-18):

1. In the case $b = 0$; there are no changes in M_n
2. In the case $a > 0$, $b < 0$; this is the first order exponential reduction, similar to M_n reduction in bulk erosion of the biodegradation (Kijchavengkul and Auras 2008), where there is a rapid reduction in the initial phase and then the reduction reaches the plateau stage.
3. In the case $a < 0$, $b > 0$; M_n decreases slowly at first and then the reduction becomes greater as the films are exposed to more radiation. This reduction pattern is similar to surface erosion of biodegradation (Kijchavengkul and Auras 2008).

The equation $M_n = y_O + ae^{bx}$ was used to fit the M_n reduction patterns of all 12 PBAT treatments (Figure 7-19). The fitted parameters, R^2, and adjusted R^2 are presented in Table 7-13.

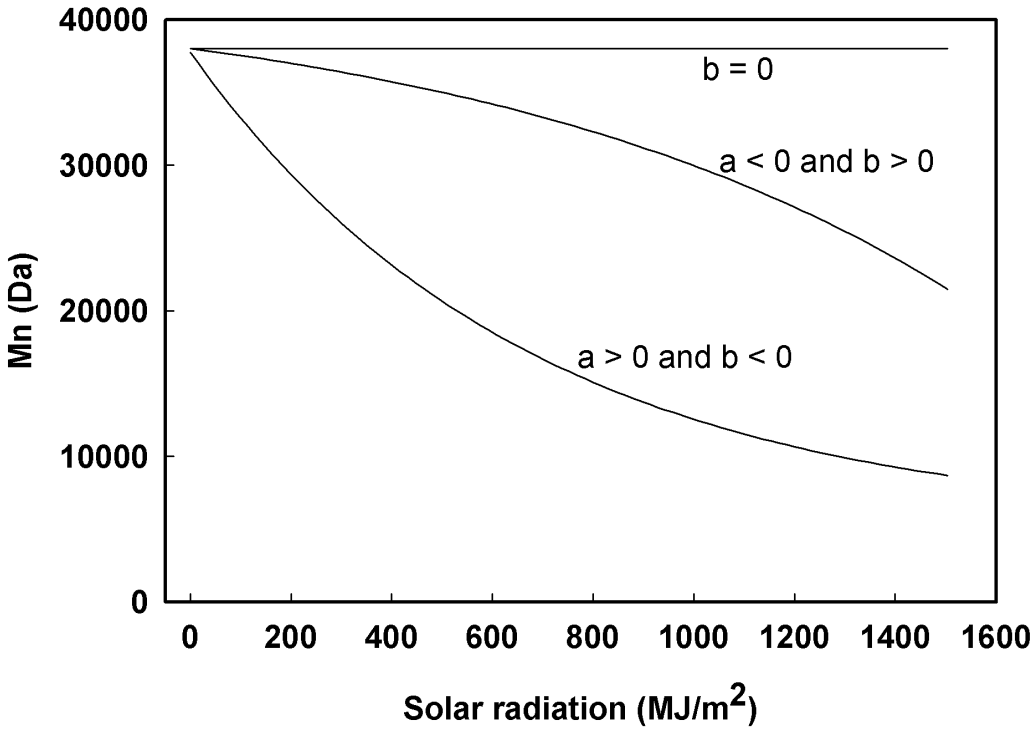

Figure 7-18. Reduction pattern of $M_n = y_O + ae^{bx}$ equation with different *a* and *b* parameters

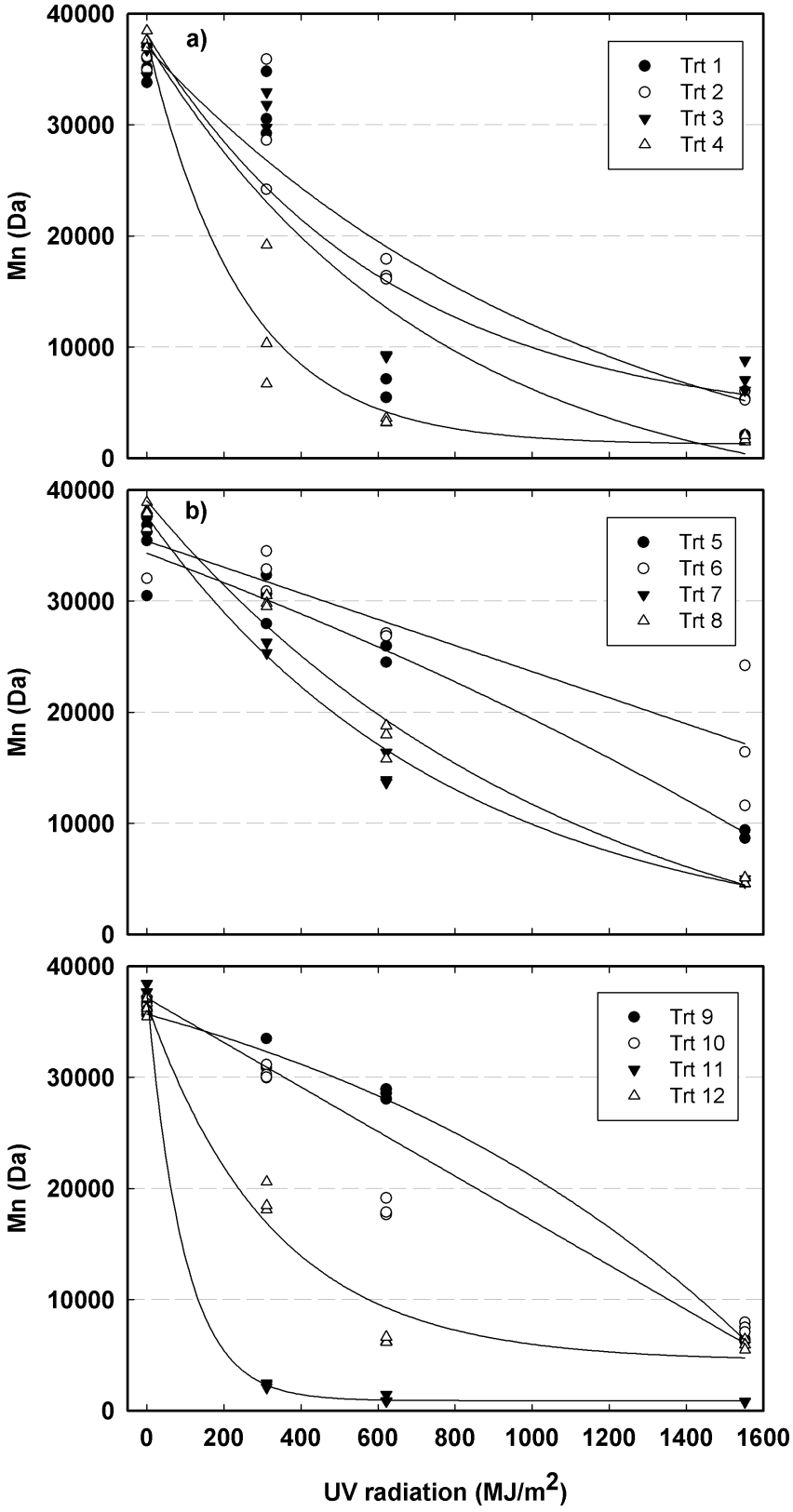

Figure 7-19. Fitted $M_n = y_O + ae^{bx}$ equation for all 12 PBAT treatments

Table 7-13. Fitted y_O, a, and b parameters, R^2, and adjusted R^2 from $M_n = y_O + ae^{bx}$ for M_n reduction of all 12 PBAT treatments

Treatment	y_o	a	b ($x10^{-3}$)	R^2	Adjusted R^2
1	1935	35864	-1.84	0.8174	0.7992
2	5240	32509	-1.49	0.9087	0.8996
3	6110	32144	-1.91	0.8316	0.8148
4	1465	36284	-4.12	0.9660	0.9626
5	36823	-4660	1.15	0.9496	0.9445
6	37521	-4167	1.03	0.7926	0.7719
7	4731	33355	-1.72	0.9588	0.9547
8	4566	35267	-1.52	0.9595	0.9555
9	36690	-2825	1.53	0.9833	0.9817
10	37144	-6330	1.02	0.8247	0.8072
11	794	36918	-10.3	0.9995	0.9995
12	5497	31168	-3.27	0.9627	0.9590

Table 7-13 shows that $M_n = y_O + ae^{bx}$ equation represents the M_n reduction pattern well, since R^2 values are at least 0.79 and the adjusted R^2 values are close to the R^2 values, which indicates that all three parameters (y_O, a, and b) are explanatory variables for M_n and none are redundant in describing the model (Kutner *et al.* 2004).

There are only 4 treatments, treatments 5, 6, 9, and 10, that have a positive b parameter. Those treatments have carbon black concentration 0.82 or greater, except treatment 10 that has 0.39% carbon black and 1% BHT.

7.3.4.1 Parameter *b*

Parameter b is critical. In this experiment, treatments 5, 6, 9, and 10 are the only four treatments with positive b parameters. The treatments with $b > 0$ were the four treatments with the lowest % light transmission (Table 7-2), the highest final tensile

strength (Table 7-4), and relatively low final gel content of less than 0.38 g gel/g polymer (Table 7-9). In the case where $b < 0$, the rapid reduction of M_n at first along with the damage from wind and animals in the field means the films will not last long. On the other hand, in the case where $b > 0$, the film will last longer in the field, since initially the film can better retain its properties and then rapidly degrade right before or after the harvest. This is desirable in vegetable production, where retention of properties early in the season is more important than later. Therefore, parameter *b* was selected as an input variable for the RSM model, since the molecular weight reduction where $b \geq 0$ is more desirable.

The relationship between the actual and predicted values of the *b* parameter from the RSM model (Table 7-14) is linear with R^2-value of 0.88 (Figure 7-20). The P-value of 0.0302 also indicates that the RSM model for the *b* parameter is well fitted (Figure 7-20). The parameter estimates shows that only the linear main effect of coded concentration of carbon black is significant with the estimate of 0.00311 (Table 7-14), indicating that greater carbon black concentration will result in an increased *b* parameter, which was previously observed. Detailed statistical results can be found in Table B-8 in Appendix B.

Table 7-14. Parameter estimates of RSM model for *b* parameter from $M_n = y_O + ae^{bx}$

Term	Estimate	Std Error	t Ratio	Prob>|t|
Intercept	-0.00166	0.000818	-2.03	0.0983
CB_C	0.0031088	0.000579	5.37	0.0030*
$AnOx_C$	0.0010584	0.000579	1.83	0.1269
CB_C x $AnOx_C$	-0.00054	0.000818	-0.66	0.5385
CB_C x CB_C	-0.00091	0.000647	-1.41	0.2186
$AnOx_C$ x $AnOx_C$	0.00072	0.000647	1.11	0.3164
Block[1]	0.00059	0.000472	1.25	0.2670

Note: * indicates a statistical significance at type I error (α) of 0.05

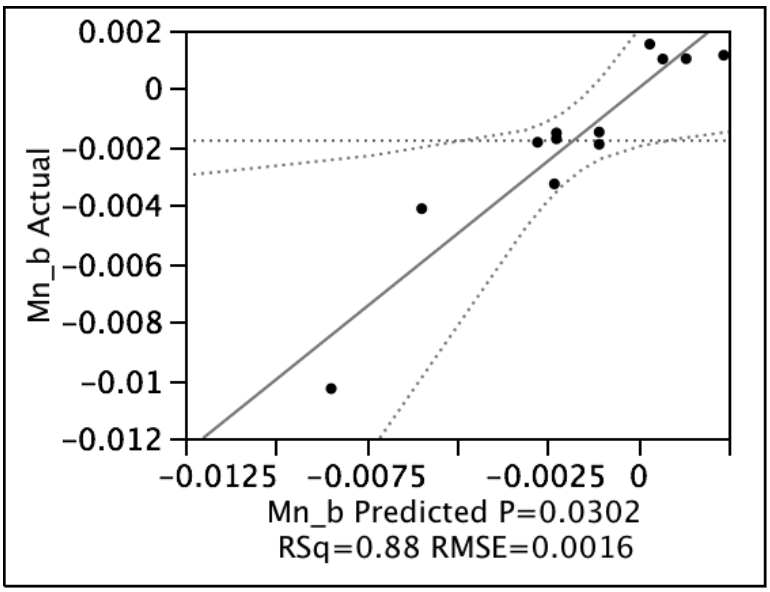

Figure 7-20. Actual vs. predicted *b* parameter from RSM model. The horizontal dotted line represents overall mean of 12 treatments. The solid diagonal line is the line of fit. Two curvature dotted lines are 95% confident interval.

Figure 7-21 is the contour plot created from the RSM model with the parameter estimates shown in Table 7-14. The curvilinear line in the contour profile was set so that parameter *b* of all the points on this line is 0. Since the fitted response surface in region of the coded level of -1 to 1 is an incline flat surface, any combination of carbon black and BHT on the right side of this curvilinear line should satisfy the biodegradation

requirement for tomato production in Michigan, since M_n reduction pattern where $b \geq 0$ is more desirable.

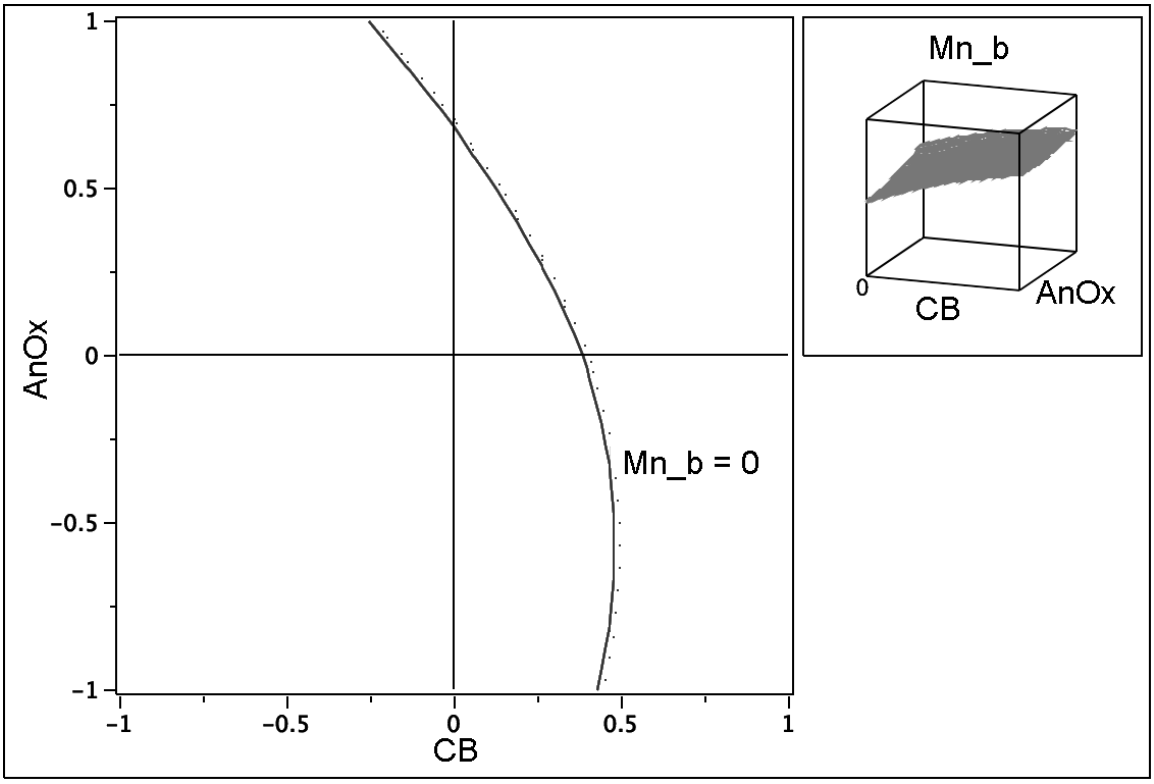

Figure 7-21. The contour profile of RSM model for parameter *b* with the curvilinear line representing $b = 0$

7.3.5 Simultaneous RSM

In order to select a suitable composition of carbon black and BHT for the PBAT mulch films for tomato production in Michigan, four-response surface models were analyzed simultaneously. Those selected four models and their criteria are shown in Table 7-15. These criteria can be changed according to the solar radiation and length of crop production season.

Table 7-15. Four response surface models and their criteria for selecting suitable carbon black and BHT composition for PBAT mulch films

Models	**Criteria**
% Light transmission	< 20%
Final tensile strength	> 6.35 MPa
Final gel content	< 0.30 g gel/g polymer
Parameter *b* in M_n reduction	> 0

The shaded area in the overlaid contour plot (Figure 7-22) is the intersection where all the four criteria are met or exceeded. Any combination of carbon black and BHT concentrations in this area should be suitable for PBAT mulch films for tomato production (3-4 months of UV exposure) in Michigan or regions with similar or lower solar radiation during the growing season from May to September, which have an average monthly solar radiation of 7.2-21.6 MJ/m^2/day or 2-6 kWh/m^2/day (Figure 7-23).

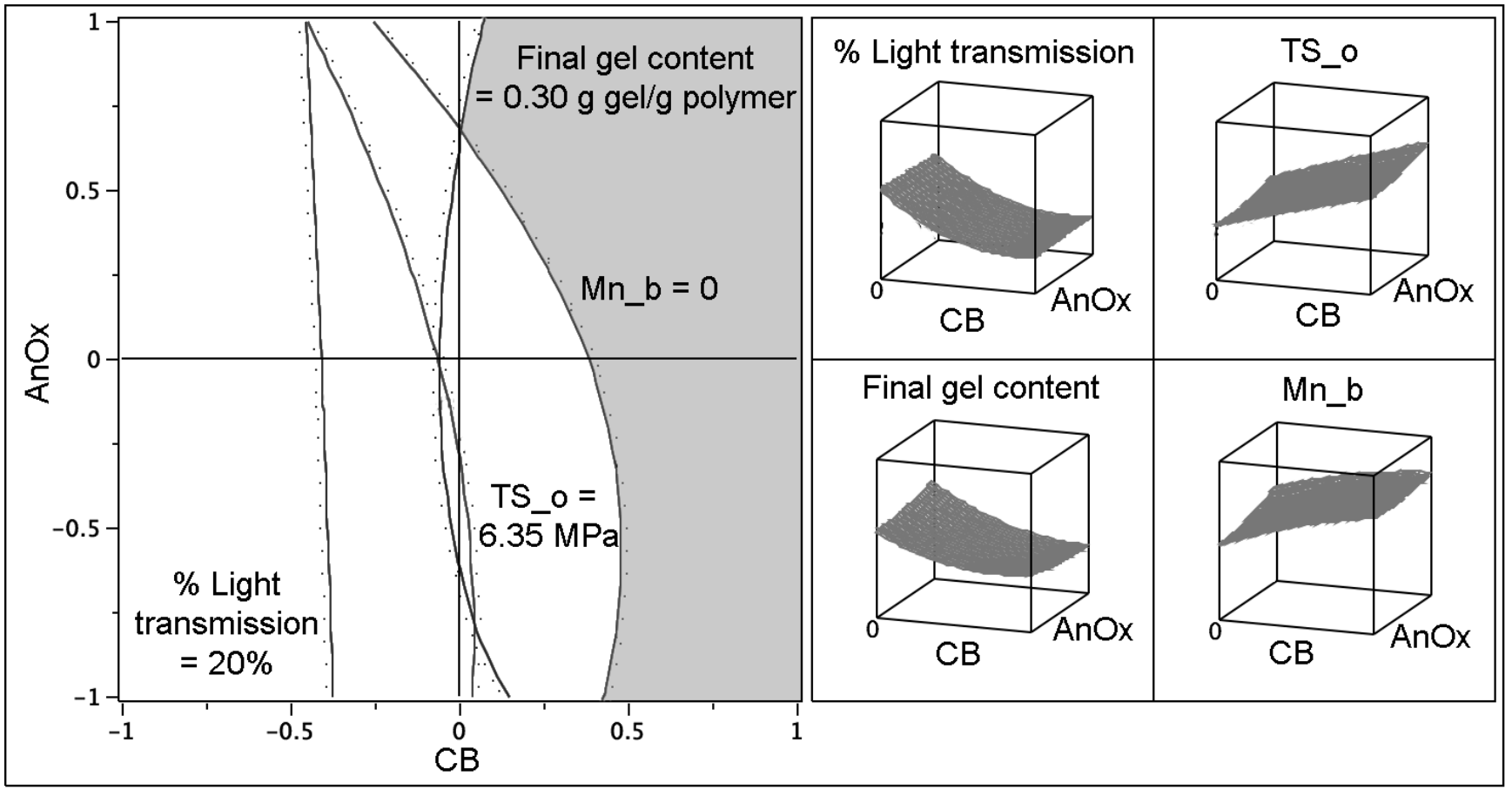

Figure 7-22. The overlaid contour plot of the four response surface models: % light transmission, final tensile strength, final gel content, and *b* parameter from M_n reduction. The shaded area is the intersection where the criteria of all four models are fulfilled

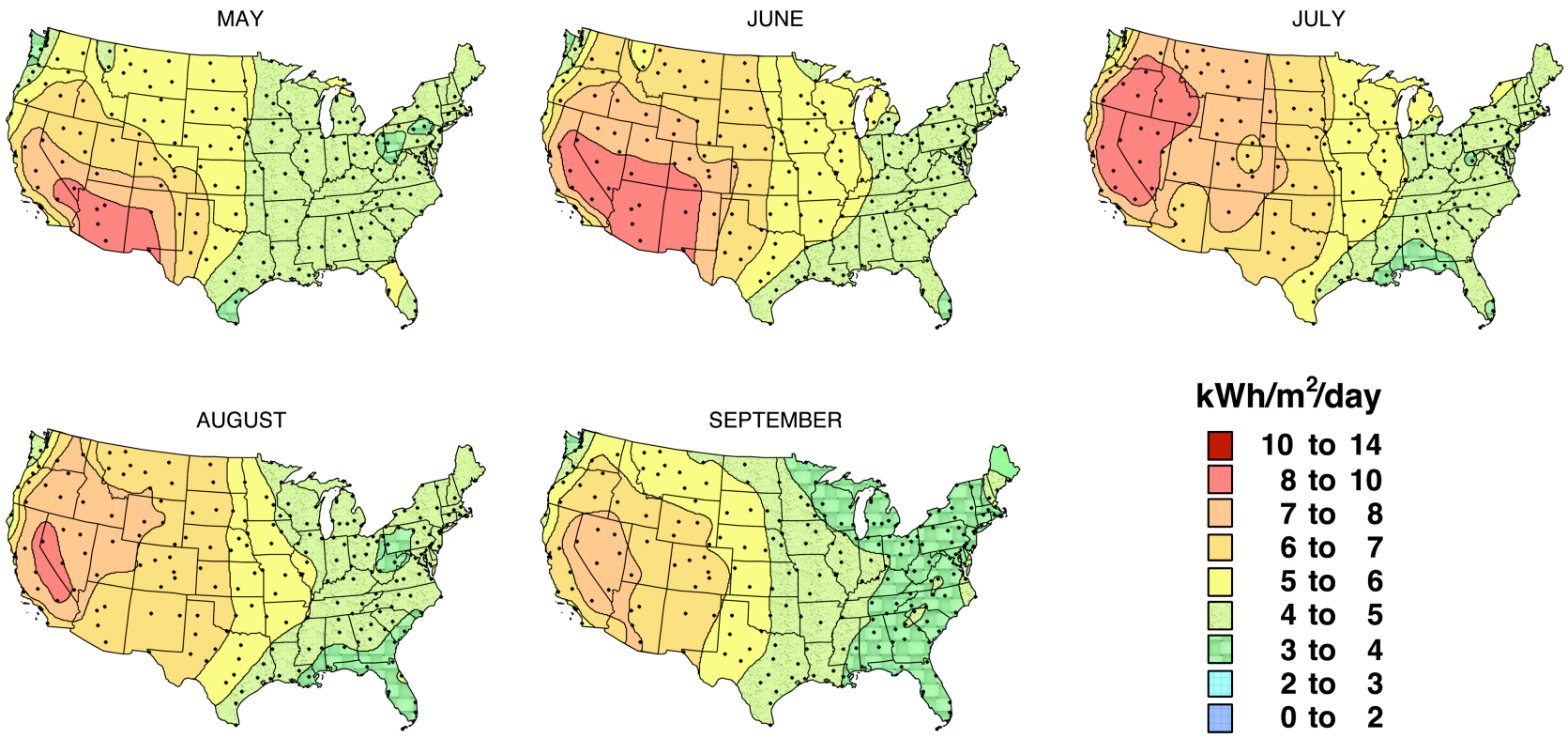

Figure 7-23. Average monthly solar radiation of the U.S. from May to September from 30-year average data from 1961-1990. The film formulation in Figure 7-22 can be used as mulch film for 3-4 month produce production during May to September season in the areas with similar solar radiation to Michigan or lower. 1 kWh/m^2/day = 3.6 MJ/m^2/day
Source: National Renewable Energy Laboratory: Resource Assessment Program (NREL 2010)
These images in this dissertation are presented in color.

Although it is statistically unsound to infer beyond the radiation boundary, since the experiment was set up for tomato production in Michigan or regions with similar solar radiation, the tentative composition of the mulch film for higher radiation exposure can be scientifically speculated. If the film were to be used in regions or for crops with higher total solar radiation, such as one-year pineapple production in Hawaii, where the films would be exposed to much higher solar radiation, it can be speculated that the appropriate composition of the PBAT mulch film would shift toward a higher carbon black concentration. From the parameter estimates (Tables. 7-3, 7-8, 7-12, and 7-14), higher carbon black concentration will produce PBAT film with more desirable properties for mulch film applications, which are lower light transmission, higher tensile strength, low gel content, and better retention of molecular weight. More detailed discussion related to film formulations for various crops and total solar radiation and how the formulation model for general radiation can be achieved is presented in section 8.2.4.

7.3.6 Effect of antioxidant

Although, from the parameter estimates from four response models (initial light transmission, estimated final tensile strength, final gel content, and parameter *b* for M_n reduction from the equation $M_n = y_O + ae^{bx}$), carbon black concentration is the main effect in improving film photo-stability, the main effects from antioxidant are not significant, except that in tensile strength. The overlaid contour plot (Figure 7-22) suggests that incorporation of a high amount of BHT allows carbon black to be used at a lower concentration. Carbon black concentration of 0.59% (coded level of 0.5) can be used when BHT concentration is greater than 0.5% (coded level of 0).

It is not that BHT does not have an effect on tensile strength and parameter *b* for M_n reduction, but the effect of coded carbon black concentration is more dominant. Besides treatments 1, 4, and 11, where carbon black concentrations were 0.1, 0.1, and 0%, respectively, treatment 12 with 0% BHT and 0.39% carbon black yields the lowest final tensile strength (Table 7-4), the lowest value of *b* parameter in M_n fitted equation (Table 7-13), and the highest gel content at the end of the test (Table 7-9) among the treatments with 0.39% carbon black or higher. Furthermore, treatment 10, which has 0.39% carbon black and the highest BHT concentration of 1.0% among all the treatments, shows the highest final tensile (Table 7-4) and lowest M_n reduction among the treatments with 0.39% carbon black (second only to the treatments with 0.82% carbon black). Treatment 10 is also the only treatment with 0.39% carbon black that has a positive value of *b* parameter in M_n fitted equation.

On the other hand, the antagonistic effect of carbon black and BHT was observed in gel-forming rate, since treatments with higher concentrations of carbon black and BHT developed gel faster than the treatment with the same BHT concentration but lower concentration of carbon black

REFERENCES

REFERENCES

ASTM (1998) D 882-98 standard test method for tensile properties of thin plastic sheeting. West Conshohocken, PA, ASTM International.

ASTM (2004) D 6400-04 standard specification for compostable plastics. West Conshohocken, PA, ASTM International.

Guan, J and Hanna, MA (2005). "Selected morphological and functional properties of extruded acetylated starch, polylactic acid foams." Industrial and Engineering Chemistry Research **44**(9): 3106-3115.

Kijchavengkul, T and Auras, R (2008). "Perspective: Compostability of polymers." Polymer International **57**(6): 793-804.

Kovács, E and Wolkober, Z (1976). "The effect of the chemical and physical properties of carbon black on the thermal and photooxidation of polyethylene." Journal of Polymer Science: Polymer Symposia **57**(1): 171-180.

Kutner, M, Nachtsheim, C, Neter, J and Li, W (2004). Applied Linear Statistical Model. New York, NY, McGraw-Hill /Irwin.

Munguia, O, Delgado, A, Farina, J, Evora, C and Llabres, M (1992). "Optimization of dl-PLA molecular weight via the response surface method." International Journal of Pharmaceutics **86**(2-3): 107-111.

NREL. (2010). "U.S. Solar radiation resource maps." Retrieved Aug 13, 2010, from http://rredc.nrel.gov/solar/old_data/nsrdb/redbook/atlas/.

Shlyapintokh, V (1984). Photochemical Conversion and Stabilization of Polymers. New York, NY, Hanser.

Zhong, QP and Xia, WS (2008). "Physicochemical properties of edible and preservative films from chitosan/cassava starch/gelatin blend plasticized with glycerol." Food Technology and Biotechnology **46**(3): 262-269.

Chapter 8 Conclusions and future work

8.1 Conclusions

The research work in this dissertation was divided into 3 phases: design and creation of assessment tools, determination of the performance of the commercial and biodegradable mulch films under field and lab studies, and design of a biodegradable film formulation for mulch film using RSM; therefore, the conclusions follow this outline.

8.1.1 Design and creation of assessment tools

An in-house direct measurement respirometric (DMR) system capable of measuring polymer biodegradability by quantifying the amount of carbon dioxide evolved during biodegradation was successfully built. This system facilitates biodegradation testing by eliminating human intervention and errors especially from titration used in the cumulative method. The data were easily interpreted since they were already converted from concentration to mass of carbon dioxide evolution and mineralization by the computer programs, and there was no further conversion and calculation required, unlike the cumulative method that requires a titration method. The main drawbacks of this system were the higher initial cost and the time-consuming process of software programming.

Besides measuring the gel content in PBAT using the gravimetric method, two additional methods (FTIR and DSC techniques) were verified and used. Crosslinking of films cause non-uniformity of the crystal lattices, making them melt at different temperatures. Polymer with a higher degree of crosslinking is indicated by a broader

melting peak and a lower onset temperature than that with a lower degree of crosslinking. Furthermore, the kinetics of the crosslinked films can be represented with the Avrami equation by observing the changes in gel content and the changes in onset temperature of the melting peak. Crosslinked samples tested with FTIR spectrophotometer showed changes of the absorbance intensities of the functional groups esters and substitutes of benzene that were related to the crosslinking.

8.1.2 Determination of the performance of the commercial and biodegradable mulch films under field and lab studies

Although the black PBAT films were slightly degraded when exposed to UV light during the season, they can still provide an acceptable level of weed control as the conventional LDPE mulch films. Because of the exposure to UV radiation, as evidenced from FTIR and molecular weight determinations, the PBAT films undergo both chain scission and crosslinking, which alter the performance of the films in the field. Chain scission causes a reduction in molecular weight and hence tensile strength. On the other hand, crosslinking from the transformation of polymer chains into a network structure, as measured using amount of gel content, reduces the film tensile elongation, increases the film brittleness, and reduces the biodegradability of the PBAT. The crosslinking mostly occurs in the amorphous regions, since X-ray diffraction analysis did not show any changes in the crystalline regions. Respirometric and scanning electron microscopy analyses indicated that the biodegradation of the crosslinked samples decreased with increasing gel content. The crosslink structures make the film samples less flexible and might prevent accessibility of the microorganisms to the polymer chains.

Biodegradation of biodegradable polyesters such as PBAT was strongly influenced by the total microbial activity of the exposure environments, which was monitored by CO_2 emissions and C/N ratio. PBAT degraded much faster in environments with high microbial activity, such as in manure compost. The ester group in the aliphatic BA unit was more susceptible to hydrolysis than that in the aromatic BT unit. Consequently, the BA unit was more vulnerable to hydrolysis and biodegradation. During biodegradation, increases in PBAT crystallinity were observed, which indicated that the amorphous regions biodegraded faster than the crystalline regions.

From the field and laboratory simulated experiments, the required criteria used in the RSM for a suitable biodegradable mulch film for 3-4 month vegetable production in Michigan or regions with similar solar radiation, such as the Midwest and New England, were obtained. Those criteria are light transmission of 20% or lower, final tensile strength of at least 6.35 MPa at the end of the season, maximum gel content of 30% at the end of the season, and positive parameter b according to the equation $M_n = y_O + ae^{bx}$ of molecular weight reduction.

8.1.3 Design of biodegradable film formulation for mulch film using response surface methodology (RSM)

From the parameter estimates from the four response models (initial light transmission, estimated final tensile strength, final gel content, and parameter b for M_n reduction), carbon black concentration was the main effect in improving film photo-stability, while the main effect from antioxidant was not significant, except that in tensile strength. It is not that BHT does not have an effect on tensile strength and parameter b for

M_n reduction, but the effect is overwhelmed by the effect of carbon black. In addition, the antagonistic effect of carbon black and BHT was observed in gel-forming rate. However, incorporation of high amount of BHT allows carbon black to be used at lower concentration, which is desirable, since an increased amount of carbon black may increase film processing difficulty.

Suitable compositions of carbon black and antioxidant for the PBAT mulch films were determined by using fitted equations and simultaneous RSM analyses of four response surfaces. As a result, a chart representing suitable combination of carbon black and BHT concentrations was obtained. PBAT mulch films produced with carbon black and BHT concentration falling in the gray area should be suitable for crop production in Michigan or regions with similar solar radiation (7.2-21.6 MJ/m^2/day or lower) and length of growing season (Figure 8-1).

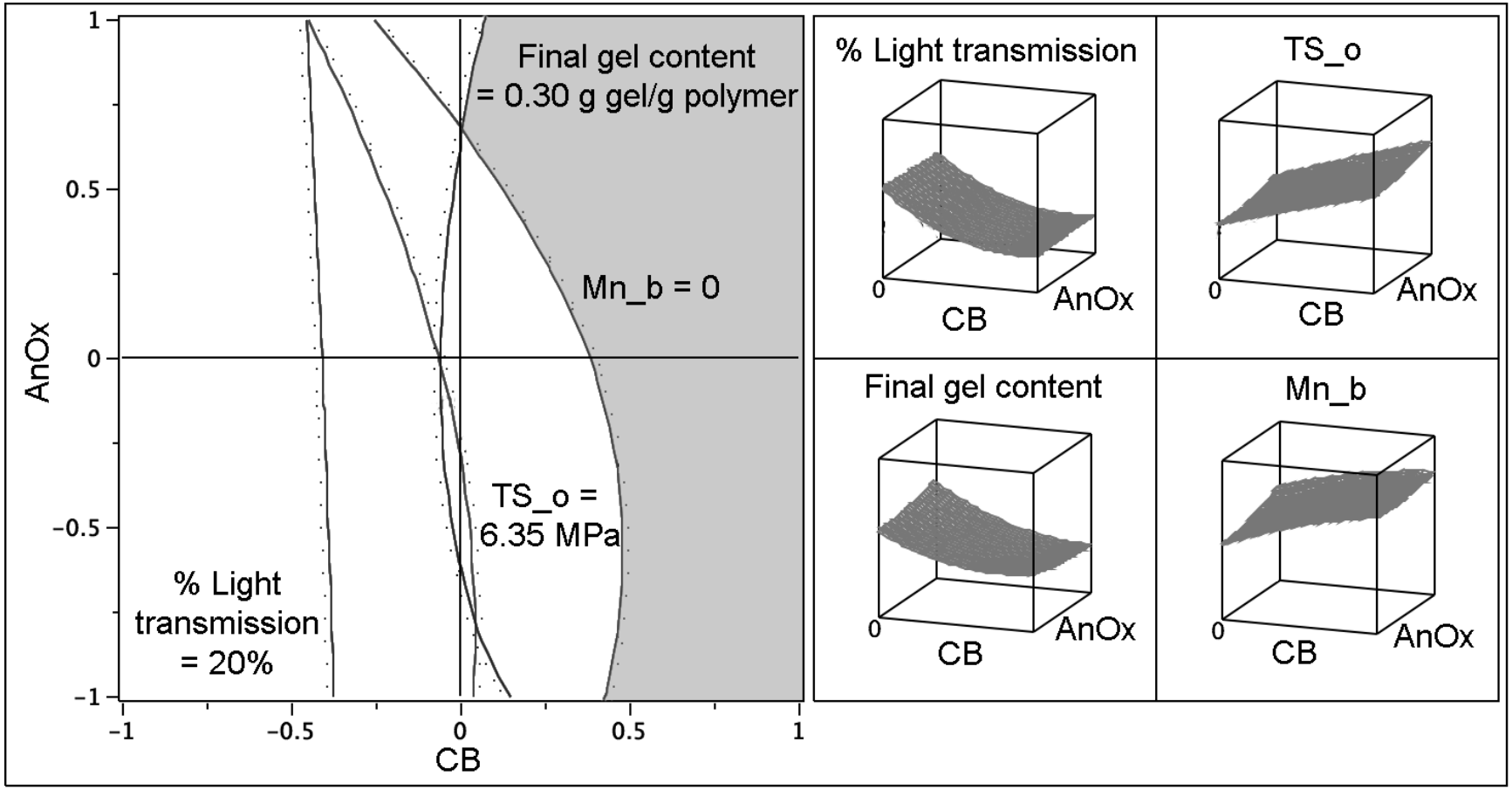

Figure 8-1. The overlaid contour plot of the four response surface models: % light transmission, final tensile strength, final gel content, and *b* parameter from M_n reduction. The shaded area is the intersection where the criteria of all four models are fulfilled. Note: CB_C = coded level of carbon black between 0.10 and 0.82 w/w and $AnOx_C$ = coded level of antioxidant between 0.15 and 0.85 w/w.

8.1.4 Overall conclusions

In regard to the hypotheses, exposure to UV light affects some properties of the biodegradable film including mechanical properties, molecular weight, chemical structure, and biodegradability. However, those changes did not always affect the performance of the biodegradable film when compared to commercial LDPE mulch film, since the weed control performance and marketable yields in fruit/plot and weight/plot of black PBAT film and LDPE mulch film were not statistically different.

In regard to the objectives, the development of crosslinking of PBAT films due to photodegradation was determined as a function of gel content and total UV radiation. Although PBAT films that did not crosslink when exposed to UV could not be produced, the formulation of biodegradable PBAT films that possesses photo-stability and strength requirements, ability to withstand the specific longevity, and biodegradability for tomato production in Michigan or regions with similar solar radiation was established.

Since the mulch film design using RSM is based on the total solar radiation in MJ/m^2 during specific time duration, it is important to translate this total solar radiation to geographical and seasonal related information in a format of length of the season in particular region, since produce growers may not fully understand the total radiation concept. For example, total solar radiation of 1,500 MJ/m^2 should equal 3-4 months of solar radiation in the Midwest region during growing season from May to September.

8.2 Future work and recommendations

8.2.1 Selective RSM boundary

The selected boundary of the RSM study was limited to 0 to 1% concentration for both carbon black and BHT, due to the ASTM D6400 specification. In addition, a center point design of carbon black was selected according to the manufacturer's specification.

From the RSM contour profiling (Figure 7-22), the concentrations of carbon black and BHT acceptable for mulch film application are on the high carbon black side with higher carbon black concentration than the manufacturer's specification. Furthermore, the area with best performance seems to be outside of the RSM boundary. Therefore, the boundary of a future recommended RSM study should be shifted toward higher carbon black concentrations, such as from 0.4 to 2% carbon black (instead of 0-1%). This indicates that the carbon black concentration according to manufacturer's specification is not high enough to protect the films from photodegradation.

From personal experience, although adding a higher concentration of carbon black facilitates the blown film extrusion process by reducing the adhesion between the extrudate and the air ring below the frost line, it can cause difficulty in controlling the thickness of the film bubble and decrease stability of the bubble below the frost line, making it break more easily. This suggests that an optimal design for RSM should be used instead of the central composite design. The optimal design is the design that its algorithm can be used when there are constraints, on some treatments or factor levels, that make them impossible to run (Kutner *et al.* 2004; Myers *et al.* 2009). As a result the total number of treatments can be reduced.

8.2.2 Addition of peroxide decomposing antioxidant in the RSM model

The type of antioxidants used in this dissertation was limited to only the chain breaking antioxidant, BHT, due to the limitation of the UV chamber sample holder capacity. Peroxide-decomposers (PD) are antioxidants that decompose hydroperoxide in a way that does not generate more free radicals. In order to completely study the effect of antioxidants on biodegradable mulch films, including the synergistic and antagonistic effects, the use of peroxide decomposers should be investigated.

8.2.3 Identification of microorganisms

Enzymatic preferences of microorganisms for different isomers and number of carbon atoms for polymers vary. Composts with appropriate C/N ratio and CO_2 emission may not directly be a suitable testing media due to lower total biodegradation of cellulose positive controls and different enzymatic specificity of microorganisms in compost. Therefore, relating the biodegradation rate to general compost composition and/or other factors may overlook the specific families of microorganisms present in the compost that may be more or less successful than others at biodegrading aliphatic aromatic polyesters. Thus, there is a critical need to understand and identify the effect of microbial population, family of microorganisms, and their enzymatic specificity in different microbial environments on the total biodegradation of biodegradable and compostable polyesters and their biodegradation rates.

8.2.4 Extended UV radiation and development of a model for general radiation

The UV radiation used in the RSM experiment (chapter 7) in this dissertation was set specifically to represent the three-to-four month use of biodegradable mulch film for vegetable production, such as tomatoes, in the Midwest and New England regions, where the films are exposed to 1,500-2,000 MJ/m^2 of radiation (average monthly solar radiation of 7.2-21.6 MJ/m^2/day or 2-6 kWh/m^2/day from May to September) (Figure 8-2). In order to expand the model to represent other U.S. regions, such as the Southwest, where the monthly average solar radiation ranges from 21.6 to 36 MJ/m^2/day (6-10 kWh/m^2/day), approximately twice that in the Midwest (Figure 8-2), the length of the UV radiation test has to be extended.

Figure 8-2indicates that the Midwest and the New England are the regions with the lowest monthly average solar radiation, while the Southwest is the highest. Therefore, the films have to be formulated differently. The produce production in the Midwest region is usually from May to September, while those in the Southwest or Florida can be all year round. In addition, season length for each crop in different geographical regions is different; for example, 3-4 months for tomato or cucumber and 1 year for pineapple. The films used for different crops will be exposed to different total solar radiation.

In order to develop an RSM model for general radiation, the total solar radiation must be included in the model as another variables, besides carbon black and antioxidant concentrations. The boundary of the total radiation has to be preselected and coded accordingly. For example, if there are three factors in the response surface model, the coded levels are -1.6818, -1, 0, 1, and 1.6818. In the case where the general model is designed for the radiation from low radiation up to one year of pineapple production in Hawaii, the coded level -1.6818 will be 0 MJ/m^2 and the coded level of 1 will be 6,275 MJ/m^2 (365 days of 17.2 MJ/m^2/day or 4.78 kWh/m^2/day, Figure 8-3). As a result, Table 8-1 represents the RSM treatment pattern, where the coded level of total radiation of -1.6818, -1, 0, 1, and 1.6818 are 0, 1,595, 3,935, 6,275, and 7,870 MJ/m^2, respectively. The total radiation of 7.870 MJ/m^2 can be achieved with 27 weeks of continuous UV exposure at 1.40 W/m^2/nm. The coded levels for carbon black and antioxidants should be modified and defined later.

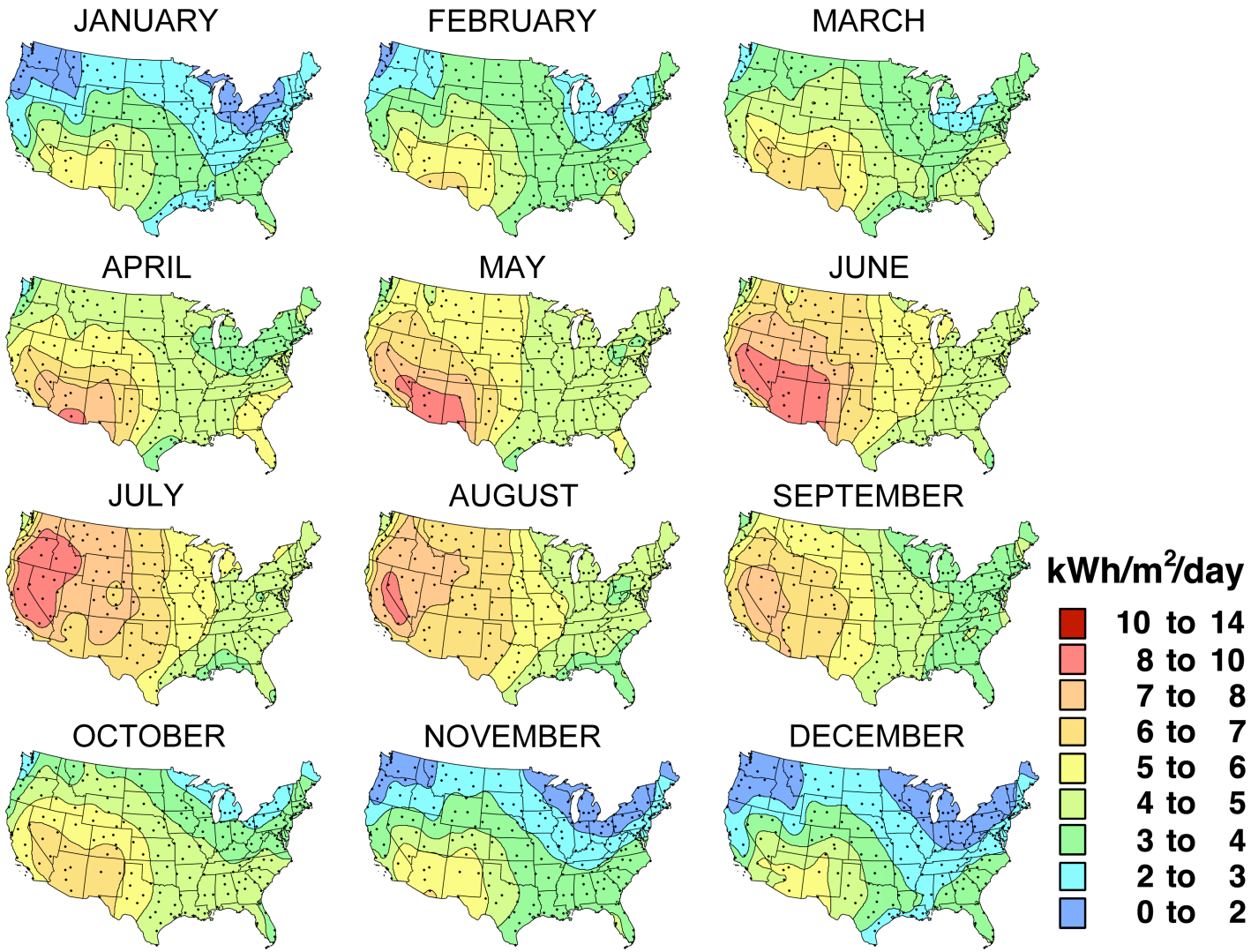

Figure 8-2. Spatial monthly average solar radiation received in the U.S. derived from the 1961-1990 National Solar Radiation Database (source: National Renewable Energy Laboratory: Resource Assessment Program (NREL 2010)); 1 kWh/m^2/day = 3.6 MJ/m^2/day. **These images in this dissertation are presented in color.**

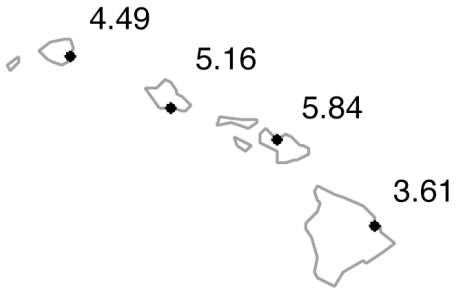

Figure 8-3. Spatial annual average solar radiation received in the Hawaii (in kWh/m^2/day) derived from the 1961-1990 National Solar Radiation Database (source: National Renewable Energy Laboratory: Resource Assessment Program (NREL 2010)); 1 kWh/m^2/day = 3.6 MJ/m^2/day

Table 8-1. Detailed list of all treatments in the proposed rotatable CCD design with 3 factors: carbon black concentration, antioxidant concentration, and radiation

Pattern	Block	Coded level		
		CB	AnOx	Radiation
−++	1	-1	1	1
++−	1	1	1	-1
000	1	0	0	0
−−−	1	-1	-1	-1
000	1	0	0	0
+−+	1	1	-1	1
+−−	2	1	-1	-1
000	2	0	0	0
+++	2	1	1	1
−−+	2	-1	-1	1
−+−	2	-1	1	-1
000	2	0	0	0
000	3	0	0	0
00A	3	0	0	1.6818
0A0	3	0	1.6818	0
0a0	3	0	-1.6818	0
000	3	0	0	0
A00	3	1.6818	0	0
00a	3	0	0	-1.6818
a00	3	-1.6818	0	0

Note: The coded level of total radiation of -1.6818, -1, 0, 1, and 1.6818 are 0, 1,595, 3,935, 6,275, and 7,870 MJ/m^2, respectively.

Once the UV exposure is complete, the light transmission, tensile strength, molecular number, and gel content of the film samples at different radiation exposure could be used as the response surfaces using the second-order polynomial model (equation 8-1). Similarly to the RSM in section 7.3.6, four response surfaces could be analyzed simultaneously. Conceptually, the overlaid contour plots with coded levels of carbon black and antioxidant as X and Y axes can be cut cross-sectionally according to any desirable total radiation from coded levels of -1 to 1 (1,595 to 6,275 MJ/m^2), and the general model for the production of mulch films to be used in the different regions of the U.S. could be obtained.

$$E\{Y\} = \beta_O + \beta_1 CB_C + \beta_2 AnOx_C + \beta_3 R_C + \beta_{11} CB_C^2 + \beta_{22} AnOx_C^2 + \beta_{33} R_C^2$$
$$+\beta_{12} CB_C \times AnOx_C + \beta_{13} CB_C \times R_C + \beta_{23} R_C \times AnOx_C + \tau(block) \quad (8\text{-}1)$$

where $E\{Y\}$ = Estimate of interested parameter

CB_C = Coded level of carbon black

$AnOx_C$ = Coded level of antioxidant

R_C = Coded level of total radiation

β_o = Intercept

β_1 = Linear main effect of carbon black

β_2	=	Linear main effect of antioxidant
β_3	=	Linear main effect of total radiation
β_{11}	=	Quadratic main effect of carbon black
β_{22}	=	Quadratic main effect of antioxidant
β_{33}	=	Quadratic main effect of total radiation
β_{12}	=	Interaction effect of carbon black and antioxidant
β_{13}	=	Interaction effect of carbon black and total radiation
β_{23}	=	Interaction effect of antioxidant and total radiation
τ	=	Blocking effect
block	=	Block number

REFERENCES

REFERENCES

Kutner, M, Nachtsheim, C, Neter, J and Li, W (2004). Applied Linear Statistical Model. New York, NY, McGraw-Hill /Irwin.

Myers, R, Montgomery, D and Anderxon-Cook, C (2009). Response Surface Methodology: Process and Product Optimization Using Designed Experiments Hoboken, NJ, John Wiley & Sons.

NREL. (2010). "U.S. Solar radiation resource maps." Retrieved Aug 13, 2010, from http://rredc.nrel.gov/solar/old_data/nsrdb/redbook/atlas/.

APPENDICES

Appendix A Response Surface Methodology (RSM)

A.1 Introduction

Myers *et al.* (2009) defines response surface methodology (RSM) as "a collection of mathematical and statistical techniques for developing, improving, and optimizing processes." In reality, RSM is usually used in the situation where several input variables (factors) could influence some performance or quality characteristic (or response) of the product or process. In general, RSM problems can be divided into these three categories (Myers *et al.* 2009):

1. "Mapping a response surface over a particular region of interest." In this case, the response will be used to predict the outcome of the process, when there are some changes of the inputs (Myers *et al.* 2009).

2. "Optimization of the response." In this case, RSM will be used to determine the optimized processing conditions, such as processing time and temperature, that result in the optimal process output, such as maximum yield (Myers *et al.* 2009).

3. "Selection of operating conditions to achieve specific requirements." In this case, several responses are used simultaneously, for example, one response for yield and another for production cost. Hence, RSM is used to maintain the yield above and keep cost below certain levels (Myers *et al.* 2009).

In this dissertation, the objective of the RSM experiment falls in the third category, which is to determine the precise factor levels (in this case concentrations of carbon black and antioxidants) that lead to optimal response (performance of biodegradable mulch film as a function of time or total solar radiation). Use of multiple response surfaces also allows more than one dependent variable Y (property) to be considered. For example, there will be one response surface for tensile strength, one for light transmission, one for molecular weight, one for gel content, one for biodegradability, and so forth. The concentrations of antioxidant and carbon black that yield the overall best performance in all the properties will be selected as the final formulation for the biodegradable PBAT mulch film.

Optimal response can be determined when the response surface is either concave (mound-shaped) (Figure A-1a and b) or convex (bowl shaped) (Figure A-1c and d). Detailed mapping of the response surface is usually done by fitted response surface (Figure A-1a and c) or contour plot (Figure A-1b and d). This methodology is applicable only when all the experimental factors (variables) are quantitative and the true response surface can be well represented by a second-order polynomial function. The second-order is widely used in RSM for several reasons (Myers *et al.* 2009):

1. The second-order model is adaptable and can fit into various functional forms.
2. The surface parameters are easy to estimate using the least squares method.
3. Considerable practical experience indicates that the second-order model usually works well for real problems.

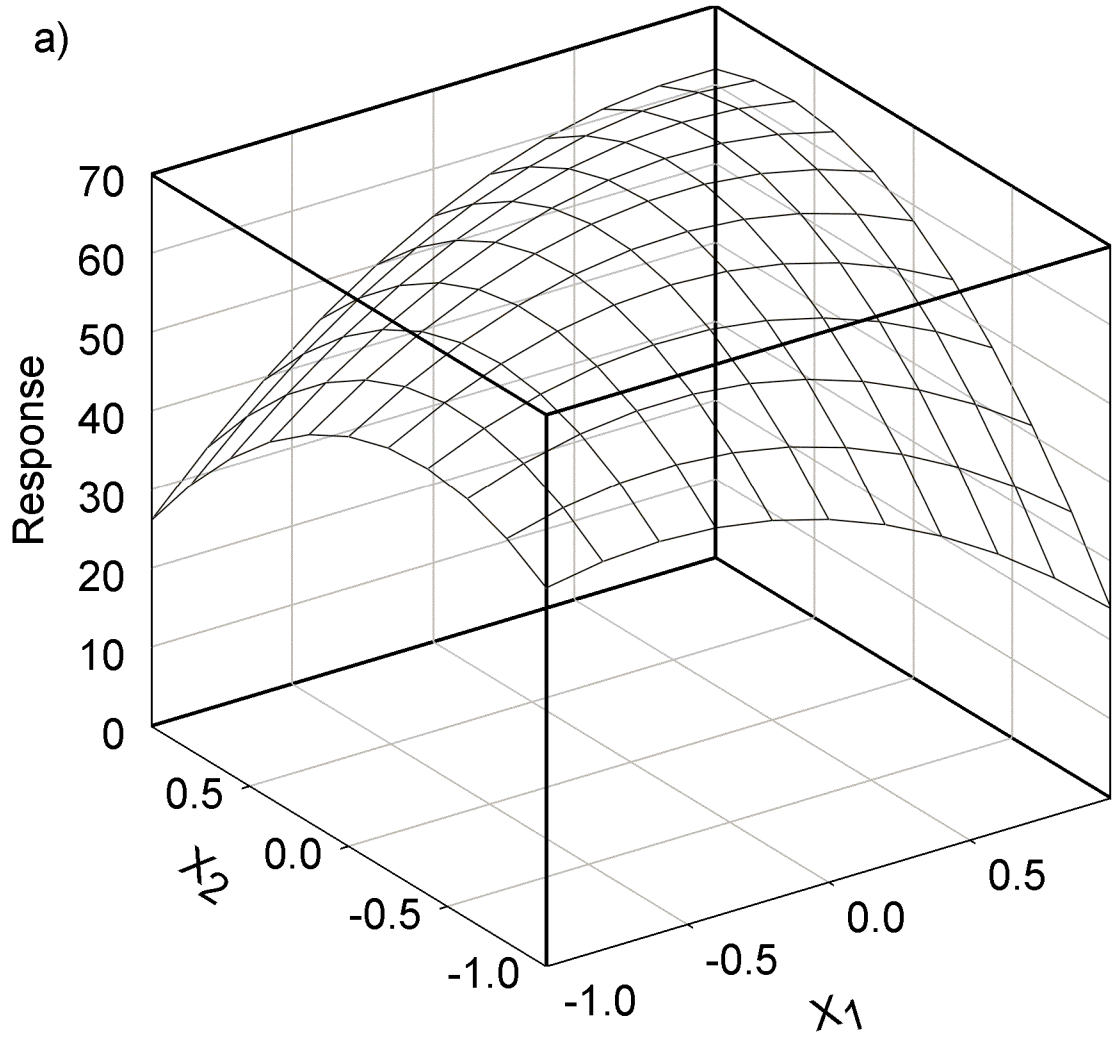

Figure A-1a. Fitted response surface of mound-shaped surface; adapted from (Kutner *et al.* 2004)

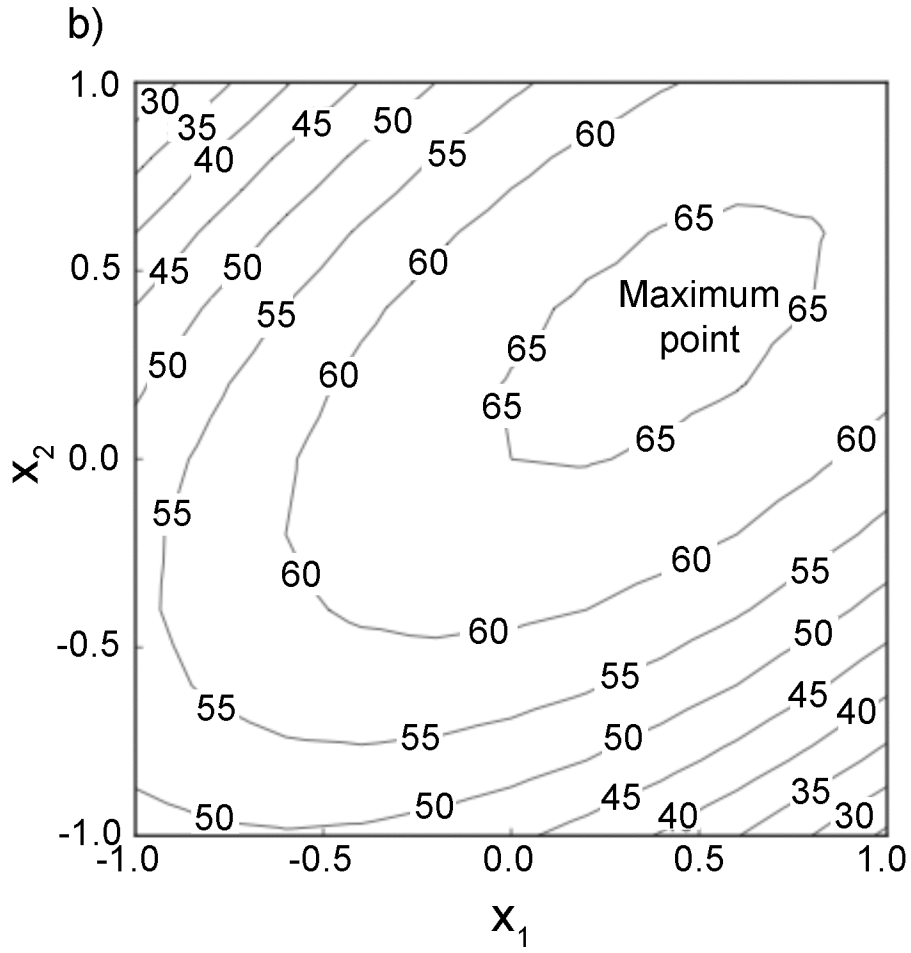

Figure A-1b. Contour plot of mound-shaped surface and its maximum point; adapted from (Kutner *et al.* 2004)

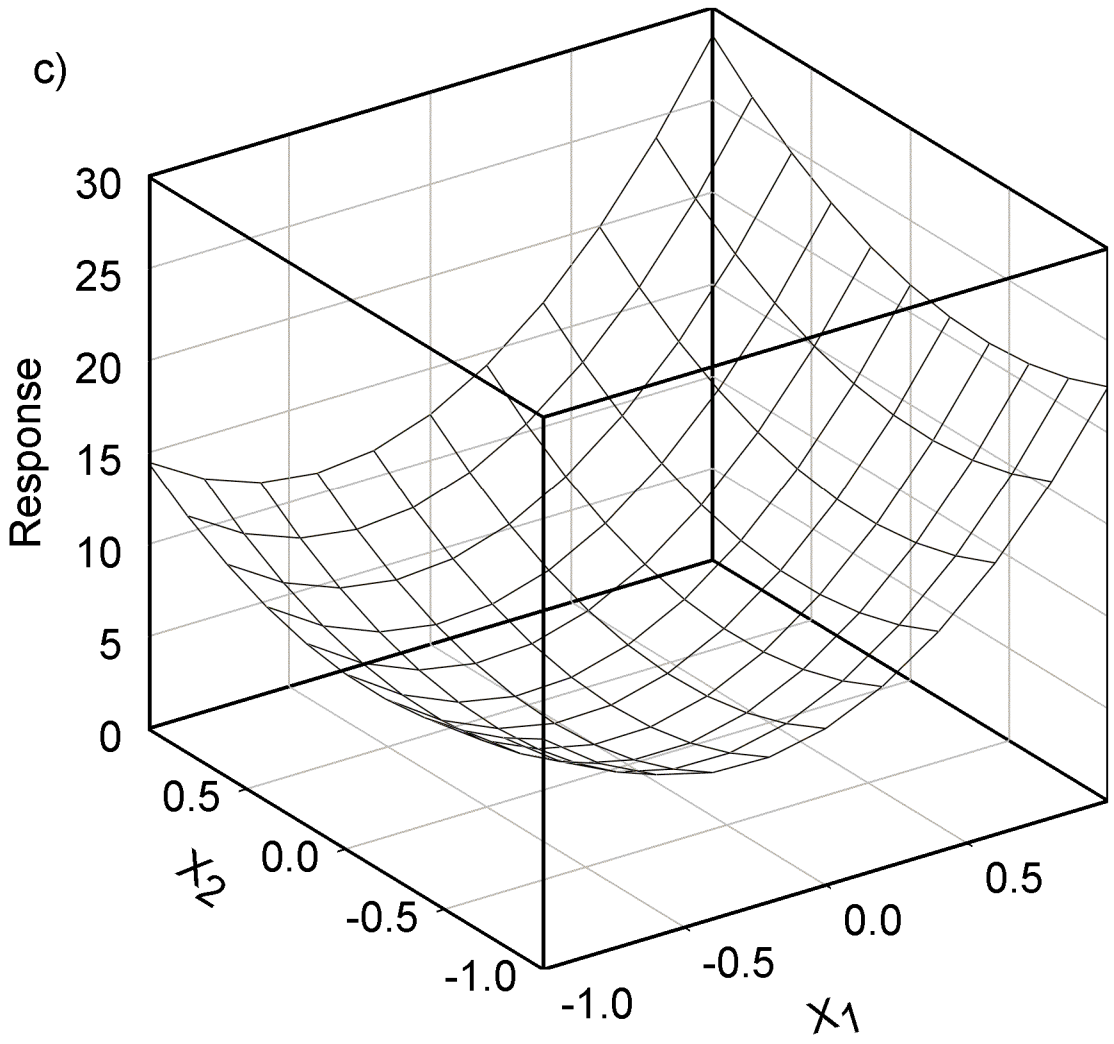

Figure A-1c. Fitted response surface of bowl-shaped surface; adapted from (Kutner *et al.* 2004)

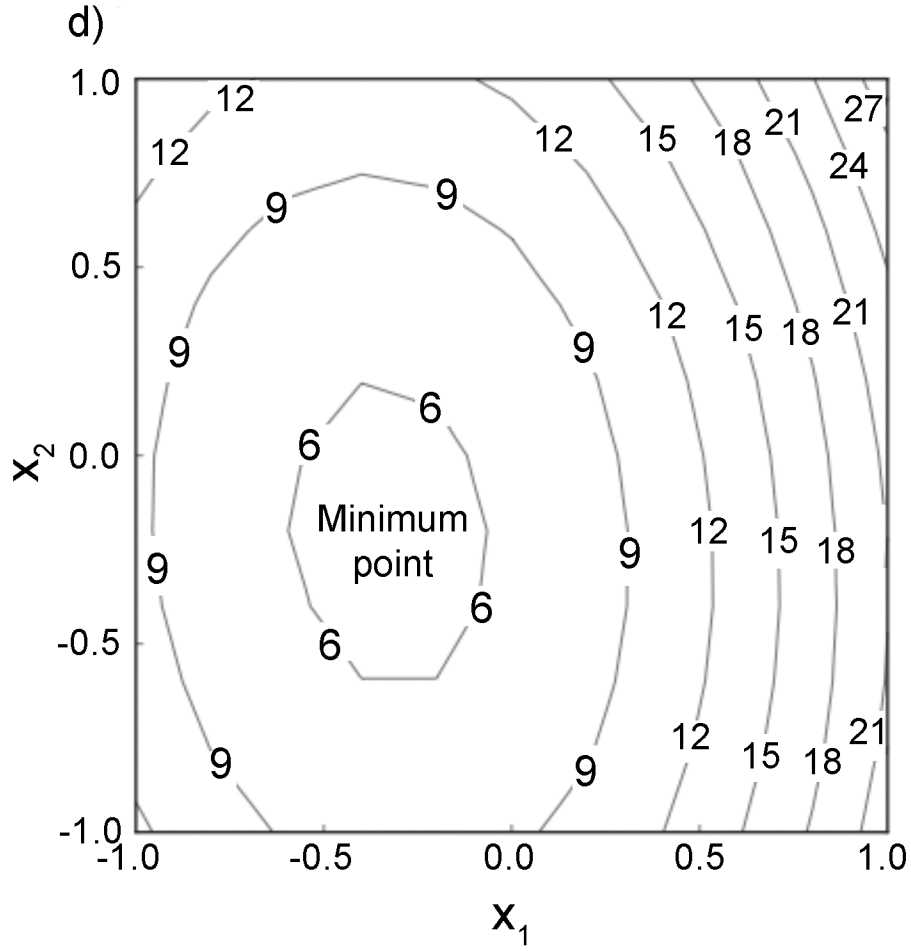

Figure A-1d. Contour plot of bowl-shaped surface and its minimum point; adapted from (Kutner *et al.* 2004)

The response surface is estimated by the second-order multiple regression model (equation A-1), based on the assumption that the main effects and second-order effects are enough to capture the response function and the third order and higher effects are unimportant (Kutner *et al.* 2004). If only two main effects are investigated, as in this dissertation, equation A-1 can be simplified to equation A-2.

$$E\{Y\} = \beta_o + \beta_1 x_1 + ... + \beta_k x_k + \beta_{11} x_{11}^2 + ... + \beta_{kk} x_k^2 + \beta_{12} x_1 x_2 + ... + \beta_{k-1,k} x_{k-1} x_k \quad \text{(A-1)}$$

$$E\{Y\} = \beta_o + \beta_1 x_1 + \beta_2 x_2 + \beta_{11} x_{11}^2 + \beta_{22} x_{22}^2 + \beta_{12} x_1 x_2 \quad \text{(A-2)}$$

Where $E\{Y\}$ = Estimate of variable Y

x_j = quantitative factors j (For example, X_1 = concentration level of carbon black and X_2 is concentration level of antioxidant.

$\beta_{1,\ldots} \beta_k$ = linear main effect coefficients

$\beta_{11,\ldots} \beta_{kk}$ = quadratic main effect coefficients

$\beta_{12,\ldots} \beta_{k-1,k}$ = interaction effect coefficients

For the second order response surface, the vector location (or the solution) where the maximum, minimum, or saddle point occurs ($\boldsymbol{X_s}$) is calculated according to Eq. A-3. The solution is located where the slope of the surface equals zero. Mound-shaped response surfaces give a maximum value, while bowl-shaped response surfaces give a minimum value. For the saddle-shaped response, the response at the solution is neither the maximum nor the minimum (Figure A-2).

$$X_S = -\frac{1}{2} B^{-1} b^* \qquad \text{(A-3)}$$

where:

$$\underset{k\times k}{B^{-1}} = \begin{bmatrix} b_{11} & \frac{b_{12}}{2} & \cdots & \frac{b_{1k}}{2} \\ \frac{b_{12}}{2} & b_{22} & \cdots & \frac{b_{2k}}{2} \\ \vdots & \vdots & \ddots & \vdots \\ \frac{b_{1k}}{2} & \frac{b_{2k}}{2} & \cdots & b_{kk} \end{bmatrix}$$

$$b^* = \begin{bmatrix} b_1 \\ b_2 \\ \vdots \\ b_k \end{bmatrix}$$

The characteristics of the matrix B are called eigenvalues, which can be used to determine whether the optimal point ($\boldsymbol{X_s}$) is a maximum, a minimum, or a saddle point. If the eigenvalues are all positive, $\boldsymbol{X_s}$ is a minimum. If the eigenvalues are all negative, $\boldsymbol{X_s}$ is a maximum. If some of the eigenvalues are positive and some are negative, then $\boldsymbol{X_s}$ is a saddle point (Figure A-2). In addition, this matrix calculation technique allows the use of more than two quantitative factors simultaneously, unlike the graphical technique, where it is limited by three-dimension graph.

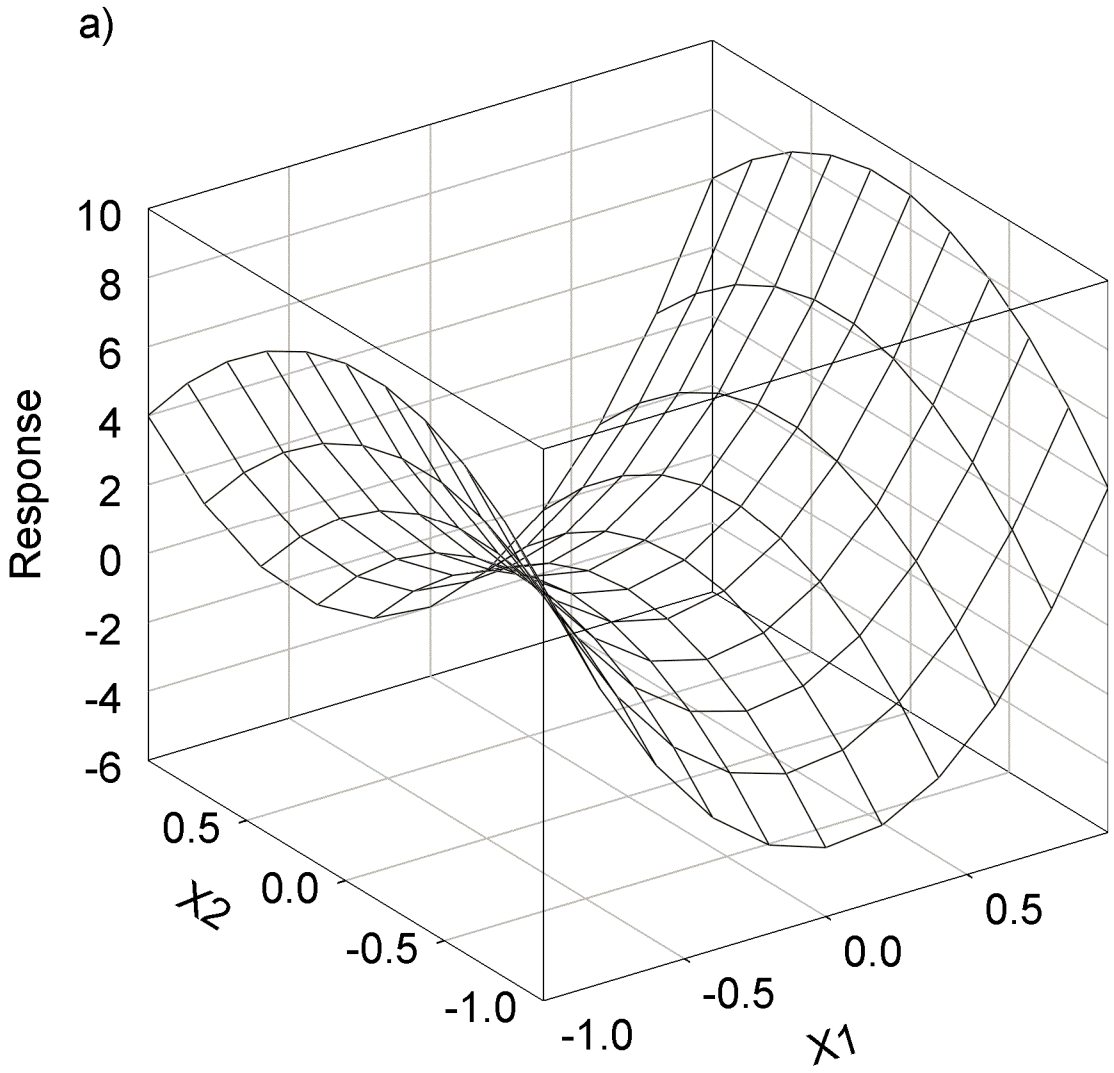

Figure A-2a. Fitted response surface of saddle-shaped surface; adapted from (Kutner *et al.* 2004)

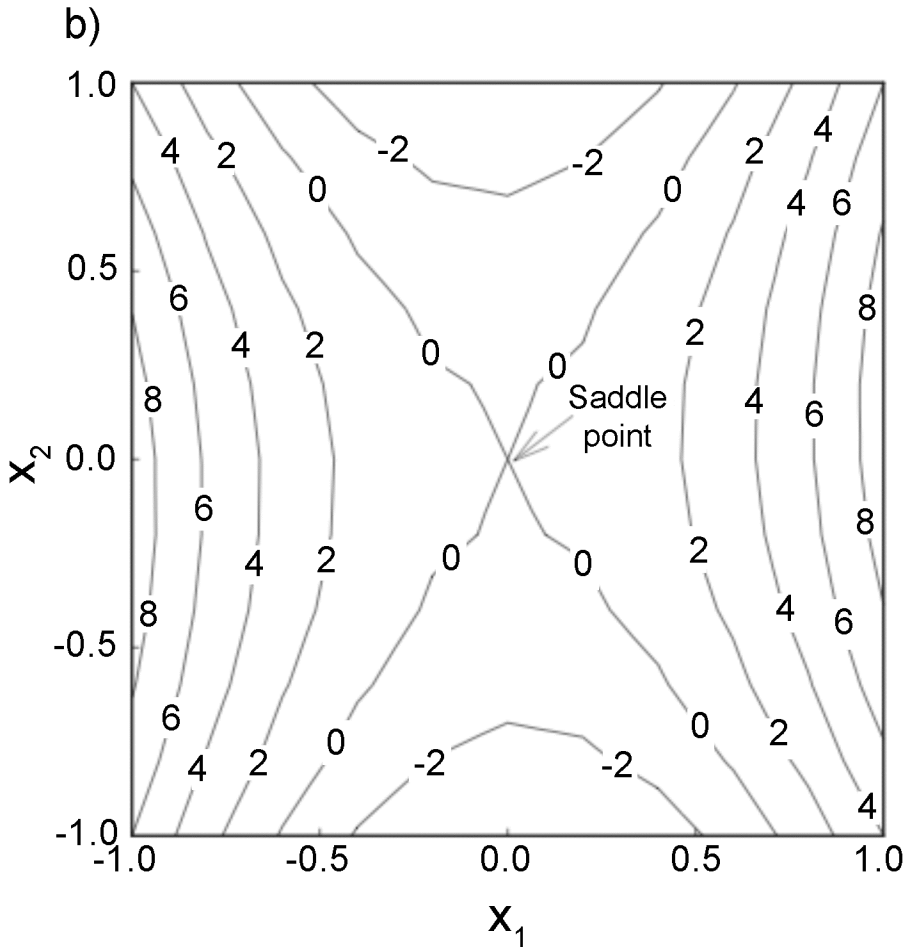

Figure A-2b. Contour plot of saddle-shaped surface and its saddle point; adapted from (Kutner *et al.* 2004)

A.2 RSM design of experiment

In RSM, coded values for factor levels are used. For example, a linear scale coding (equation A-4) results in a coded value of -1 for low level, 0 for mid level, and 1 for high level. Other coding schemes, such as log transformation, can also be used.

$$x = \frac{\text{Actual level} - \frac{\text{High level} + \text{Low level}}{2}}{\frac{\text{High level} - \text{Low level}}{2}} \qquad \text{(A-4)}$$

The most used design in RSM is the central composite designs (CCD). According to Kutner *et al.* (2004), central composite designs are "two-level full or fractional factorial designs that have been designed with a number of carefully selected treatments to allow the estimation of the second-order response surface model." Two types of CCD are shown in Figure A-3. The distance from the center point to the star point (or axial point) is called α. The distances α are 1 and $\sqrt{2}$ in Figure A-3a, and Figure A-3b, respectively. Cubic and quadratic curvature effect can only be tested when α is greater than 1 (Kutner *et al.* 2004).

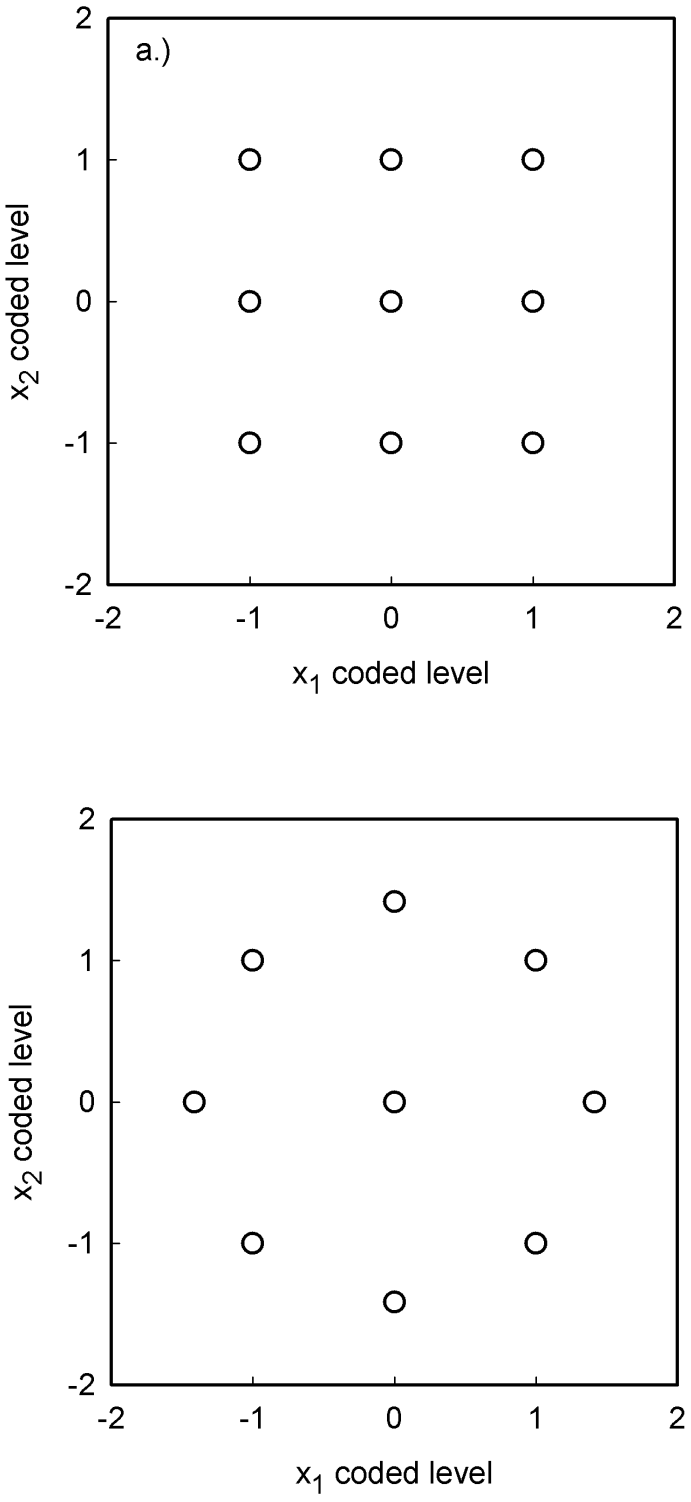

Figure A-3. Two types of central composite designs (CCD) for two-factor RSM: (a) $\alpha = 1$ and (b) $\alpha = \sqrt{2}$.

For k factors and f fractionation (2^{k-f}) design, CCD consists of three main components:

1. 2^{k-f} corner points. The coded coordinates for two-factor CCD are (±1,±1).

2. $2k$ star points. The coded coordinates for two-factor CCD are (0,± α) or (±α,0).

3. n_o center points. If $n_o > 1$, estimation of variance and lack of fit test can be performed. The coded coordinates for two-factor CCD are (0,0).

Kutner *et al.* (2004) summarizes the CCD design for 2-8 factors, as shown in Table A-1.

Table A-1. Example of CCD from Kutner *et al.* (2004).

Characteristic	**Number of factors**						
	2	3	4	5	6	7	8
Factorial design	2^2	2^3	2^4	2^{5-1}	2^{6-1}	2^{7-1}	2^{8-2}
Star points	4	6	8	10	12	14	16
Center point	1	1	1	1	1	1	1
α for rotatability	1.1412	1.16818	2	2	2.3784	2.8284	3.3636
Total number of trials (n_o = 4)	12	18	28	30	48	82	84

From Table A-1, the value α for rotatability is the α value that leads to a rotatable CCD. Generally, a rotatable design is desirable, since the variance of the response at the same distance in any direction is the same (Kutner *et al.* 2004). This is an advantage over

the non-rotatable design, since it is not known which direction from the center point will be of interest later on. Therefore, only the distance from the center point, but not the direction, will affect the variance of the fitted value on the response surface, for the rotatable designs.

Appendix B Supplement Tables

Table B-1. Statistical results of RSM model for % light transmission

Summary of Fit

R^2	0.990566
Adjusted R^2	0.979245
Root Mean Square Error	4.096733

Analysis of Variance

Source	**DF**	**Sum of Squares**	**Mean Square**	**F Ratio**
Model	6	8810.9163	1468.49	87.4973
Error	5	83.9161	16.78	**Prob > F**
Total	11	8894.8324		<.0001*

Note: * indicates a statistical significance at type I error (α) of 0.05

Table B-2. Statistical results for of RSM model TS_a parameter

Summary of Fit

R^2	0.849518
Adjusted R^2	0.66894
Root Mean Square Error	1.577087

Analysis of Variance

Source	**DF**	**Sum of Squares**	**Mean Square**	**F Ratio**
Model	6	70.205231	11.7009	4.7044
Error	5	12.436021	2.4872	**Prob > F**
C. Total	11	82.641252		0.0552

Table B-3. Statistical results of RSM model for TS_b parameter

Summary of Fit

R^2	0.598599
Adjusted R^2	0.116918
Root Mean Square Error	0.001335

Analysis of Variance

Source	**DF**	**Sum of Squares**	**Mean Square**	**F Ratio**
Model	6	0.00001328	2.214e-6	1.2427
Error	5	0.00000891	1.7816e-6	**Prob > F**
C. Total	11	0.00002219		0.4149

Table B-4. Statistical results of RSM model for TS_o parameter

Summary of Fit

R^2	0.937525
Adjusted R^2	0.862555
Root Mean Square Error	0.487182

Analysis of Variance

Source	**DF**	**Sum of Squares**	**Mean Square**	**F Ratio**
Model	6	17.808617	2.96810	12.5054
Error	5	1.186733	0.23735	**Prob > F**
C. Total	11	18.995350		0.0070*

Note: * indicates a statistical significance at type I error (α) of 0.05

Table B-5. Statistical results of RSM model for Gel_a parameter

Summary of Fit

R^2	0.764613
Adjusted R^2	0.482149
Root Mean Square Error	0.084054

Analysis of Variance

Source	**DF**	**Sum of Squares**	**Mean Square**	**F Ratio**
Model	6	0.11474849	0.019125	2.7069
Error	5	0.03532541	0.007065	**Prob > F**
C. Total	11	0.15007390		0.1470

Note: * indicates a statistical significance at type I error (α) of 0.05

Table B-6. Statistical results of RSM model for Gel_b parameter

Summary of Fit

R^2	0.895875
Adjusted R^2	0.770925
Root Mean Square Error	0.001281

Analysis of Variance

Source	**DF**	**Sum of Squares**	**Mean Square**	**F Ratio**
Model	6	0.00007058	0.000012	7.1699
Error	5	0.00000820	1.641e-6	**Prob > F**
C. Total	11	0.00007878		0.0236*

Note: * indicates a statistical significance at type I error (α) of 0.05

Table B-7. Statistical results of RSM model for final gel content

Summary of Fit

R^2	0.857417
Adjusted R^2	0.686318
Root Mean Square Error	0.068206

Analysis of Variance

Source	**DF**	**Sum of Squares**	**Mean Square**	**F Ratio**
Model	6	0.13987653	0.023313	5.0112
Error	5	0.02326054	0.004652	**Prob > F**
C. Total	11	0.16313707		0.0488*

Note: * indicates a statistical significance at type I error (α) of 0.05

Table B-8. Statistical results of RSM model for *b* parameter from $M_n = y_O + ae^{bx}$

Summary of Fit

R^2	0.884271
Adjusted R^2	0.745397
Root Mean Square Error	0.001637

Analysis of Variance

Source	**DF**	**Sum of Squares**	**Mean Square**	**F Ratio**
Model	6	0.00010234	0.000017	6.3674
Error	5	0.00001339	2.679e-6	**Prob > F**
C. Total	11	0.00011574		0.0302*

Note: * indicates a statistical significance at type I error (α) of 0.05

REFERENCES

References

Kutner, M, Nachtsheim, C, Neter, J and Li, W (2004). Applied linear statistical model. New York, NY, McGraw-Hill /Irwin.

Myers, R, Montgomery, D and Anderxon-Cook, C (2009). Response surface methodology: Process and product optimization using designed experiments Hoboken, NJ, John Wiley & Sons.